DISSERTATION

SKIN TISSUE OPTICAL AND THERMAL REACTIONS TO PULSE SEQUENCES OF THULIUM YTTRIUM ALUMINUM GARNET LASER IRRADIATION

Submitted by

David Nicholas Schaaf Jr.

Department of Environmental and Radiological Health Sciences

In partial fulfillment of the requirements

For the Degree of Doctor of Philosophy

Colorado State University

Fort Collins, Colorado

Summer 2010

COLORADO STATE UNIVERSITY

May10, 2010

WE RECOMMEND THAT THE DISSERTATION PREPARED UNDER OUR SUPERVISION BY DAVID NICHOLAS SCHAAF JR. ENTITLED SKIN TISSUE OPTICAL AND THERMAL REACTIONS TO PULSE SEQUENCES OF THULIUM YTTRIUM ALUMINUM GARNET LASER IRRADIATION BE ACCEPTED AS FULFILLING IN PART REQUIREMENTS FOR THE DEGREE OF DOCTOR OF PHILOSOPHY.

Committee on Graduate Work

William J. Brazile

Joseph F. Harmon

Robert Woody

John D. Zimbrick

Advisor: Thomas E. Johnson

Department Head: Jac A. Nickoloff

ABSTRACT OF DISSERTATION

SKIN TISSUE OPTICAL AND THERMAL REACTIONS TO PULSE SEQUENCES OF THULIUM YTTRIUM ALUMINUM GARNET LASER IRRADIATION

The increasing interest in new lasers operating in the mid-infrared region has produced a need for better understanding of tissue reactions for safety purposes. One of the lasers of interest for skin irradiation is the Tm:YAG which produces 2.0 micron wavelength light. However, there are many vital pieces of knowledge missing to calculate thermal effects of two micron light interactions with human skin. This work aims to fill several of these deficiencies. The first unresolved issue is the fundamental optical absorption coefficient of skin layers for 2.0 μm because current published values span two orders of magnitude. A new method for measuring optical absorption rates which avoids most of the factors introducing uncertainties in current approaches is therefore presented. The second issue unaddressed in literature is the effect of delivering the laser energy in multiple pulses which nullifies the normal assumption of thermal confinement. The third issue that published literature leaves confused is the values of thermal constants used in heat modeling. The wide ranging values of these constants is shown to allow models to drastically differ from measured temperatures. The final issue

to be resolved for the first time is the effective depth of measurement of thermal imaging non-contact temperature measurement instruments.

David Nicholas Schaaf Jr.
Department of Environmental and
Radiological Health Sciences
Colorado State University
Fort Collins, CO 80523
Summer 2010

ACKNOWLEDGEMENTS

This dissertation, and the research to support it, has been conducted under the guidance of my graduate committee. First, I am forever grateful to my advisor Dr. Tom Johnson, who has always supported my efforts and helped me overcome many hurdles in the path. Next, I wish to express my gratitude to my committee members, Dr. William Brazile, Dr. Fred Harmon, Dr. Robert Woody, and Dr. John Zimbrick. These distinguished scholars have given me time, insights, suggestions, critiques, and support to make this possible. I have been blessed with a committee of gentlemen of the highest caliber.

As a multi-disciplinary research project, I have had to seed assistance outside the department. I would like to thank Dr. Sandeep Kohli for assistance and access to the Chemistry Department's spectrophotometer. I would like to thank Dr. Robert E. Lee of the Veterinary Anatomy Department for assistance with the Animal Care and Use Committee and generosity in providing the pig skin. I would like to thank Dr. Semi Kumruh for helpful discussions of optical measurement techniques. I would like to thank Dr. Jake Roberts for one of the most challenging courses, in which I learned so much.

I could not have accomplished the experiments or prepared manuscripts for publication without the assistance of Ms. Aimee Oke. I thank Mr. Antonio Serpa for all

his expert help with my electronics. I offer my thanks to Ms. Julie Asmus for her kind guidance through the bureaucracy.

I would also like to thank all the Health Physics Program students who have become friends along the journey, and from whom I have learned a great deal. In particular Mr. Dan Dugan, Ms. Jerri Walter, Ms. Lisa Manglass, Ms. Margaret Cervera, and Eric the Anonymous.

Lastly, I need to acknowledge the support of the program managers at AFIT/CI and the staff of AFROTC Detachment 90 who have been so helpful.

The views expressed in this dissertation are those of the author and do not reflect the official policy or position of the United States Air Force, the Department of Defense, or the U.S. Government.

> "Suspicion is a thing very few people can entertain without letting the hypothesis turn, in their minds, into fact ... only scientists can walk around and around a hypothesis without even beginning to confuse it with truth." – *David Cort*

> "An investment in knowledge always pays the best interest."
> – *Benjamin Franklin*

DEDICATION

This dissertation, these years, and all, I dedicate to my Jenn.

TABLE OF CONTENTS

Chapter 1

SKIN TISSUE OPTICAL AND THERMAL REACTIONS TO PULSE SEQUENCES OF THULIUM YTTRIUM ALUMINUM GARNET LASER IRRADIATION

1.1 Introduction

The profession of Health Physics combines scientific research and understanding with their practical application for protection of people from radiation. Radiation is most commonly thought of as x-rays, gammas and particles such as alphas and betas. However, the Health Physics Society and the National Council on Radiation Protection and Measurements both consider non-ionizing radiation to also be within the field of Health Physics. The safe use of infrared lasers is the particular Health Physics sub-field of this proposal. A laser (Light Amplification by Stimulated Emission of Radiation) is an optical amplifier which produces a coherent beam of light. In North America, laser safety is primarily governed by regulations of the Food and Drug Administration's Center for Devices and Radiological Health (CDRH) and the Department of Labor's Occupational Safety and Health Administration (OSHA). OSHA implements its regulations concerning lasers, found in 29CFR1910 subpart I, with its standard *Guidelines for Laser Safety and Hazard Assessment*.[1] The CDRH issues many guidance

documents for users and manufacturers including the classification criteria. The federal regulations of the CDRH concerning lasers are found in 21CFR1040. Both CDRH and OSHA recognize and utilize the recommendations of the American National Standards Institute which publishes the "Safe Use of Lasers" series of standards in ANSI Z136.[2]

A laser is a unique instrument in that it can transfer energy in very short times and in very confined volumes. The benefits of energy transfer to tissue was recognized soon after the debut of lasers. Lasers were quickly applied in such endeavors as surgical incisions[3] or medical coagulation to stop bleeding.[4] The laser has also been identified as a precise tool in neurological research.[5] Analogous to the evolution of discovery and utilization of ionizing radiation, lasers were also recognized to present health hazards soon after their first appearance. Within the first year after Maiman published the invention of the first laser,[6] accidental eye injuries from lasers had been reported in literature.[7] After just two more years, skin injuries had been investigated on rabbits and humans.[8]

As with most activities in Health Physics, this work crosses disciplines to investigate methods to predict and measure infrared laser thermal effects in human skin while avoiding the permanent effects of laser interactions.

1.2 Laser Background

The now common laser can be considered an amplifier of a particular type of energy, Electro-Magnetic energy in the optical region of the spectrum, through the conversion of input energy. The theory of this process was first proposed by Einstein in one of his many seminal papers.[9] Einstein described the phenomena of blackbody

radiation in terms of discrete energy levels as postulated by Max Planck.[10] Einstein's description first proposed the ability of incident energy to stimulate an atom to produce an exact duplicate quanta of radiated energy by dropping its own energy level. The probabilities of this stimulated emission of energy, and of the atom's ability to absorb or spontaneously emit a particular packet of energy have become known as the Einstein *A* and *B* coefficients. The first demonstration of the theoretical stimulated emission of energy was produced not with light but with microwaves by Charles H. Townes and colleagues in 1955.[11] The principle of stimulated emission was then successfully transferred into the optical portion of the electro-magnetic spectrum when Theodore H. Maiman produced the first stimulated optical radiation with a ruby crystal.[6] However, other labs were also thinking of stimulating light emission. The lab notebook of Jack Gould in fact contains the earliest mention of the acronym LASER, which he wrote for Light Amplification by Stimulated Emission of Radiation on the 13th of November 1957.[12]

Since this first demonstration of the theory, lasers have become common, ubiquitous instruments in a wide variety of fields from academic research such as Raman Spectroscopy[13] to nano-scale imaging,[14] household entertainment, and a wide variety of medical diagnosis and treatment.[15-18] Many lasers have been used in neurological research looking at variables such as reaction times[19] and small-diameter afferent nerve fiber viability in patients with peripheral neuropathies.[20] Treede et al found at least 20 different medical diagnoses are possible using Laser Evoked Potentials (LEP) in brain activity. The conditions can arise from a variety of causes such as lesions on the spinal column or brainstem, diabetes, and dementia.[21] The laser is the instrument of choice in

these studies because electrical and mechanical stimulation methods preferentially excite the large-diameter afferent nerves, while laser parameters can be selected to activate both Aδ and C receptors.[22]

The uses and types of lasers continue to grow. From the maser in the low-frequency microwave portion of the spectrum up to low-energy x-rays, a laser can produce almost any frequency of radiation. The specific laser type of interest in this project provides infrared light at a wavelength of 2.01 microns. The 2-micron wavelength is important because it is close to the peak photon absorption in water at 1.94 microns.[23-25] For this reason, the Ho:YAG laser at 2.12 micron wavelength has found popularity in soft tissue medical applications such as urological procedures.[26] Recently, the introduction of commercially available Tm:YAG lasers at 2.01 micron wavelength has opened even more possibilities for near-infrared laser uses.[27] A thulium-doped fiber laser operating at 2-micron wavelength was first reported in 1990[28] with Jackson and King surpassing the single Watt power output level in a laboratory eight years later.[29] Jackson and King also established the method of adjusting the wavelength of thulium fiber lasers by means of changing fiber length.

The laser produces several unique characteristics in its amplified emission. The output energy from a laser is bound within a very narrow bandwidth. The output waves all have a uniform polarization. The light waves are traveling in the same direction, with a relatively small angle of divergence, depending on the laser cavity and wavelength. The light waves are in the same phase, which is called coherent light.[30]

Lasers can be produced in many configurations from gas, liquid, amorphous solids, and crystals. The first laser was produced by coating two parallel surfaces of a

ruby crystal with metal to reflect some light, and pumping it with an external flashlamp.[6] Today, lasers are made of a wide variety of materials and powered with many types of energy pumps, including other lasers. Table 1.1 lists a representative sampling of the common types of lasers, their pumping mechanism, and significant characteristics as described by Pedrotti[30] and by Niemz.[26]

The optical laser beam is characterized by six major parameters. These include the duration of the beam, the wavelength of the beam, the beam diameter and shape, the beam divergence, the polarization of the light, and the beam's Transverse Electro-Magnetic (TEM) mode(s).

The laser beam duration is generally considered to be continuous if it remains on and constant for longer than one quarter second.[2] It is said to be pulsed if it is on for less than one quarter second, either in a single burst or in a repetitive pattern. The pulsed beam may be created by external control of the input pump energy, a mechanical shutter on the beam exit, or induced by internal conditions of the laser. In the first case the pump energy is turned on and off at the desired times, each time creating a new population inversion. For the third case the laser pump energy remains constant while an internal switch creates the conditions to lase and then turns the lasing action off. This is generally done by creating a high loss condition in the beam path which can be quickly switched to low loss. This is called Q-switching because the amount of loss in the cavity is called the Quality of the cavity. The special case of creating a low loss condition or phase modulation at the internal round trip time of the internally reflected beam is known as mode-locking.[31] The mode-locked pulse is a very short pulse (typically less than a microsecond down to picoseconds) with a very large intensity.

The beam wavelength, or alternatively the frequency, describes the energy of the photons produced by a laser. The photon energy is determined by the energy states of the gain medium and the input pump. Each laser system will naturally tend to lase at a single wavelength. However, a particular gain medium can have multiple energy levels which can lase under different cavity and pump conditions. The common HeNe laser with its industry standard visible red beam can also produce a green light with changes to the pump and cavity. The spread of wavelengths from a laser, its bandwidth, is very low in comparison to other amplifying systems.

The beam diameter and shape are determined by the gain medium, mirrors, and optical components of the laser. Most beams have a Gaussian shape in the transverse plane. A small aperture, in relation to the natural beam size, can produce the "top hat" laser beam shape which approximates a square wave shape. However, far from the aperture, the top hat beam from this method will return to a Gaussian shape. A "top hat" beam cross section can also be achieved by mixed TEM modes. The beam radius is usually called the spot size. It is normally reported as the width of the beam at $1/e^2$ of its maximum intensity. However, in the context of laser safety, a beam size is described at the 1/e intensity level. This provides a margin of safety as the total beam energy is then considered to be concentrated in the smaller area, triggering safety precautions based on aerial energy levels.[2]

The beam divergence is a function of the minimum beam radius and the beam wavelength, before beam focusing with lenses. One of the singular features of a laser is the ability to produce a very low rate of beam divergence. However, some lasers, such

as most diode lasers, can have a very large angle of divergence which is overcome with a strong lens.

The light from a laser is usually polarized, which is to say all the light has the same orientation of its transverse electric field. The laser may operate in different transverse electro-magnetic (TEM) modes with different optical cavity configurations. Most commercial lasers operate predominantly in the lowest order, $TEM_{0,0}$, mode which produces the single circular beams familiar today. The lasers used in this study all operated in the $TEM_{0,0}$ mode with a circular shape and Gaussian intensity distribution.

1.3 Laser Radiation Interactions With Tissue - Health Physics

Laser radiation, whether it is visible, UV, or IR, can deliver enough energy, in very little time, to living tissue to produce transient and permanent effects. Examples of temporary effects are induction of pigmentation production and swelling from capillary dilation. Some permanent effects include heating, burning, coagulation of blood or proteins, and tissue ablation. A laser can deliver energy at a rate which overwhelms the ability of the local tissue to dissipate the heat. The primary interaction of concern for this dissertation is thermal interactions utilizing medium laser power levels with millisecond scale pulses. The distinction between heating and burning is determined by the rate of heating relative to the rate of heat removal. Generally, if human tissue is heated to above 50° it will be destroyed as the cellular material begins to break down.[32] Moritz (Figure 1.1) showed that, the threshold for skin burns depends upon a combination of time and temperature.[33] Modern lasers in fact can easily deposit energy so quickly that the reciprocal relation of time and temperature to produce injury as

described by Moritz and Henriquez is invalid.[34] The extreme power can create vaporization and mechanical shocks in addition to heat.

Laser energy can induce blood to coagulate when several hundred to a few thousand J/cm^2 are applied at a rate of a few Watts and produce a temperature rise to 60 – 70 °C.[35] The human body can maintain a thermal equilibrium with no external heat removal for up to about six hours when the tissue temperature remains no higher than 44°C.[32] This is the maximum temperature of most hot tubs. A laser can deliver energy at a rate which overwhelms the ability of the local tissue to dissipate the heat.

Early investigation into cellular damage from ruby lasers concluded that necrosis was caused by denaturation and coagulation of cell proteins, combined with vaporization of intercellular and intracellular water.[36] This suggests the injury is also power dependent. Rate process models of thermal denaturation predict that the complete temperature history over time governs the degree of denaturation rather than just the peak temperature attained.[37] Albumins begin to coagulate between 45 °C and 60 °C.[38] Studies then showed that in addition to protein denaturation, DNA and RNA melting also contributes to cellular death at temperatures as low as 43 °C.[39] Continued interest into the cellular thermal effects confirm the 43 °C temperature for cell killing, but also discovered potential heat resistance induced by so called Heat Shock Proteins (HSP).[40] The resistance has been termed thermo tolerance and is defined as a transient resistance to cell death from heat induced by prior exposure to thermal stress.[41] The activation energy for killing cells has been reported to be approximately 600 kJ.[42]

There are five general categories of laser tissue interactions, as described by Niemz.[26] These include photochemical, thermal, photoablation, plasma-induced

photoablation, and photodisruption. The first involves all processes where light imparts energy for chemical reactions, usually with the help of a photosensitizer.[26] Photochemical processes use low power irradiations (less than 1W/cm^2) for several seconds. Thermal interactions can produce a range of effects from coagulation, vaporization, carbonization, and melting. Coagulation, the denaturing of proteins and collagen, will be induced at temperatures exceeding 60°C. Coagulated tissues appear opaque white and will become necrotic.

Photo-ablation, or more commonly ablation, is the process of removing tissue as water expands into gas as it boils, generally at 100°C. The sudden expansion of vaporized water produces microscopic explosions from the pressure which eject particles of the tissue. Photo-ablation is a distinct removal of tissue with minimal coagulation, charring or other thermal damage in surrounding tissue. It is used for laser incisions, skin resurfacing, and dental drilling with laser pulses on the order of nanoseconds and megawatts per square centimeter. Studies of ablation generally report the depth of ablation craters per incident laser energy per unit area.

Carbonization occurs in tissue which exceeds 150°C. Melting can occur in hard tissues such as teeth and bone when temperatures of a few hundred degrees Celsius are reached. Thermal effects are associated with power density up to 1 MW/cm^2. Power density exceeding 10^{11} W/cm^2 can produce a state of matter called plasma, when the energy produces an optical breakdown of atoms producing a cloud of free electrical charges. The plasma ionization can produce very clean ablation cavities, even in tissue which is not absorptive of the particular light. The optical breakdown is usually created using picosecond scale pulses from mode locked lasers. Photo-disruption is a term

applied to laser energy inducing mechanical effects such as shock waves or cavitation splitting or breaking tissue. Photo-disruption is produced with femtosecond scale pulses. A common use of this phenomenon is laser lithotripsy of kidney and gall stones.[26] This work will be concerned with the thermal laser-tissue interactions.

Laser irradiation can quickly induce temperature increases which will produce a burn in the tissue. While most commonly thought of as a danger to eye tissue, lasers are also known to cause accidental burns to other tissue. A recent review of the three most prominent laser injury and incident databases found that 35% of 551 injuries since the early 1960s have been to tissue other than the eye.[43] Skin burns are one of the primary hazards of laser use, as these burns are difficult injuries to treat. Treatment of burns is among the earliest form of medical care recorded, with evidence of Neanderthals using plant juice and Egyptians experimenting with milk treatments.[44] Lasers can deliver energy to a very small portion of an organism, with beams that can be much smaller than the spacing of vasculature or other structures of the skin such as sweat glands or hair follicles.

1.4 Anatomy and Physiology

The skin is a very complex organ which performs many different functions and varies in structure at different locations.[45] Skin is also a large organ, with surface area of $1.2 - 2\ m^2$ and fractionally accounting for 12 to 16% of a human's mass.[46] While the skin type of interest is human, in this study pig skin was used as a substitute during irradiation experiments.[47] Several structures of the skin, such as hair follicles and sweat glands, are often not considered in modeling as their concentration, location, and

influence vary tremendously. Sweat glands are distributed within the human skin with an average of 92 glands cm^{-2} for females and 77 glands cm^{-2} for males.[48] But the density of the glands can vary to extremes of 360 glands cm^{-2} on the forehead and a maximum concentration of over 600 glands cm^{-2} on the sole of the feet.[49-50] The human skin also contains hair at an areal density of 40 hairs cm^{-2} on males and 45 hair cm^{-2} on female arms.[51] The average thickness of the hairs is approximately 18 μm.[52] The skin also contains many nerves, with one study quoting 23% of the skin surface area containing nerve fibers.[53] Pig skin is considered a suitable substitute for laser exposure experiments.[47,54-59]

The relevant anatomic features to this study for modeling temperatures are the distinct layers of the skin: the stratum corneum, the epidermis, and the dermis, from exterior inward, as shown in Figure 1.2. The stratum corneum is the outermost layer and is composed of cells ready to be sloughed off. It provides the first layer of protection from incident light. Early studies of skin that included the stratum corneum are Kligman in 1964[60] and Holbrook in 1974.[61] Several other skin studies have also reported stratum corneum thickness for a variety of sites and from various populations, which will be discussed in detail in Chapter 2. The typical thickness given for stratum corneum is 10 – 20 μm. Depending on the author and perspective, the stratum corneum is sometimes considered the first layer of the epidermis.

The epidermis of the skin is characterized by the absence of blood vessels. The different sub-layers of the epidermis are fed by diffusion from the capillaries beneath. The layers include, from the exterior inward, the stratum lucidum, stratum granulosum, stratum mucosum (sometimes referred to as spinosum), and stratum germinativum. The

stratum germinativum is significant to this study as it is the layer which re-populates an injured epidermis. The undulations of the stratum mucosum are relevant in the geometry of heating in that the location of the stratum germinativum is not at a fixed depth. The lack of vasculature is significant to the transport of heat as there is no convection in the epidermis. The epidermis also contains no nerve fibers. The epidermis is composed almost entirely of live cells. One other potentially significant skin property for optics is the presence of melanin in the epidermis. Melanin absorbs light at different wavelengths as a function of the individual pigment particles' size, but does not absorb infrared light so will not be considered further.[62-64] There have been numerous studies measuring the thickness of the epidermal layer of human skin, which will be presented in Chapter 2. The typical epidermal typical thickness is 50 – 100 μm.

Underneath the epidermal layer is the dermis. The dermal layer of the skin is significant as it is the location of blood vessels and capillaries, sweat glands, hair follicles and nerve endings in the skin. The volume density of vasculature within the dermis has been found to be 22.4% in the forearm, 31.1% in the shoulder and 29.6% in the buttocks.[65] In contrast to the cells of the epidermis, the dermis is primarily proteins making up the elastins and collagen fibers (which are about 70% by weight of the dermis).[66] The reported thicknesses of the dermis from the ICRP varies from one to two and a half millimeters depending on anatomic location.[67] Results of specific studies of human dermis thickness will be presented in Chapter 2.

1.5 Dissertation Research and Presentation

The objective of this dissertation is to investigate human skin tissue reactions from 2-μm IR laser irradiation. Each chapter addresses a particular gap in the scientific body of knowledge in this field. The chapters are presented in the format of individual works because the chapters have been or will be submitted as papers to scientific journals or presented at scientific conferences. Therefore they all have the structure of a stand-alone paper including an Introduction, Materials and Methods, Results, and Discussion sections. Due to the shared goal of describing 2-μm laser irradiation of tissue, some background material may be found to overlap in the multiple chapters. The data and analyses are unique for each chapter.

The first step toward this goal was to clarify discrepancies between absorption coefficients of skin, particularly the epidermis, at the 2-μm wavelength. Investigation was required into the absorption rate of IR radiant energy and subsequent conversion to thermal energy within live skin tissue. Specifically, the first efforts centered on supplying a novel approach to measuring the optical absorption rate of two micron IR light in epidermis by growing optically thin layers of epidermis in culture. This work has been published in the Journal of BioPhotonics.[68]

The next chapter focuses on the ability to measure skin temperature *in vivo* during 2-μm IR laser irradiation. Investigations were made into the capabilities and limitations of several thermal measurement instruments. The market offers a variety of non-contact temperature measurement instruments with a large range of capabilities. As many authors from a wide range of disciplines have used these instruments without verification of their readings, the second set of experiments thoroughly evaluated the temperature measurement instruments available. The goal was to establish the

capabilities and limitations of two types of instruments suitable for measuring human skin temperature while being heated by IR lasers. Parts of Chapter Three have been presented at the SPIE Conference in San Jose in January 2009.

The fourth chapter's area of investigation was in measuring the temperature of a series of pulse sequences of 2-μm laser irradiation on skin using *ex vivo* pig skin. While there have been studies which recorded the surface temperature during single pulses of Tm:YAG laser 2.01 μm irradiation, measurement at both surface and depth within skin is unavailable. This section has produced the first simultaneous temperature measurements at multiple skin depths during laser irradiation. This work is the first comparison of multiple millisecond-scale pulse-sequence effects on maximal temperature rise of laser irradiation of skin. This work has been accepted for publication in the Journal of Biomedical Optics.

The methods of chapter four were continued on further pig skin samples to obtain measurements at more depths and across the beam profile to optimize theoretical models of skin heating from laser irradiation. A variety of analytical solutions to the air-interface bioheat condition were considered, including several forms of Green's function. Because all analytical solutions utilize the optical absorption coefficient and various thermal properties of skin, several published values were evaluated and the combination best matching measured values were identified. While the laws of physics readily describe, and often can predict, the transfer of energy in inanimate materials, living biological tissue presents a large variety of heat dissipation mechanisms. Therefore, experimental measurements matching the model are necessary to validate a

model for specific conditions. This work is being prepared for submission to the Journal of Biomedical Optics for publication.

The results of these modeling investigations were combined to compare surface and depth temperatures during laser irradiations. The non-contact temperature instrument's measurements were found to correspond to temperatures within pig skin from a region between 50 and 120 microns deep rather than at the air-skin interface as assumed by most authors. This depth was determined considering both the wavelength of the incident laser and also the spectral region of the far IR to which the detector is sensitive, as well as the particular type of tissue being irradiated. This work is to be prepared for submission to the Journal of BioPhotonics for publication.

1.6 References

1. Occupational Safety and Health Administration, "Guidelines for laser safety and hazard assessment," Report STD 01-05-001 [Pub 8-1-7],(1991)

2. American National Standards Institute, "American national standard for safe use of lasers," Report No. ANSI Z136-1-2007, 2007.

3. T. G. Polanyi, Bredemei.Hc, and T. W. Davis, "CO_2 laser for surgical research," Medical & Biological Engineering **8** (6), 541-& (1970).

4. N. S. Kapany, Silbertr.N, and N. A. Peppers, "Laser retinal photocoagulator," Applied Optics **4** (5), 517-518 (1965).

5. B. Bromm and R.D. Treede, "CO_2 laser radiant heat pulses activate c nociceptors in man," Pflügers Archiv European Journal of Physiology **399** (2), 155-156 (1983).

6. T. H. Maiman, "Stimulated optical radiation in ruby," Nature **187** (4736), 493-494 (1960).

7. M. M. Zaret, G. M. Breinin, I. M. Siegel, H. Ripps, and H. Schmidt, "Ocular lesions produced by an optical maser (laser)," Science **134** (348), 1525-& (1961).

8. L. Goldman, D. J. Blaney, D. J. Kindel, and E. K. Franke, "Effect of the laser beam on the skin," Journal of Investigative Dermatology **40** (3), 121-122 (1963).

9. A. Einstein, "On the quantum theory of radiation," in *The old quantum theory*, edited by D. Ter Haar (Pergamon, New York NY, 1966), pp. 167-183 Original publication: Physikalische Zeitschrift 18:121 (1917).

10. M. Planck, "Law of energy distribution in normal spectra," Annalen Der Physik **4** (3), 553-563 (1901).

11. J. P. Gordon, H. J. Zeiger, and C. H. Townes, "The maser—new type of microwave amplifier, frequency standard, and spectrometer," Physical Review **99** (4), 1264-1274 (1955).

12. J. Gould, "Lab notebook," (1957), pp. 14.

13. M. Gniadecka, O.F. Nielsen, D.H. Christensen, and H.C. Wulf, "Structure of water, proteins, and lipids in intact human skin, hair, and nail," Journal of Investigative Dermatology **110** (4), 393-398 (1998).

14. F. Pedaci, Y. Wang, M. Berrill, B. Luther, E. Granados, and J. J. Rocca, "Highly coherent injection-seeded 13.2 nm tabletop soft x-ray laser," Optics Letters **33** (5), 491-493 (2008).

15. M. M. Zaret, "Laser application in field of medicine," Zeitschrift Fur Angewandte Mathematik Und Physik **16** (1), 178-& (1965).

16. K. M. Diette, B. R. Bronstein, and J. A. Parrish, "Histologic comparison of argon and tunable dye lasers in the treatment of tattoos," J Invest Dermatol **85** (4), 368-373 (1985).

17. A. Schindl and R. Neumann, "Low-intensity laser therapy is an effective treatment for recurrent herpes simplex infection. Results from a randomized double-blind placebo-controlled study," Journal of Investigative Dermatology **113** (2), 221-223 (1999).

18. R. Splinter and B. A. Hooper, *An introduction to biomedical optics*. (CRC Press, Boca Raton, 2007).

19. L. Arendt-Nelsen and P. Bjerring, "Reaction times to painless and painful CO_2 and argon laser stimulation," European Journal of Applied Physiology and Occupational Physiology **58** (3), 266-273 (1988).

20. J. P. Lefaucheur, A. Brusa, A. Creange, X. Drouot, and G. Jarry, "Clinical application of laser evoked potentials using the Nd: Yag laser," Neurophysiologie Clinique/Clinical Neurophysiology **32** (2), 91-98 (2002).

21. R. D. Treede, J. Lorenz, and U. Baumgärtner, "Clinical usefulness of laser-evoked potentials," Neurophysiologie Clinique/Clinical Neurophysiology **33** (6), 303-314 (2003).

22. G. Cruccu and L. Garcia-Larrea, "Clinical utility of pain--laser evoked potentials," Supplements to Clinical neurophysiology **57**, 101 (2004).

23. J. A. Curcio and C. C. Petty, "The near infrared absorption spectrum of liquid water," Journal of the Optical Society of America **41** (5), 302-304 (1951).

24. G. M. Hale and M. R. Querry, "Optical-constants of water in 200-nm to 200-mum wavelength region," Applied Optics **12** (3), 555-563 (1973).

25. M. R. Querry and G. M. Hale, "Optical-constants of water in 200-nm to 0.2-mm wavelength region," Journal of the Optical Society of America **62** (11), 1381-1381 (1972).

26. MH Niemz, *Laser-tissue interactions: Fundamentals and applications*. (Springer Verlag, 2003).

27. B. Chen, H. W. Kang, S. L. Thomsen, and A. J. Welch, "Modeling thermal response of skin to 2000 nm laser irradiation," Lasers in Surgery and Medicine, 274 (2006).

28. D. C. Hanna, I. R. Perry, J. R. Lincoln, and J. E. Townsend, "A 1-watt thulium-doped cw fibre laser operating at 2 μm," Optics Communications **80** (1), 52-56 (1990).

29. S. D. Jackson and T. A. King, "High-power diode-cladding-pumped Tm-doped silica fiber laser," Optics Letters **23** (18), 1462-1464 (1998).

30. F. L. Pedrotti, L. S. Pedrotti, and L. M. Pedrotti, *Introduction to optics*, 3 ed. (Prentice Hall, Upper Saddle River NJ, 2007).

31. C. B. Hitz and J. Falk, "Utilization of simultaneous loss and phase modulation to mode lock the frequency-doubled Nd: Yag laser," presented at the IEEE International Ecetronic Devices Meeting, 1972.

32. J.A. Moncrief, "The body's response to heat," in *Burns, a team approach*, edited by C. Artz, J.A. Moncrief, and B. Pruitt (Saunders, Philadelphia PA, 1979).

33. A. R. Moritz, "Studies of thermal injury v.3. The pathology and pathogenesis of cutaneous burns an experimental study," American Journal of Pathology **23** (6), 915-941 (1947).

34. A. R. Moritz and F. C. Henriques, "Studies of thermal injury v.2. The relative importance of time and surface temperature in the causation of cutaneous burns," American Journal of Pathology **23** (5), 695-720 (1947).

35. R. Vanhillegersberg, H. J. Vanstaveren, W. J. Kort, P. E. Zondervan, and O. T. Terpstra, "Interstitial ndyag laser coagulation with a cylindrical diffusing fiber tip in experimental liver metastases," Lasers in Surgery and Medicine **14** (2), 124-138 (1994).

36. G. C. Faith, M. N. Stein, J. R. Hayes, and R. E. Stowell, "Cellular effects of laser radiation - light microscopic studies on injury of mouse liver," Archives of Pathology **86** (3), 262-& (1968).

37. F. Hillenkamp, "Interaction between laser radiation and biological systems," in *Lasers in biology and medicine*, edited by F. Hillenkamp, R. Pratesi, and C. A. Sacci (Plenum Press, New York NY, 1979), pp. 37-75.

38. A. Vassiliadis, "Ocular damage from laser radiation," in *Laser applicaation in medicine and biology*, edited by M. L. Wobarsht (Plenum Press, New York, 1971), Vol. 1, pp. 125-161.

39. J. R. Lepock, H. E. Frey, A. M. Rodahl, and J. Kruuv, "Thermal-analysis of chl v79 cells using differential scanning calorimetry - implications for hyperthermic cell killing and the heat-shock response," Journal of Cellular Physiology **137** (1), 14-24 (1988).

40. J. L. R. Roti, H. H. Kampinga, R. S. Malyapa, W. D. Wright, R. P. vanderWaal, and M. Xu, "Nuclear matrix as a target for hyperthermic killing of cancer cells," Cell Stress & Chaperones **3** (4), 245-255 (1998).

41. H. H. Kampinga, "Thermotolerance in mammalian-cells - protein denaturation and aggregation, and stress proteins," Journal of Cell Science **104**, 11-17 (1993).

42. J. R. Lepock, "Membrane lipids and proteins," in *Thermotolerance*, edited by K. J. Henle (CRC Press, Boca Raton FL, 1987), Vol. 2, pp. 47–82.

43. T. E. Johnson, J. C. Dunn, and W. P. Roach, "Survey of laser injury," in *Laser tissue interaction xiii: Photochemical, photothermal, and photomechanical*, edited by S. L. Jacques, D. D. Duncan, S. J. Kirkpatrick et al. (2002), Vol. 4617, pp. 125-133.

44. C. Artz, "History of burns," in *Burns, a team approach*, edited by C. Artz, J.A. Moncrief, and B. Pruitt (Saunders, Philadelphi, 1979).

45. W. F. W Southwood, "The thickness of the skin," Plastic and Reconstructive Surgery **15** (5), 423 (1955).

46. P. F. MILLINGTON and R. WILKINSON, *Skin (biological structure & function books, n 9)*. (Cambridge University Press, London, 2009).

47. T. A. Eggleston, W. P. Roach, M. A. Mitchell, K. Smith, D. Oler, and T. E. Johnson, "Comparison of two porcine (sus scrofa domestica) skin models for in vivo near-infrared laser exposure," Comparative Medicine **50** (4), 391-397 (2000).

48. A. S. Knip, "Measurement and regional distribution of functioning eccrime sweat glands in male and female caucasians," Human Biology **41** (3), 380-& (1969).

49. O. P. Kreyden and E. P. Scheidegger, "Anatomy of the sweat glands, pharmacology of botulinum toxin, and distinctive syndromes associated with hyperhidrosis," Clinics in Dermatology **22** (1), 40-44 (2004).

50. G Szabo, "The regional anatomy of the human integument with special reference to the distribution of hair follicles, sweat glands and melanocytes," Philosophical Transactions of the Royal Society of London. Series B, Biological Sciences **252** (779), 447 (1967).

51. K. Hwang and S. H. Baik, "Distribution of hairs and sweat glands on the bodies of korean adults: A morphometric study," Acta Anatomica **158** (2), 112-120 (1997).

52. N. Otberg, H. Richter, H. Schaefer, U. Blume-Peytavi, W. Sterry, and J. Lademann, "Variations of hair follicle size and distribution in different body sites," Journal of Investigative Dermatology **122** (1), 14-19 (2004).

53. I. Besne, C. Descombes, and L. Breton, "Effect of age and anatomical site on density of sensory innervation in human epidermis," Archives of Dermatology **138** (11), 1445-1450 (2002).

54. P. C. M. Williams, G. C. H. Winston, D. Q. Randolph, T. A. Neal, T. Eurell, and T. E. Johnson, "Comparison of experimental models for predicting laser tissue interaction from 3.8 micron lasers," Proceedings of SPIE **5312**, 334-340 (2004).

55. A. V. Lukashev, S. E. Sverchkov, V. P. Solovyev, B. I. Denker, V. V. Engovatov, and P. P. Pashinin, "Investigation of laser damage on skin by 1540 nm er-glass laser," Report Contract F61708-94-C-0008,(1995)

56. D Tata, VI Villavicencio, MC Cook, TE Dayton, CD Clark III, CA Moreno, JA Ross, JS Eggers, P Kennedy, and D Christensen, "Infra red laser induced skin damage and perception," Report No. Technical Report AFRL-HEBRTR-2005-0139, 2005.

57. E. B. Helwig, W. A. Jones, J. R. Hayes, and E. H. Zeitler, "Anatomic and histochemical changes in skin after laser irradiation," Federation Proceedings **24** (1S14), S83-& (1965).

58. J. G. Kuhns, J. Hayes, M. Stein, and E. B. Helwig, "Laser injury in skin," Laboratory Investigation **17** (1), 1-& (1967).

59. A. S. Brownell, W. H. Parr, and D. K. Hysell, "Skin and carbon dioxide laser radiation," Journal Name: Arch. Environ. Health, 18: 437-42(Mar. 1969).; Other Information: Orig. Receipt Date: 31-DEC-69, Medium: X (1969).

60. A. M. Kligman, "The biology of the stratum corneum," in *The epidermis*, edited by W. Montagna and W. C. Lobitz (Academic Press, New York, 1964), pp. 387-433.

61. K. A. Holbrook and G. F. Odland, "Regional differences in the thickness of the human stratum corneum," Journal of Investigative Dermatology **62**, 415-422 (1974).

62. M. R. Chedekel, "Photochemistry and photobiology of epidermal melanins," Photochem Photobiol **35**, 881-885 (1982).

63. M. R. Chedekel, "Photophysics and photochemistry of melanin," in *Melanin: Its role in human photoprotection*, edited by L. Zeise, M. R. Chedekel, and T. B. Fitzpatrick (1995), pp. 11-22.

64. M. R. Chedekel, "Photophysics and photochemistry of melanin," Journal of Investigative Dermatology **102** (2), 264-264 (1994).

65. J. Sandby-Moller, T. Poulsen, and H.C. Wulf, "Epidermal thickness at different body sites: Relationship to age, gender, pigmentation, blood content, skin type and smoking habits," Acta dermato-venereologica **83** (6), 410-413 (2003).

66. E. J. Wood and P.T. Bladon, *The human skin*. (Edward Arnold, London, 1985).

67. International Commission on Radiological Protection and Measurements, "The biological basis for dose limitations in the skin," Report No. ICRP Report 59, 1991.

68. D. Schaaf, T. Eurell, and T. Johnson, "Cultured human keratinocytes for optical transmission measurement," Journal of Biophotonics **3** (3), 161-168 (2010).

Table 1.1. Examples of types of lasers.

Type	Gain Medium	Pump	Wavelength (nm)	Typical Power
Gas, Atomic	Helium-neon	electric discharge	632.8	0.1-50mW
Gas, Ion	Argon	electric discharge	488, 514.5	20W
Gas, Molecular	Carbon Dioxide	electric discharge	10,600	20kW
Gas, Excimer	Argon Fluoride	electric discharge	193	50W avg.
Liquid	various Dyes	laser, flashlamp	tunable	1W
Solid State	Nd:YAG	flashlamp, diode laser	1,064	10kW
Solid State	Ho:YAG	diode array	2,100	1W
Solid State	Er:YAG	flashlamp, diode	2,940	10W
Amorphous	Er:glass	flashlamp	1,540	10W
Fiber	Tm:YAG	diode array	2,010	20W
Semiconductor	InGaAsP	electric current	1,100 – 1,600	1W

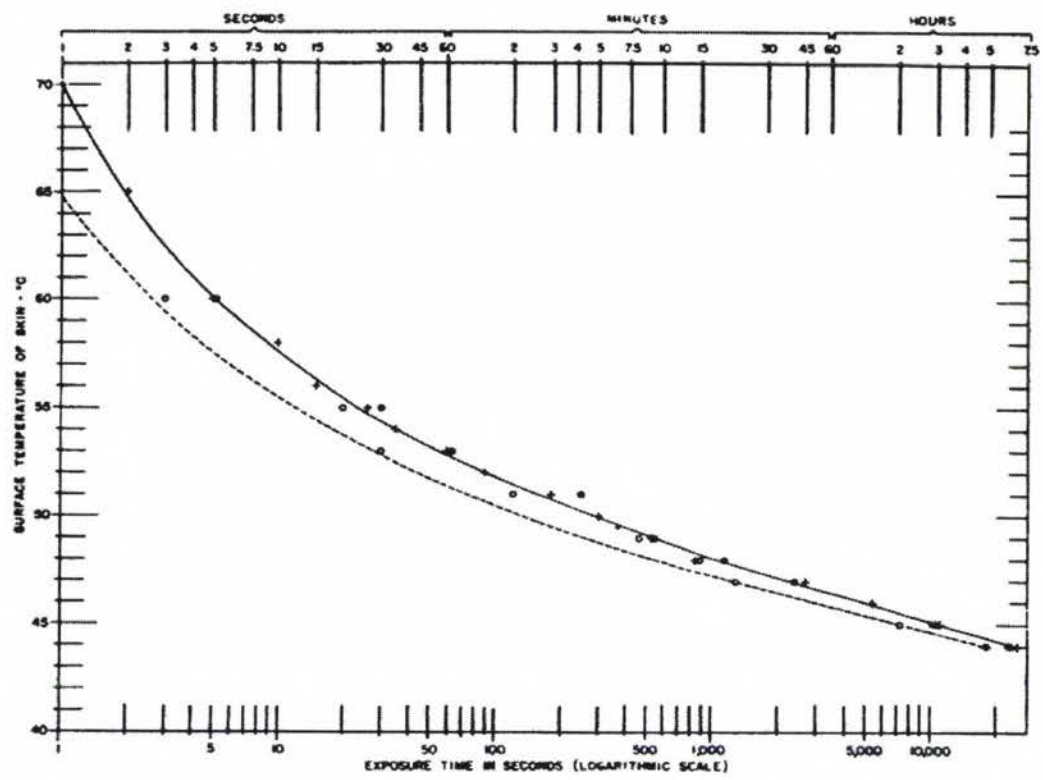

Figure 1.1. Time-temperature threshold for irreversible epidermal injury in porcine skin (dash line). Threshold for epidermal necrosis in porcine skin (solid line). (Reprinted from Moritz in Am. J. Pathol, **23**(5):679-693, 1947, with permission from the American Society for Investigative Pathology).

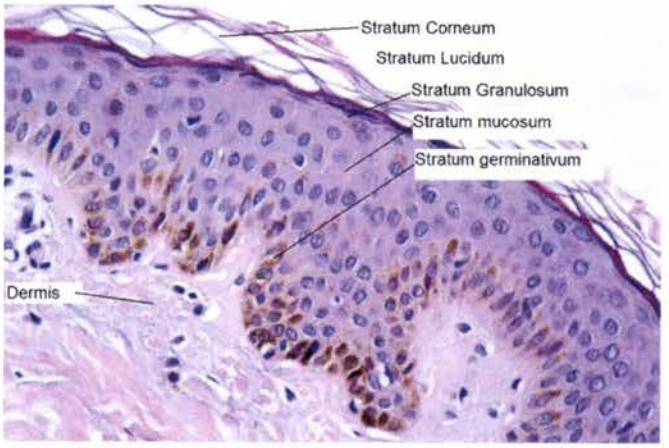

Figure 1.2 Structure of typical human skin. Photo original magnification is 400X.

Chapter 2

Cultured Human Keratinocytes for Optical Transmission Measurement

2.0 Abstract

The challenges of measuring optical properties of human tissues include the thickness of the sample, homogenization, or crystallization from freezing of the tissue. This investigation demonstrates a method to avoid these problems by growing optically thin samples of human keratinocytes as a substitute for ex vivo epidermis samples. Several methods of growth were investigated. Resulting samples were measured on a spectrophotometer for transmission between 300 nm and 2600 nm. The efficacy of the cell growth was confirmed with histological examination of several cultured keratinocyte samples. Limitations were the requirement to measure samples immediately after removal from the incubation environment, and the absence of the irregular structures of normal skin such as hair and glands.

2.1 Introduction

The attenuation and scatter of light by human skin has been studied for many years for optical therapy,[1-3] diagnosis,[4-6] cosmetics,[7] and safety.[8-9] The first surgical use of laser light was reported[10] just four years after the first demonstration of a working laser.[11] The transmission and scatter through the human skin are of vital importance for

non-invasive procedures and diagnostics. Many methods have been developed for directly and indirectly determining the absorption and scattering properties of skin.[12-13] The recent interest in mid-infrared light[14] has revealed a lack of accepted absorption and scattering data in the 2 μm region of the spectrum. Several published reviews of tissue optical properties do not include absorption or scattering coefficients between 1.064 μm from the Nd:YAG and 10.6 μm from the CO_2 laser.[15-18]

There have been many methods described to measure light transport in biological tissue from interstitial probes, time resolved, variable distance probes, goniometers, spectrophotometers, and integrating spheres. Measuring the fundamental optical properties has been described as the most difficult task of tissue optics.[19] Most methods involve measuring the total reflected light intensity, the total transmitted light intensity (which includes forward scattered light), and the ballistic transmitted light intensity (which excludes scattered light).[12-13] From these measurements, several calculation methods may be utilized to determine the optical properties of scattering coefficient μ_s, absorption coefficient μ_a, scattering anisotropy g, and index of refraction n. Chen also introduced a method to calculate the attenuation coefficient of skin from thermal imaging of skin heating during irradiation.[20]

In order to avoid introducing uncertainty by using modeling to render the optical properties, a direct measurement is appealing. The limiting factor for direct measurement is the requirement for an optically thin sample.[21] An optically thin sample is defined as one in which there is only one scattering event likely before exiting the sample. This generally limits the sample to roughly 10 μm.[21] In order to prepare such thin samples, either sectioning frozen tissue or homogenization of the tissue is usually

necessary. Both methods introduce significant thermal, chemical, and mechanical alterations of the tissue which likely alter the optical properties .[22] Of the three main layers of skin, only the stratum corneum approaches the requirement for an optically thin sample as the thickness of the epidermis is several times the 10 μm requirement and the dermis is roughly 100 times too thick. A review of the skin component thickness found in literature is presented in Table 2.1.

There are few and conflicting published values of optical properties of skin in the infrared beyond 1064 nm (Nd:YAG). Troy et al were unable to produce absorption coefficients from their transmittance and reflectance data between 1900 nm and 2050 nm.[23] The samples were whole skin from surgical procedures. The optical properties of blood have also been measured further out in the infrared.[24-25] Bashkatov et al recently presented an absorption curve for whole human skin showing a coefficient of 1.75 cm^{-1}, and a reduced scattering coefficient of 13.25 cm^{-1} at 2 μm wavelength.[26] Bashkatov performed measurements on postmortem samples of whole skin. Frequently, the optical properties of water or animal tissues are substituted for human skin. One of the popular studies to reference lists no less than six different optical absorption coefficients (ranging from 6 cm^{-1} to 73 cm^{-1}) for different thickness of pig skin as a substitute for human skin.[27] Other authors have used skin attenuation coefficients of 28 cm^{-1} without explanation.[28-29] Table 2.2 lists the optical properties of skin and water found in the literature for a wavelength of 2.0 μm.

As the absorption coefficient values have such a large spread, further inquiries are warranted. This study investigated the use of cultured human epidermal keratinocytes to measure optical transmission and found the technique affords several

advantages. Cultured cells meet the criteria for optically thin samples without the problems of freezing, compression, or amalgamation. The difficulty of separating the stratum corneum, epidermis, and dermis has been avoided. The measurement of accurate optical properties of human tissue is dependent on the sample preparation. Chan *et al* report that compression of an excised sample will increase optical transmission.[30] Optical properties also depend on the temperature of the tissue during measurement.[31] The process of skin excision and preparation for histology also changes the thickness of samples. Tan et al presented skin thickness increase between in vivo and *in vitro* measurement of 28% and 46% for xerographic and ultrasound techniques respectively.[32] Their in vitro measurements matched within 10 μm their histological results. This further complicates the transmission measurement from *ex vivo* samples.

The potential to produce a uniform, optically thin sample is presented by methods of culturing structurally correct epidermis.[33-34] The growth of cultured epithelial cells on collagen more closely resembles the regular, hexagonal, columnar structure typical of epidermis.[35-36] Without air-interface growth, the submerged cultured cells do not produce the membrane-coating granules of *in vivo* epidermis.[37] The keratins produced by epidermal cells grown in culture are similar to those of natural human epidermis.[38] Cells grown on membranes containing type I collagen may grow into tissue resembling epidermis with identifiable layers equivalent to stratum spinosum, stratum granulosum, and stratum corneum.[39] Growing epidermal cells without using a basement membrane on the growth medium still can produce epidermis with basal, spinous, and granular layers.[40] Growth of an optically thin layer of cells should overcome the problems of freezing, contraction, and cold sample temperatures.

2.2 Materials and Methods

2.2.1 Sample Culture Growth

Human epithelial keratinocytes were grown in vitro from Clonetics® NHEK-Ad-Adult Normal Human Epidermal Keratinocytes primary cells in Cascade Biologics Epilife growth medium with EDGS supplement (Invitrogen, Portland OR). The keratinocytes were seeded at 2,000 cells per square cm. The cells reached confluence at seven days growth, with growth medium changed every two days, in a 37 °C humidified incubator at 5% CO_2. The cells were then stratified in layers by interfacing the upper layer of the membrane with air by placing them on membranes. The stratification period was between 6 and 7 days producing an epidermal layer 3 cells thick on one side of the growth medium membrane. Two membrane types were utilized, the Transwell and the Snapwell (Corning Inc., Acton MA). The Transwell membranes are circular with diameters of 10 mm and are 10 μm thick (50 μm thick for collagen coated membranes). The Snapwell membranes are the same membrane material and thickness mounted in specialized holders with 12 mm diameters. Cells were grown both with and without collagen on the membrane. The cultured epithelial keratinocytes were placed in a spectrophotometer to measure total attenuation when they had grown several layers.

The membranes were secured between two zinc titanium glass slide coverslips (Corning Inc, Lowell MA) which were between 0.13 mm and 0.16 mm thick. The glass has a refractive index of 1.523 at the Sodium D line (589 nm). The glass is rated to have 100% transmission above 400 nm. The membranes were mounted on the coverslips

using a phosphate buffered saline solution to avoid air bubbles and provide adhesion. The optical transmission measurements were performed within one hour of mounting on glass. During the first session with live cell samples, the first sample was repeated at middle and the end of the session to evaluate the duration of viability of the samples. Nine batches, six samples each, of cells were grown on the Transwell membrane and measured. Two of these batches were grown with collagen in the growth medium. One batch of samples on Transwell membrane was grown with the membrane fully submerged (no air interface). Two batches of cells were grown on the Snapwell membrane and measured.

2.2.2 Measurements

The transmission of light through the cells was measured on a Cary 500 Scan UV-Vis-NIR spectrophotometer (Varian Analytical Instruments, CA). The transmission was measured over a range of 300 nm to 2,600 nm. Transmission beyond 2,600 nm was too low to provide useful data. The spectrophotometer data was read in one-nm increments at one fifth second per reading. An open beam baseline was performed on the spectrophotometer prior to each measurement session to remove instrument variation from the data. The baseline served to normalize the detector and source combination at each wavelength as the tungsten filament may produce minor spectral emission variations with voltage or current fluctuations. Measurements were taken with the samples oriented both with the beam incident on the cells prior to the membrane and reversed with the beam through the membrane preceding the cells. The spectrophotometer utilizes a split beam in order to remove any variability in light output

from the source. The samples were held in an aluminum mount with a 5 mm diameter beam limiting aperture positioned 10 cm from the detector surface.

The attenuation by the cells was isolated by two methods. In the first, a blank growth membrane mounted in the same manner as the cell membrane was positioned in the reference beam of the spectrophotometer. This physically removed the influence of the coverslip glass, the growth membrane, the saline solution. For samples grown on collagen, a collagen membrane was used and the method repeated. The second method employed was to remove these influences by post-acquisition subtraction of a transmission spectrum through the blank membrane and glass. Transmission measurements were taken of two blank coverslips, coverslips with saline, coverslips with saline and a Tran-swell growth membrane, and coverslips with saline and a collagen coated growth membrane. These curves were then subtracted from the corresponding cultured keratinocyte transmission spectra to isolate the transmission through the cells alone.

In order to establish the validity of the transmission measurements, pure water was also scanned for comparison to published water attenuation data. Laboratory deionized water was purified to biology grade water by reverse osmosis in a Barnstead filtration system (Sybron, Boston MA). A thin layer of water was held between two cover slips by surface tension. The water thickness was 145 ± 15 μm determined by spacers cut from cover slip glass. The transmission data was used to calculate a total attenuation coefficient, μ_t, using Beer's Law as demonstrated by Profio.[41]

2.2.3 Histological examination

Histological cross section samples of the cultured keratinocytes were examined for cell layer thickness and uniformity of growth under an Olympus BX45 optical microscope (Olympus America, Center Valley PA). The cultured keratinocyte sample was prepared with 95% Eosin alcohol based stain, which presents the cytoplasm red. Frozen sections were cut 8 μm thick on a Cryomicrotome (Hacker Instruments, Fairfield NJ). The microscope's digital camera provided images for thickness measurements with ImagePro Discovery morphometric tools (Media Cybernetics, Bethesda MD) at 40 locations across both the keratinocyte layer and also the membrane thickness to establish the degree of thickness variation.

2.3 Results

Transmission measurements of biological grade water at room temperature of 22 °C were obtained from 300 nm to 2600 nm as shown in Figure 2.1. The artifact seen in all figures at 870 nm is a result of the spectrophotometer changing detectors at this wavelength. Also shown is the transmission through the zinc titania glass used in all transmission measurements. The transmittance was used to calculate total attenuation coefficient, μ_t, in units of cm^{-1}, which is shown in Figure 2.2. Several published water attenuation curves extending into the infra-red are also plotted for comparison.[42-45] The data for these curves were taken from the Oregon Medical Laser Center website (http://omlc.ogi.edu/spectra/water/index.html, downloaded July 2008).

The transmission of light through a thin sample held between coverslips in the spectrophotometer has been confirmed with water. As seen in Figure 2.2, the derived

attenuation coefficient from 400 nm to 2500 nm follows closely the results of several other studies. The physical technique of positioning a blank coverslip into the reference beam produced the closest match to the published water attenuation data with a chi-squared value of 2.6 versus 3.4 for the subtraction method using the Hale and Querry [45] spectrum as the reference. In Figure 2.4 the post-acquisition subtraction method can be seen to amplify the noise in the spectrum in the region around 1,200 nm and 2,400 nm.

Histological cross sections of cultured keratinocyte samples grown with collagen are shown in Figure 2.3. Under low magnification, in Figure 2.3a, the keratinocytes are seen to grow into a uniform layer across the Transwell growth membrane. In Figure 2.3b the cells are not individually recognizable without the hematoxilyn to show nuclei, but the cytoplasm is stained red and shows a homogenous monolayer layer of cells. The uniform straight vertical pores in the membrane demonstrate the histological cut is clean and perpendicular to the membrane. The membrane measured an average 11.1 μm thick with a standard deviation of 0.4 μm and the total keratinocyte layer thickness was 4.6 μm with a standard deviation of 0.7 μm.

The two methods of removing the attenuation of the light by the membrane, saline, and coverslip glass are compared in Figure 2.4, which presents the transmission of epidermal cells grown on a collagen membrane using both methods. In the black curve the raw spectrum has been post-processed with a spectrum from a blank growth membrane with saline between two coverslips. The blue curve was the transmission taken with this blank positioned in the spectrophotometer's reference beam. Both were air-interfaced for 6 days. The transmission through cultured keratinocytes grown without collagen is shown in Figure 2.5. Here the blue line is the transmission through

cells grown with an air-interface time of 6 days for comparison to cells grown submerged in growth medium for the entire time (black curve).

Transmission measurements initiated at approximately 22 minutes and 60 minutes after removal from the growth incubator are shown in Figure 2.6. The repeated measurement shows an increased transmission throughout the spectrum, but most dramatic at the strong water absorption regions in the infrared (centered at 1450 nm and 1950 nm).

2.4 Discussion and Conclusions

Attempts to extend the measurement to 3000 nm demonstrated inadequate signal strength. The air interface period during cell growth has been shown to produce a noticeable optical difference in addition to the previously reported histological differences.

The histology images show that cultured keratinocytes can be grown into an optically thin sample with uniform thickness and free of defects. This should be useful for measuring optical properties of human tissue without the sample preparation problems identified by Roggan et al, Chan et al, Tan et al, and Laufer et al. The images do not clearly illustrate individual cells as an alcohol-based hematoxilyn stain was not available commercially which would have identified nuclei. The aqueous-based hematoxilyn stain washed the cells off the membrane in the mounting process and was therefore discontinued. However, the uniform thickness of the keratinocyte layer shows that a uniform sample without holes or large variations in thickness can be produced for use as an optical measurement sample.

The cultured keratinocyte samples have been shown to produce different optical properties when grown with collagen. Comparing Figures 2.4 and 2.5 (blue), the random cell pattern grown without collagen absorbs more light. The columnar structure of the cells grown in a collagen environment appears to transmit approximately 15% more light in the near and far infrared (at 800 nm and 1,900 nm). Towards the other end of the spectrum, the collagen grown cells transmit 60% while the unorganized cells grown without collagen transmit only 20% at 400 nm.

The transmission spectrum through cells grown with an air interface period in Figure 2.4 (blue) is much smoother, particularly in the visible region. The cultured keratinocyte samples demonstrated greater absorption throughout the spectral range measured when it was interfaced with air to stratify. The increased absorption by the air interfaced cells relative to the submerged cells can be attributed to the membrane granules described by Bruls.[46-47]

All the transmission spectra measured have some characteristics in common. They all demonstrate the strong influence of water in the infrared region with similar drops in transmission centered at 1450 nm and 1950 nm. None of the spectra demonstrated the strong but smoothly falling absorption reported for melanin[48] as only keratinocytes were present.

The cultured tissue method also presents some unique challenges. The samples must be measured without delay as the cells will dry out and will not survive long outside the incubator. Even with the measurement beam half the diameter of the growth sample, dehydration was seen in the data taken at one hour post mounting on the slides. Therefore, the thickness of an individual sample to be used in a transmission

measurement cannot be known. In order to obtain a tissue thickness for use in calculating absorption coefficients, several membranes would have to be grown under identical conditions to provide several for histology and several for transmission.

The growth of human keratinocytes in culture has been shown to produce an optically thin sample for transmission measurements. The samples' optical transmission has been measured from 300 nm to 2600 nm. The measurement technique has been shown to provide ample signal within these limits on this particular spectrophotometer. Cultured samples of cells of a particular tissue avoid the variables of expansion and contraction of freezing tissue for sectioning. This approach also eliminates the compression of excised samples and provides an optically thin sample.

2.5 References

1. J. Mnitentag, E. F. Marques, M. P. Ribeiro, G. A. Braga, M. R. Navarro, A. B. Veratti, E. Armelin, R. Macruz, and A. D. Jatene, "Thermographic study of laser on arteries," Lasers in Surgery and Medicine **7** (4), 307-329 (1987).

2. N. S. Kapany, Silbertr.N, and N. A. Peppers, "Laser retinal photocoagulator," Applied Optics **4** (5), 517-518 (1965).

3. L. O. Svaasand, T. Boerslid, and M. Oeveraasen, "Thermal and optical-properties of living tissue - application to laser-induced hyperthermia," Lasers in Surgery and Medicine **5** (6), 589-602 (1985).

4. A. L. McKenzie and J. A. S. Carruth, "Lasers in surgery and medicine," Physics in Medicine and Biology **29** (6), 619-641 (1984).

5. Y. Mendelson, B. C. Lin, R. A. Peura, and A. C. Clermont, "Carbon-dioxide laser based multiple atr technique for measuring glucose in aqueous-solutions," Applied Optics **27** (24), 5077-5081 (1988).

6. J. S. Maier, S. A. Walker, S. Fantini, M. A. Franceschini, and E. Gratton, "Possible correlation between blood-glucose concentration and the reduced scattering coefficient of tissues in the near-infrared," Optics Letters **19** (24), 2062-2064 (1994).

7. J. L. Solan and K. Laden, "Factors affecting penetration of light through stratum-corneum," Journal of the Society of Cosmetic Chemists **28** (3), 125-137 (1977).

8. J. A. S. Carruth, A. L. McKenzie, and A. C. Wainwright, "The carbon-dioxide laser - safety aspects," Journal of Laryngology and Otology **94** (4), 411-417 (1980).

9. J. A. S. Carruth and A. L. McKenzie, "The argon-laser in dermatology - safety aspects," Clinical and Experimental Dermatology **7** (3), 247-253 (1982).

10. P. E. McGuff, F. Roeber, L. S. Gottlieb, D. Bushnell, R. A. Deterling, and H. D. Fahimi, "Laser treatment of experimental malignant tumours," Canadian Medical Association Journal **91** (21), 1089-1089 (1964).

11. T. H. Maiman, "Stimulated optical radiation in ruby," Nature **187** (4736), 493-494 (1960).

12. MH Niemz, *Laser-tissue interactions: Fundamentals and applications.* (Springer Verlag, 2003).

13. V.V. Tuchin, *Tissue optics*, 2nd ed. (SPIE Press, Bellingham WA, 2007).

14. B. Chen, D. C. O'Dell, S. L. Thomsen, B. A. Rockwell, and A. J. Welch, "Threshold damage of in vivo porcine skin at 2000 nm laser irradiation - art. No. 60840c," in *Optical interactions with tissue and cells xvii*, edited by S. L. Jacques and W. P. Roach (2006), Vol. 6084, pp. C840-C840.

15. W. F. Cheong, S. A. Prahl, and A. J. Welch, "A review of the optical-properties of biological tissues," IEEE Journal of Quantum Electronics **26** (12), 2166-2185 (1990).

16. V. Tuchin, "Light scattering study of tissues," Physics-Uspekhi **40** (5), 495-515 (1997).

17. I. V. Meglinski and S. J. Matcher, "Quantitative assessment of skin layers absorption and skin reflectance spectra simulation in the visible and near-infrared spectral regions," Physiological Measurement **23** (4), 741-753 (2002).

18. G. Baronoski and A. Krishnaswamy, "An introduction to light interaction with human skin," Revista de Informatica Teorica e Aplicada **11** (1), 33 - 62 (2004).

19. A. Welch, M. van Gemert, W. Star, and B. Wilson, "Overview of tissue optics," in *Optical-thermal response of laser-irradiated tissue*, edited by A. Welch and M. van Gemert (Plenum Press, New York, NY, 1995).

20. B. Chen, S. L. Thomsen, R. J. Thomas, and A. J. Welch, "Modeling thermal damage in skin from 2000-nm laser irradiation," Journal of Biomedical Optics **11** (6) (2006).

21. B. Wilson, "Measurement of tissue optical properties: Methods and theories," in *Optical thermal response of laser irradiated tissue*, edited by A Welch and M. van Gemert (Plenum Press, New York NY, 1995).

22. A. Roggan, D. Schadel, U. Netz, J. P. Ritz, C. T. Germer, and G. Muller, "The effect of preparation technique on the optical parameters of biological tissue," Applied Physics B-Lasers and Optics **69** (5-6), 445-453 (1999).

23. T.L. Troy and S.N. Thennadil, "Optical properties of human skin in the near infrared wavelength range of 1000 to 2200 nm," Journal of Biomedical Optics **6**, 167 (2001).

24. A. Roggan, M. Friebel, K. Dorschel, A. Hahn, and G. Muller, "Optical properties of circulating human blood in the wavelength range 400-2500 nm," Journal of Biomedical Optics **4** (1), 36-46 (1999).

25. A. N. Yaroslavsky, I. V. Yaroslavsky, T. Goldbach, and H. J. Schwarzmaier, "Influence of the scattering phase function approximation on the optical properties of blood determined from the integrating sphere measurements," Journal of Biomedical Optics **4**, 47 (1999).

26. A. N. Bashkatov, E. A. Genina, V. I. Kochubey, and V. V. Tuchin, "Optical properties of human skin, subcutaneous and mucous tissues in the wavelength range from 400 to 2000 nm," Journal of Physics D Applied Physics **38** (15), 2543-2555 (2005).

27. A. N. Takata, L. Zaneveld, and W. Richter, "Laser-induced thermal damage of skin," Report SAM-TR-77-38,(1977)

28. L. Plaghki and A. Mouraux, "How do we selectively activate skin nociceptors with a high power infrared laser? Physiology and biophysics of laser stimulation," Neurophysiologie Clinique-Clinical Neurophysiology **33** (6), 269-277 (2003).

29. J. Spiegel, C. Hansen, and R.D. Treede, "Clinical evaluation criteria for the assessment of impaired pain sensitivity by thulium-laser evoked potentials," Clinical Neurophysiology **111** (4), 725-735 (2000).

30. E. K. Chan, B. Sorg, D. Protsenko, M. Oneil, M. Motamedi, and A. J. Welch, "Effects of compression on soft tissue optical properties," Ieee Journal of Selected Topics in Quantum Electronics **2** (4), 943-950 (1996).

31. J. Laufer, R. Simpson, M. Kohl, M. Essenpreis, and M. Cope, "Effect of temperature on the optical properties of ex vivo human dermis and subdermis," Physics in Medicine and Biology **43** (9), 2479-2489 (1998).

32. C. Y. Tan, B. Statham, R. Marks, and P.A. Payne, "Skin thickness measurement by pulsed ultrasound: Its reproducibility, validation and variability," British Journal of Dermatology **106** (6), 657-667 (1982).

33. M. Prunieras, M. Regnier, and D. Woodley, "Methods for cultivation of keratinocytes with an air-liquid interface," Journal of Investigative Dermatology **81** (1), S28-S33 (1983).

34. J. H. Lillie, D. K. Maccallum, and A. Jepsen, "Fine-structure of subcultivated stratified squamous epithelium grown on collagen rafts," Experimental Cell Research **125** (1), 153-165 (1980).

35. I. C. Mackenzi and J. E. Linder, "Examination of cellular organization within stratum corneum by a silver staining method," Journal of Investigative Dermatology **61** (4), 245-250 (1973).

36. I. C. Mackenzie and N. E. Fusenig, "Regeneration of organized epithelial structure," Journal of Investigative Dermatology **81** (1), S189-S194 (1983).

37. W. A. G. Bruls, H. Slaper, Leun Van Der, J. C., and L. Berrens, *Transmission of human epidermis and stratum corneum as a function of thickness in the ultraviolet and visible wavelengths.* (Blackwell Publishing, Malden, MA, 1984).

38. T. T. Sun and H. Green, "Keratin filaments of cultured human epidermal-cells - formation of inter-molecular disulfide bonds during terminal differentiation," Journal of Biological Chemistry **253** (6), 2053-2060 (1978).

39. I. A. Schafer, M. Kovach, R. L. Price, and R. B. Fratianne, "Human keratinocytes cultured on collagen gels form an epidermis which synthesizes bullous pemphigoid antigens and alpha-2-beta-1 integrins and secretes laminin, type-iv collagen, and heparan-sulfate proteoglycan at the basal-cell surface," Experimental Cell Research **195** (2), 443-457 (1991).

40. M. Guo and F. Grinnell, "Basement-membrane and human epidermal differentiation invitro," Journal of Investigative Dermatology **93** (3), 372-378 (1989).

41. A. E. Profio, "Light transport in tissue," Applied Optics **28** (12), 2216-2221 (1989).

42. K. F. Palmer and D. Williams, "Optical-properties of water in near-infrared," Journal of the Optical Society of America **64** (8), 1107-1110 (1974).

43. D. M. Wieliczka, S. Weng, and M.R. Querry, "Wedge shaped cell for highly absorbent liquids: Infrared optical constants of water," Applied Optics **28**, 1714-1719 (1989).

44. L. H. Kou, D. Labrie, and P. Chylek, "Refractive-indexes of water and ice in the 0.65-μm to 2.5-μm spectral range," Applied Optics **32** (19), 3531-3540 (1993).

45. G. M. Hale and M. R. Querry, "Optical-constants of water in 200-nm to 200-mum wavelength region," Applied Optics **12** (3), 555-563 (1973).

46. Bruls, G. W. A, Slaper, H, Leun Van Der, C. J, Berrens, and L, *Transmission of human epidermis and stratum corneum as a function of thickness in the ultraviolet and visible wavelengths.* (Blackwell Publishing, Malden, MA, ETATS-UNIS, 1984).

47. W. A. Bruls and J. C. van der Leun, "Forward scattering properties of human epidermal layers," Photochem Photobiol **40** (2), 231-242 (1984).

48. A. Vogel and V. Venugopalan, "Mechanisms of pulsed laser ablation of biological tissues," Chemical Reviews **103** (2), 577-644 (2003).

49. K. A. Holbrook and G. F. Odland, "Regional differences in the thickness of the human stratum corneum," Journal of Investigative Dermatology **62**, 415-422 (1974).

50. C. Blair, "Morphology and thickness of human stratum corneum," British Journal of Dermatology **80** (7), 430-& (1968).

51. J. P. Hulsbergen Henning, E. G. J. Beerens, and J. C. Leun, "A non-invasive microscopic method for measuring epidermal thickness in vivo," Archives of Dermatological Research **258** (1), 25-32 (1977).

52. J. Sandby-Moller, T. Poulsen, and H.C. Wulf, "Epidermal thickness at different body sites: Relationship to age, gender, pigmentation, blood content, skin type and smoking habits," Acta dermato-venereologica **83** (6), 410-413 (2003).

53. W. F. W Southwood, "The thickness of the skin," Plastic and Reconstructive Surgery **15** (5), 423 (1955).

54. J. T. Whitton and J. D. Everall, "The thickness of the epidermis," The British Journal of Dermatology **89** (5), 467 (1973).

55. J.A. Moncrief, "The body's response to heat," in *Burns, a team approach*, edited by C. Artz, J.A. Moncrief, and B. Pruitt (Saunders, Philadelphia PA, 1979).

56. J. Welzel, E. Lankenau, R. Birngruber, and R. Engelhardt, "Optical coherence tomography of the human skin," Journal of the American Academy of Dermatology **37** (6), 958-963 (1997).

57. T. A. Eggleston, W. P. Roach, M. A. Mitchell, K. Smith, D. Oler, and T. E. Johnson, "Comparison of two porcine (sus scrofa domestica) skin models for in vivo near-infrared laser exposure," Comparative Medicine **50** (4), 391-397 (2000).

58. Y. Lee and K. Hwang, "Skin thickness of korean adults," Surgical and Radiologic Anatomy **24** (3-4), 183-189 (2002).

59. L. Overgaard Olsen, H. Takiwaki, and J. Serup, "High-frequency ultrasound characterization of normal skin. Skin thickness and echographic density of 22 anatomical sites," Skin Research and Technology **1** (2), 74-80 (1995).

60. R. L. Anderson and J. M. Cassidy, "Variations in physical dimensions and chemical composition of human stratum corneum," Journal of Investigative Dermatology **61** (1), 30-32 (1973).

61. F. Pirot, Y. Kalia, A Stinchcomb, G. Keating, A Bunge, and R Guy, "Characterization of the permeability barrier of human skin in vivo," Proceedings of the National Academy of Sciences of the United States of America **94**, 1562-1567 (1997).

62. E. Salomatina, B. Jiang, J. Novak, and A. N. Yaroslavsky, "Optical properties of normal and cancerous human skin in the visible and near-infrared spectral range," Journal of Biomedical Optics **11**, 064026 (2006).

63. A. R. Young, "Chromophores in human skin," Physics in Medicine and Biology **42**, 789-802 (1997).

64. J. D. Hardy, H. T. Hammel, and D. Murgatroyd, "Spectral transmittance and reflectance of excised human skin," Journal of Applied Physiology **9** (2), 257-264 (1956).

65. G. J. Tearney, M. E. Brezinski, J. F. Southern, B. E. Bouma, M. R. Hee, and J. G. Fujimoto, "Determination of the refractive index of highly scattering human tissue by optical coherence tomography," Optics Letters **20** (21), 2258 (1995).

66. A. Knuttel and M. Boehlau-Godau, "Spatially confined and temporally resolved refractive index and scattering evaluation in human skin performed with optical coherence tomography," Journal of Biomedical Optics **5** (1), 83-92 (2000).

67. R. R. Anderson and J. A. Parrish, "The optics of human-skin," Journal of Investigative Dermatology **77** (1), 13-19 (1981).

Table 2.1. Reported skin thickness in micrometers.

Anatomic Location	Stratum Corneum	Epidermis	Dermis	Whole Skin	Date	Study
Forearm	12.9				1974	[49]
Forearm	16.9				1968	[50]
Forearm	17.9	60			1977	[51]
Forearm	18.3	56.6			2003*	[52]
Forearm		52	994		1955	[53]
Forearm		60.9			1973	[54]
Forearm		48	995		1979	[55]
Forearm		113			1997	[56]
Forearm		68			2000	[57]
Forearm		74	1123		2002 **	[58]
Forearm				1120M/1310F	1995***	[59]
Chest		44	1400		1955	[53]
Chest		39	1319		1979	[55]
Chest (front upper trunk)		37.6			1973	[54]
Chest		98	1337		2002 **	[58]
Chest (pectoral)				1770M/1920F	1995***	[59]
Leg (posterior)		58	1183		1955	[53]
Leg (posterior)		74.9			1973	[54]
Leg (posterior)		63	1264		1979	[55]
Leg (posterior)		129	981		2002 **	[58]
Leg (posterior)				1300M/1340F	1995***	[59]
Abdomen	8.2				1974	[49]
Hip	11.8				1973	[60]
Buttock	14.9	81.5			2003*	[52]
Interscapular	14.7				1968	[50]
Shoulder	11	70.3			2003*	[52]
Neck		65			2000	[57]
Face		68			2000	[57]
Back	26	69			1984	[37]
Body Average	10-20				1997	[61]
Body Average		80			2002	[17]
Body Average		60 to 100	100 - 780		2006	[62]
Body Average	10	100 to 150	2000 - 4000		1997	[63]
Body Average	16	29.5	220.5		2001	[23]

* Study of Nordic Adults; ** Study of Korean Adults; *** Results for Male/Female Subjects

Table 2.2. Published index of refraction *n*, absorption μ_a, reduced scatter μ_s', and attenuation μ_t coefficients for 2 micron IR light.

Material	*n*	μ_a [cm^{-1}]	μ_s' [cm^{-1}]	Date	Study
Skin (in vitro)	--	1.75	13.25	2005	[26]
Skin	1.36	48*	10*	2001	[23]
Skin		28		2003	[28]
Skin		28		2000	[29]
Skin (0.157 mm)		26		1977	[27]
Skin (0.053 mm)		73		1977	[27]
Skin (highly pigmented)		32.6		1956	[64]
Skin (sparse pigment)		26.9		1956	[64]
Stratum Corneum	1.51			1995	[65]
Epidermis	1.34			1995	[65]
Epidermis	1.36			2000	[66]
Dermis	1.41			1995	[65]
Dermis	1.43			2000	[66]
Dermis		82	10	1981	[67]
Epidermis (porcine)		21.76		2006	[20]
Dermis (porcine)		58.02**		2006	[20]

* calculated from 70% water model, not measured; ** calculated using 80% water content; ***2.20 μm light

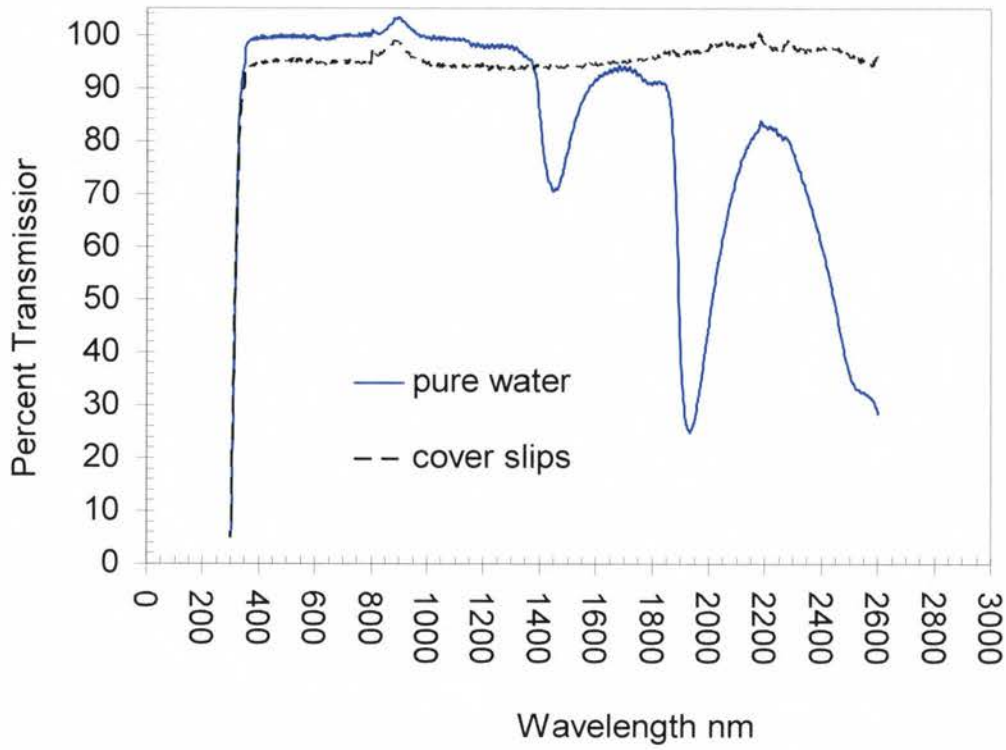

Figure 2.1 Measured optical transmission through pure water and blank cover slips.

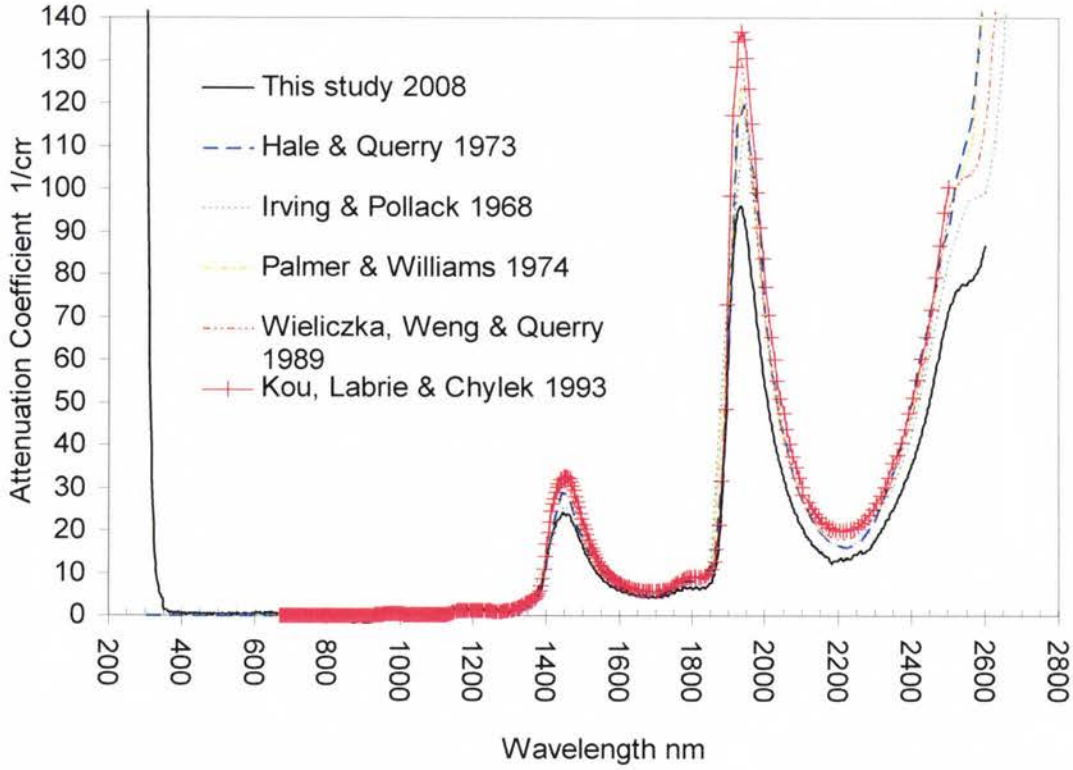

Figure 2.2 Optical attenuation coefficient of water.

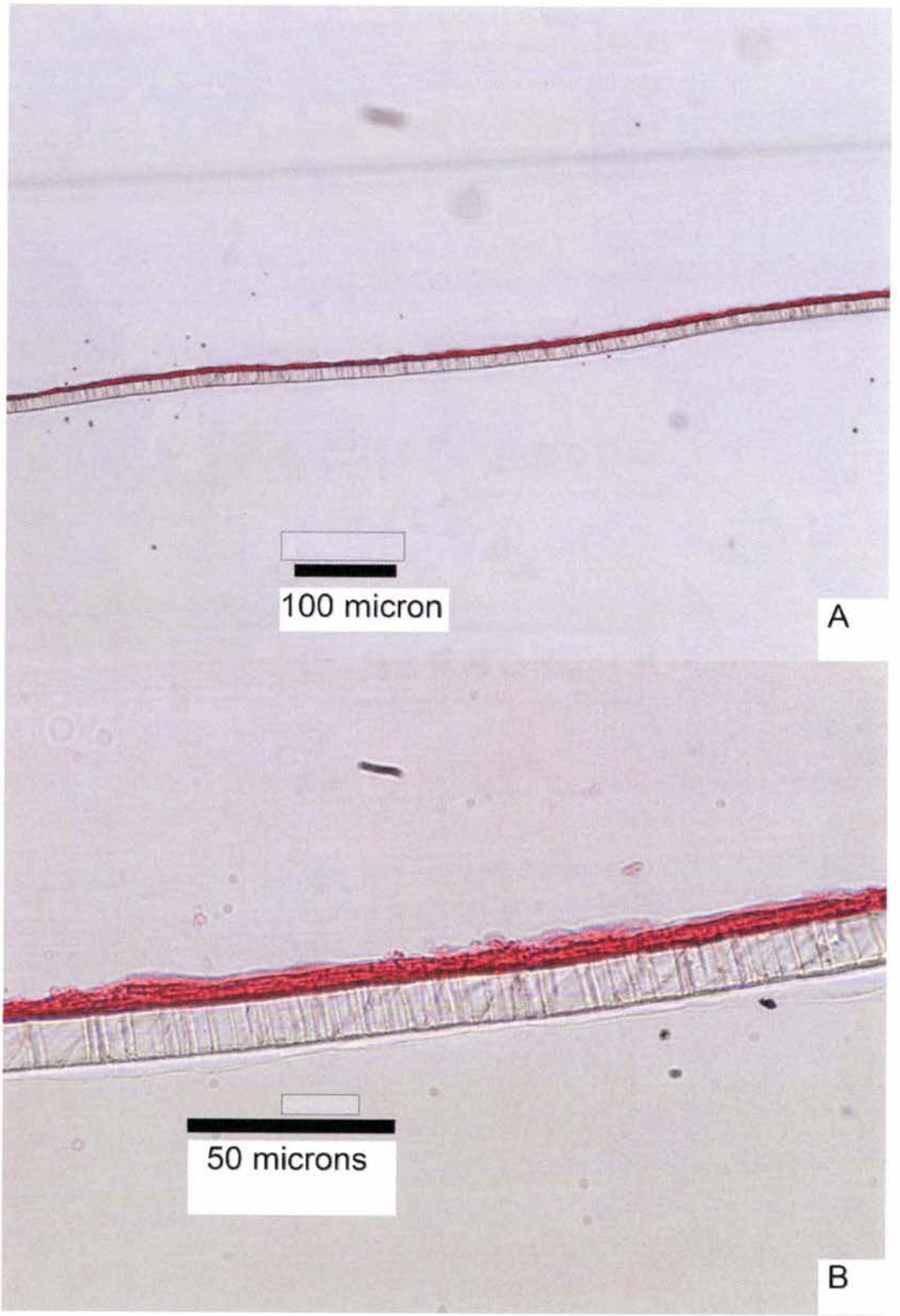

Figure 2.3 Histological cross section image of epidermis grown from stem cells A) at 10X magnification and B) at 40X magnification.

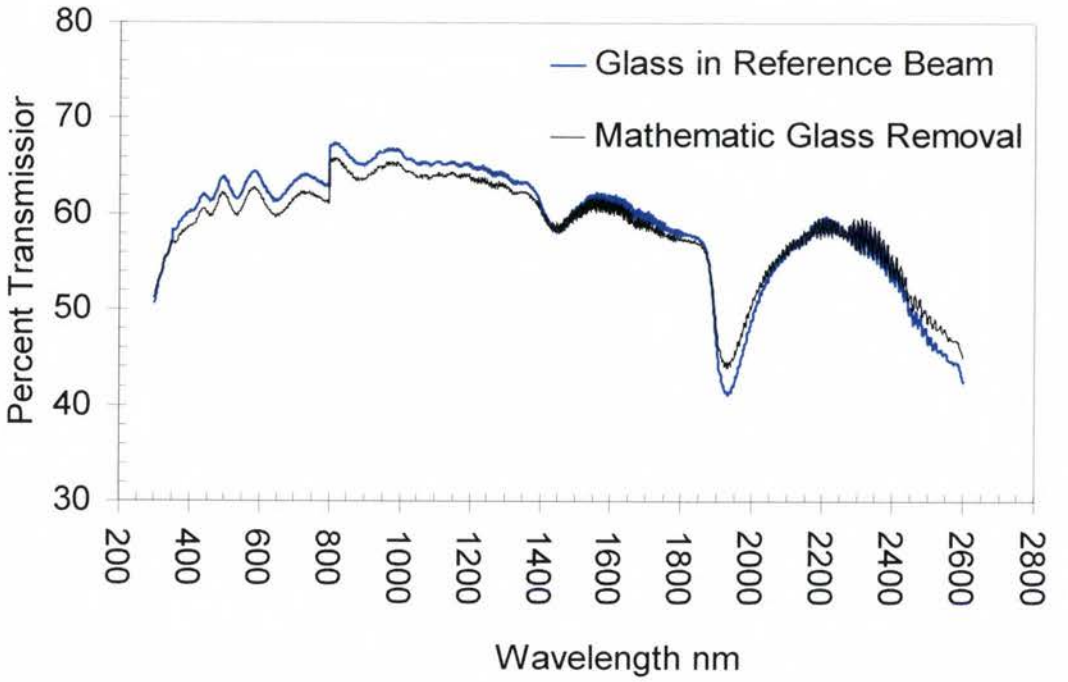

Figure 2.4 Transmission curves for keratinocytes grown with collagen; glass and membrane removed by post-processing (black) and by physical method (blue).

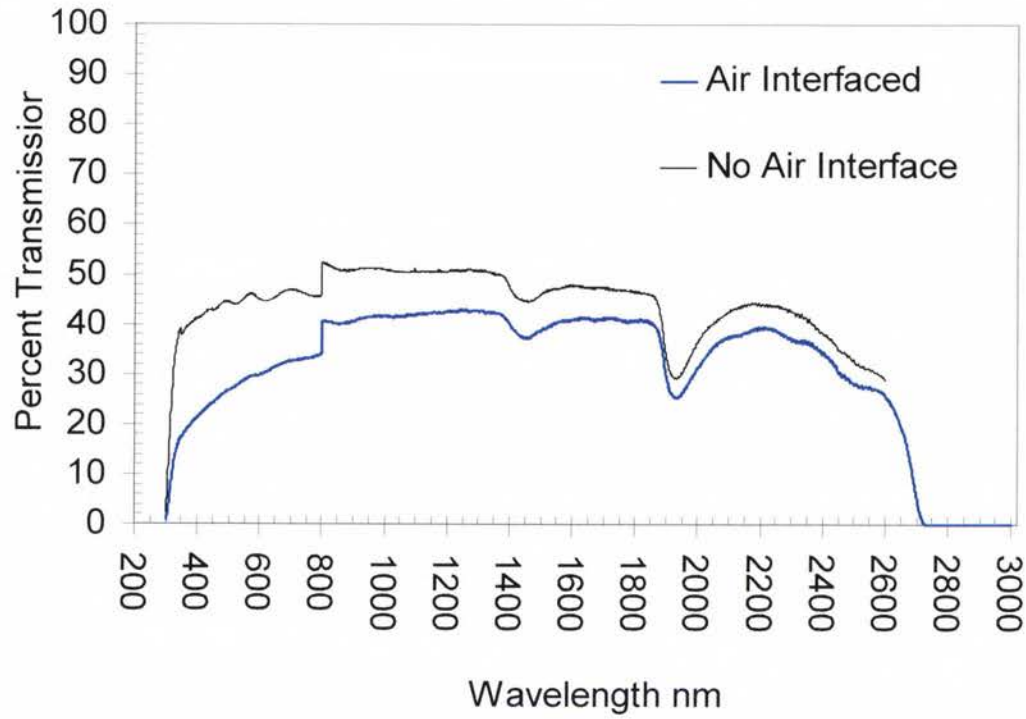

Figure 2.5 Transmission through keratinocytes grown without collagen, glass and membrane attenuation present; air interfaced (blue) and submerged entire time (black).

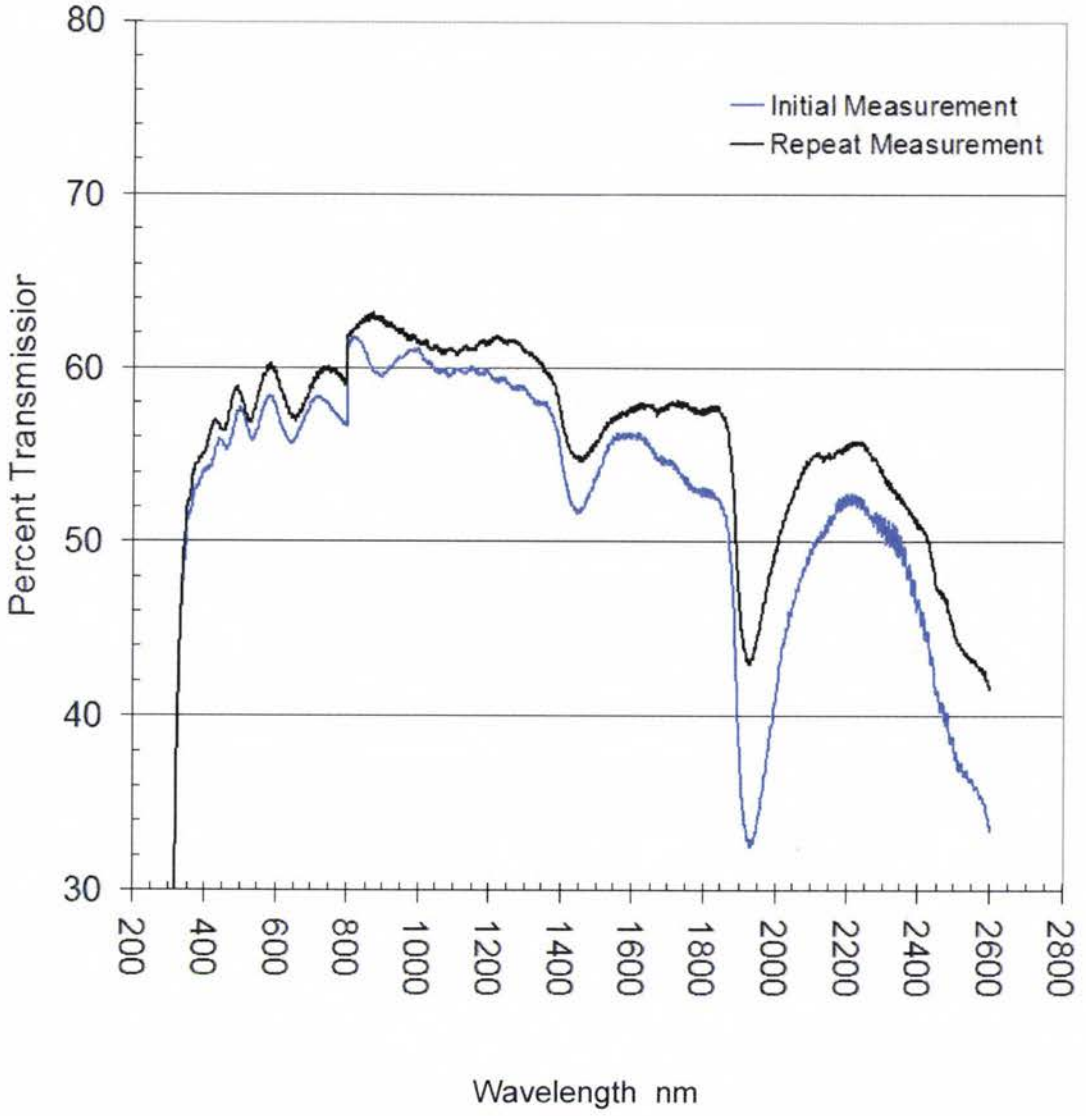

Figure 2.6 Transmission through same sample of keratinocytes at beginning of measurement session (blue) and at the conclusion (black).

Chapter 3

Temperature Instrument Comparison For Measurement of Laser Irradiation

3.0 Abstract

Non-contact temperature measurement and imaging instruments are widely used in studies of laser interaction with tissue. For reliable results, independent verification of the instrument's abilities and limitations is necessary. Two common types of heat measuring instruments are the $LiTaO_3$ type II pyrometer and the microbolometer array thermal imager. This study found that when considering the Signal to Noise Ratio, the temporal resolution, and the spatial dependency of the temperature measured by the instrument, the microbolometer was superior for measurements of incident beams of five mm diameter and all pulse frequencies investigated.

3.1 Introduction

Laser irradiation of human and animal tissue is frequently recorded to measure heat, irradiation area, and cooling. Measuring skin temperature has been an area of interest for a decades.[1-2] Measuring other types of live tissue temperatures has also been studied for several decades.[3] There are three main types of instruments used for measuring temperature rise during and following IR laser irradiation. The first is a thermal imaging camera using bolometers.[4-8] Secondly, a pyrometer may be used to measure temperature in many situations.[9-11] A third group is the newer Indium

Antimonide (InSb) detector cameras that have become popular in laser studies.[12-13] An array of micro-bolometers produces a resistance change in each pixel proportional to the incident IR flux. The pyrometer detector is a crystal which produces an electric field proportional to the IR radiation.[14-15] The InSb detector elements operate as a photovoltaic cell producing a linear voltage response to incident IR flux.[16-18] Another novel heat imaging technique is optical frequency domain imaging utilizing frequency domain information from an optical coherence tomography system, which one study found to have a depth resolution of 8 μm and a temporal resolution of 0.1 msec.[19] These non-contact temperature measurement instruments have been inconsistently investigated for performance characteristics suitable to specific tasks. Every instrument has its strengths and weaknesses. Some of the most comprehensive reports of instrument capabilities have been in cases of modified instruments such as the InSb camera described by Riccio et al.[20]

The wide variety of performance characteristics, and measurement techniques of non-contact temperature instruments have been the basis for several investigations for over twenty years. The American Academy of Thermology published technical guidelines introducing infrared thermography in 1986.[21] More recent descriptions of thermal instruments have included specific measurement parameters of the instruments such as spectral range, spatial resolution, temperature sensitivity, and temporal resolution. Many other authors simply report the manufacturer's instrument specification.[8,22-23] On occasion a parameter is given as an estimate such as "image spatial resolution was approximately 40 μm per pixel" without explanation.[24] However, a few have independently investigated the characteristics of their instruments. An early

study utilizing thermal imaging utilized a pair of IR LEDs spaced at 10 cm within each image of a subject for spatial calibration.[25] Holmes et al calculated the pixel size of their IR camera at their distance of interest for comparison to the manufacturer's specification.[26] Sherman and Woerman compared three types of skin temperature measurement instruments in terms of features and relative temperature changes using a blackbody.[27] In one of the most comprehensive evaluations, Torres et al examined three imaging cameras which utilized a "flying spot" detector for response to a thermal step change, accuracy for small thermal targets, and spatial resolution in terms of the Point Spread Function (PSF).[28]

This work compares a micro-bolometer array thermal camera and a pyrometer under conditions appropriate to the *in vivo* measurement of human skin temperature during laser irradiation. This work uses the tests on a scanned HgCdTe (Mercury Cadmium Telluride) detector camera by Torres, then modifies and expands those tests for the focal plane array of detectors a micro-bolometer camera. In our tests of the pyrometer and micro-bolometer array camera, the thermal camera was found to provide superior results in all tests of Signal to Noise Ratio, temporal resolution, and spatial influence on readings for small targets. The pyrometer nominally has much higher temporal resolution, but its high noise masked any useful data of msec laser pulses producing temperature changes on the order of 10 degrees.

3.2 Materials and Methods

3.2.1 Instruments

Two infrared temperature instruments were investigated for performance in areas relevant to measuring human skin temperature during laser irradiation. The first was a model KT15.82 IIP pyrometer (Heitronics , Wiesbaden Germany). The second instrument was a ThermaCam S65 microbolometer array (FLIR Systems, Boston).

The pyrometer was originally configured with a germanium lens (f = 60 mm). As germanium is not transparent in the visible regime the lens had a window for a red diode aiming laser. The unit was calibrated with NIST traceable black bodies by the distributor (Wintronics, NJ) following ANSI Z540-1-1994 procedures.[29] The pyroelectric detector had a $LiTaO_3$ type II material sensitive in the infrared from 8 to 14 μm. This lens and detector combination produced a 4.4 mm diameter measurement spot at 151 mm from the lens, as seen in curve number 4 from the manufacturer's diagrams in Figure 3.1.

The pyrometer was upgraded to the larger detector A to reduce the specified minimum resolvable temperature difference from 7.9 °C to 2.15 °C. In order to maintain a similar measurement spot, the lens was changed to a ZnSe f=50 mm lens which is transparent in the visible. From the manufacturer's specifications, this configuration produced a nominal measurement focal spot of 4.4 mm diameter at 85 mm from the lens. The new lens glass did not need a window for the red aiming laser, which was required in the original configuration, that blocked some of the IR signal. The pyrometer was controlled by the manufacturer's software EasyMeasure version 3.0.2 (Heitronics, Weisbaden Germany). In both configurations the pyrometer used the chopped radiation method for stability. In this method, an optical chopper blade was used as a reference

level of radiation with defined temperature to cancel electronic drift. The KT15.82 model's chopper wheel was rated for a reading cycle of 400 Hz producing data intervals of 5 msec. The Heitronics pyroelectric detectors allow a minimum setting of 5 msec time to reach 90% of full response. The 5 msec read and response time of the pyrometer was the primary capability of interest to our laser studies.

The model S65HSV thermal imaging camera (FLIR Systems, Wiesbaden Germany) was composed of a 320 × 240 array of uncooled microbolometer detectors. The sensitivity is quoted at 0.05 °C with an accuracy specification of + 2 °C. Image sequences were collected and sent to a PC at a rate of 60 Hz, giving a temporal resolution of 17 msec. The images were read and analyzed using Researcher Pro version 2.8 (FLIR Systems, Wiesbaden Germany) which offers region of interest and line profile extraction. The camera is sensitive in the spectral range of 7.5 to 13 μm. The lens has a minimum focusing distance of 0.3 m, with a quoted spatial resolution of 1.1 mrad of divergence. The camera was calibrated by the manufacturer using NIST traceable blackbody sources.

3.2.2 Tests to Compare Instruments

The performance investigation was undertaken in three parts. The first parameter to be measured was the Signal to Noise Ratio (SNR) achieved by the instruments for temperature ranges expected on human skin. For this investigation, the instruments were mounted above the surface of a thin piece of blackened Teflon plastic. The pyrometer in original configuration (Detector B) was held at its focal distance, 15 cm, from the plastic. The upgraded pyrometer was at its focal point of 8.5 cm, normal to the

plastic. The thermal camera was mounted on a tripod at 150 cm above the surface. The black teflon was measured at constant temperatures of both 30 °C and 35 °C maintained in a large, insulated water bath; the plastic measured by the pyrometer in original configuration was at 22 °C and 27 °C. The emissivity of both instruments was set to 0.98 to match skin emission rate, though the Teflon approaches blackbody conditions of 1.00 emissivity.[30-33] While the thermal camera was only used at its maximum frame rate of 60 Hz, the pyrometer was tested with five combinations of response time settings and data intervals, as listed in Table 3.1, for both temperatures.

The second objective was to determine the limitations in the temporal domain of both systems. The instruments were positioned as above, except in this experiment the camera was approximately 10° off of normal to the surface in order to read the same laser pulse as the pyrometer. In these tests a 2 μm laser was pulsed at increasing frequencies onto the plastic. The 2.0 μm model TLR-50 Tm:YAG fiber laser (IPG Photonics, Oxford MA) was chosen to heat the plastic as neither instrument is sensitive to this wavelength. Both instruments were set to measure the same laser pulse sequence for comparison. The pulse sequences were repeated twelve times to investigate the effects of different response and read time settings on the pyrometer.

The laser pulse sequences were created by two 15 MHz digital waveform generators (model 33120A; serial numbers US34015616 and US36020133; Hewlett Packard, Englewood, CO) in series to control the duration and number of laser pulses respectively. A single 2 ms laser pulse was created by setting the first waveform generator to deliver a single 250 Hz square wave pulse, thereby generating a 2 ms TTL signal that served as a trigger for the laser control. The ten-pulse sequences were

repetitions of the 2 msec single pulses as triggered by the second waveform generator which is set to the frequency desired (see Figure 3.2 for illustration of the multi-pulse sequence timing). The 50 W laser was set to 35% power to produce an approximately one degree temperature rise per pulse.

The 2-μm laser pulses were aligned to be colinear with a commercial HeNe laser (model 05-LLR-811, Melles-Griot, Carlsbad, CA). The HeNe beam is essential to the laser operator for aiming the beam. The IR beam had a Gaussian shape and was 4.5 mm in diameter at the $1/e^2$ level using a knife-edge technique. The IR laser beam was directed onto the plastic at 30° from normal in order to allow the pyrometer to be directly vertical to the surface. The Teflon was maintained at 33 °C on the surface of a water bath to approximate human skin baseline temperature.

While the thermal camera was only used at its maximum frame rate of 60 Hz, the pyrometer was interrogated at several combinations of response time settings and data point recording frequencies as listed in Table 3.2. The temporal resolution was examined by plotting the measured values on a time scale with the laser pulses and recording the signal to noise ratio (SNR) if the laser energy was detected.

The third area investigated was the spatial influence on temperature accuracy of the instruments. The test consisted of taking readings of uniform temperature targets with a range of sizes. An imaging test pattern was employed composed of consecutively smaller circles in a matte black sheet of 1.6 mm thick aluminum (Irwin model HG03305, Huntersville NC). The test object was attached to one inch diameter aluminum rods which held the object in position and also acted as a heat sink to maintain the test object at 21 °C. The contrast was provided by a piece of black plastic located 3.5 cm behind

the test object which was maintained at 28 °C in a water bath. The temperature difference of 7 °C was chosen to simulate temperature differences of interest in skin heating studies. The microbolometer camera spatial resolution test was repeated at four distances from 1.5 m to 0.3 m. The Researcher Pro software was used to find the maximum temperature within each target, effectively giving a contrast – detail response curve.[34-38] The pixel size at the four distances was calculated from the known dimensions of the test object and used to determine the divergence angle for comparison to the specified angle.

The pyrometer spatial resolution was investigated by measuring the test object's consecutively smaller circles and determining target diameter at which temperature accuracy begins to depend on target size. This method was performed at the focal distance of 8.5 cm and repeated at 7.5 cm and 9.5 cm to determine any effects of detector positioning. The pyrometer was set to read at 10-msec intervals with a response time of 10 msec. Each target was measured for 10 seconds producing one thousand data points for averaging and evaluation of variation.

3.2.3 Tests to Further Characterize Micro-Bolometer Focal Plane Array

Additional testing of the micro-bolometer focal plane array detector was undertaken because it would be the only non-contact temperature instrument used in future studies. One of the fundamental requirements for a measurement instrument is to be reproducible. The micro-bolometer focal plane array reproducibility was evaluated by taking ten successive measurements of single laser pulses ranging from 100 msec down to 2 msec. The laser irradiated the black Teflon which was held at a constant

background temperature in a water bath. The reproducibility was quantified as the Coefficient of Variation calculated as the standard deviation of the ten measurements divided by the average of the ten. Similarly the detector's stability at background was quantified by ten measurements of the black Teflon at three background temperatures covering the expected tissue sample temperatures.

As an imaging system of lenses, the Flir ThermaCam was investigated to determine if there were focusing effects. The Camera was set at four distances from the uniform temperature Teflon to cover the range of focal distances of interest. At each distance a 2 second (120 data points) measurement was taken of the uniform temperature Teflon with careful focusing and separate measurements were taken with the lens out of focus by two steps close and then two steps in the far direction. The average reading of the 120 frames for each of the three focal conditions at all four distances using a region of interest of 100 pixels was calculated.

The spatial resolution of the camera system as a whole is best represented by the Modulation Transfer Function (MTF).[16,39-40] The MTF was calculated from data generated by an edge step function similar to that of Torres except that instead of the detector sweeping across the edge, the data comes from separate individual detectors of the array. The step function is formed from a machined straight 2-mm thick aluminum piece held 2 cm above a constant temperature black Teflon warmed in a water bath to a temperature difference of 10 °C. The camera is positioned directly above the target with the aluminum edge centered in either the vertical or horizontal direction as appropriate. The Edge Response Data is transformed into a Line Spread Function (LSF) by averaging 35 rows of pixels in the direction of the edge, and then taking the derivative in the

direction across the edge.[41-44] The MTF is then calculated from the LSF with a discrete Fourier Transform.[45-52] The MTF was measured vertically and horizontally at distances of 30 cm, 60 cm, 100 cm, and 150 cm.

3.3 Results

The SNR of black plastic at a temperature difference of 5 °C for the pyrometer operated with different settings is presented in Table 3.3. The difference between SNR of the three instruments is graphically presented in Figure 3.3.

The temporal resolution of the instruments is shown in Figure 3.4 which graphs the temperature response of the two instrument during the laser pulse sequence. All laser pulses are 2 msec square waves of equal irradiance. Note that the bolometer array resolves only the 30 Hz pulses; all pulses more frequent than 30 msec are beyond its Nyquist frequency in the time domain. The bolometer array also gives a baseline temperature of 22.4 °C versus the pyrometers average baseline of 20.7 °C. However, the pyrometer's baseline of any one reading contains far more noise with an average standard deviation of 0.8 versus the average standard deviation of a bolometer baseline reading of 0.04.

The spatial resolution for the range of target diameters is shown in Figure 3.5 for the upgraded pyrometer and the bolometer. The off-focus pyrometer measurements were lower than those at the focal distance when the target is larger than the minimum spot size. The targets were all maintained at a constant temperature. A thermal image of the spatial resolution test object is shown in Figure 3.6. The measured camera pixel

sizes at four distances are shown in Figure 3.7 along with the manufacturer's specifications for comparison.

Several further tests were conducted to explore the micro-bolometer focal plane array. The detector's reproducibility for short laser pulses is shown in Figure 3.8. The micro-bolometer's stability at background temperatures was measured to be even lower, at 25 °C the CoV was 0.1%, at 30 °C and 35 °C the CoV was 0.07%.

The impact of lens focal adjustment on temperature measurement by the thermal camera was investigated and is presented in Figure 3.9. The difference between the out-of-focus measurements from the focused measurements was maximum at a distance of 60 cm, with a disparity of 1.3°C.

The spatial resolution of the focal plane array camera system was calculated as the MTF which represents the fidelity of the imaging system to reproduce an image with increasing spatial information in the frequency domain. The MTF of the micro-bolometer focal plane array system is presented in Figure 3.10.

3.4 Discussion and Conclusions

The SNR found for the original pyrometer was so low that the instrument was unable to distinguish temperature changes of 5°C with its fastest two settings of 5 and 10 msec data intervals. The upgraded pyrometer was able to identify changes of 5°C but the results were unreliable as the noise induced a wide range of responses. The micro-bolometer array demonstrated very little noise and consistently identified the 5 °C temperature changes in this comparison. The thermal camera SNR was not found to be adequate for small temperature increases of 10 msec duration.

The temporal resolution was evaluated subjectively from the response graphs. The pyrometer demonstrated no temporal resolution advantage over the microbolometer as the individual laser pulses were often lost in the noise. The pyrometer in either configuration was unable to reduce noise sufficiently at short data collection intervals of 5 msec or 10 msec to offer an advantage over the microbolometer. At response settings long enough to suppress the noise (100 msec), the short laser pulses were entirely missed.

Among the most relevant attributes of thermal imaging systems listed by Gore and Xu are the spatial resolution, spectral range, temperature sensitivity, and temporal data collection rate.[22] The spatial resolution usually reported is the divergence angle of the optics rather than an absolute, distance-specific, spatial descriptor such as minimum resolved object size. The pyrometer displayed a loss of accuracy in a linear manner when the object was smaller that its 4.4 mm focal spot. The pyrometer gave readings roughly a half and a full degree less when the pyrometer was measuring large objects relative to its focal spot at a centimeter closer or further away from its focal distance of 8.5 cm.

The microbolometer accuracy began to drop as the target diameter fell below 5 mm. The fall in temperature readings was not linear. The thermal camera pixel size was found to vary close to manufacturer's specification out to a distance of 1.5 m. The image divergence angle was found to match the quoted 1.3 mrad over the same distance.

The micro-bolometer array is marketed as a general purpose thermal camera with a wide range of applications. The pyrometer is marketed as a configurable instrument to match the user's specific application. In spite of this, for the narrow range of distances,

target sizes, and heating/cooling cycles investigated, the bolometer was found to be more precise in all categories. The pyrometer with either detector size produced excess noise and was not useful for fast temperature changes. Both instruments lost accuracy when the target size diminished below 5 mm. When measuring temperatures of laser beams, therefore, the user should be aware of the spatial dependency of the individual instrument. Simple specifications such as spot size, pixel size or image divergence specified by the manufacturer will not reveal the accuracy dependence on target size. Overall, the microbolometer was found to be the superior instrument for measuring laser pulses with repetition rates between 30 Hz and 180 Hz, and with spot sizes larger than 5 mm. The pyrometer would only be useful for an immobile target larger than 5 mm diameter, with the pyrometer normal to the target surface, when the temperature changes are larger than 10 °C.

3.5 References

1. M. Lipkin and J. D. Hardy,"Measurement of some thermal properties of human tissues," Journal of Applied Physiology **7** (2), 212-217 (1954).

2. E. Hendler, R. Crosbie, and J. D. Hardy,"Measurement of the skin during exposure to infrared radiation," J. Appl. Physiol **12**, 177-185 (1958).

3. J. A. Pearce, A. J. Welch, M. Motamedi et al., in *Heat and mass transfer in the microcirculation of thermally significant vessels*, edited by K. Diller and R. B Roemen (ASME, Anaheim CA, 1986), pp. 49-54.

4. C. Cain, T. Milner, S. Telenkov et al., in *Laser interaction with tissue and cells xv*, edited by S. L. Jacques and W. P. Roach (2004), Vol. 5319, pp. 313-324.

5. N. M. Fried, B. Choi, A. J. Welch et al.,"Radiometric surface temperature measurements during dye-assisted laser skin closure: In vitro and in vivo results," Lasers in Surgery and Medicine **25** (4), 291-303 (1999).

6. B. J. F. Wong, J. Neev, and M. J. C. vanGemert,"Surface temperature distributions in carbon dioxide, argon, and ktp (Nd:YAG) laser ablated otic capsule and calvarial bone," American Journal of Otology **18** (6), 766-772 (1997).

7. B. Choi, J. K. Barton, E. K. Chan et al.,"Imaging of the irradiation of skin with a clinical CO_2 laser system: Implications for laser skin resurfacing," Lasers in Surgery and Medicine **23** (4), 185-193 (1998).

8. G Litscher,"Infrared thermography fails to visualize stimulation-induced meridian-like structures," BioMedical Engineering OnLine **4** (1), 38 (2005).

9. G. D. Iannetti, M. Leandri, A. Truini et al.,"A delta nociceptor response to laser stimuli: Selective effect of stimulus duration on skin temperature, brain potentials and pain perception," Clinical Neurophysiology **115** (11), 2629-2637 (2004).

10. M. Leandri, M. Saturno, L. Spadavecchia et al.,"Measurement of skin temperature after infrared laser stimulation," Neurophysiologie Clinique-Clinical Neurophysiology **36** (4), 207-218 (2006).

11. I. A. Strigo, F. Carli, and M. C. Bushnell,"Effect of ambient temperature on human pain and temperature perception," Anesthesiology **92** (3), 699-707 (2000).

12. C. Boue, F. Cassagne, C. Massoud et al.,"Thermal imaging of a vein of the forearm: Analysis and thermal modelling," Infrared Physics & Technology **51** (1), 13-20 (2007).

13. P. A. Campbell, A. B. Cresswell, T. G. Frank et al.,"Real-time thermography during energized vessel sealing and dissection," Surgical Endoscopy and Other Interventional Techniques **17** (10), 1640-1645 (2003).

14. W.L. Wolfe and G.J. Zissis, *The infrared handbook*. (ERIM, Ann Arbor MI, 1989).

15. E.L Derniak and D.G. Crowe, *Optical radiation detectors*. (Wiley & Sons, New York NY, 1984).

16. E.L Derniak and G.D. Borememan, *Infrared detectors and systems*. (Wiley & Sons, New York NY, 1996).

17. D. G. Avery, D. W. Goodwin, and A. E. Rennie,"New infra-red detectors using indium antimonide," Journal of Scientific Instruments **34** (10), 394-395 (1957).

18. P. J. Treado, I. W. Levin, and E. N. Lewis,"Indium-antimonide (InSb) focal-plane array (FPA) detection for near-infrared imaging microscopy," Applied Spectroscopy **48** (5), 607-615 (1994).

19. B. J. Vakoc, G. J. Tearney, and B. E. Bouma,"Real-time microscopic visualization of tissue response to laser thermal therapy," Journal of Biomedical Optics **12** (2) (2007).

20. M. Riccio, G. Breglio, A. Irace et al.,"An equivalent time temperature mapping system with a 320x256 pixels full-frame 100 khz sampling rate," Review of Scientific Instruments **78** (10) (2007).

21. R. Pochaczevsky, M. Abernathy, M. Borten et al.,"Technical guidelines," Thermology **2**, 108-112 (1986).

22. J.P. Gore and L.X. Xu, in *Biomedical photonics*, edited by V. Tuan (CRC Press, Boca Raton FL, 2003).

23. S. P. Niehof, Fjpm Huygen, R. W. P. van der Weerd et al.,"Thermography imaging during static and controlled thermoregulation in complex regional pain syndrome type 1: Diagnostic value and involvement of the central sympathetic system," Biomedical Engineering Online **5** (2006).

24. B. Choi and A. J. Welch,"Infrared imaging of 2-d temperature distribution during cryogen spray cooling," Journal of Biomechanical Engineering-Transactions of the Asme **124** (6), 669-675 (2002).

25. P. H. Goodman, M. G. Murphy, G. L. Siltanen et al.,"Normal temperature asymmetry of the back and extremities by computer-assisted infrared imaging," Thermology **1**, 195-202 (1986).

26. L. C. Holmes, E. M. Gaughan, D. A. Gorondy et al.,"The effect of perineural anesthesia on infrared thermographic images of the forelimb digits of normal horses," Canadian Veterinary Journal-Revue Veterinaire Canadienne **44** (5), 392-396 (2003).

27. R. A. Sherman, A. L. Woerman, and K. W. Karstetter,"Comparative effectiveness of videothermography, contact thermography, and infrared beam thermography for scanning relative skin temperature," Journal of Rehabilitation Research and Development **33** (4), 377-386 (1996).

28. J. H. Torres, T. A. Springer, A. J. Welch et al.,"Limitations of a thermal camera in measuring surface-temperature of laser-irradiated tissues," Lasers in Surgery and Medicine **10** (6), 510-523 (1990).

29. American National Standards Institute, "Calibration laboratories and measuring and test equipment—general requirements," Report (1994)

30. T. Togawa,"Noncontact skin emissivity - measurement from reflectance using step change in ambient radiation temperature," Clinical Physics and Physiological Measurement **10** (1), 39-48 (1989).

31. T. Togawa,"Non-contact skin emissivity measurement by switching two shades of different temperature," Phys. Med. Biol **33** (S1), 409 (1988).

32. D. Mitchell, C. H. Wyndham, and T. Hodgson,"Emissivity and transmittance of excised human skin in its thermal emission wave band," Journal of Applied Physiology **23** (3), 390-& (1967).

33. D. J. Watmough and R. Oliver,"Wavelength dependence of skin emissivity," Physics in Medicine and Biology **14** (2), 201-& (1969).

34. A. Rose,"A unified approach to the performance of photographic film, television pickup tubes, and the human eye," J. Soc. Motion Pict. Eng **47**, 273–294 (1946).

35. A. Rose,"The sensitivity performance of the human eye on an absolute scale," Journal of the Optical Society of America **38** (2), 196-208 (1948).

36. A. E. Burgess,"The rose model, revisited," Journal of the Optical Society of America A **16** (3), 633-646 (1999).

37. Z. F. Lu, EL Nickoloff, JC So et al.,"Comparison of computed radiography and film/screen combination using a contrast-detail phantom," Journal of Applied Clinical Medical Physics **4** (1), 91 (2003).

38. X. J. Rong, CC Shaw, X Liu et al.,"Comparison of an amorphous silicon/cesium iodide flat-panel digital chest radiography system with screen/film and computed radiography systems—a contrast-detail phantom study," Medical Physics **28**, 2328 (2001).

39. G. D. Boreman, *Modulation transfer function in optical and electro-optical systems*. (SPIE Press, Bellingham, WA, 2001).

40. P. W. Kruse, *Uncooled thermal imaging: Arrays, systems, and applications*. (SPIE, Bellingham WA, 2001).

41. S. M. Bentzen,"Evaluation of the spatial resolution of a CT scanner by direct analysis of the edge response function," Medical Physics **10**, 579 (1983).

42. J. M. Boone and JA Seibert,"An analytical edge spread function model for computer fitting and subsequent calculation of the lsf and mtf," Medical Physics **21**, 1541 (1994).

43. T. D. Cradduck,"Assessing the performance of radioisotope scanners: Data acquisition," Journal of Nuclear Medicine **9** (6), 210 (1968).

44. R. Cubeddu, A Pifferi, P Taroni et al.,"Spatial resolution of imaging with diffusing light: Edge spread function measurements on a realistic tissue phantom," Medical Physics **26**, 462 (1999).

45. J. C. Dainty, R Shaw, and LJ Cutrona,"Image science: Principles, analysis and evaluation of photographic-type imaging processes," Physics Today **29**, 71 (1976).

46. R. T. Droege and RL Morin,"A practical method to measure the MTF of CT scanners," Medical Physics **9**, 758 (1982).

47. W. A. Goldsmith and M. L, Nusynowitz,"Determination of the modulation transfer function (mtf) using a programmable calculator," American Journal of Roentgenology **112** (4), 806 (1971).

48. P. F. Judy,"The line spread function and modulation transfer function of a computed tomographic scanner," Medical Physics **3**, 233 (1976).

49. E. L. Nickoloff and R. Riley,"A simplified approach for modulation transfer-function determinations in computed-tomography," Medical Physics **12** (4), 437-442 (1985).

50. E. Samei, M.J Flynn, and D.A. Reimann,"A method for measuring the presampled MTF of digital radiographic systems using an edge test device," Medical Physics **25**, 102 (1998).

51. N. J. Schneiders and S.C. Bushong,"Single-step calculation of the MTF from the ERF," Medical Physics **5**, 31 (1978).

52. J. A. Sorenson and M.E. Phelps, *Physics in nuclear medicine*. (Grune & Stratton Orlando FL, 1987).

Table 3.1 Pyrometer settings for SNR evaluation

Response Time [msec]	Data Point Intervals [msec]
5	5
10	10
30	50
100	100
300	500

Table 3.2 Pyrometer settings examined for temporal resolution

Response Time [msec]	Data point intervals [msec]	Laser Pulse Rate [Hz]	Laser Pulse Interval [msec]
100	100	30	33
5	10	30	33
5	5	30	33
5	5	60	17
5	5	90	11
5	5	120	8
5	5	180	6

Table 3.3 SNR for various pyrometer settings.

Response Time [msec]	Data point intervals [msec]	SNR	
		Detector A	Detector B
300	500	79.8	
100	100	39.9	
30	50	21.9	
10	10	7.9	2.2
5	5	6.8	1.7

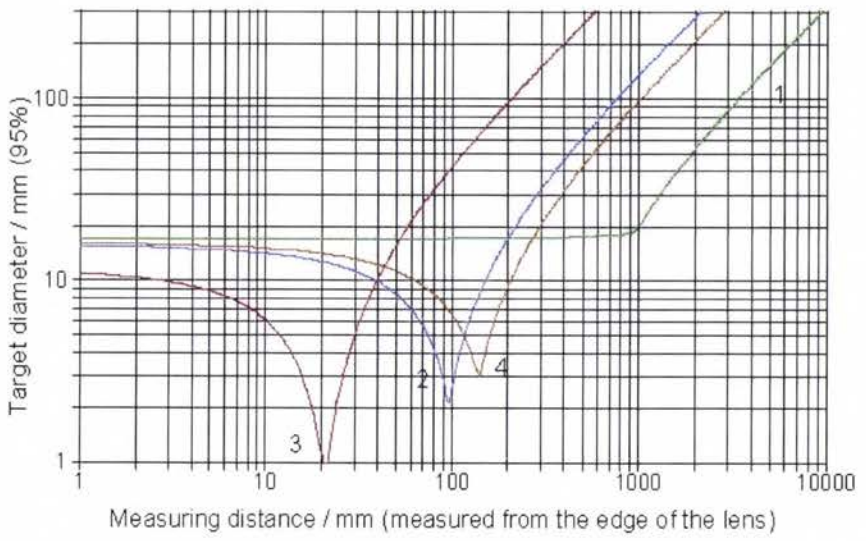

Figure 3.1 Heitronics KT15D Series Pyrometers Field of View Diagrams. The lens/detector combination originally configured on the instrument is represented by curve 4 (orange). The curves show the effective measurement area of the instrument over a range of distances.

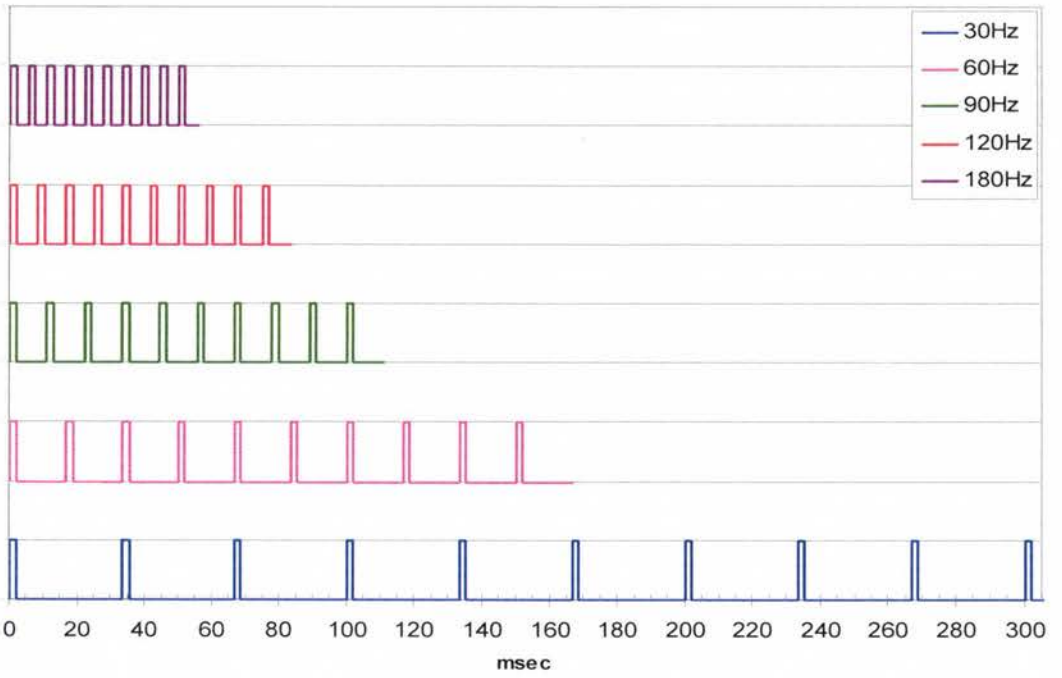

Figure 3.2 Laser pulse sequences for temporal resolution, each square-wave pulse length is 2 msec. Vertical axis is arbitrary for illustration.

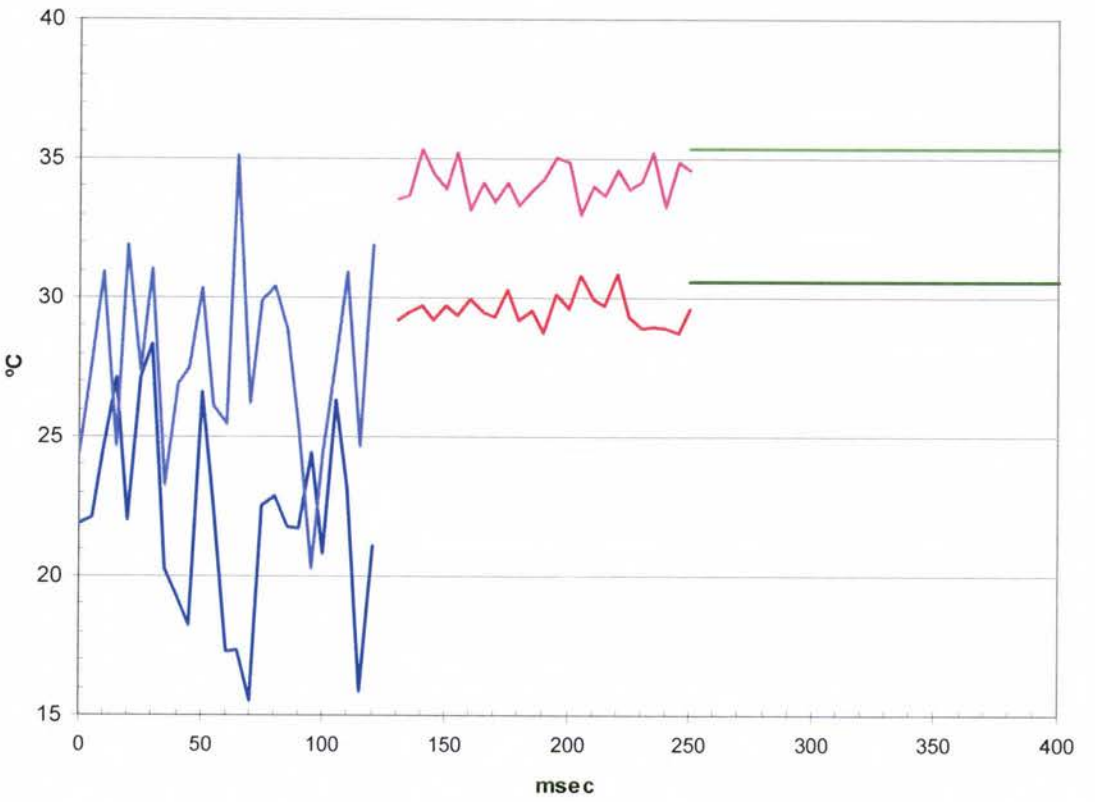

Figure 3.3 SNR comparison with 5°C temperature difference for: Original pyrometer (blue), Upgraded pyrometer (red), micro-bolometer array (green). Pyrometer settings are 5 msec response time, 5 msec data intervals; 120 msec (25 data points) shown for both configurations. Bolometer was operating at 60 Hz (16.7 msec); 151 msec (10 data points) shown.

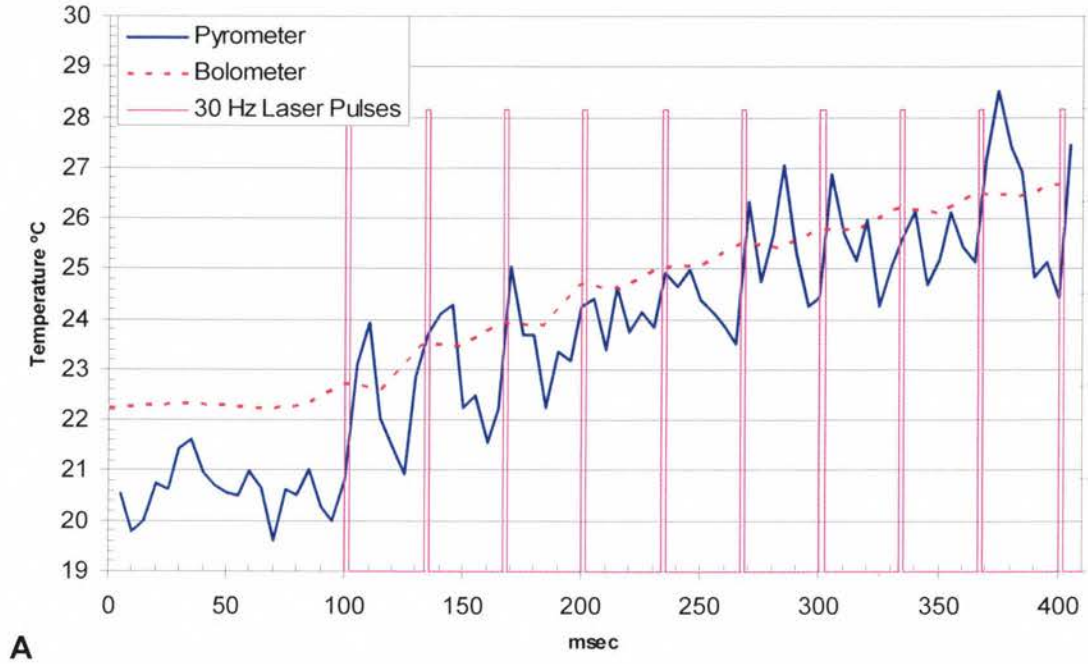
Pyrometer
Bolometer
30 Hz Laser Pulses
Temperature °C
msec
30
29
28
27
26
25
24
23
22
21
20
19
0
50
100
150
200
250
300
350
400

A

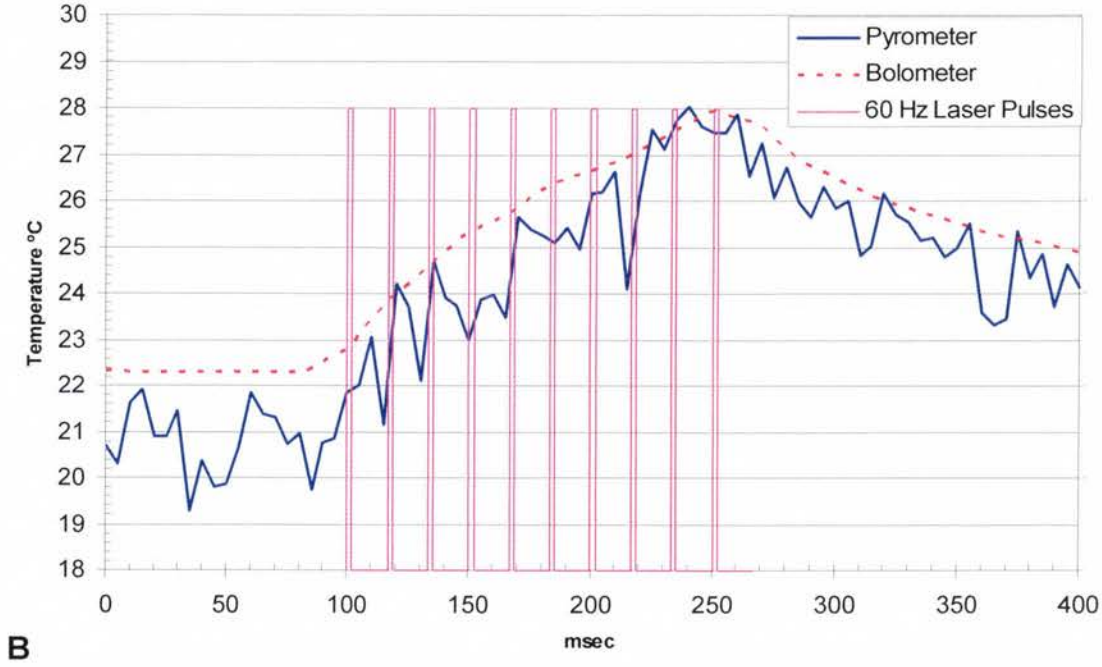
Pyrometer
Bolometer
60 Hz Laser Pulses
Temperature °C
msec
30
29
28
27
26
25
24
23
22
21
20
19
18
0
50
100
150
200
250
300
350
400

B

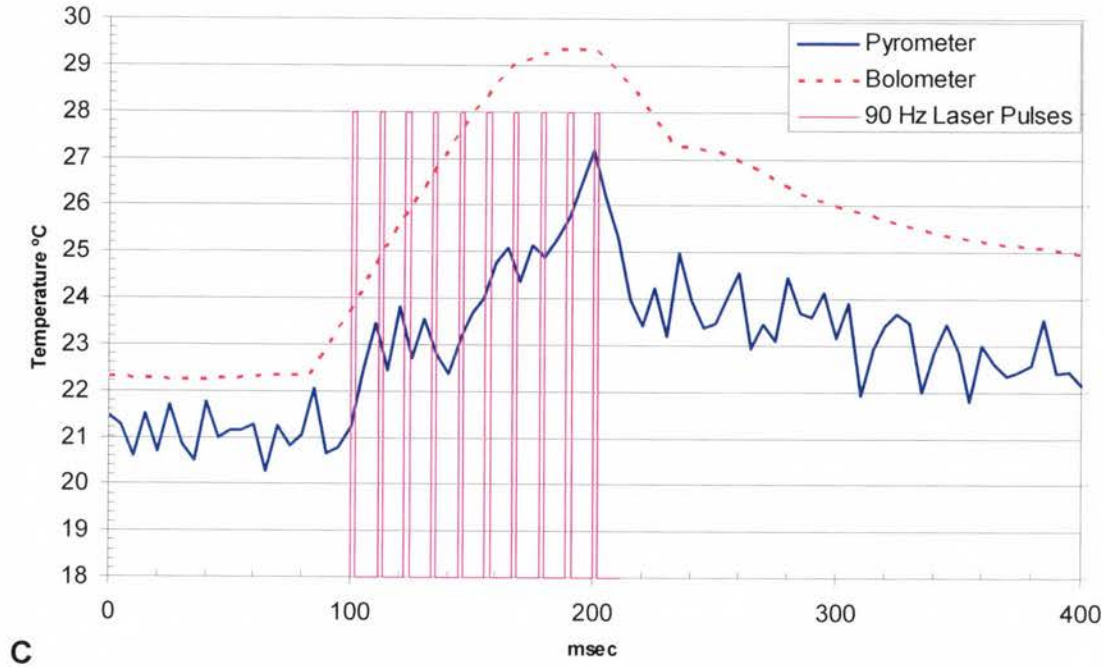
Pyrometer
Bolometer
90 Hz Laser Pulses
Temperature °C
msec
30
29
28
27
26
25
24
23
22
21
20
19
18
0
100
200
300
400

C

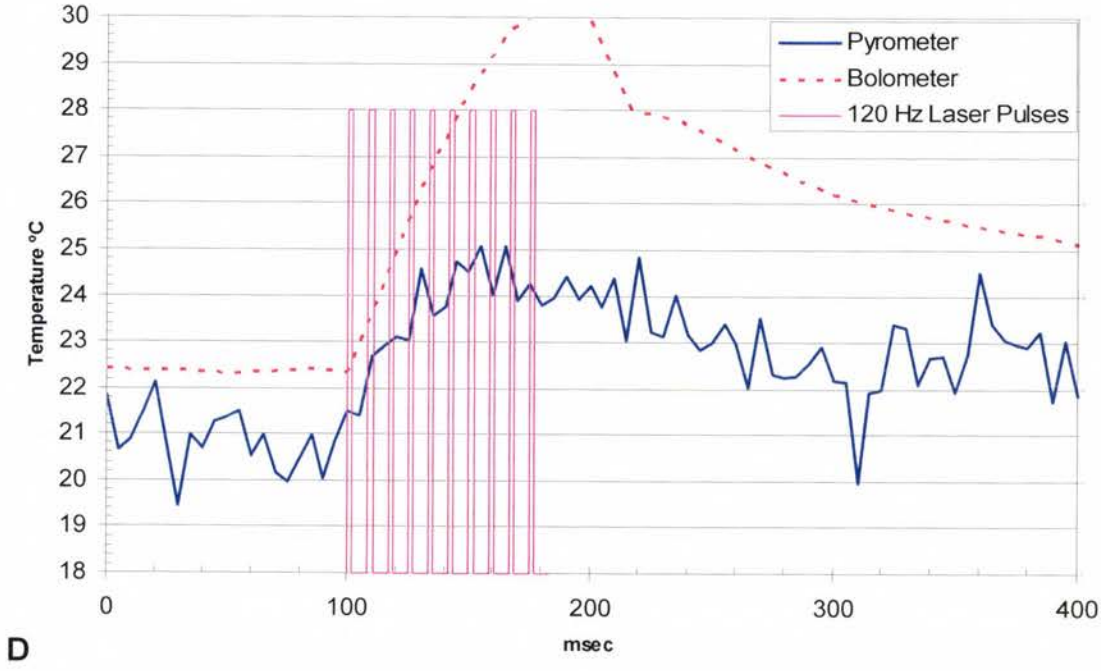
Pyrometer
Bolometer
120 Hz Laser Pulses
Temperature °C
msec
30
29
28
27
26
25
24
23
22
21
20
19
18
0
100
200
300
400

D

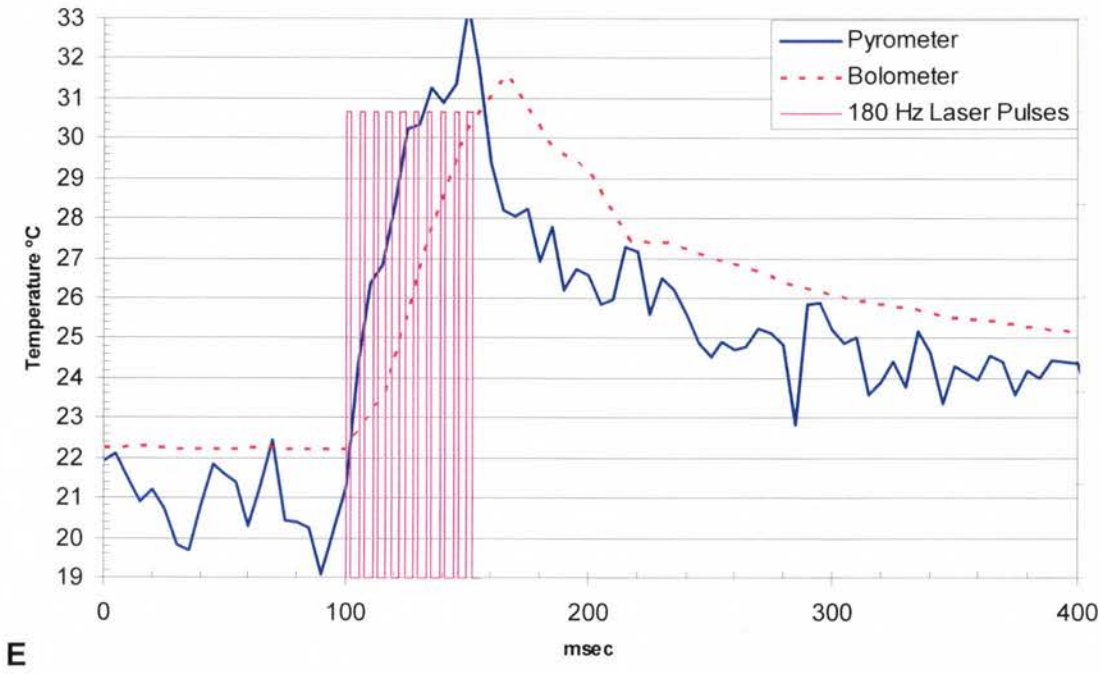

Figure 3.4 Temporal resolution of pyrometer and micro-bolometer A) 33 msec interval between laser pulses, B) 17 msec interval between laser pulses, C) 11 msec interval between laser pulses, D) 8 msec interval between laser, E) 6 msec interval between laser pulses. The pyrometer is set for 5 msec detector response with data sampled at 5 msec. The micro-bolometer data rate is 16.7 msec. The height of the laser pulse curve is arbitrary to illustrate the comparison to instrument response.

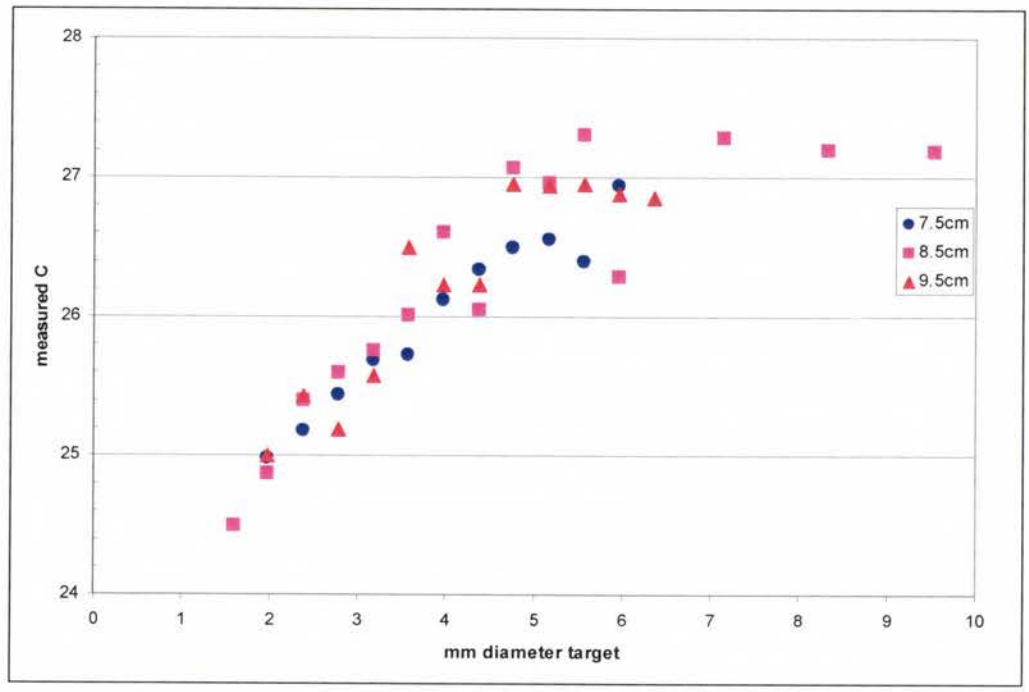

A

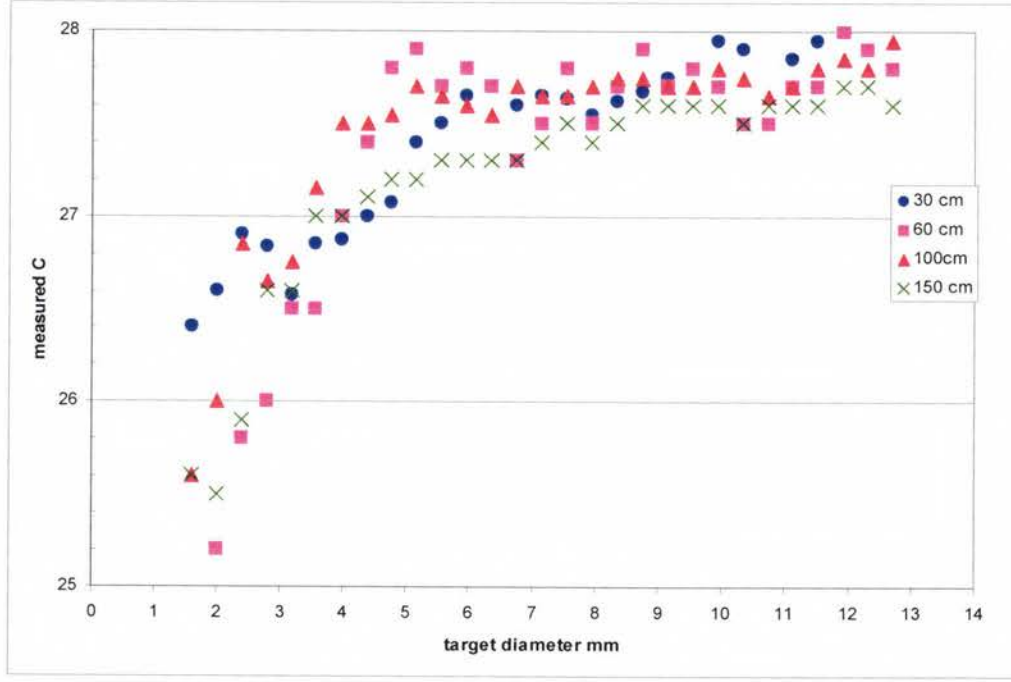

B

Figure 3.5 Instrument spatial dependence of accuracy. A) Pyrometer at fixed focal distance of 8.5 cm (squares) and off focal distances of 7.5 cm (circles) and 9.5 cm (triangles). B) Micro-bolometer array at distances of 30 cm (circles), 60 cm (squares), 100 cm (triangles), and 150 cm (x).

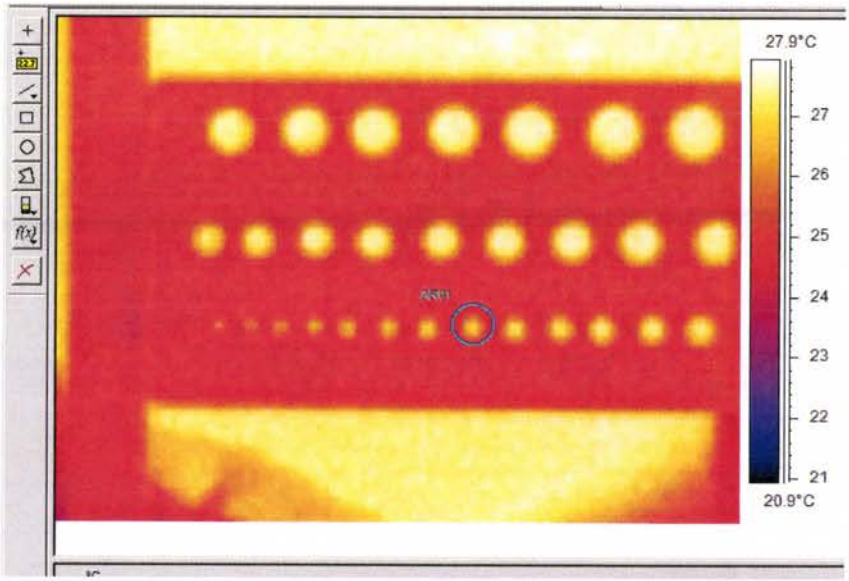

Figure 3.6 Thermal camera image of spatial resolution test object at 150 cm. Temperature was taken from the average of the four central pixels of each circle.

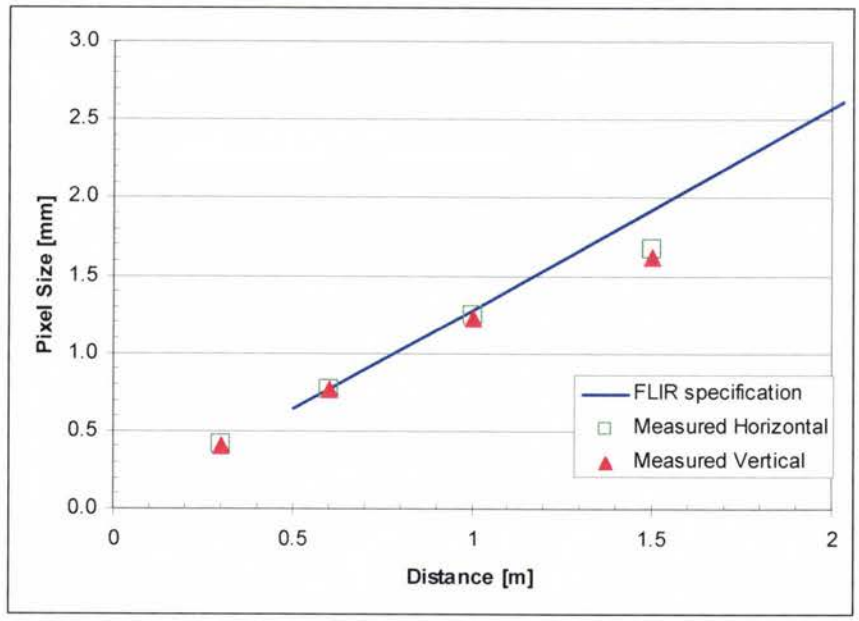

Figure 3.7 Thermal camera measured pixel size in horizonatal and vertical direction of array. Manufacturer's specified dimension is straight line.

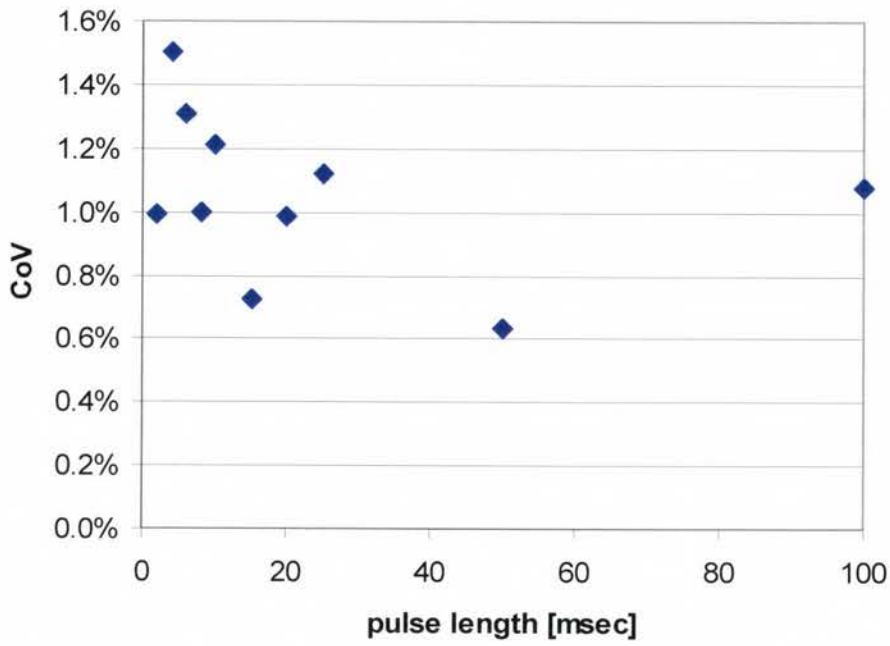

Figure 3.8 Micro-bolometer detector reproducibility to ten laser pulses presented as the Coefficient of Variability for a variety of pulse durations.

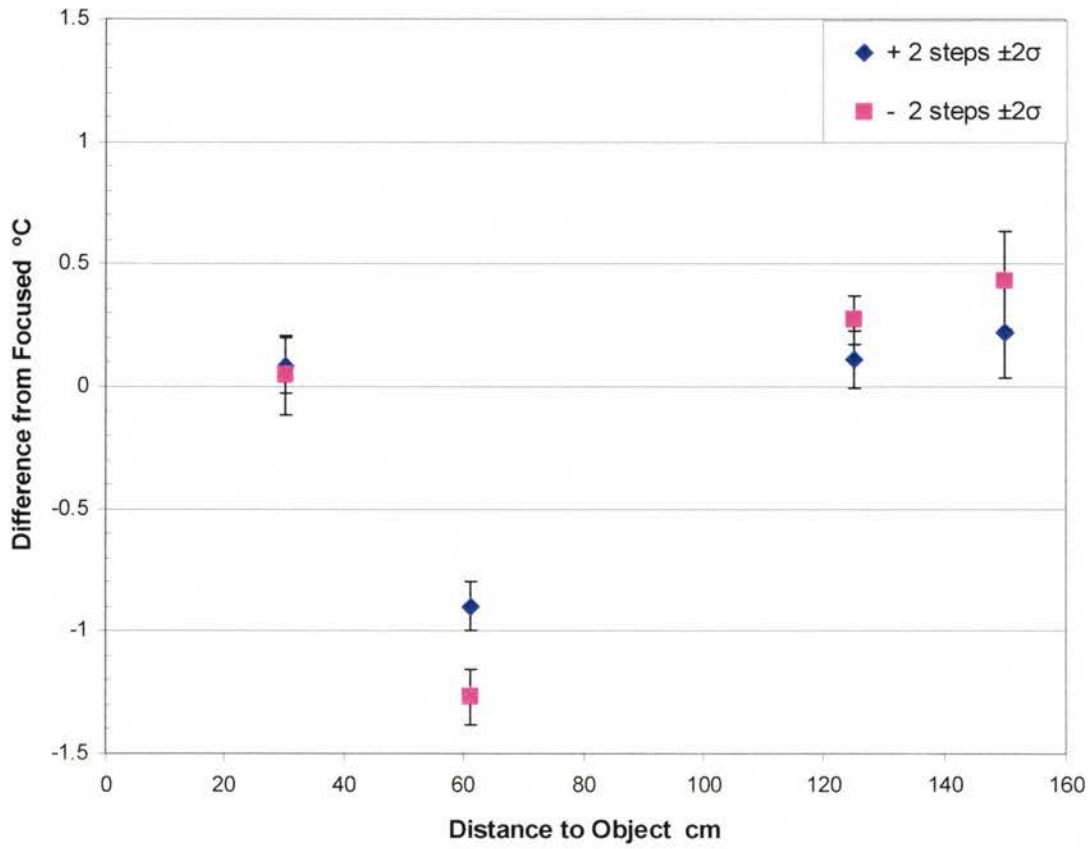

Figure 3.9 Focal effects on IR camera temperature measurements over a range of distances from object to camera. Error bars represent two standard deviation of the 120 data points for each condition.

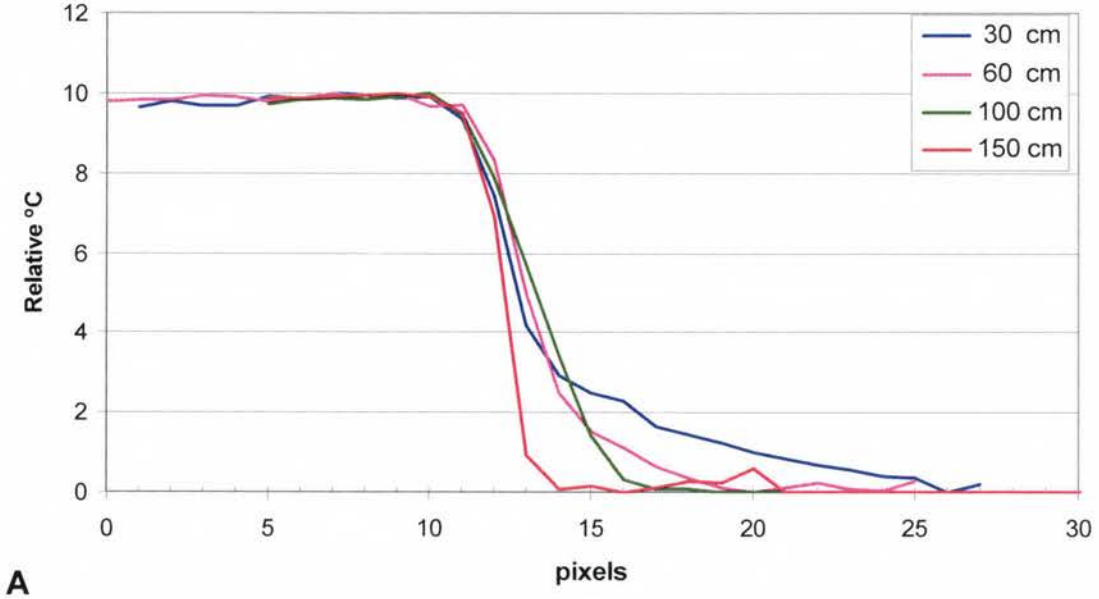
12
10
8
6
4
2
0
Relative °C
0
5
10
15
20
25
30
pixels
30 cm
60 cm
100 cm
150 cm

A

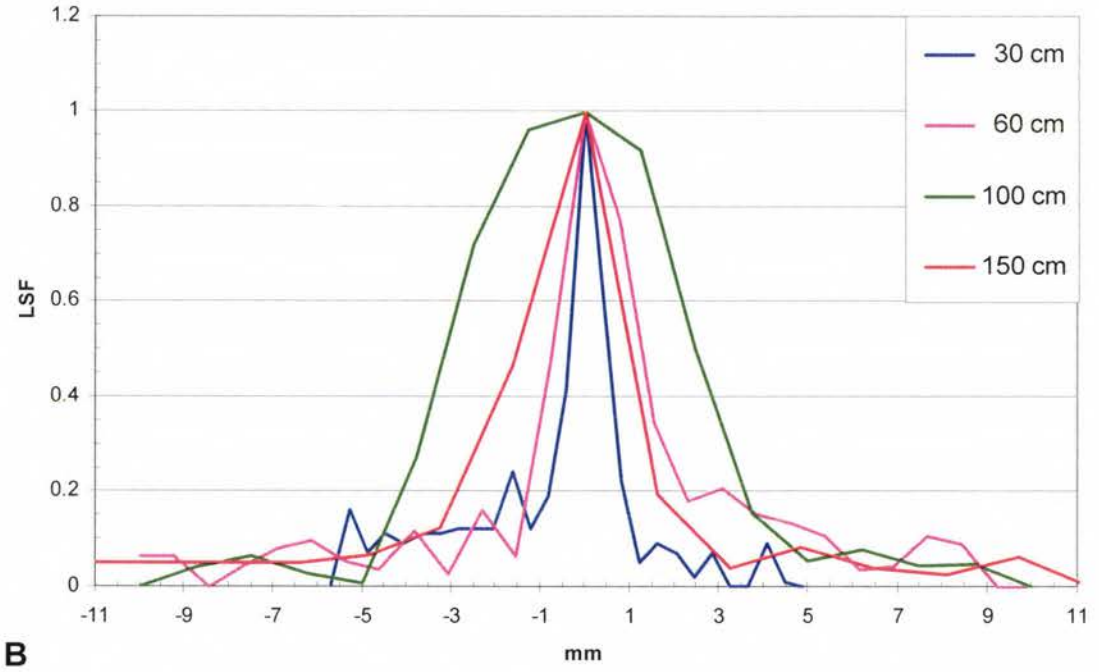
1.2
1
0.8
0.6
0.4
0.2
0
LSF
-11
-9
-7
-5
-3
-1
1
3
5
7
9
11
mm
30 cm
60 cm
100 cm
150 cm

B

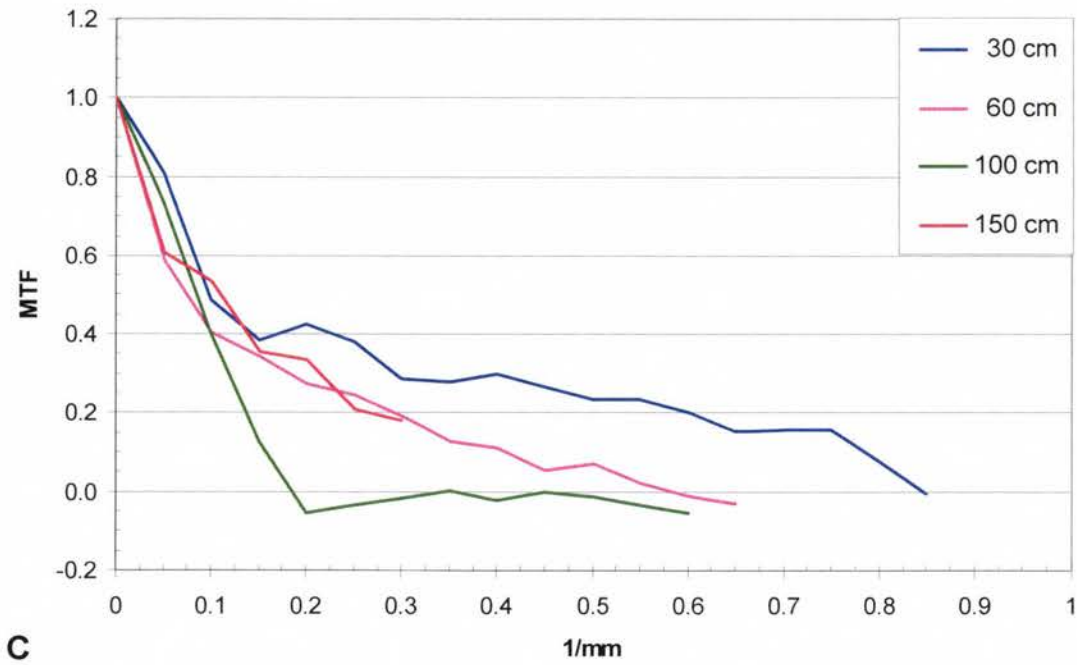

Figure 3.10 Spatial resolution of the micro-bolometer focal plane array imaging system. A) ESF at varying distances, and B) LSF calculated from ESF with pixel sizes from Figure 3.7, C) MTF calculated from LSF in the frequency domain.

Chapter 4

Relationships of skin depths and temperatures when varying pulse repetition frequencies from 2.0 μm laser light incident on *ex vivo* pig skin

4.0 Abstract

Human perception of 2.0 μm IR lasers irradiation has become significant in such disparate fields as law enforcement, neuroscience, and pain research. Several recent studies have found damage thresholds for single pulse and CW irradiations at this wavelength. However, the only publication using multiple pulse irradiations investigated the cornea rather than skin. Previous studies have claimed that the 2.0 μm light characteristic thermal diffusion time was as long as 300 msec. Irradiating the skin with 2.0 μm lasers to produce sensation should be optimal with published recommendations of pulses on the order of ten to 100 milliseconds, which approach the theoretical thermal diffusion time. Therefore, investigation of the heating of skin for a variety of laser pulse combinations was undertaken. Temperatures of *ex-vivo* pig skin were measured at the surface and at three depths from pulse sequences of six different duty factors. Differences were found in temperature rise per unit exposure which did not follow a linear relation to duty factor. The differences can be explained by significant heat conduction during the pulses. Therefore the common heat modeling assumption of

thermal confinement during a pulse may need to be experimentally verified if the pulse approaches the theoretical thermal confinement time.

4.1 Introduction

The irradiation of skin by laser light has been a subject of study since shortly after the ruby laser was introduced in 1960,[1] with the first publication on rabbit and human skin in 1963.[2] From very early in the history of lasers, skin irradiation safety limits have been based on both pulsed (0.1 J/cm^2) and CW (1.0 W/cm^2) operation.[3] Current safety standards from the American National Standards Institute (ANSI) set the skin exposure limit in the infrared (IR) at $0.56 \times t^{0.25}$, in units of J cm^{-2} where t is the exposure time between 10^{-3} and 10 seconds.[4] The ANSI report is based on observed damage thresholds to the cornea of the eye, quantified in radiant exposure, H (J/cm^2).[5] From dermatology, skin damage is described in units of temperature. Accurate temperature prediction is important because the gap between skin tolerance and injury is as narrow as 3 – 6 °C depending on duration of heating.[6-8]

The skin temperature change due to IR laser irradiation has been measured in many studies with temperature and time as predictors of skin damage.[6] Moncrief sets the threshold for irreversible damage to the basal cells of the epidermis at 44 °C for extended time in minutes. For brief exposures Moncrief gives 51 °C as the limiting temperature.[7] Leach et al had reported 47 °C as critical temperature for visible change to skin and 50 – 55 °C as the threshold for permanent damage.[8]

Establishing injury thresholds from laser irradiation with very short durations often focuses on the energy and leaves temperature to calculation rather than

measurement.[9] The most frequent method of skin temperature measurement during laser irradiation has been the non-contact IR camera. This type of instrument was used for single pulses of 2.0 μm laser by Chen et al.[5] Pulsed irradiation of skin with 2.94 μm laser was measured by a thermal imaging camera.[10] IR pyrometers have also been used to measure surface temperatures during laser irradiation.[11-12] Leandri et al again demonstrated the difficulties in temperature measurement with a correlation of temperature to laser energy, but not to pulse duration.[11] Temperatures deep within tissue during and following continuous wave (CW) laser irradiation have also been measured with thermocouples.[13-14]

Tissue effects comparing different laser pulse conditions have been investigated for many purposes including medical uses and injury investigation. Different results have been found when one or more of the following parameters have been varied: pulse repetition frequency (PRF), pulse width combinations of different widths, different spacing (i.e. not a repetitive frequency), or sequences with different power per pulse. Pulse sequence optimization of Er:YAG lasers has been of particular interest to dermatologists to replace their CO_2 lasers.

A summary of representative studies of pulse sequence effects is given in Table 4.1. As seen in Table 4.1, pulse width can change the amount of radiant energy to produce damage in tissue or change the extent of damage. Pulse repetition frequency can change the observed temperature or type of tissue damage. Increasing the number of pulses can affect the depth of injury per pulse.

Many studies use ablation or coagulation depth as a metric for pulse sequence comparison.[10,15-16] For those modeling the temperature from laser pulse irradiation, the

energy deposition is assumed to be an instantaneous impulse confined within the volume of deposition.[17-21] The conditions required for this assumption to be valid depend on the optical penetration in the tissue and the rate of heat flow or thermal diffusivity of the tissue.

The optical penetration depth, *d*, is a measure of how deep the energy fluence will travel before being absorbed. Optical penetration depth depends on the absorption and scatter of the light in the tissue and the beam width.[22-23] For absorption-dominated tissue, the optical penetration depth is $d = 1/\mu_a$. For optically turbid material, the optical penetration depth is defined by Ritz[23] as

$$d = [3\mu_a(\mu_a + \mu'_s)]^{-1/2} \qquad (4.1)$$

where μ_a is the absorption coefficient and μ_s' is the reduced scattering coefficient ($\mu_s' = \mu_s(1-g)$, with g being the anisotropy factor). The optical zone, where the incident energy fluence has been reduced by 1/e, in turbid media has an additional factor to account for backscattered reflections.[22]

The 2.0 μm Tm:YAG laser has yet to have optical absorption and scatter properties conclusively established. The diversity of published attenuation coefficients produces a wide range of optical penetration depths, as seen in Table 4.2.

The heating of tissue below the skin surface is complicated by the flow of heat into or out of the volume of interest during the irradiation. Therefore, models of tissue heating are simplified if they assume that the energy is deposited as an impulse with no heat flow until the pulse has terminated. The conventional criteria for neglecting heat transfer from the irradiated tissue is for the laser pulse to be significantly smaller than the thermal diffusion time[22] τ_{diff}, also known as the thermal relaxation time, expressed

by Equation 4.2, where D is the thermal diffusivity coefficient. The thermal relaxation time, τ_{diff}, is considered to confine the heat transferred within the optical penetration depth.[22]

$$\tau_{diff} = \frac{d^2}{D} \qquad (4.2)$$

Thermal analysis of laser pulses assumes no residual thermal influence of prior pulses if the pulse length is much less than the thermal relaxation time[24], however, these analysis do not address the pulse repetition frequency, that is the time between "impulses" of energy deposited. This assumption has been applied to pulse durations up to 300 msec.[25] Some analytic functions have been reported to fit tissue temperature changes best for short (microsecond) pulses[26-27] while others fit best for longer pulse widths (>100 msec).[28] However, both of these solutions were evaluated for a single laser pulse rather than for a series of pulses as a whole.[27]

The skin tissue is composed of three anatomical layers, which have different optical properties. The exterior skin layer is the stratum corneum, which ranges from 10 μm to 20 μm thick depending on anatomic site and study. Underneath is the epidermis ranging from 30 μm to 150 μm thick. Lastly, the dermis has been reported to be from 981 μm to 4,000 μm thick.[29] This places the optical penetration depth of 2.0 μm laser light within the dermis if absorption is dominant in skin. If skin is a turbid medium with scatter dominant, then the penetration depth is deeper into or beyond the dermis. If skin is a mildly turbid medium with both absorption and scatter, then the optical zone is close to the border between the epidermis and dermis.

Considering pulses of 2.01 μm infrared from Tm:YAG fiber lasers, the range of published values of thermal constants listed in Table 4.3, combined with the range of

optical zones, *d*, found above in Table 4.2, produce thermal diffusion times that would indicate virtually any pulse widths are thermally confined. As shown in Table 4.4, different combinations of constants can produce thermal diffusion times over a range of four orders of magnitude. The thermal diffusivity, *D*, depends on the tissue type and any vascular perfusion.

This work explores the relationship of computed and measured temperatures of 2 μm laser light incident on pig skin with varying pulse repetition frequencies and skin depths. The objective of this work is to investigate the validity of the common assumption of isolated, thermally confined pulses used in analytical temperature modeling. The variable of interest is the duty cycle of pulsed irradiations. Measurements of temperature at the surface and internal temperature at three depths beyond the optical penetration depth were evaluated for differences of heating between sequences of varying PRF, while total energy is held constant. Temperatures predicted by models which rely on the assumption of thermal confinement within a thermal relaxation time were found to have varying agreement depending on pulse cycle duty factor. Temperature rise per unit exposure was found to be different between pulse sequence duty factors at all four depths.

4.2 Materials and Methods

4.2.1 Temperature Measurements

Temperature measurements of six distinct pulse sequences were taken at four *ex-vivo* skin depths, nominally at the surface, 300 μm, 400 μm and at 650 μm. The entire

skin sample and holder with thermocouple in place was centered in the beam of a 2.0 μm laser by scanning the probe through the beam on a 2D optical stage with a micrometer (model TXS, Melles-Griot, Albuquerque, NM) in 500 μm increments first in the N-S direction and then in the E-W direction. The measurements at central axis (CAX) of the IR beam were repeated four times for each pulse sequence on each sample of pig skin. The first sequence was also repeated another four times in order to show that the skin conditions had not changed during the measurements. Three different samples of pig skin were used at each depth for a total of nine skin samples (surface measurements were performed concurrently).

Temperatures were measured with two instrument systems: an infrared camera with micro-bolometer array for skin surface measurements and with a type T (Copper-Constantan) micro-thermocouple for below surface depths. The model S65HSV thermal imaging camera (FLIR Systems, Wiesbaden Germany) detector was composed of a 320 × 240 array of uncooled microbolometer detectors. The sensitivity is calibrated at 0.05 °C with an accuracy specification of + 2 °C. Image sequences were collected and sent to a PC (XPS, Dell, Round Rock TX) at a rate of 60 Hz, giving a temporal resolution of 17 msec per data point. The images were read and analyzed using Researcher Pro version 2.8 (FLIR Systems, Wiesbaden Germany) which offers region of interest and line profile extraction. The camera is sensitive in the spectral range of 7.5 to 13 μm. The lens has a minimum focusing distance of 0.3 m, with a quoted spatial resolution of 1.1 mrad of divergence. The thermal camera was positioned in the same location for all exposures at one meter from the skin surface, approximately 30° from normal to the skin in the E-W direction in order to not interfere with the beam delivery

arm. The camera was calibrated by the manufacturer using NIST traceable blackbody sources.

The model HYP-0 thermocouple (Omega Engineering, Stamford CT) consisted of the thermocouple junction imbedded in the tip of a stainless steel 33 gauge hypodermic needle. The outer diameter of the needle was 200 μm. The thermocouple response was recorded using iNet software (Omega Engineering Inc., Stamford CT). The iNET settings were 150 readings per second, with the noise filter set to exclude signals over 200 Hz, signal integrate time set to 0.001 second, with 4,000 readings collected for 26 seconds of monitoring. The iNet system recording was initiated by the same pulse triggering the laser via connection to the output of the HP model 33120A waveform generator (Hewlett Packard, Palo Alta CA) with a coaxial T connector. The IPG model TLR-50-2010 Tm:YAG laser (IPG Photonics, Oxford MA) fired as the TTL signal reached its maximum of 5 V while the iNet was set to begin collecting data at a TTL signal of 0.5 V in order to measure the initial temperature of the tissue prior to the laser pulse. Prior to each exposure session, the thermocouple – iNet system was self tested for connectivity with results stored to disk. The thermocouple relative accuracy and constancy was verified three times during the study by immersion into a water bath at four different temperatures ranging from boiling to ice-water. The water temperature was determined by the average reading of four Barnstead Ever-safe N16B organic liquid filled thermometers (Thermo Scientific, Waltham MA). The thermocouple probe was inserted in the pig skin in the N-S direction.

Direct heating of the thermocouple probe by the 2.0 μm beam rather than the surrounding tissue, considered a significant impact in several laser studies,[30-32] was

judged to be negligible in this experiment for three reasons. First, the thermocouple used was considerably smaller than the one used in the Manns study[30]. The 33 gauge needle presents a 0.21 mm diameter as opposed to their 23 gauge needle's 0.61 mm to intercept the direct beam fluence. Second, the 2.01 μm wavelength IR of the Tm:YAG laser does not penetrate to the depth of the needle as did the 1.06 μm beam of Manns' Nd:YAG laser. For example, consider the difference 1 μm of wavelength makes in the two beams' attenuation coefficient in water. From Hale and Querry, the coefficients are 69.12 cm^{-1} at 2,000 nm but only 0.12 cm^{-1} at 1,060 nm wavelength.[33] Using these attenuation coefficients, weighted by water content of skin,[22,34] the 2.0 μm beam is reduced to 19% of original intensity by Beer's Law at the 0.3 mm depth of the probe. In contrast, the Nd:YAG beam in the Manns study would still be at 95% at the 5 mm distance to their closest thermocouple. Finally, the graphs of skin temperature rise during the laser pulse recorded with this thermocouple did not exhibit the instantaneous temperature jump which has been claimed to be the indication of direct thermocouple absorption of laser beam energy.[31-32]

4.2.2 Skin Samples

Pig skin (*Sus scrofa domestica*) was obtained via an agreement with the professional veterinary program at Colorado State University. Approval to utilize tissue samples from these pigs was obtained from the University Institutional Animal Care and Use Committee. Tissue sample disposal procedures were approved by the Institutional Biosafety Committee (IBC) of the Research Integrity and Compliance Office.

Skin samples were excised from the rear flank of pigs within 24 hours of animal euthanasia. Skin excision was performed in the Veterinary Medicine Anatomy Lab. After identifying a suitable area of skin free of injury or scars, with uniform pigmentation, the hair was removed with electric clippers set to the closest setting which would not scratch the skin. This left hair of approximately 1.5 mm length on the skin. Skin samples of approximately 100 cm^2 were taken with approximately 0.5 cm of fatty tissue thickness. The samples were maintained at 5 °C in airtight containers with 1 ml saline solution to maintain moisture. Skin samples were handled from the sides and edges to avoid any abrasion or tearing of the surfaces to be irradiated.

Under optical magnification, a 25 gauge, 5/8 inch, hypodermic needle (Becton Dickenson, Franklin Lakes NJ) was used to pierce the surface of the skin and was directed parallel to the skin surface. The HYP-0 thermocouple needle was immediately inserted through the 25 g needle until it extended 10 mm past the tip. This method proved to be the most reliable to insert the probe as the 33 gauge needle construction of the thermocouple was too fragile to penetrate the skin by itself. The thermocouple insertion is shown in Figure 4.1.

Insertion attempts were balanced between the goal of positioning the probe at shallow depth and the tendency to penetrate the delicate epidermal tissue from the inside (see Figure 4.1b). When this occurred, the needle was withdrawn from the hole and the process begun again 5 mm lateral to the ruptured hole site. The sample with the thermocouple inserted was then mounted on the optical translation stage using screws and rubber washers to clamp down a Petri dish containing the skin sample.

4.2.3 Laser and Optics

The pig skin was irradiated with a commercial 50 W Tm:YAG fiber laser (IPG Photonics, Oxford MA) producing a 2.01 μm wavelength beam. The laser pulse sequences were created by two model 33120A 15 MHz digital waveform generators (Hewlett Packard, Englewood CO) connected in series to control the duration and number of laser pulses respectively. A single 10 ms laser pulse was created by setting the first waveform generator to deliver a single 50 Hz square wave pulse, and offsetting the voltage by half the amplitude, thereby generating a TTL signal that served as a trigger for the laser control. The six pulse sequences were repetitions of the 10 msec single pulses as triggered by the second waveform generator which was set to the desired PRF (see Figure 4.2 for illustration of the multi-pulse sequence timing). In all sequences, individual 10 msec pulses were fired within a 250 msec period. The 50 W laser was adjusted in power to produce approximately equal total radiant exposures for each sequence.

The IR laser pulses were aligned to be colinear with a commercial HeNe laser (model 05-LLR-811, Melles-Griot, Carlsbad, CA) using a dual-axis adjustable gold mirror (model PF20-03-M01, ThorLabs, Newton NJ) with average reflectivity greater than 98% from 1 μm to 5 μm. This HeNe was selected in part for the low divergence of its beam at 1.7 mrad in the far field. The HeNe beam was essential to the laser operator for aiming the beam. The co-linear beams were then directed into a custom optical articulating arm assembly (Oxid Corp. Farmington Hills, MI). This arm used seven articulating joints with gold mirrors to allow both the visible and IR beams to be directed to the measurement site safely. The laser and optics are diagramed in Figure 4.3.

The 2% of the IR beam reflected by the HeNe alignment mirror was measured and recorded for each exposure of the pig skin. The IR laser output from the articulating arm was calibrated to the split beam sample prior to each exposure session. A total of 21 exposures were simultaneously measured by both the sampling probe and another probe placed on the optical stage in place of the skin sample. The beam probes were PM10 air-cooled thermopile sensors (Coherent, Santa Clara CA) calibrated by the manufacturer with an uncertainty of ± 1 %. The sensors were read by an EPM2000 model meter (Coherent, Santa Clara CA). The meter was also calibrated by the manufacturer with a stated resolution of ± 0.03% of full scale reading. The beam output and sampling data points covered laser settings from 30 % to 100 % power output and were fit to a straight line with correlation coefficient greater than 0.98 without forcing the intercept to zero. This provided a high confidence in the calculated beam energy for each exposure.

The IR beam incident on the pig skin had a Gaussian shape with a 3.28 mm $1/e^2$ radius using a pinhole technique[35] in both directions. Beam diameter was measured in both directions on five occasions throughout the study with a standard deviation of 0.33 mm between all results. Beam shape was confirmed to be uniform, circular in the lowest order mode, and aligned with the HeNe beam with Zap-It thermal paper (Kentek, Pittsfield NH) prior to each measurement session. Exposures were made on the thermal paper prior to the beam entering the armature and after the beam exiting the arm at the level of the skin sample. The thermal paper impressions were then visually compared to previous sessions' marks to identify any changes. The thermal paper exposures were performed using a four-pulse sequence with the laser set to 50% power to produce

reasonable beam patterns both entering and exiting the articulating arm with the same laser settings.

4.2.4 Histology

After the laser exposures were completed, the surface of the pig skin was marked with black ink parallel to the needle from the insertion point to the end of the probe. The HYP-O probe was then withdrawn from the sample and from the 25 g needle. Before the 25 g needle was withdrawn, a 3 cc syringe containing yellow tissue marking dye (Cancer Diagnostics Inc., Birmingham MI) was connected to the Leur-lock of the needle. As the 25 g needle was withdrawn from the skin, gentle pressure on the syringe injected the dye into the cavity evacuated by the needle. This prevented the cavity from collapsing on itself, and rendered it clearly distinguishable under a microscope. The pressure on the syringe plunger was minimal, to prevent the dye from being forced into the surrounding tissue and expand or rupture the cavity. The sample was then cut down with 2 mm margins around the ink marks and submerged in the freezing solution, Tissue-Tek OCT (Sakura Fintek, Torrance CA), as shown in Figure 4.4.

In order to freeze the sample in a known orientation, the skin was held in place with cotton thread sutured to the edges deep in the muscle layer of the sample. This was necessary to prevent sectioning geometry uncertainty. The sample container was marked with the needle direction and sample number. It was then frozen for 24 hours at -80 °C. The frozen sample was affixed to a ball joint holder with OCT solution and mounted in the microtome (Bright Instruments, Huntington UK) as shown in Figure 4.5. The sample was aligned perpendicular to the knife edge and trimmed down until the

black ink markings on the surface, indicating the needle insertion, were visible. As soon as the black ink was identified, sections of 15 μm thickness were cut and mounted on slides. Digital images were taken of the slides at 4X magnification on a BH2 microscope (Olympus, Center Valley PA), as shown in Figure 4.6. Depths were measured on the images to the center of the dye stained hole using Spot software version 4.09 (Digital Instruments Inc., Sterling Heights, MI). Measurements from the four distal images showing the probe cavity were averaged with a maximum standard deviation of a sample being 0.065 mm at the 0.650 mm depth. The distance measurement function of the Spot software was calibrated for the 4X lens with a digital test pattern, model USAF1951 (Edmund Optics, Barrington NJ).

4.2.5 Data Analysis

Temperature for each exposure was measured simultaneously both at depth and on the surface. The relative temperature rise per exposure in $^{\circ}C\ mJ^{-1}\ mm^2$ was calculated. In the case of the thermocouple temperature, baseline was taken as the first data point. The thermal camera was set to take twenty data points prior to the exposure for background subtraction.

The maximum temperature rise per exposure ($\Delta\ ^{\circ}C\ mJ^{-1}\ mm^2$) for each pulse sequence was examined with an analysis of variance (ANOVA) to determine if any differences existed between the pulse sequences. The data were then compared with Fisher's Least Significant Difference (LSD) procedure to find which sequences produced a different temperature rise at the 95% confidence level. The LSD is given by

$$LSD = t_{\alpha/2}\sqrt{S_W^2\left(\frac{1}{n_i}+\frac{1}{n_j}\right)} \qquad (4.3)$$

where t is the percentage point of student's t distribution for α=0.05 and degrees of freedom from within the groups, S_W^2 is the within sample sum of squares variability, n_i and n_j are the numbers of samples of each population compared.

The measured temperatures were then compared to expected temperatures calculated with an adaptation of the Green's function solution to the tissue bioheat differential equation from Vyas and Rustgi (Equation 4.4).[27] As there was no blood flow in the pigskin samples the first exponential term from the published solution is one and is dropped. The second exponential term from Vyas and Rustgi is also one for these central axis (r = 0) temperatures, and is therefore omitted. For the multiple pulse exposures, the calculated temperatures from the individual pulses were summed at the end of the pulse sequence. The Vyas solution was chosen over the Grossweiner[26] or the Roider[18] solutions as it describes the temperature in both the depth and radial directions with time.

$$T(z,t) = \left(\frac{\mu_a E_o}{\pi \rho C}\frac{1}{(a^2+8Dt)}\right)\left[\exp\left(-\mu_a z+\mu_a{}^2 Dt\right)\right]\ \mathrm{Erfc}\left(\frac{2D\mu_a t - z}{\sqrt{4Dt}}\right) \qquad (4.4)$$

In Equation 4.4, μ_a is the optical absorption coefficient for the tissue, E_o is the energy deposited, ρ is the tissue density, C is the specific heat capacity, a is the laser beam $1/e^2$ radius, D is the tissue thermal diffusivity, z is the depth in tissue, and t is the time. The literature provides a wide range of values for the thermal constants for skin tissue, as listed in Table 4.2. The constants used in this study were as follows: μ_a = 2.176 mm^{-1};[34]

$\rho = 0.00107$ g mm^{-3};[36-37] $C = 3.4$ J g^{-1} °C^{-1};[36] $D = 0.12$ mm^2 sec^{-1},[27,38] beam radius $a =$ 3.2 mm. These values were chosen because they fall near the middle of the range of published values and the diffusivity value was also used by Vyas and Rustgi.

4.3 Results

The temperature of pig skin was measured simultaneously on the surface and at depth during six different pulsing sequences of 2.0 μm laser exposure. Four measurements of each sequence on three different skin samples produced at least twelve data points for each sequence at depths of 300 μm, 400 μm, and 650 μm. The IR camera provided surface temperature readings during each irradiation. The measurements produced repeatable temperature increases per incident exposure with the maximum variance of a data group at 0.013 °C mJ^{-1} mm^2 for the single pulse (duty factor 0.04) surface data. The depth of measurement was determined by histological examination of the irradiated skin with a maximum variance of 0.004 mm, attributed to the irregular surface of skin within a sample. The measurements were compared to expected temperatures calculated with an analytical expression.

4.3.1 Temperature Rise per Exposure - Measured

The temperature rise per H in °C mJ^{-1} mm^2 was measured at four depths in pig skin using six different laser pulse patterns. The measured results, shown in Figure 4.7, reveal a different pattern on the surface at low duty factor compared to the measurements below the optical penetration depth. As the duty factor increases, the temperature rise per exposure levels off.

4.3.2 Temperature Rise per Exposure - Calculated

The difference between the temperatures calculated using the Vyas equation for the pulse sequences under consideration and the corresponding measured temperatures are shown in Figure 4.8. Here, the surface temperature calculated was dramatically less than measured for all but the single pulse sequence. Below the surface, the temperatures calculated from the model were higher than measured results. The calculated temperatures at 0.4 mm depth were five to ten °C higher than measured. This corresponds to the measurements at 0.4 mm being equivalent to the temperatures at 0.65 mm seen in Figure 4.7. Calculated temperatures at 0.65 mm depth matched the measured temperatures reasonably well for all duty factors. The model results gave maximum temperatures at depths between 90 μm and 170 μm as shown in Figure 4.9.

4.3.3 Statistical Analysis

Comparing the measured temperatures per exposure between the different pulse sequences, the ANOVA showed that there were significant differences between pulse sequences at each depth at the 95% confidence level. A summary of the p-values and variance within each group are given in Table 4.5. The LSD procedure performed for each depth showed that the differences were between the low duty factor sequences and the high duty factor sequences. The relations between sequences are given in Tables 4.6 through 4.9 for depths from surface to 650 μm. Within each depth's table, the italicized results indicate that the two sequences produced insignificantly different temperature

rise per unit exposure to 2.0 μm laser irradiation. The bold values were found to be statistically different from each other

The different pulse sequences were found to produce statistically different temperature rise per total exposure at all four depths, with p-values less than 0.001 from ANOVA results. At all depths, the 2 pulse, 3 pulse and the 4 pulse sequences were equivalent. The 300 μm and 400 μm depths produced temperatures that were not significantly different in the temperature rise produced between adjoining sequences.

4.4 Discussion

The temperature rise per exposure on the surface was found to follow a different trend at low duty factor (single pulse) than the temperatures measured at depths below the surface. The measurements below the surface represent direct heating as well as heat flow from tissue above. The increase in temperature appears to rise as the duty factor increases for depths below the surface. In contrast, from the IR camera measurements, this trend does not hold for the single pulse (low duty factor) sequence on the surface.

However, as seen in Figure 4.8, the calculated temperatures using the Vyas model demonstrate the model was very good at predicting temperature for 650 μm depth for all duty factors from one pulse up to CW. The model's predicted temperatures were 5° to 10° C high for the 400 μm depth for all duty factors, with the largest difference at the medium duty factor of 0.16. The modeling results using these optical constants confirm the assumption that the skin behaves as a partially turbid medium at 2.0 μm wavelength. The linear superposition of multiple pulses exaggerated the model's difference from measured temperature. At a 300 μm depth in skin, the calculations were

within 1°C for duty factors of 0.16 and higher, but increasingly diverged to 7 °C from measurements at lower duty factors. The divergence of actual from modeled temperatures was unexpected as this model was originally validated with microsecond pulse widths.

The Vyas model did not predict surface temperatures well. For all duty factors, the model predicted a temperature rise which exhibits a buildup from the surface to a maximum and then a decreases with further depth. At shallow depths, either exact skin surface ($z = 0$ μm) or at the depths of calculated maximum temperatures, the model underestimated temperature rise as seen in Figure 4.8. The Vyas model was best at predicting temperatures for the smallest duty factor (0.04). The predicted maximum temperature rise at shallow depth (dashed curve) fell significantly below measured temperatures by approximately 5-7 °C for the middle duty factors (0.08 to 0.16). As the duty factor increased to 0.36 and above, the model underestimated the temperatures by 10 °C. At the air – skin interface ($z = 0$ μm), the predicted temperatures (solid pink curve) were an additional 6 °C lower than camera measurements while following the same pattern as the predictions at the depth of maximum over the range of duty factors. The significantly better agreement of measurements to calculated temperatures near, but not at the air-skin interface, appears to indicate that the IR camera's microbolometer is responding to IR emitted by a region below the skin surface. The Vyas model produced maximum temperatures at increasing depths between 90 μm and 170 μm as seen in Figure 4.9. The disagreement between the model and the measurements becomes larger as the maximum temperature occurs deeper in the skin. This discrepancy is most

significant because it occurs in the region of the basal layer of the epidermis in human skin.

The analysis of measured temperature rise per exposure between pulse sequences of different duty factors showed a significant difference between some of the sequences, but not the same ones at different depths. For the surface and 650 μm depths of Tables 4.4, and 4.7, the measured rise per exposure was found to be statistically different between any combination two sequences including one with a duty factor of 0.04 or above 0.36. The single pulse, the nine pulse and the CW irradiations were different from any other sequence. At 300 μm and 400 μm depths in Tables 4.5 and 4.6, the single pulse sequence was equivalent to the double pulse sequence, but different from all higher duty factors. The 300 μm and 400 μm depths were unique in the temperature rise per exposure relations between sequences of higher duty factor. At 300 μm depth a sequence with duty factor of 0.36 was equivalent to both a CW irradiation and a pulse sequence with duty factor of 0.16. At 400 μm depth, a sequence with duty factor of 0.36 was different from the CW irradiation but equivalent to both a 0.16 and 0.12 duty factor sequence. Therefore, while there were several combinations of pulse sequence duty factors producing equivalent temperature rise per radiant energy, only the 9 pulse sequence with duty factor 0.36 heated the tissue the same as a CW beam at 300 μm. At all depths then, the pulsed beams produced lower temperatures per radiant exposure than did the CW beam for equivalent energy input.

The maximum temperatures measured at the 400 μm and 650 μm depths were virtually the same for all duty factors, all within one standard deviation. By a simple Beer's law calculation, there is at least an order of magnitude difference in incident

beam energy at these two depths. Chen's attenuation coefficient of 21.76 cm^{-1} gives the closest beam intensities at depths of 400 μm and 650 μm from among the various attenuation coefficient values from Table 4.1. This attenuation coefficient used in Vyas's model also predicted temperatures closest to the measurements. Therefore, there appears to be rapid heat transfer in the axial direction to bring the deeper measurements to the same maximum temperature. However, the significant differences between pulse sequences of 0.36 duty factor at 650 μm that are not found at 400 μm indicates that the heat flows fast enough to distinguish each separate pulse at duty factors between 0.04 and 0.36.

The differences in temperature normalized to radiant energy indicates that the assumption of linear superposition of successive pulses does not represent the thermal dynamics of pulsed irradiation of skin for pulse sequences with duty factors between 0.04 and 0.36 at depths from the surface to 650 μm, roughly the middle of the dermis. The ANSI Z136.1 limit of radiant exposure for 250 msec pulse sequences of 2.0 μm IR is $MPE=0.56 \times 0.250^{0.25} = 0.396$ J cm^{-2}, which is roughly ten times less than the maximum exposure of 3.17 J cm^{-2} delivered in this study. It is worth noting that while the exposures delivered in this study were very close to the ED_{50} levels of Chen *et al* [5] for *in-vivo* pig skin (3.6 J cm^{-2} and 2.9 J cm^{-2} for beams of radii of 2.4 mm and 4.8 mm respectively) no reddening of the *ex-vivo* skin was observed. Furthermore, the maximum absolute temperature increase recorded was 36.2 °C from the IR camera surface measurement of an exposure sequence with 0.16 duty factor. The maximum temperature increase for any one exposure beneath the surface was 20.7 °C above background for a 0.16 duty factor sequence at 300 μm depth. This increase is over twice

Moncrief's "brief" temperature tolerated by skin, yet even with no vascular heat removal no damage was observed visually or on the histology slides. Therefore the ANSI Z136.1 limitations for skin exposure are shown to be inherently conservative as they do not apply the "Rule 3" correction factor based on number of pulses to skin. However, a correction factor based on pulse sequence duty factor may be appropriate in this region of the far infrared.

The differences in temperature rise per unit exposure between the pulse sequences can be explained by significant heat conduction during the pulses. Therefore the common assumption of thermal confinement needs to be experimentally verified for a modeled temperature rise to be accepted.

4.5 References

1. T. H. Maiman, "Stimulated optical radiation in ruby," Nature **187** (4736), 493-494 (1960).

2. L. Goldman, D. J. Blaney, D. J. Kindel, and E. K. Franke, "Effect of the laser beam on the skin," Journal of Investigative Dermatology **40** (3), 121-122 (1963).

3. C. H. Powell and L. Goldman, "Recommendations of laser safety conference," Archives of Environmental Health **18** (3), 448-& (1969).

4. American National Standards Institute, "American national standard for safe use of lasers Report" No. ANSI Z136-1-2007, 2007.

5. B. Chen, D. C. O'Dell, S. L. Thomsen, B. A. Rockwell, and A. J. Welch, "Porcine skin ED50 damage thresholds for 2,000 nm laser irradiation," Lasers in Surgery and Medicine **37** (5), 373-381 (2005).

6. A. R. Moritz and F. C. Henriques, "Studies of thermal injury v.2. The relative importance of time and surface temperature in the causation of cutaneous burns," American Journal of Pathology **23** (5), 695-720 (1947).

7. J.A. Moncrief, "The body's response to heat," in *Burns, a team approach*, edited by C. Artz, J.A. Moncrief, and B. Pruitt (Saunders, Philadelphia PA, 1979).

8. E. H. Leach, R. A. Peters, and R. J. Rossiter, "Experimental thermal burns, especially the moderate temperature burn," Quarterly Journal of Experimental Physiology and Cognate Medical Sciences **32**, 67-U20 (1944).

9. R. J. Rockwell Jr and L. Goldman, "Research on human skin laser damage thresholds[final report, nov. 1971- jun. 1974], 1974.

10. R. Hibst and R. Kaufmann, "Effects of laser parameters on pulsed Er-YAG laser skin ablation," Lasers in Medical Science **6** (4), 391-397 (1991).

11. M. Leandri, M. Saturno, L. Spadavecchia, G. D. Iannetti, G. Cruccu, and A. Truini, "Measurement of skin temperature after infrared laser stimulation," Neurophysiologie Clinique-Clinical Neurophysiology **36** (4), 207-218 (2006).

12. B. Bromm and R. D. Treede, "CO-2 laser radiant heat pulses activate c-nociceptors in man," Pflügers Archiv European Journal of Physiology **399** (2), 155-156 (1983).

13. Y. Ito, R. P. Kennan, E. Watanabe, and H. Koizumi, "Assessment of heating effects in skin during continuous wave near infrared spectroscopy," Journal of Biomedical Optics **5** (4), 383-390 (2000).

14. J. Howard, P. Arango, J. Ossoff, R. H. Ossoff, and L. Reinisch, "Healing of laser incisions in rat dermis: Comparisons of the carbon dioxide laser under manual and computer control and the scalpel," Lasers in Surgery and Medicine **20** (1), 90-96 (1997).

15. R. M. Adrian, "Pulsed carbon dioxide and erbium-YAG laser resurfacing: A comparative clinical and histologic study," Journal of Cosmetic and Laser Therapy **1** (1), 29-35 (1999).

16. A. D. Zweig and H. P. Weber, "Mechanical and thermal parameters in pulsed laser cutting of tissue," Ieee Journal of Quantum Electronics **23** (10), 1787-1793 (1987).

17. S. L. Jacques and S. A. Prahl, "Modeling optical and thermal distributions in tissue during laser irradiation," Lasers in Surgery and Medicine **6** (6), 494-503 (1987).

18. J. Roider, F. Hillenkamp, T. Flotte, and R. Birngruber, "Microphotocoagulation - selective effects of repetitive short laser-pulses," Proceedings of the National Academy of Sciences of the United States of America **90** (18), 8643-8647 (1993).

19. N. A. Peppers, "Corneal damage thresholds for CO_2 laser radiation," Applied Optics **8** (2), 377-381 (1969).

20. P. Parsa, S. L. Jacques, and N. S. Nishioka, "Optical-properties of rat-liver between 350 and 2200 nm," Applied Optics **28** (12), 2325-2330 (1989).

21. R. Birngruber, F. Hillenkamp, and V.P. Gabel, "Theoretical investigations of laser thermal retinal injury," Health Physics **48** (6), 781-796 (1985).

22. S. L. Jacques, "Role of tissue optics and pulse duration on tissue effects during high-power laser irradiation," Applied Optics **32** (13), 2447-2454 (1993).

23. J. P. Ritz, A. Roggan, C. Isbert, G. Muller, H. J. Buhr, and C. T. Germer, "Optical properties of native and coagulated porcine liver tissue between 400 and 2400 nm," Lasers in Surgery and Medicine **29** (3), 205-212 (2001).

24. A. Vogel and V. Venugopalan, "Mechanisms of pulsed laser ablation of biological tissues," Chemical Reviews **103** (2), 577-644 (2003).

25. N. P. Furzikov, "Different lasers for angioplasty: Thermo-optical comparison," Journal Name: IEEE J. Quant. Electron.; (United States); Journal Volume: QE-23:10, Medium: X; Size: Pages: 1751-1755 (1987).

26. L. I. Grossweiner, A. M. Alkarmi, P. W. Johnson, and K. R. Brader, "Modeling of tissue heating with a pulsed Nd-YAG laser," Lasers in Surgery and Medicine **10** (3), 295-302 (1990).

27. R. Vyas and M. L. Rustgi, "Green-function solution to the tissue bioheat equation," Medical Physics **19** (5), 1319-1324 (1992).

28. C. Cain, "Measured and predicted laser-induced temperature rises in the rabbit fundus " Investigative Opthalmology and Visual Science **13** (1), 60-70 (1974).

29. D. Schaaf, T. Eurell, and T. Johnson, "Cultured human keratinocytes for optical transmission measurement," Journal of Biophotonics **3** (3), 161-168 (2010).

30. F. Manns, P. J. Milne, X. Gonzalez-Cirre, D. B. Denham, J. M. Parel, and D. S. Robinson, "In situ temperature measurements with thermocouple probes during laser interstitial thermotherapy (litt): Quantification and correction of a measurement artifact," Lasers in Surgery and Medicine **23** (2), 94-103 (1998).

31. C. Cain, "Thin-film temperature sensors for biological measurements," IEEE Transactions of Biomedical Engineering **21** (5), 421-423 (1974).

32. J. W. Valvano and J. A. Pearce, "Temperature measurements," in *Optical thermal response of laser irradiated tissue*, edited by A Welch and M. van Gemert (SPIE, Bellingham WA, 1995), pp. 518.

33. G. M. Hale and M. R. Querry, "Optical-constants of water in 200-nm to 200-mum wavelength region," Applied Optics **12** (3), 555-563 (1973).

34. B. Chen, S. L. Thomsen, R. J. Thomas, and A. J. Welch, "Modeling thermal damage in skin from 2000-nm laser irradiation," Journal of Biomedical Optics **11** (6) (2006).

35. P. J. Shayler, "Laser-beam distribution in focal region," Applied Optics **17** (17), 2673-2674 (1978).

36. J. J. Crochet, S. C. Gnyawali, Y. C. Chen, E. C. Lemley, L. H. V. Wang, and W. R. Chen, "Temperature distribution in selective laser-tissue interaction," Journal of Biomedical Optics **11** (3) (2006).

37. T. S. Sandhu, "Measurement of blood-flow using temperature decay - effect of thermal conduction," International Journal of Radiation Oncology Biology Physics **12** (3), 373-378 (1986).

38. L. O. Svaasand, T. Boerslid, and M. Oeveraasen, "Thermal and optical-properties of living tissue - application to laser-induced hyperthermia," Lasers in Surgery and Medicine **5** (6), 589-602 (1985).

39. C. P. Cain, K. J. Schuster, J. J. Zohner, K. L. Stockton, D. J. Stolarski, R. J. Thomas, B. A. Rockwell, and W. P. Roach, "Visible lesion thresholds with pulse duration, spot size dependency, and model predictions for 1.54-mu m, near-infrared laser pulses penetrating porcine skin," Journal of Biomedical Optics **11** (2) (2006).

40. A. Jain, M. S. Blumenkranz, Y. Paulus, M. W. Wiltberger, D. E. Andersen, P. Huie, and D. Palanker, "Effect of pulse duration on size and character of the lesion in retinal photocoagulation," Archives of Ophthalmology **126** (1), 78-85 (2008).

41. J. M. Garden, O. T. Tan, R. Kerschmann, J. Boll, H. Furumoto, R. R. Anderson, and J. A. Parrish, "Effect of dye-laser pulse duration on selective cutaneous vascular injury," Journal of Investigative Dermatology **87** (5), 653-657 (1986).

42. K. A. Khatri, "The effects of variable pulse width of Er:YAG laser on facial skin," Dermatologic Surgery **27** (4), 332-334 (2001).

43. E. V. Ross, J. R. McKinlay, F. P. Sajben, C. H. Miller, D. J. Barnette, K. J. Meehan, N. P. Chhieng, M. J. Deavers, and B. D. Zelickson, "Use of a novel Erbium laser in a yucatan minipig: A study of residual thermal damage, ablation, and wound healing as a function of pulse duration," Lasers in Surgery and Medicine **30** (2), 93-100 (2002).

44. E. D. Jansen, T. H. Le, and A. J. Welch, "Excimer, Ho-YAG, and q-switched Ho-YAG ablation of aorta - a comparison of temperatures and tissue-damage invitro," Applied Optics **32** (4), 526-534 (1993).

45. M. A. Trelles, S. Mordon, V. Benitez, and J. L. Levy, "Er:YAG laser resurfacing using combined ablation and coagulation modes," Dermatologic Surgery **27** (8), 727-734 (2001).

46. R. E. Fitzpatrick, S. R. Smith, and S. Sriprachya-anunt, "Depth of vaporization and the effect of pulse stacking with a high-energy, pulsed carbon dioxide laser," Journal of the American Academy of Dermatology **40** (4), 615-622 (1999).

47. J. Spiegel, C. Hansen, and R.D. Treede, "Clinical evaluation criteria for the assessment of impaired pain sensitivity by thulium-laser evoked potentials," Clinical Neurophysiology **111** (4), 725-735 (2000).

48. A. N. Bashkatov, E. A. Genina, V. I. Kochubey, and V. V. Tuchin, "Optical properties of human skin, subcutaneous and mucous tissues in the wavelength range from 400 to 2000 nm," Journal of Physics D Applied Physics **38** (15), 2543-2555 (2005).

49. T. L. Troy and S. N. Thennadil, "Optical properties of human skin in the near infrared wavelength range of 1000 to 2200 nm," Journal of Biomedical Optics **6**, 167 (2001).

50. R. R. Anderson and J. A. Parrish, "The optics of human-skin," Journal of Investigative Dermatology **77** (1), 13-19 (1981).

51. F. Xu, T. J. Lu, and K. A. Seffen, "Biothermomechanical behavior of skin tissue," Acta Mechanica Sinica **24** (1), 1-23 (2008).

52. T. J. Pfefer, D. J. Smithies, T. E. Milner, M. J. C. van Gemert, J. S. Nelson, and A. J. Welch, "Bioheat transfer analysis of cryogen spray cooling during laser treatment of port wine stains," Lasers in Surgery and Medicine **26** (2), 145-157 (2000).

53. T. R. Gowrishankar, D. A. Stewart, G. T. Martin, and J. C. Weaver, "Transport lattice models of heat transport in skin with spatially heterogeneous, temperature-dependent perfusion," Biomed Eng Online **3** (1), 42 (2004).

54. A. M. Stoll, "Thermal-properties of human-skin related to nondestructive measurement of epidermal thickness," Journal of Investigative Dermatology **69** (3), 328-332 (1977).

55. M. L. Cohen, "Measurement of thermal-properties of human-skin - review," Journal of Investigative Dermatology **69** (3), 333-338 (1977).

56. H. F. Bowman, E. G. Cravalho, and M. Woods, "Theory, measurement, and application of thermal properties of biomaterials," Annual Review of Biophysics and Bioengineering **4** (1), 43-80 (1975).

57. B. Anvari, T. E. Milner, B. S. Tanenbaum, and J. S. Nelson, "A comparative study of human skin thermal response to sapphire contact and cryogen spray cooling," Ieee Transactions on Biomedical Engineering **45** (7), 934-941 (1998).

58. Z. S. Deng and J. Liu, "Analytical study on bioheat transfer problems with spatial or transient heating on skin surface or inside biological bodies," Journal of Biomechanical Engineering-Transactions of the ASMA **124** (6), 638-649 (2002).

59. O. S. Khalil, S. Yeh, M. G. Lowery, X. Wu, C. F. Hanna, S. Kantor, T. W. Jeng, J. S. Kanger, R. A. Bolt, and F. F. de Mul, "Temperature modulation of the

visible and near infrared absorption and scattering coefficients of human skin," Journal of Biomedical Optics **8** (2), 191-205 (2003).

60. J. A. Parrish, R. R. Anderson, T. Harrist, B. Paul, and G. F. Murphy, "Selective thermal effects with pulsed irradiation from lasers - from organ to organelle," Journal of Investigative Dermatology **80**, S75-S80 (1983).

61. B. Choi, J. A. Pearce, and A. J. Welch, "Modelling infrared temperature measurements: Implications for laser irradiation and cryogen cooling studies," Physics in Medicine and Biology **45** (2), 541-557 (2000).

62. M. K. Loze and C. D. Wright, "Temperature distributions in laser-heated biological tissue with application to birthmark removal," Journal of Biomedical Optics **6** (1), 74-85 (2001).

63. V.V. Tuchin, *Tissue optics*, 2nd ed. (SPIE Press, Bellingham WA, 2007).

64. J. C. Chato, "Selected thermophysical properties of biological materials," in *Heat transfer in medicine and biology*, edited by A Shitzer and R. C. Eberhart (Plenum Press, New York NY, 1985), pp. 413-418.

65. M. Lipkin and J. D. Hardy, "Measurement of some thermal properties of human tissues," Journal of Applied Physiology **7** (2), 212-217 (1954).

66. J. C. Chato, "Thermal properties of tissues," in *Handbook of bioengineering*, edited by R. Skalak and S. Chien (McGraw-Hill, New York NY, 1987).

Table 4.1. Sampling of laser pulse sequence manipulation studies.

Variable	Change	Constant	Result	Wavelength (μm)	Study
Pulse Width	Reduced t_p	Equal tissue damage	Required H reduced	1.5	39
				0.532	40
				0.577	41
Pulse Width	Increase t_p	Equal radiant energy	No change in depth of coagulation	2.94	42
Pulse Width	Increase t_p	Equal radiant energy	Increase depth of coagulation	2.94	43
				2.94	15
PRF	Increase PRF	Equal radiant energy	Reduced temperature	2.09	44
PRF	Reduce PRF	Equal radiant energy	Change effect from ablation to coagulation	2.94	45
PRF	Increase PRF	Equal radiant energy	Increase ablation depth	2.94	10
Number of pulses	Increase N_p	Equal radiant energy	Increase depth of injury	10.6	46

Table 4.2 Optical penetration depth [mm], using published constants and optical zone for beam with a $1/e^2$ radius of 3.28 mm.

μ_a [cm^{-1}]	μ_s' [cm^{-1}]	Optical Penetration Depth, δ	Optical Zone, *d* Depth	Radial	Study
Absorption					
21.76*		0.460	0.460	0.460	[34]
28		0.357	0.357	0.357	[47]
58.02**		0.172	0.172	0.172	[34]
Turbid					
1.75	13.25	1.127	2.209	2.017	[48]
48	10	0.109	0.214	0.214	[49]
82	10	0.066	0.130	0.130	[50]

* absorption coefficient for epidermis, ** absorption coefficient for dermis

Table 4.3 Thermal constants of human and pig skin.

Tissue (depth or specifier)	Conductivity κ $W\ m^{-1}\ ^oC^{-1}$	Diffusivity D $m^2\ sec^{-1}$	Density ρ $g\ cm^{-3}$	Specific Heat C $J\ kg^{-1}\ ^oC^{-1}$	Year
Human					
stratum corneum	0.235		1.5	3600	2008 [51]
epidermis	0.21			3600	2000 [52]
epidermis	0.2			2244	2006 [34]
epidermis	0.23		1.2	3590	2004 [53]
epidermis	0.235		1.190	3600	2008 [51]
epidermis (forearm)	0.569				1977 [54]
epidermis (in vitro)	0.209				1977 [55]
dermis	0.53			3800	2000 [52]
dermis	0.49			3663	2006 [34]
dermis	0.45		1.2	3300	2004 [53]
dermis	0.445		1.116	3680	2008 [51]
dermis (forearm)	0.837				1977 [54]
dermis (in vitro)	0.293				1977 [55]
skin	0.23 - 0.414				1975 [56]
skin	0.45	1.10×10^{-7}			1998 [57]
skin	0.5			4200	2002 [58]
skin	0.39		1.116	3200	2003 [59]
skin		1.30×10^{-7}			1983 [60]
skin	0.37		1	4180	2000 [61]
skin	0.53				2001 [62]
skin (0.26 mm)		0.4×10^{-7}			1975 [56]
skin (0.45 mm)		0.6×10^{-7}			1975 [56]
skin (0.90 mm)		0.85×10^{-7} - 1.20×10^{-7}			1975 [56]
skin (0-2 mm)	0.376				1975 [56]
skin	0.56		1.07	3400	2006 [36]
skin (in vitro)		0.82×10^{-7} - 1.2×10^{-7}			2000 [63]
skin (in vitro)	0.21 - 0.41	0.82×10^{-7} - 1.2×10^{-7}			1985 [64]
skin (in vitro)	0.293		1.2	3389	1954 [65]
skin (in vivo)	0.5 – 2.8	0.4×10^{-7} – 1.6×10^{-7}			1987 [66]
tissue		1.20×10^{-7}			1985 [38]
tissue	0.44		1.070	3500	1986 [37]
Animal					
pig epidermis, in vitro	0.209				1977 [55]
pig skin, opaque	0.414	0.82×10^{-7} - 0.86×10^{-7}			1975 [56]

Table 4.4 Thermal relaxation times, τ, for 2.0 μm light in both depth and radial direction using published constants [sec].

μ_a [cm^{-1}]	μ_s' [cm^{-1}]	Slow Thermal Diffusivity* Depth	Radial	Fast Thermal Diffusivity* Depth	Radial	Study
Absorption						
21.76**		5.28	5.28	1.32	1.32	34
28		3.19	3.19	0.80	0.80	47
58.02***		0.74	0.74	0.19	0.19	34
Turbid						
1.75	13.25	121.90	101.70	30.5	25.4	48
48	10	1.10	1.15	0.29	0.29	49
82	10	0.42	0.42	0.11	0.11	50

*Fast $D = 4 \times 10^{-4}$ cm^2 sec^{-1} from Bowman[56], Slow D = 1.6×10^{-3} cm^2 sec^{-1} from Chato[66];
** epidermis; ***dermis

Table 4.5 ANOVA results

Depth	p-value	S_w^2
Surface	1.47×10^{-23}	0.00874
300 μm	0.000914	0.00875
400 μm	0.000852	0.00290
650 μm	8.07×10^{-10}	0.00073

Table 4.6 Significant Difference in Temperature per Exposure at Surface (significant differences in bold, differences less than Fisher's LSD, 0.031, are in italics)

Pulse Sequence	1 pulse	2 pulse	3 pulse	4 pulse	9 pulse	25 (CW)
1 pulse	--	**-0.16**	**-0.14**	**-0.13**	**-0.07**	**0.04**
2 pulse	**0.16**	--	*0.02*	*0.02*	**0.09**	**0.19**
3 pulse	**0.14**	*-0.02*	--	*0.01*	**0.07**	**0.18**
4 pulse	**0.13**	*-0.02*	*-0.01*	--	**0.07**	**0.17**
9 pulse	**0.07**	**-0.09**	**-0.07**	**-0.07**	--	**0.10**
25 (CW)	**-0.04**	**-0.19**	**-0.18**	**-0.17**	**-0.10**	--

Table 4.7 Significant Difference in Temperature per Exposure at 0.30 mm (significant differences in bold, differences less than Fisher's LSD, 0.054, are in italics)

Pulse Sequence	1 pulse	2 pulse	3 pulse	4 pulse	9 pulse	25 (CW)
1 pulse	--	*0.03*	**0.06**	**0.07**	**0.12**	**0.15**
2 pulse	*-0.03*	--	*0.03*	*0.05*	**0.09**	**0.12**
3 pulse	**-0.06**	*-0.03*	--	*0.01*	**0.06**	**0.09**
4 pulse	**-0.07**	*-0.05*	*-0.01*	--	*0.05*	**0.08**
9 pulse	**-0.12**	**-0.09**	**-0.06**	*-0.05*	--	*0.03*
25 (CW)	**-0.15**	**-0.12**	**-0.09**	**-0.08**	*-0.03*	--

Table 4.8 Significant Difference in Temperature per Exposure at 0.40 mm (significant differences in bold, differences less than Fisher's LSD, 0.031, are in italics)

Pulse Sequence	1 pulse	2 pulse	3 pulse	4 pulse	9 pulse	25 (CW)
1 pulse	--	*0.01*	**0.03**	**0.04**	**0.05**	**0.09**
2 pulse	*-0.01*	--	*0.02*	*0.03*	**0.05**	**0.08**
3 pulse	**-0.03**	*-0.02*	--	*0.01*	*0.02*	**0.06**
4 pulse	**-0.04**	*-0.03*	*-0.01*	--	*0.02*	**0.05**
9 pulse	**-0.05**	**-0.05**	*-0.02*	*-0.02*	--	**0.03**
25 (CW)	**-0.09**	**-0.08**	**-0.06**	**-0.05**	**-0.03**	--

Table 4.9 Significant Difference in Temperature per Exposure at 0.65 mm (significant differences in bold, differences less than Fisher's LSD, 0.015, are in italics)

Pulse Sequence	1 pulse	2 pulse	3 pulse	4 pulse	9 pulse	25 (CW)
1 pulse	--	**0.03**	**0.04**	**0.04**	**0.06**	**0.09**
2 pulse	**-0.03**	--	*0.00*	*0.01*	**0.03**	**0.05**
3 pulse	**-0.04**	*0.00*	--	*0.00*	**0.03**	**0.05**
4 pulse	**-0.04**	*-0.01*	*0.00*	--	**0.02**	**0.04**
9 pulse	**-0.06**	**-0.03**	**-0.03**	**-0.02**	--	**0.02**
25 (CW)	**-0.09**	**-0.05**	**-0.05**	**-0.04**	**-0.02**	--

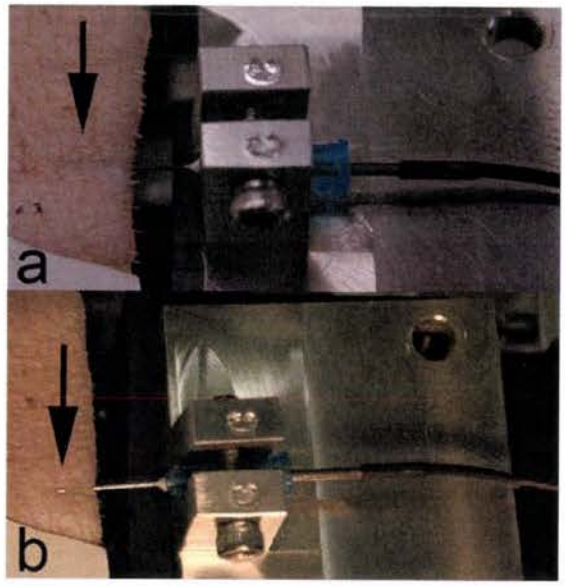

Figure 4.1 Needle insertion into pig skin; (a) successful placement of probe, (b) needle has re-surfaced. Also in (b) the HYP-0 thermocouple can be seen entering the 25 g needle.

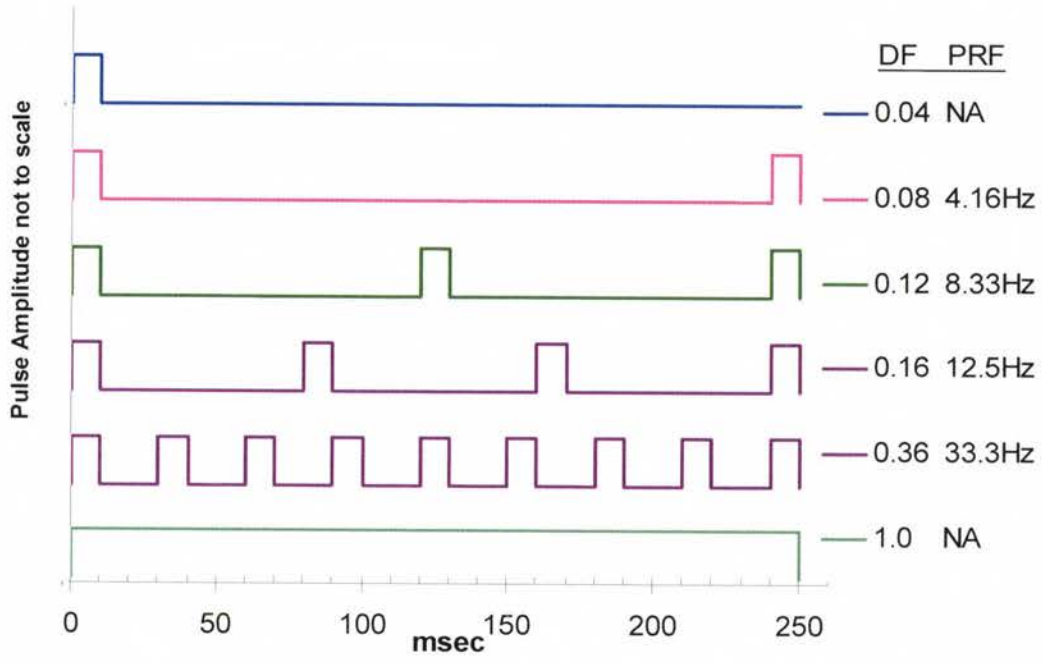

Figure 4.2 TTL signal laser pulse sequences, with duty factors (DF) and pulse repetition frequencies (PRF) listed.

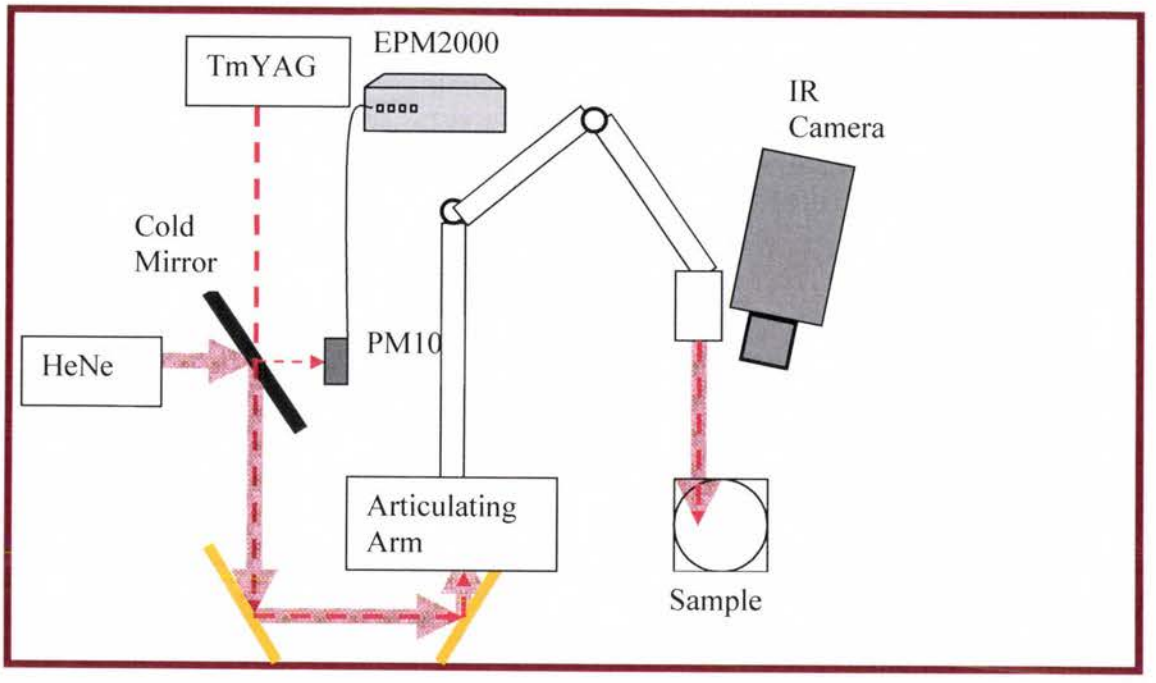

Figure 4.3 Optics path, IR beam is dashed, red positioning beam is gray. The "Cold Mirror" is highly reflective to visible light while transparent (>98% transmission) to IR. The small reflection is measured by the PM10 probe with the EPM2000 meter to record the exposure energy of each irradiation.

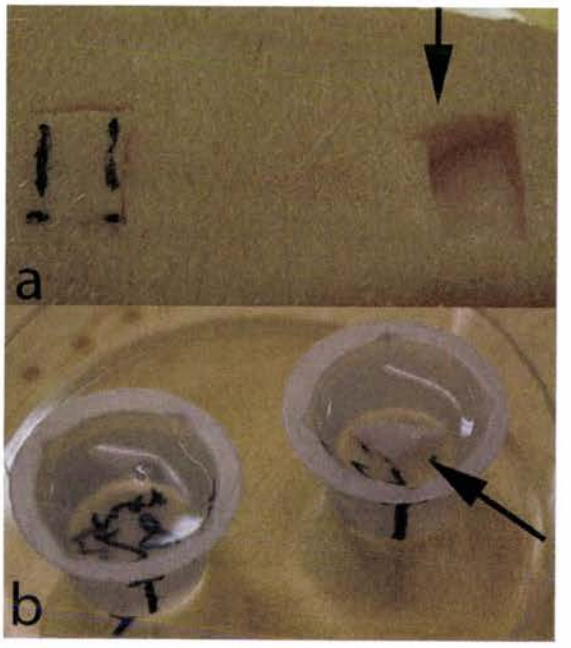

Figure 4.4 Pig skin after exposure during preparation for freezing, (a) needle insertion marked with ink on left and sample cut out on right; (b) inked and cut sample in OCT solution in labeled freezing cup on right, at left is OCT for unexposed skin.

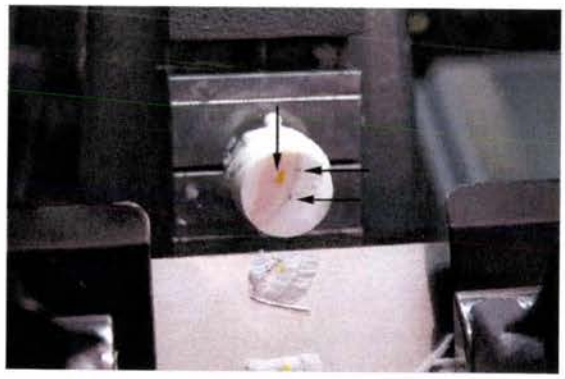

Figure 4.5 Pig skin sample frozen in OCT mounted in the microtome. Note the black ink marks visible on the surface (horizontal arrows) and the large yellow dye spot (vertical arrow) from excessive pressure on the syringe during needle withdrawal (yellow dye from successful injection yields inadequate contrast to identify in photographs).

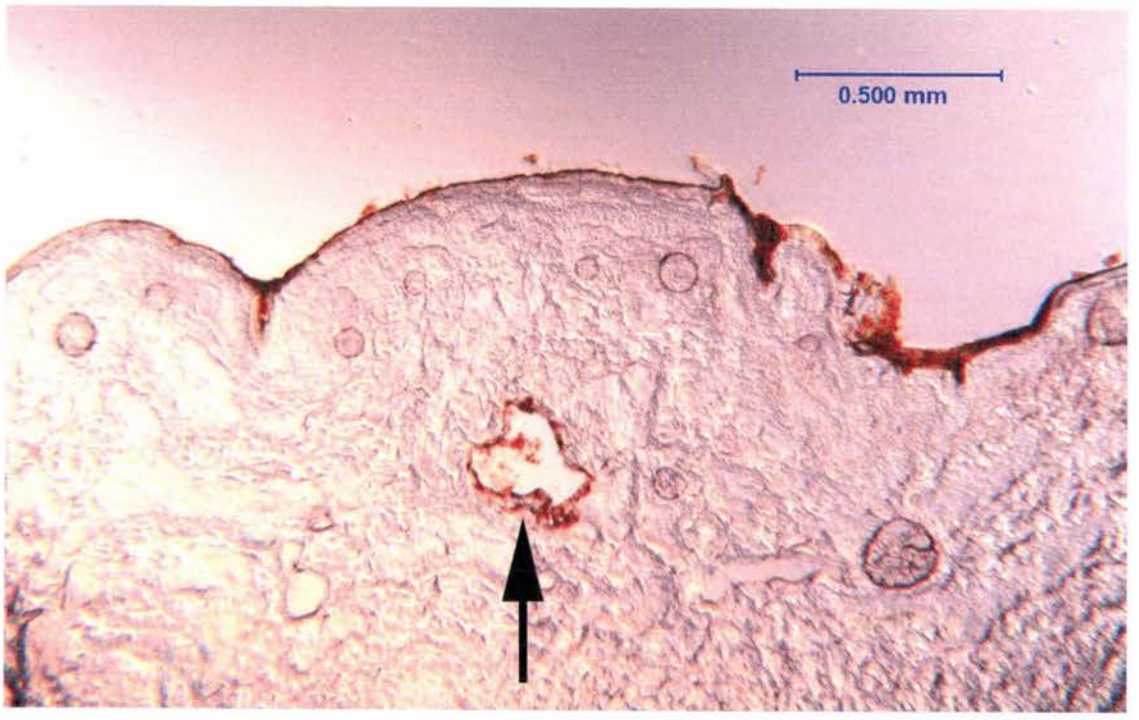

Figure 4.6 Histology image of pigskin showing the dye marked thermocouple probe hole (arrow) and the ink marked surface (ink appears brown in the two valleys on either side of the hole).

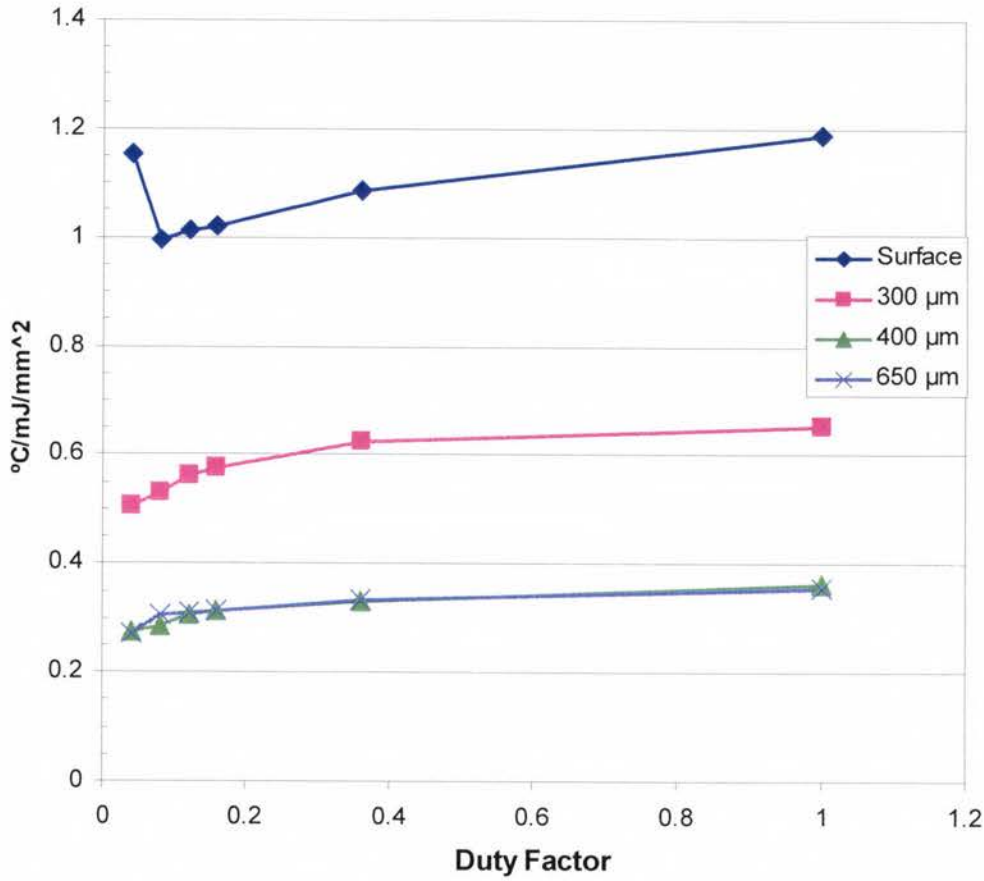

Figure 4.7 Graph of measured temperature rise per exposure at four depths in pig skin versus duty factor of the pulse sequence.

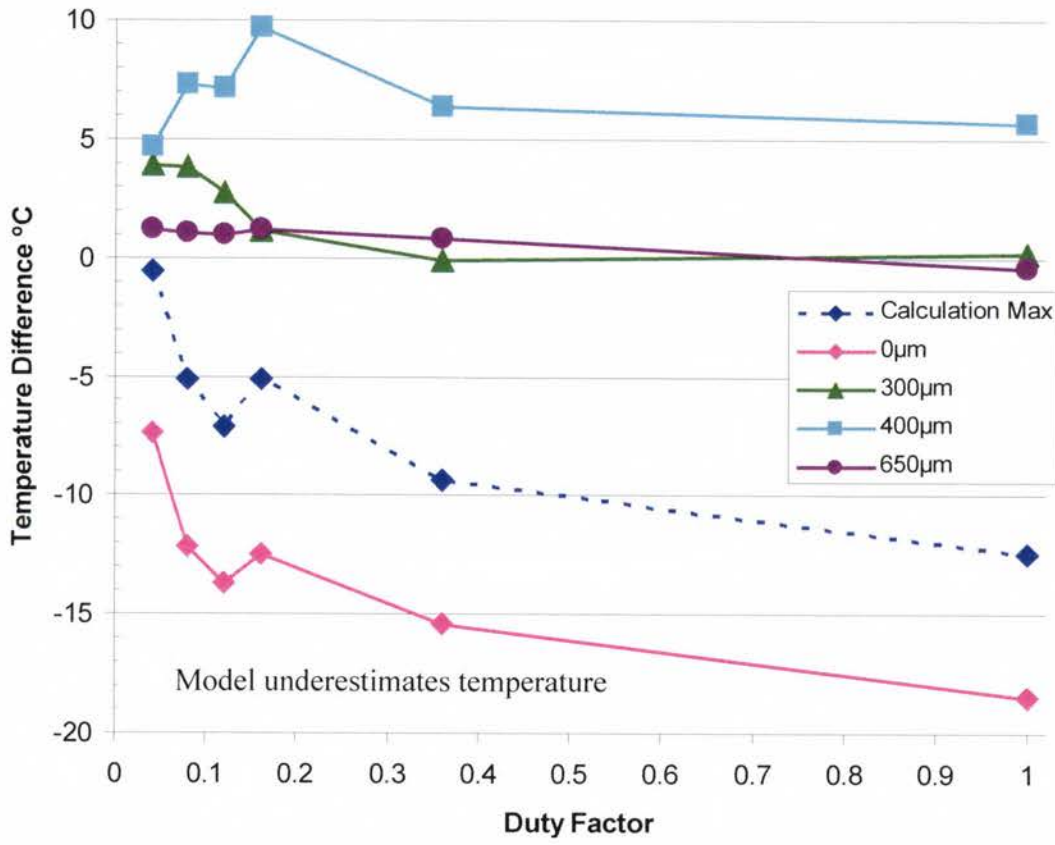

Figure 4.8 Difference between calculated and measured temperature rise for exposures used in study. Calculation maximum temperature and the calculated zero depth temperatures are compared to IR camera measurements while temperatures at depth relate to thermocouple measurements. The depths of the calculated maximum temperatures are given in Figure 9.

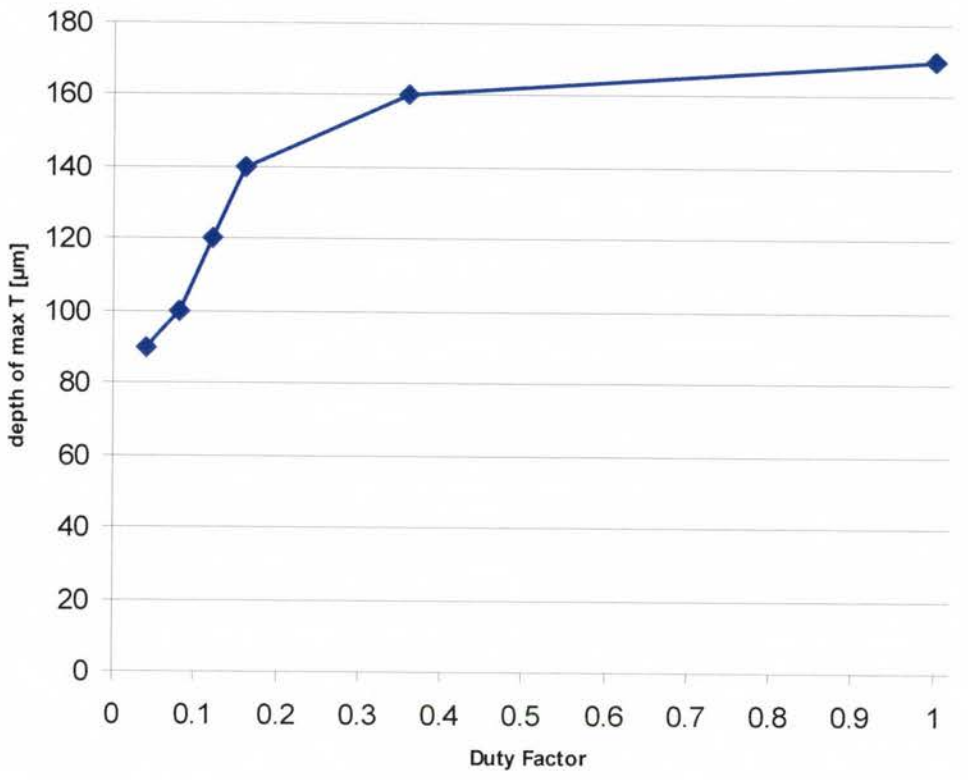

Figure 4.9 Calculated skin depth of maximum temperature from exposure to Tm:YAG laser.

Chapter 5

Temperature Rise Modeling Comparison with Measurements in Pig Skin Irradiated with a Tm:YAG Laser

5.0 Abstract

The risk of injury to skin is a function of both time and temperature. In order to determine the risk of injury to skin, measurements of the specific conditions of laser irradiation can be made. Otherwise, a model can be used to predict the temperature. However, the model must be shown to apply to the type of irradiation under consideration. Prior models have considered two conditions; a continuous wave irradiation or a single pulse treated as a delta function impulse. This chapter will evaluate the accuracy of a Green's function solution to the heating of tissue interfaced to air with respect to measured temperatures for 2.0 μm infrared laser on skin when the pulses approach thermal diffusion time. From among the many published optical and thermal properties of skin, those that best predict measured results were determined.

5.1 Introduction

In the interest of preventing skin injury from invisible infrared laser light, it is normal in the United States to calculate the Maximum Permissible Exposure by the methodology of the American National Standards Institute.[1] However, for a wavelength of 2.0 μm from a Tm:YAG laser, this safety evaluation method provides an approximate

value for the energy level one tenth of the ED_{50}, the exposure expected to produce lesions in 50% of the irradiations and is based on little experimental data.[2]

On a macroscopic scale, thermal damage to skin is known to be a product of time, temperature and depth in Dermatology.[3] Studies at the cellular level have identified specific temperatures for particular skin effects. Thomsen gives a 40 °C – 45 °C range for reversible cell injury, while above this range of temperatures cell death is reported to result from deactivation of enzymes.[4] For one particular strain of cells, the critical temperature for death has been found to be 46.3 °C.[5] An early study of laser heating proposed loss of cellular water with denaturation and coagulation of cellular proteins as the mechanisms of injury.[6] Additional causes of cellular damage were identified as melting of membrane lipids between 20 °C and 40 °C, denaturation of the ribosome at 47 °C, and melting of tRNA at 75 °C.[7] Another study identifies the nuclear matrix as the target for cell killing at 43 – 45 °C.[8] Skin death at the cell level has also been reported in terms of IR laser radiant exposure for a Ho:YAG laser (λ=2.1 μm) to be 9.6 J cm^{-2}.[9] Other authors have investigated the laser irradiation of tissue from the opposite perspective and found that temperatures under 43 °C will produce no irreversible damage of normal tissue.[10] The cornea of the eye has been reported to have a damage threshold of 44 °C.[11] Another identified effect of raised tissue temperature is vascular destruction in tumors at 42.5 °C.[12] On the cellular level, the time and temperature relation can work in reverse to produce a thermotolerance when temperatures are raised to less than 42 °C for extended periods.[13]

Thermal skin damage is also attributed to the denaturation of the collagen support matrix, though studies disagree on the temperature for damage. Collagen

damage has been reported to begin at 45 °C and collagen breakage at 57 °C.[14] Later the same authors report 60 °C is required to start collagen denaturation and subsequent fracture point at 65 °C.[15] Another study puts the initial change of collagen at 54 °C.[16] Still others claim that collagen denaturation is governed by both temperature and time, and also influenced by hydration and variety of chemicals in its environment.[17]

The behavior of collagen is of great interest to the medical laser community. Heating the dermis to sub-lethal temperatures has been found to stimulate growth of new collagen fibers, which is one approach to wrinkle reduction.[18] This has prompted studies to optimize laser instruments for heating of deep dermal layers, often with pulse sequences in the range of this study (4 Hz to 33 Hz). For example, Majaron et al studied pulse sequences of 10 Hz and 33 Hz pulse an Er:YAG (λ=2.9 μm) laser.[19] Ophthalmic laser procedures are also interested in the collagen response of heating the cornea. The shrinkage of collagen prior to denaturation is a primary cause of refractive change.[20,21] Oncologists have begun to use laser energy delivered via an optical fiber with a wavelength appropriate diffuser implanted in a tumor. Temperatures of 69.7 °C were found to coagulate the tumor without charring.[22] The ability of IR lasers to precisely heat collagen has created many new surgical and dermatological procedures benefiting many people.

The popularity of laser procedures has led to multiple studies on the process of laser light conversion to heat in the form of vibrational, rotational, and translational energy.[23] But lasers can deliver such intense pulses of energy that other methods of dissipation may occur such as acoustic and mechanical waves.[24] Further complicating the energy transfer is the specific optical properties of individual tissues with varying

wavelengths of light. The small difference in wavelength between the Ho:YAG (λ=2.1 μm) and the Tm:YAG (λ=2.0 μm) has been shown in an ablation study to require different amounts of total energy per volume of tissue removal.[25] Another confounding factor is the tissue's tendency to change optical behavior during a laser pulse as the energy is being delivered. One study proposed that the cause of the dynamic optical absorption rate the change is alterations of the hydrogen-bonding structure as the energy is delivered.[26] Rastegar et al attempted to characterize the changes in optical properties during a laser pulse with an analytical integral of energy during the pulse.[27] Another study identifies the optimal OH bond energy absorption band at a wavelength of 1.9 μm.[28]

Many attempts have been made to devise models for predicting temperature rise from laser irradiations. Some approach from the optical perspective of absorption and scatter of light in a medium using Monte Carlo methods.[29-30] Another approach is from a thermodynamic viewpoint, starting with the Pennes tissue bioheat equation, shown here in the Oane et al format in cylindrical coordinates as Equation 5.1.[31-32]

$$\frac{\partial^2 T}{\partial r^2}+\frac{1}{r}\frac{\partial T}{\partial r}+\frac{\partial^2 T}{\partial z^2}+\frac{1}{D}\frac{\partial T}{\partial t} = -\frac{A(r,\varphi,z,t)}{k} \qquad (5.1)$$

Here T is the temperature rise, r radial distance, z is the depth beyond the air-tissue boundary, D is the thermal diffusivity, and k is the thermal conductivity. The differential equation is usually solved with a Green's function in cylindrical coordinates following the first attempt by Mainster.[33] Several of these solutions have been evaluated in the visible portion of the spectrum.[34] Other studies have attempted to verify a Green's

function solution without presenting the formula.[11,35] A third approach to modeling laser tissue interactions is the optical thermal diffusion approximation to radiative transfer.[36-39]

Both macroscopic and microscopic analysis of skin injury identifies specific temperatures, accompanied by the time maintained at the temperature, as predictive of injury. Therefore, precise knowledge of induced temperatures is needed for planning IR laser irradiations of skin. However, the use of tissue optical parameters currently published is controversial as Graaf et al state "most of the published data did not prove to be appropriate when applied to data from *in vivo* measurements."[40] The validity of the values of constants combined with the wide variance of published optical parameters for tissue in the mid-infrared wavelengths raises doubts to modeled temperatures without experimental confirmation. The additional complication of delivering the energy for heat in short and repetitive pulses, possibly nullifying some of the modeling assumptions, leads to the conclusion that experimental measurements are necessary for validating models under specific conditions.[41]

5.2 Materials and Methods

5.2.1 Laser and Optics

Irradiations were performed with a commercial 50 W Tm:YAG fiber laser (IPG Photonics, Oxford MA) producing a 2.01 μm wavelength beam. The irradiations consisted of six medium duty cycle pulse sequences contained within a period of 250 msec. Two different beam sizes were investigated. The laser pulse sequences were created by two model 33120A 15 MHz digital waveform generators (Hewlett Packard,

Englewood CO) connected in series to control the duration and number of laser pulses respectively. A single 10 ms laser pulse was created by setting the first waveform generator to deliver a single 50 Hz square wave pulse, and offsetting the voltage by half the amplitude, thereby generating a TTL signal that served as a trigger for the laser pump diodes. The six pulse sequences were repetitions of the 10 msec single pulses as triggered by the second waveform generator which was set to the desired PRF (see Figure 5.1 for illustration of the multi-pulse sequence timing). The 50 W laser power was adjusted for the number of pulses in a sequence to produce an approximately equal total energy for each sequence.

The 2.01 μm laser pulses were aligned to be colinear with a commercial HeNe laser (model 05-LLR-811, Melles-Griot, Carlsbad, CA) using a dual-axis adjustable cold mirror (model PF20-03-M01, ThorLabs, Newton NJ) with specified transmission greater than 98% from 1 μm to 5 μm. The alignment was established by removing the first gold mirror so the beam could travel over 3 meters to the wall. Coincidence of the red HeNe and the invisible Tm:YAG beams was found with commercial thermally active Zap-It paper (Kentek, Pittsfield NH). This model HeNe was selected in part for the low divergence of its beam at 1.7 mrad in the far field. The red HeNe beam was essential to the laser operator for aiming the beam. The co-linear beams were then steered into a custom optical articulating arm assembly (Oxid Corp. Farmington Hills, MI) with a pair of adjustable gold mirrors which reflect both visible and IR. This arm used seven articulating joints with gold mirrors to allow both the visible and IR beams to be directed to the target safely. The laser path and optics are diagramed in Figure 5.2.

The 2% of the IR beam reflected by the HeNe alignment mirror was measured and recorded for each exposure of the sample. The IR laser output from the articulating arm was calibrated to the split beam sample prior to each exposure session. A total of 21 exposures were simultaneously measured by both the sampling probe and another probe placed on the optical stage in place of the skin sample. The beam probes were PM10 air-cooled thermopile sensors (Coherent, Santa Clara CA) calibrated by the manufacturer with an uncertainty of ± 1 %. The sensors were read by an EPM2000 model meter (Coherent, Santa Clara CA). The meter was also calibrated by the manufacturer with a stated resolution of ± 0.03% of full scale reading. The beam output and sampling data points covered laser settings from 30 % to 100 % output and were fit to a straight line with a correlation coefficient greater than 0.98 without forcing the intercept to zero. This provided a high confidence in the calculated beam energy for each exposure.

The IR beam incident on the sample had a Gaussian shape with a 3.2 mm $1/e^2$ radius using a pinhole technique in both directions.[42] Beam width was measured in both directions on five occasions throughout the study with a standard deviation of 0.33 mm between all results. Beam shape was confirmed to be uniform, circular in the lowest order TEM mode, and aligned with the HeNe beam with Zap-It thermal paper (Kentek, Pittsfield NH) prior to each measurement session. Exposures were made on the thermal paper prior to the beam entering the armature and after the beam exiting the arm at the level of the skin sample. The thermal paper impressions were then visually compared to previous sessions' marks to identify any changes. The thermal paper exposures were performed using a four-pulse sequence with the laser set to 50% power to produce

reasonable beam patterns both entering and exiting the articulating arm with the same laser settings.

The IR beam was expanded for irradiation of one sample with a pair of lenses made from BK7 glass (ThorLabs, Newton NJ) which is chosen for its ability to transmit and refract IR light, as shown in Figure 5.4. The 25 mm diameter plano-convex lenses were mounted at a separation of their combined nominal focal distances on rails to fix their planar surfaces parallel to ensure a uniform collimated beam exiting the system, as seen in Figure 5.5 where the lenses are fixed beneath the articulating arm. A $1/e^2$ radius of 6.3 mm was measured with the pin-hole method just prior to beam output calibration for sample irradiation.

5.2.2 Temperature Measurements

Temperature measurements on the beams' central axis (CAX) were taken at depths ranging from 204 μm to 1,145 μm in *ex-vivo* pig skin. A total of 22 samples were measured on the CAX. Temperature measurements across the beams' profiles were performed on 22 samples at depths ranging from 0.1 mm to 0.6 mm.

The pig skin sample and holder with thermocouple fixed in place was centered in the beam of the 2.0 μm laser by scanning the probe through the beam on a 2D optical stage with a micrometer (model TXS, Melles-Griot, Albuquerque, NM) in 500 μm increments first in the N-S direction and then in the E-W direction. The measurements at central axis (CAX) of the IR beam were repeated four times for each pulse sequence on each sample of pig skin. The temperature measurements along beam profile were taken at radial increments of 0.5 mm on each side of CAX and also at 0.25 mm from

CAX out to 4 mm. Temperature profile measurements of the expanded beam were taken at 0.5 mm increments out to 6 mm. The measurements of the first pulse sequence were repeated another four times at the conclusion of a measurement session in order to confirm that the skin conditions had not changed during the measurements.

Temperatures were measured with two instrument systems: an infrared micro-bolometer array for skin surface measurements and a type T (Copper-Constantan) micro-thermocouple for below-surface depths. The model S65HSV thermal imaging camera (FLIR Systems, Wiesbaden Germany) was composed of a 320 × 240 array of uncooled microbolometer detectors. The camera sensitivity was calibrated at 0.05 °C with an accuracy specification of ± 2 °C. Image sequences were collected and sent to a PC (XPS, Dell, Round Rock TX) at a rate of 60 Hz, giving a temporal resolution of 17 msec per data point. The images were read and analyzed using Reasercher Pro version 2.8 (FLIR Systems, Wiesbaden Germany) which offers region-of-interest and line-profile extraction. The camera is sensitive in the spectral range of 7.5 to 13 μm. The lens has a minimum focusing distance of 0.3 m, with a quoted spatial resolution of 1.1 mrad of divergence. The thermal camera was positioned in the same location for all exposures at one meter from the skin surface, approximately 30° from normal to the skin in the E-W direction in order to not interfere with the beam delivery arm. The camera was calibrated by the manufacturer using NIST traceable blackbody sources.

The model HYP-0 thermocouple (Omega Engineering, Stamford CT) consisted of the thermocouple junction imbedded in the tip of a stainless steel 33 gauge hypodermic needle. The outer diameter of the needle was 200 μm. The thermocouple probe was inserted in the pig skin in the N-S direction. The thermocouple response was

recorded using iNet software (Omega Engineering Inc., Stamford CT). The iNET settings were 150 readings per second, with the noise filter set to exclude signals over 200 Hz, signal integrate time set to 0.001 second, with 4,000 readings collected for 26 seconds of monitoring. The iNet system recording was initiated by the same pulse triggering the laser via connection to the output of the HP model 33120A waveform generator (Hewlett Packard, Palo Alta CA) with a coaxial T connector. The IPG model TLR-50-2010 Tm:YAG laser (IPG Photonics, Oxford MA) fires as the TTL signal reaches its maximum of 5 V while the iNet begins collecting data at a TTL signal of 0.5 V in order to measure the initial temperature of the tissue prior to the laser pulse. Prior to each exposure session, the thermocouple – iNet system was self tested for connectivity with results stored to disk. The thermocouple relative accuracy and constancy were verified three times during the study by immersion into a water bath at four different temperatures ranging from boiling to ice-water. The water temperature was determined by the average reading of four Barnstead Ever-safe N16B organic liquid filled thermometers (Thermo Scientific, Waltham MA).

Direct heating of the thermocouple probe by the 2.0 μm beam rather than the surrounding tissue has been considered a significant impact in several prior laser studies.[43-45] This was not an obstacle to this study for three reasons. First, the thermocouple used was considerably smaller than the one used in the Manns study. The 33 gauge needle presents a 0.21 mm diameter as opposed to their 23 gauge needle's 0.63 mm to intercept the direct beam fluence. Second, the 2.01 μm wavelength IR of the Tm:YAG laser does not penetrate to the depth of the needle as did the 1.06 μm beam of Manns' Nd:YAG laser. For example, consider the difference 1μm of wavelength makes

in the two beams' attenuation coefficient in water. From Hale and Querry, the coefficients are 69.12 cm-1 at 2,000 nm but only 0.12 cm-1 at 1,060 nm wavelength.[46] Using these attenuation coefficients, weighted by water content of skin as commonly done,[47-48] the 2.0 μm beam is reduced to 19% of original intensity by Beer's Law at the 0.3 mm depth of the probe. In contrast, the Nd;YAG beam in the Manns study would still be at 95% at the 5 mm distance to their closest thermocouple. Finally, the graphs of skin temperature rise during the laser pulse recorded with this thermocouple did not exhibit the instantaneous temperature jump which Cain and Valvano claim to be the indication of direct thermocouple absorption of laser beam energy.[44-45]

5.2.3 Skin Samples

Pig skin (*Sus Scrofa Domestica*) was obtained via an agreement with the professional veterinary program at Colorado State University. Approval to utilize tissue samples from these pigs was obtained from the University Institutional Animal Care and Use Committee. Tissue sample disposal procedures were approved by the Institutional Biosafety Committee (IBC) of the Research Integrity and Compliance Office.

Skin samples were excised from the rear flank of pigs within 24 hours of animal euthanasia. Skin excision was performed in the Veterinary Medicine Anatomy Lab. After identifying a suitable area of skin free of injury or scars, with visually uniform pigmentation, the hair was removed with electric clippers set to the closest setting which would not scratch the skin. This left hair of approximately 1.5 mm length on the skin. Skin samples of approximately 100 cm^2 were taken with approximately 0.5 cm of fatty tissue thickness. The samples were maintained at 5 °C in airtight containers with 1 ml

saline solution to maintain moisture. Skin samples were handled from the sides and edges to avoid any abrasion or tearing of the surfaces to be irradiated.

Under optical magnification, a 25 gauge, 5/8 inch, hypodermic needle (Becton Dickenson, Franklin Lakes NJ) was used to pierce the surface of the skin and was directed parallel to the skin surface. The HYP-0 thermocouple needle was immediately inserted through the 25 g needle until it extended 10 mm past the tip. This method proved to be the most reliable to insert the probe as the 33 gauge needle construction of the thermocouple was too fragile to penetrate the skin by itself. The thermocouple insertion is shown in Figure 5.6.

Insertion attempts were balanced between the goal of positioning the probe at shallow depth and the tendency to penetrate the delicate epidermal tissue from the inside (see Figure 5.6b). When this occurred, the needle was withdrawn from the hole and the process begun again 5 mm lateral to the ruptured hole site. The sample with the thermocouple inserted was then mounted on the optical translation stage using screws and rubber washers to clamp down a Petri dish containing the skin sample. The Petri dish was positioned with the thermocouple needle parallel to the North-South axis of travel of the stage, and the needle tip centered visually with the red HeNe beam.

5.2.4 Depth Measurement – Histology and Ultrasound

The depth of the thermocouple was measured by two methods. The thermocouple in samples for profile measurements was imaged with high-frequency ultrasound. With the HYP-0 needle still in place in the skin, the wires were disconnected and the sample was transported to the Veterinary Teaching Hospital

Imaging Department. A Sonaline Antares ultrasound unit with a 13.5 MHz VF13.5SP probe (Siemens Medical Solutions USA, Malvern PA). The system was set to 11.43 MHz with 60 dB gain in the linear 2D imaging mode, using the standard MSK (superficial muscular-skeletal) protocol. The needle was visually located in images taken in both a transverse cross section and in a long-axis cross section. The transverse image provided an image with less noise. The image along the needle's long-axis was necessary to identify the tip of the needle as seen in Figure 5.7. The Anteres US unit's measurement tools were used to determine depth by placing cursers on the top edge of the image (skin surface) and at the center of the needle's image. The uncertainty estimate for the ultrasound measurement process was determined by repeating measurements on one sample ten times in both directions and calculating the standard deviation.

The location of the thermocouple needle in samples from CAX measurement sessions was determined with a post-irradiation histological examination.
After the laser exposures were completed for CAX sample, the surface of the pig skin was marked with black ink parallel to the needle from the insertion point to the end of the probe. The HYP-O probe was then withdrawn from the sample and from the 25 g needle. Before the 25 g needle was withdrawn, a 3 cc syringe containing yellow tissue marking dye (Cancer Diagnostics Inc., Birmingham MI) was connected to the Leur-lock of the needle. As the 25 g needle was withdrawn from the skin, gentle pressure on the syringe injected the dye into the cavity evacuated by the needle. This prevented the cavity from collapsing on itself, and rendered it clearly distinguishable under a microscope. The pressure on the syringe plunger was minimal, to prevent the dye from

being forced into the surrounding tissue and expand or rupture the cavity. The sample was then cut down with 2 mm margins around the ink marks and submerged in the freezing solution, Tissue-Tek OCT (Sakura Fintek, Torrance CA), as shown in Figure 5.8.

In order to freeze the sample in a known orientation, the skin was held in place with cotton thread sutured to the edges deep in the muscle layer of the sample. This was necessary to prevent sectioning geometry uncertainty. The sample container was marked with the needle direction and sample number. It was then frozen for 24 hours at -80 °C. The frozen sample was affixed to a ball joint holder with OCT solution and mounted in the microtome (Bright Instruments, Huntington UK) as shown in Figure 5.9. The sample was aligned perpendicular to the knife edge and trimmed down until the black ink markings on the surface, indicating the needle insertion, were visible. As soon as the black ink was identified, sections of 15 μm thickness were cut and mounted on slides. Sections were mounted at intervals of approximately 100 μm, sometimes up to 200 μm if mounting was unsuccessful for the intended section . Digital images were taken of the slides at 4X magnification on a BH2 microscope (Olympus, Center Valley PA), as shown in Figure 5.10. Depths were measured on the images to the center of the dye stained hole using Spot software version 4.09 (Digital Instruments Inc., Sterling Heights, MI). Measurements from the four distal images showing the probe cavity were averaged with a maximum standard deviation of a sample being 0.065 mm at the 0.650 mm depth. The distance measurement function of the Spot software was calibrated for the 4X lens with a digital test pattern, model USAF1951 (Edmund Optics, Barrington NJ).

5.2.5 Data Analysis

Temperature for each exposure was measured simultaneously both at depth and on the surface. The relative temperature rise per exposure in °C mJ^{-1} mm^2 was calculated. In the case of the thermocouple temperature, baseline was taken as the first data point. The thermal camera was set to take twenty data points prior to the laser exposure for background subtraction.

The measured temperatures were then compared to expected temperatures calculated with an adaptation of the Green's function solution to the tissue bioheat differential equation from Vyas and Rustgi (Equation 5.2).[49] As there was no blood flow in the pigskin samples the first exponential term from the published solution is one and is dropped. The second exponential term in the Vyas and Rustgi equation describes the temperature decrease in the radial direction, and is therefore omitted for CAX points. For the multiple pulse exposures, the calculated temperature rise from the individual pulses were summed at the end of the pulse sequence. The Vyas solution was chosen over the Grossweiner[50] or the Roider[51] solutions as it describes the temperature in both the depth and radial directions with time.

$$T(r,z,t) = \left(\frac{\mu_a E_o}{\pi t_o \rho C}\right) t_o \frac{e^{-bt}}{(a^2+8Dt)} \exp\left(\frac{-2r^2}{a^2+8Dt}\right) \exp\left(-\mu_a z + \mu_a^2 Dt\right) \mathrm{Erfc}\left(\frac{2D\mu_a t - z}{\sqrt{4Dt}}\right) \quad (5.2)$$

$$T(z,t) = \left(\frac{\mu_a E_o}{\pi \rho C} \frac{1}{(a^2+8Dt)}\right) \left[\exp\left(-\mu_a z + \mu_a{}^2 Dt\right)\right] \mathrm{Erfc}\left(\frac{2D\mu_a t - z}{\sqrt{4Dt}}\right) \quad (5.3)$$

In Equation 5.2, μ_a is the optical absorption coefficient for the tissue, E_o is the energy deposited, ρ is the tissue density, C is the specific heat capacity, a is the laser beam $1/e^2$ radius, D is the tissue thermal diffusivity, z is the depth in tissue, and t is the time. The literature provides a wide range of values for the thermal constants for skin tissue, as listed in Table 4.3, selected values from which were used in the modeling experiments are listed in Table 5.1. Temperatures were calculated with combinations of thermal and optical constants to determine which produced the closest match to measured temperature rise per incident mJ. The CAX temperatures were evaluated first to narrow down the possible combinations and assure the best fit for the worst case (i.e. maximum temperatures) in the beam center.

Modeled temperatures were compared to measured data using Pearson's Chi-Squared method. The number of measured data points was chosen to provide an overall uncertainty, E, in the temperature per radiant energy of ± 0.5 °C mJ^{-1} at the 95% confidence level (setting $\alpha = 0.05$).

$$n \cong 2 z_{\alpha/2}^2 \sigma^2 E^{-2} \qquad (5.4)$$

Taking a test statistic of $z = 1.96$ from the standard normal curves and an estimated uncertainty of measurement, σ, at 0.68 °C mJ^{-1}, the number of measurement repetitions for each point is found from Equation 5.4 to be $n \geq 3.6$. Therefore for the measured temperature rise for a particular pulse sequence, four repetitions were performed consecutively and then averaged. This is four readings of the particular pulse sequence in a particular sample of pig skin. This process was repeated on each of the 22 pig skin samples in order to obtain an evenly distributed sampling of probe depths.

5.3 Results

5.3.1 Temperature Measurements

Skin temperatures were measured on the beam central axis on 22 pig skin samples consisting of over two thousand laser exposures. Each skin sample was used to measure both the surface temperature using the IR thermal camera and temperature at one depth using the HYP-0 thermocouple needle. Temperature profiles were measured on an additional 21 pig skin samples producing over three thousand exposure measurements in orthogonal radial directions. The large number of data points were used to determine temperature rise per radiant energy input with an uncertainty of less than ±0.5 °C from the true value for 95% of the points.

The thermocouple probe depths during CAX session were distributed from 0.204 mm to 1.145 mm. Positioning of the probe was based upon at least three histology images covering the distal 1 mm of the needle insertion position. The measurement depths are presented in Figure 5.11 with error bars representing one standard deviation of the mean of the histology measurements from that sample. The standard deviation was larger than one tenth of a millimeter for five of the 22 skin samples demonstrating the extreme variability possible in the wrinkles of natural skin.

The depths of thermocouple placement from the profile sessions, measured with ultrasound imaging, are presented in Figure 5.12. There were twenty profile measurement sessions performed. However, results from six of the samples had to be set aside due to difficulties of determining the depth of measurement. In one case, the needle visibly ruptured the epidermis in transit to the VTH for ultrasound measurement.

In another case, the needle was apparently not deep enough to be imaged. In the third case the US measured a depth of 2 mm which was beyond the depths of interest. In the fourth case the computer recording the thermocouple readings crashed before being backed up, losing the data. The failures of the fifth and sixth cases were not conclusive, but the needle appeared to have moved during transit, so were eliminated. There are no error bars presented with the graph in Figure 5.12 as the depth is a single point measured from the clearest image obtained. The uncertainty estimate for the ultrasound measurement process was found to be ±0.16 mm, the standard deviation of ten repetitions on the same sample. Another uncertainty which remains unresolved was the thickness of the acoustic gel necessary for the US waves to propagate from the transducer into the tissue. This large standard deviation, and the high rate of loss during transit to the VTH, led to developing the histology depth measurement methods described in section 5.2.4.

The laser beam output calibration was performed prior to each pig skin sample irradiation session and, for the CAX measurement sessions, after the tissue was set in the freezer. The calibration produced a linear relation between the sampled beam reflection and the radiant energy delivered at the plane of the pig skin surface. The correlation coefficient, R^2, was better than 0.98 in all cases. This gave high confidence in the calculation of energy delivered from the reflected beam measurement recorded for each exposure. The calibration linear relation was found to predict the beam energy measured for confirmation taken at the end of a session. This is shown in the representative calibration and confirmation data from the 16 July 2009 measurement session graphed in Figure 5.13. The four pulse sequences shown were chosen from the six to demonstrate

the agreement between the beginning calibration with the final confirmation readings. Additionally, the minor differences between calibrations can be seen.

The laser beam at the plane of the tissue sample was measured and found to produce a Gaussian shaped beam in the lowest order mode. The average $1/e^2$ beam radius was 3.2 mm with a standard deviation of 0.28 mm between the ten measurements. The expanded beam was measured to have a $1/e^2$ beam radius of 6.3 mm. Measured and fit beam profiles are shown in Figure 5.14.

Temperatures were measured with a temporal resolution of 16.7 msec and 6.7 msec from the IR thermal camera at 60 frames per second and the thermocouple sampled at 150 Hz. Representative temporal graphs of temperature rise in pig skin during laser irradiations using the six pulse sequences are presented in Figure 5.15. The IR camera data are presented with just one data point prior to temperature rise to facilitate comparison with the thermocouple data. These graphs show results from the third measurement session on 15 July 2009 which had a thermocouple depth of 0.306 mm.

The first sequence measured on a sample was repeated at the end of the session to confirm inter-sample consistency. As an example, Figure 5.16 shows the measured temperature rise of a two-pulse sequence taken on the CAX at the beginning and at the end of the first session on 15 July 2009 which placed the thermocouple at 0.440 mm deep in the pig skin. Over the duration of the measurement session the pig skin sample base temperature has risen 2.3 °C which is evident in both the surface and the deep curves. The temperature rise per mJ is consistent between exposures for both the thermocouple (0.00826 °C mJ^{-1} and 0.00817 °C mJ^{-1}) and the IR bolometer (0.02928 °C mJ^{-1} and 0.02931 °C mJ^{-1}), which illustrates the importance of the background readings

for each exposure. The measurement session included 28 exposures (four repetitions of six sequences plus four confirmation exposures of the first sequence) which would take roughly one minute each.

5.3.2 Modeling Results on the Beam Central Axis

Temperature rises per unit radiant energy were calculated for the six pulse sequences in pig skin with the range of thermal and optical constants listed in Table 5.1 using appropriate modifications of the Vyas and Rustgi Green's function solution of heat transfer with an air interface (Equation 5.3). Representative results are presented here in graphical and tabular form.

The optical absorption coefficient had the most dramatic effect as shown in Figure 5.17 in which a one order of magnitude difference produces a temperature rise two orders of magnitude higher. Temperatures calculated are displayed at the end of the 250 msec pulse train. The maximum rise in temperature was always calculated to be at the end of the 250 msec pulse train in the model.

The impact of the thermal diffusivity is displayed in Figure 5.18 which shows calculated temperatures with the four values of D for the two optical absorption coefficients from Chen and Takata for a 3-pulse sequence. The model results correspond to higher values of thermal diffusivity conducting heat faster to the deeper tissue with which the IR laser light does not directly interact. Note that the curves cross over at approximately 0.5 mm depth, at which the 2.0 μm IR light will have been attenuated to approximately one quarter of its original intensity.

The specific heat capacity, C, and relative density, ρ, have an inverse relation to the temperature calculated as shown in Figure 5.19. The lines are model results and the dots are the measured temperatures over depth. Notice that the curves do not cross, though the impact of the different values for C and ρ are less noticeable deeper in the skin. Also note that the temperature axis is different from the previous graphs in order to show the maximum calculated temperature when $C = 2.244$.

The combination of thermal and optical constants with the lowest value of Pearson's Chi-Squared residuals from the measured data were the optical absorption from Takata, $\mu_a = 2.6\ mm^{-1}$, the thermal diffusivity from Bowman, $D = 0.04\ mm^2\ sec^{-1}$, the specific heat capacity from Deng, $C = 4.2\ J\ g^{-1}\ °C^{-1}$, and the relative density from Xu and Deng, $\rho = 0.001116\ g\ mm^{-3}$. The model results for the six-pulse sequences are shown in Figure 5.20 with the measured results.

The values of the optical and thermal constants providing best fit to the IR camera "surface" measurements are listed in Table 5.2. Best fit was defined as absolute difference between peak temperature rise modeled and the measured rise by the IR camera nominally on the "surface".

The model results for the beam expanded to a $1/e^2$ radius of 6.4 mm are shown in Figure 5.21. The model uses the values of thermal and optical constants determined above for the original 3.2 mm radius beam. Measured results for the single-pulse sequence were indistinguishable from noise due to the power limit of the laser and are therefore not shown. The modeled temperature rise curves for the remaining five pulse sequences are not significantly different from each other. The dispersed energy of the expanded beam lessens the differences between the model's predictions. The model

calculated the temperature rise at the single depth very well, but predicted a "surface" maximum of roughly half of the measured value. The surface and depth measured temperature rise from the original 3.2 mm beam during this session are also shown on the graph to illustrate the dramatic drop in temperature caused by doubling the beam diameter. However, neither at the measurement depth of 0.337 mm nor at the surface did the temperature rise drop to one quarter of the original beam as the area over which the energy is spread was increased by four times.

5.3.3 Profile Modeling

Using the optical and thermal properties' values determined from the CAX modeling, the Vyas model was expanded to predict off-axis temperature rise per radiant exposure. The model results with the measured values are presented in Figure 5.22 for the 3.2 mm radius beam incident on pig skin for the six-pulse sequences studied. Measured temperatures are from one sample at 0.1 mm depth, two samples for depths of 0.2 mm, 0.3 mm, and 0.6 mm, and three samples with the probe measured at 0.4 mm and 0.6 mm.

5.4 Discussion

5.4.1 Depth of Thermocouple

The HYP-0 thermocouple probe proved to be difficult to insert into the pig skin samples. After several methods were tried, using a small 25 g hypodermic needle as a guide proved to be the most effective and repeatable. Initial attempts to enter the skin

from the side failed due to movement of the distensible tissue, even with a guide needle. This failure eliminated the *a priori* knowledge of depth intended with a micrometer operating a vertically translating optical mount. Depth determination was then attempted with the superficial ultrasound probe from the VTH during profile measurements. Several temperature measurement sessions data were rendered useless when the HYP-0 needle was found to have ripped the epidermis or slid back out of the tissue after transport to the VTH for imaging. Upon developing satisfactory transportation methods, the US system appeared to be satisfactory, until several samples had been measured and analyzed. Comparisons between measurements on different tissue samples which had been imaged to be at the same depth revealed remarkable differences in temperature results. Additionally, the 0.1 mm resolution of the US system was determined to need improvement if results were to be compared to models. Therefore, inquiries were made to find histology equipment and expertise. Initial trials at histological sample preparation and measurement revealed two major issues to be addressed. First the tissue sample had to be carefully held in a known position in order to minimize geometry distortions during sectioning. Second, the cavity created by the HYP-0 probe would usually collapse upon itself and be indistinguishable under the low power microscope. Injecting tissue marking dye solved this problem both by enhancing contrast of the probe position and filling the void to prevent collapse.

The thermocouple measurements were distributed between 0.1 mm to 1.1 mm as seen in Figures 5.11 and Figures 5.12. The depths for the profiles determined with US are assumed to have a uniform uncertainty of 0.7 mm as the measured depth comes from the single image showing the best resolution of the probe in a particular sample. The

depths from the CAX measurements determined by histology are shown with individual standard deviations of the depths measured based on several sections taken from a tissue sample. A minimum of three to a maximum of seven sections were measured and averaged for each sample point depth, depending on the success of mounting sliced sections on microscopy slides. The sections proved to require delicate handling and a freshly sharpened cutting blade. Lack of experience in this technique limited the numbers of sections for initial CAX depth measurements.

5.4.2 CAX Measurements and Modeling

Temperature measurements from 2.0 μm laser irradiations utilizing six different pulse sequences were performed on the beam's central axis. The instruments provided reproducible measurements of temperature rise per incident energy. The thermocouple sampling at 150 Hz provided ample temporal resolution to visualize individual pulses within a sequence. The IR camera imaging rate of 60 Hz provided reasonable temporal resolution to capture the maximum surface temperatures with inter-sample coefficient of variation within a series of measurements for a sequence of 1% to 2 %. The individual pulses of a series could be distinguished on both instruments for up to four pulses per 250 msec. The thermocouple could distinguish the nine-pulse sequence, but the IR camera did not. Tissue considerations such as dehydration kept the number of repetitions for each pulse sequence to the minimum of four to provide reasonable data quality. The agreement of the initial measurements with the confirmation data, as demonstrated in Figures 5.13 and 5.15, showed that tissue dehydration or changes in baseline temperature were insignificant during a measurement session, when background

temperature is subtracted out. The base tissue temperature offset between the two is clearly visible throughout the lasing sequence and cooling period.

Modeling temperature rise for sequences of 2.0 μm laser pulses demonstrated both the extreme and minor influences that available values for optical and thermal constants can have on predictions. As seen in Figure 5.16, the optical absorption coefficient has the most profound impact on predicted temperatures. Not only will the magnitude of the modeled temperature rise be affected, but the entire shape of the curve with respect to depth in tissue will drastically change. The predictions for a two-pulse sequence in Figure 5.14 were representative of the magnitude and shape of changes seen between using $\mu_a = 2.176\ mm^{-1}$ and the Bashkatov value of $\mu_{eff} = 13.425\ mm^{-1}$. The lower absorption coefficients produced a distinct build up to a maximum temperature at a depth between 50 μm and 100 μm. In sharp contrast, the absorption coefficients greater than 10 mm^{-1} locate the maximum temperature directly on the interface of the air and skin (depth = 0.000 mm) with an almost inverse exponential form.

Increasing the value of thermal diffusivity produced intuitive results in reducing the maximum temperature (heat diffusing faster to surrounding and deeper tissue) and increasing the temperature predictions for deep tissue beyond optical penetration. The overall shape of the predicted curves retains the distinct buildup with little change in depth of maximum temperature. The curves in Figure 5.17 crossed as the thermal diffusivity increased at a depth of 0.4 mm.

The specific heat capacity and the tissue relative density are found in the prefactor denominator of the Vyas model (Equation 5.4). Therefore, their influence is seen in Figures 5.18 as a direct amplification in the magnitude of the curves.

With four variables in the model, a best fit was found by reducing the possible values of the variables to four each, representing the range of published values. The best fit for all six pulse sequences was found to be the Takata optical absorption coefficient of 2.6 mm^{-1}. The combination of variables giving the best fit used diffusivity from Bowman with $D = 0.04$ mm^2 sec^{-1}, i.e. the fastest heat transfer rate. The value of the specific heat constant producing the best fit was $C = 4.2$ J g^{-1} $°C^{-1}$, the highest value of energy required to increase temperature published. The value of tissue density used in predicting the best fit to measured data was $\rho = 0.001116$ g mm^{-1}, a value in the middle of published results.

As seen in the series of graphs in Fig 5.19, modeling with the above values for the constants trends lower in peak temperature as the number of pulses increases. This trend is opposite to that of the IR camera readings as the number of pulses in a sequence went from single pulse to continuous wave. In order to best match the IR camera measured temperature rise, the constants needed to be selected for each pulse sequence, with no apparent pattern emerging among the constants.

The model was less sensitive to different pulse sequences with the expanded beam. The five curves of predicted temperature are almost indistinguishable. The model predicted the temperature at 0.337 mm very well, but underestimated the peak temperature rise.

The measurements were performed on *ex-vivo* skin samples. Therefore the modeling ignored heat convection by blood circulation in the capillaries of the dermis. Blood or plasma flow would serve to remove heat in the axial direction while leaving the heat transfer in the radial direction as conduction. The model's blood flow component is

a simple inverse exponential with a blood flow rate constant and time post exposure. This would serve to shift the entire curve lower with time. The agreement at deeper measurements would improve, but the more important agreement with maximum temperature at shallow depths would suffer.

5.4.3 Profile Measurements and Modeling

Using the values of the thermal and optical constants determined from the central axis modeling, radial profiles were generated with the Vyas model, seen in the six graphs of Figure 5.21 for the six pulse sequences. The modeled profiles are seen to fall in the midst of the measured values for the single and double pulse sequences at depths of 0.1 mm, 0.2 mm, and 0.3 mm. For the sequences with higher numbers of pulses, the profiles lie on the lower edges of the measured data points, even at the shallow depths. For all sequences at depths of 0.4 mm and 0.5 mm, the model predicts temperatures below the measurements. However, the measured data for 0.4 mm in all sequences appears to overlap the data at 0.3 mm. In contrast the 0.6 mm depth measurements are significantly less than the model prediction. The measured data appears to show greater lateral heat flow than the model predicts.

5.5 Conclusion

Temperature rise in pig skin irradiated with 2.0 μm infrared laser light has been performed on the surface and at depths from 0.1 mm to 1.1 mm for six different sequences of pulses. A Green's function solution to the tissue – interface thermal condition has been used to isolate the published values of thermal and optical constants which best predict the rise in temperature per incident radiant energy.

5.6 References

1. American National Standards Institute, "American national standard for safe use of lasers Report" No. ANSI Z136-1-2007, 2007.

2. B. Chen, D. C. O'Dell, S. L. Thomsen, B. A. Rockwell, and A. J. Welch, "Porcine skin ed50 damage thresholds for 2,000 nm laser irradiation," Lasers in Surgery and Medicine **37** (5), 373-381 (2005).

3. K. Buettner, "Effects of extreme heat and cold on human skin .1. Analysis of temperature changes caused by different kinds of heat application," Journal of Applied Physiology **3** (12), 691-702 (1951).

4. S. Thomsen, "Pathologic analysis of photothermal and photomechanical effects of laser-tissue interactions," Photochem Photobiol **53** (6), 825-835 (1991).

5. J. R. Lepock, H. E. Frey, A. M. Rodahl, and J. Kruuv, "Thermal-analysis of chl v79 cells using differential scanning calorimetry - implications for hyperthermic cell killing and the heat-shock response," Journal of Cellular Physiology **137** (1), 14-24 (1988).

6. G. C. Faith, M. N. Stein, J. R. Hayes, and R. E. Stowell, "Cellular effects of laser radiation - light microscopic studies on injury of mouse liver," Archives of Pathology **86** (3), 262-& (1968).

7. B. M. Mackey, C. A. Miles, S. E. Parsons, and D. A. Seymour, "Thermal-denaturation of whole cells and cell components of escherichia-coli examined by differential scanning calorimetry," Journal of General Microbiology **137**, 2361-2374 (1991).

8. J. L. R. Roti, H. H. Kampinga, R. S. Malyapa, W. D. Wright, R. P. vanderWaal, and M. Xu, "Nuclear matrix as a target for hyperthermic killing of cancer cells," Cell Stress & Chaperones **3** (4), 245-255 (1998).

9. J. T. Beckham, M. A. Mackanos, C. Crooke, T. Takahashi, C. O'Connell-Rodwell, C. H. Contag, and E. D. Jansen, "Assessment of cellular response to thermal laser injury through bioluminescence imaging of heat shock protein 70," Photochemistry and Photobiology **79** (1), 76-85 (2004).

10. G. Müller, K. Dörschel, and H. Kar, "Biophysics of the photoablation process," Lasers in Medical Science **6** (3), 241-254 (1991).

11. R. L. McCally, R. A. Farrell, and C. B. Bargeron, "Cornea epithelial damage thresholds in rabbits exposed to Tm-YAG laser-radiation at 2.02 μm," Lasers in Surgery and Medicine **12** (6), 598-603 (1992).

12. V. G. Liu, T. M. Cowan, S. M. Jeong, S. L. Jacques, E. C. Lemley, and W. R. Chen, "Selective photothermal interaction using an 805-nm diode laser and indocyanine green in gel phantom and chicken breast tissue," Lasers in Medical Science **17** (4), 272-279 (2002).

13. H. H. Kampinga, "Thermotolerance in mammalian-cells - protein denaturation and aggregation, and stress proteins," Journal of Cell Science **104**, 11-17 (1993).

14. S. J. Lin, C. Y. Hsiao, Y. Sun, W. Lo, W. C. Lin, G. J. Jan, S. H. Jee, and C. Y. Dong, "Monitoring the thermally induced structural transitions of collagen by use of second-harmonic generation microscopy," Optics Letters **30** (6), 622-624 (2005).

15. M. G. Lin, T. L. Yang, C. T. Chiang, H. C. Kao, J. N. Lee, W. Lo, S. H. Jee, Y. F. Chen, C. Y. Dong, and S. J. Lin, "Evaluation of dermal thermal damage by multiphoton autofluorescence and second-harmonic-generation microscopy," Journal of Biomedical Optics **11** (6) (2006).

16. Y. Sun, W. L. Chen, S. J. Lin, S. H. Jee, Y. F. Chen, L. C. Lin, P. T. C. So, and C. Y. Dong, "Investigating mechanisms of collagen thermal denaturation by high resolution second-harmonic generation imaging," Biophysical Journal **91** (7), 2620-2625 (2006).

17. N. T. Wright and J. D. Humphrey, "Denaturation of collagen via heating: An irreversible rate process," Annual Review of Biomedical Engineering **4**, 109-128 (2002).

18. T. Kuo, M. T. Speyer, W. R. Ries, and L. Reinisch, "Collagen thermal damage and collagen synthesis after cutaneous laser resurfacing," Lasers in Surgery and Medicine **23** (2), 66-71 (1998).

19. B. Majaron, S. M. Srinivas, H. E. L. Huang, and J. S. Nelson, "Deep coagulation of dermal collagen with repetitive Er :YAG laser irradiation," Lasers in Surgery and Medicine **26** (2), 215-222 (2000).

20. R. Brinkmann, N. Koop, J. Kampmeier, A. Bruhns, M. AsiyoVogel, R. Engelhardt, and R. Birngruber, "Corneal collagen denaturation in laser thermokeratoplasty (LTK)," Investigative Ophthalmology & Visual Science **38** (4), 2514-2514 (1997).

21. R. Brinkmann, B. Radt, C. Flamm, J. Kampmeier, N. Koop, and R. Birngruber, "Influence of temperature and time on thermally induced forces in corneal

collagen and the effect on laser thermokeratoplasty," Journal of Cataract and Refractive Surgery **26** (5), 744-754 (2000).

22. R. Vanhillegersberg, H. J. Vanstaveren, W. J. Kort, P. E. Zondervan, and O. T. Terpstra, "Interstitial NdYAG laser coagulation with a cylindrical diffusing fiber tip in experimental liver metastases," Lasers in Surgery and Medicine **14** (2), 124-138 (1994).

23. R. Splinter and B. A. Hooper, *An introduction to biomedical optics*. (CRC Press, Boca Raton, 2007).

24. M. M. Pankratov, Donald F. Perrault, Jr., M. Shapshay Stanley, F. Pinto Joseph, Esterowitz Dina, and H. Thomas Aretz, "Comparative laser-tissue interaction effects at 1.96 and 2.01 um of cr; Tm:YAG laser," Proceedings of SPIE **1646**, 30-41 (1992).

25. N. S. Nishioka and Y. Domankevitz, "Comparison of tissue ablation with pulsed holmium and thulium lasers," IEEE Journal of Quantum Electronics **26** (12), 2271-2275 (1990).

26. J. P. Cummings and J. T. Walsh, "Erbium laser ablation - the effect of dynamic optical-properties," Applied Physics Letters **62** (16), 1988-1990 (1993).

27. S. Rastegar, B. M. Kim, and S. L. Jacques, "Role of temperature dependence of optical properties in laser irradiation of biological tissue," Proceedings of SPIE **1646**, 228-235 (1992).

28. M. C. Pierce, S. D. Jackson, M. R. Dickinson, and T. A. King, "Laser-tissue interaction with a high-power 2-μm fiber laser: Preliminary studies with soft tissue," Lasers in Surgery and Medicine **25** (5), 407-413 (1999).

29. M. Keijzer, S. L. Jacques, S. A. Prahl, and A. J. Welch, "Light distributions in artery tissue - monte-carlo simulations for finite-diameter laser-beams," Lasers in Surgery and Medicine **9** (2), 148-154 (1989).

30. S. T. Flock, M. S. Patterson, B. C. Wilson, and D. R. Wyman, "Monte-carlo modeling of light-propagation in highly scattering tissues .1. Model predictions and comparison with diffusion-theory," IEEE Transactions on Biomedical Engineering **36** (12), 1162-1168 (1989).

31. H. H. Pennes, "Analysis of tissue and arterial blood temperatures in the resting human forearm," Journal of Applied Physiology **1** (2), 93-122 (1948).

32. M. Oane, A. Peled, F. Scarlat, I. N. Mihailescu, A. ScarisoreanU, and G. Georgescu, "Multi-photon temperature profile modeling in solids during

powerful pulse laser irradiation," Infrared Physics & Technology **51** (3), 242-245 (2008).

33. M. A. Mainster, T. J. White, J. H. Tips, and P. W. Wilson, "Transient thermal behavior in biological systems," Bulletin of Mathematical Biophysics **32** (3), 303 (1970).

34. J. H. Torres, M. Motamedi, J. A. Pearce, and A. J. Welch, "Experimental evaluation of mathematical-models for predicting the thermal response of tissue to laser irradiation," Applied Optics **32** (4), 597-606 (1993).

35. C. B. Bargeron, R. L. McCally, and R. A. Farrell, "Calculated and measured endothelial temperature histories of excised rabbit corneas exposed to infrared radiation," Experimental Eye Research **32** (2), 241-250 (1981).

36. S. L. Jacques and S. A. Prahl, "Modeling optical and thermal distributions in tissue during laser irradiation," Lasers in Surgery and Medicine **6** (6), 494-503 (1987).

37. G. Yoon, S. A. Prahl, and A. J. Welch, "Accuracies of the diffusion-approximation and its similarity relations for laser irradiated biological media," Applied Optics **28** (12), 2250-2255 (1989).

38. J. L. Karagiannes, Z. Zhang, B. Grossweiner, and L. I. Grossweiner, "Applications of the 1-d diffusion-approximation to the optics of tissues and tissue phantoms," Applied Optics **28** (12), 2311-2317 (1989).

39. M. Oane, F. Scarlat, and I. N. Mihailescu, "The semi-analytical solution of the fourier heat equation in beam - 3d inhomogeneous media interaction," Infrared Physics & Technology **51** (4), 344-347 (2008).

40. R. Graaff, A. C. M. Dassel, M. H. Koelink, F. F. M. Demul, J. G. Aarnoudse, and W. G. Zijlstra, "Optical-properties of human dermis invitro and invivo," Applied Optics **32** (4), 435-447 (1993).

41. S. T. Flock, B. C. Wilson, and M. S. Patterson, "Monte-carlo modeling of light-propagation in highly scattering tissues .2. Comparison with measurements in phantoms," IEEE Transactions on Biomedical Engineering **36** (12), 1169-1173 (1989).

42. P. J. Shayler, "Laser-beam distribution in focal region," Applied Optics **17** (17), 2673-2674 (1978).

43. F. Manns, P. J. Milne, X. Gonzalez-Cirre, D. B. Denham, J. M. Parel, and D. S. Robinson, "In situ temperature measurements with thermocouple probes during

laser interstitial thermotherapy (LITT): Quantification and correction of a measurement artifact," Lasers in Surgery and Medicine **23** (2), 94-103 (1998).

44. C. Cain, "Thin-film temperature sensors for biological measurements," IEEE Transactions of Biomedical Engineering **21** (5), 421-423 (1974).

45. J. W. Valvano and J. A. Pearce, "Temperature measurements," in *Optical thermal response of laser irradiated tissue*, edited by A Welch and M. van Gemert (SPIE, Bellingham WA, 1995), pp. 518.

46. G. M. Hale and M. R. Querry, "Optical-constants of water in 200-nm to 200-mum wavelength region," Applied Optics **12** (3), 555-563 (1973).

47. S. L. Jacques, "Role of tissue optics and pulse duration on tissue effects during high-power laser irradiation," Applied Optics **32** (13), 2447-2454 (1993).

48. B. Chen, S. L. Thomsen, R. J. Thomas, and A. J. Welch, "Modeling thermal damage in skin from 2000-nm laser irradiation," Journal of Biomedical Optics **11** (6) (2006).

49. R. Vyas and M. L. Rustgi, "Green-function solution to the tissue bioheat equation," Medical Physics **19** (5), 1319-1324 (1992).

50. L. I. Grossweiner, A. M. Alkarmi, P. W. Johnson, and K. R. Brader, "Modeling of tissue heating with a pulsed Nd-YAG laser," Lasers in Surgery and Medicine **10** (3), 295-302 (1990).

51. J. Roider, F. Hillenkamp, T. Flotte, and R. Birngruber, "Microphotocoagulation - selective effects of repetitive short laser-pulses," Proceedings of the National Academy of Sciences of the United States of America **90** (18), 8643-8647 (1993).

Table 5.1 Optical and thermal constants for modeling 2.0 μm light on pigskin, representing the range of published values, (reference in parenthesis) in each category used in the Vyas model.

Optical Absoption μ_a [mm^{-1}]	Heat Capacity C [$J\ g^{-1}\ °C^{-1}$]	Density ρ [$g\ mm^{-3}$]	Thermal Diffusivity D [$mm^2\ sec^{-1}$]
2.176 (Chen)	2.244 (Chen)	0.001 (Choi)	0.04 (Bowman)
2.60 (Takata)	3.4 (Crochet)	0.00107 (Sandu)	0.082 (Tuchin)
5.802 (Chen*)	3.68 (Xu)	0.001116 (Xu)	0.12 (Svaasand)
13.425 (Bashkatov)	4.2 (Deng)	0.0012 (Lipkin)	0.16 (Chato)

* absorption coefficient for dermis

Table 5.2 Modeled peak temperature rise (and depth at which it occurred), with the values of optical and thermal constants which best matched measured surface temperature rise per incident 2.0 μm laser energy for the six pulse sequences.

	1 pulse	2 pulse	3 pulse	4 pulse	9 pulse	CW
Temperature Rise °C mJ^{-1} (mm)						
Measured	0.03220	0.02859	0.02896	0.02995	0.03151	0.03457
Surface Match	0.03209	0.02864	0.02802	0.02751	0.02936	0.02543
	(0.06)	(0.08)	(0.08)	(0.09)	(0.10)	(0.12)
Overall Match	0.02911	0.02409	0.02317	0.02294	0.02279	0.02115
	(0.05)	(0.06)	(0.08)	(0.09)	(0.10)	(0.10)
Values of Constants						
μ mm^{-1}	2.176	2.6	2.6	2.6	2.6	2.176
D mm^2 sec^{-1}	0.04	0.12	0.82	0.82	0.04	0.04
ρ g cm^{-3}	1.07	1.07	1.07	1.07	1.07	1.07
C J g^{-1} $°C^{-1}$	3.4	3.4	3.4	3.4	3.4	3.4

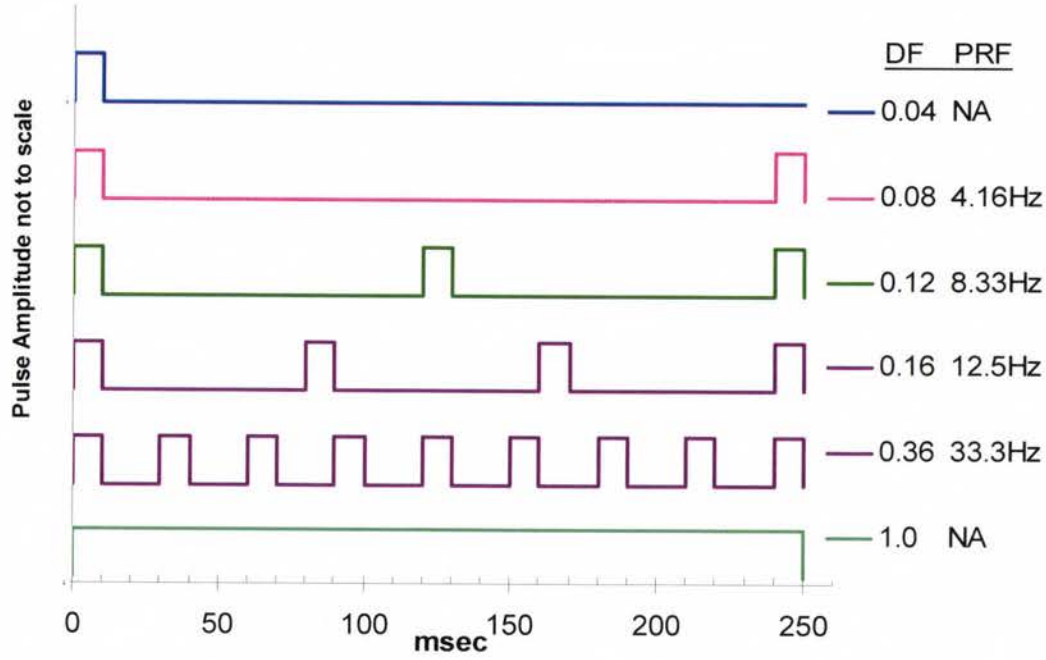

Figure 5.1 TTL signal laser pulse sequences, with corresponding duty factors (DF) and pulse repetition frequencies (PRF) listed adjacent.

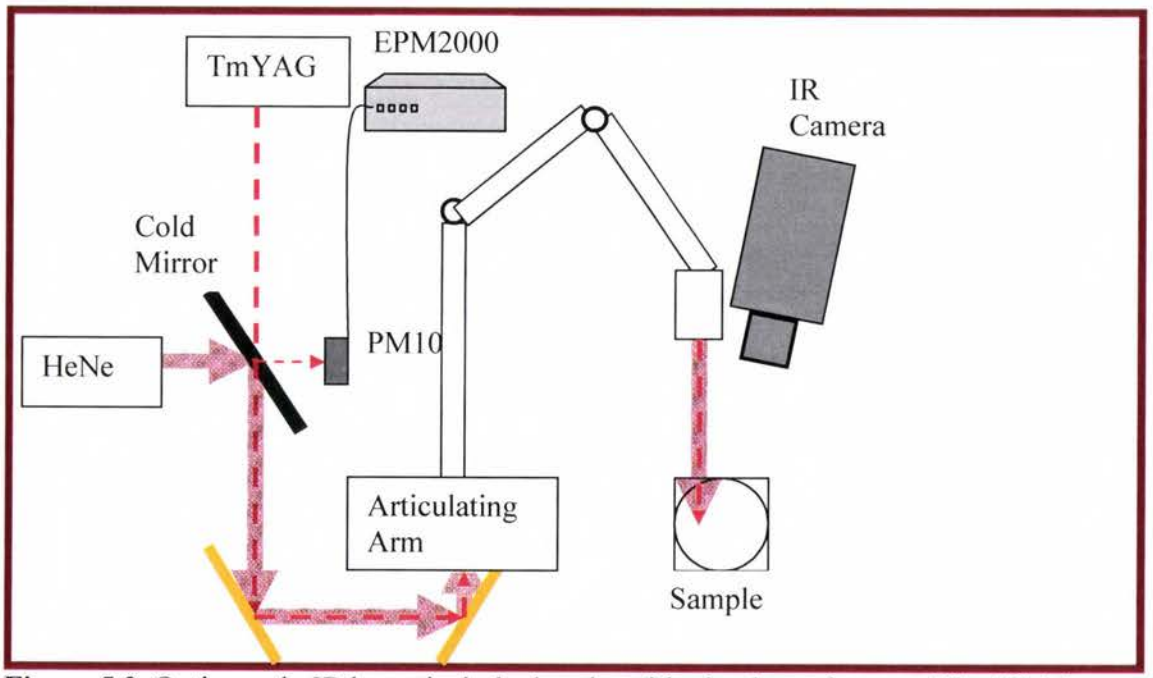

Figure 5.2 Optics path, IR beam is dashed, red positioning beam is gray. The "Cold Mirror" is highly reflective to visible light while transparent (>98% transmission) to IR. The small reflection is measured by the PM10 probe with the EPM2000 meter to record the exposure energy of each irradiation.

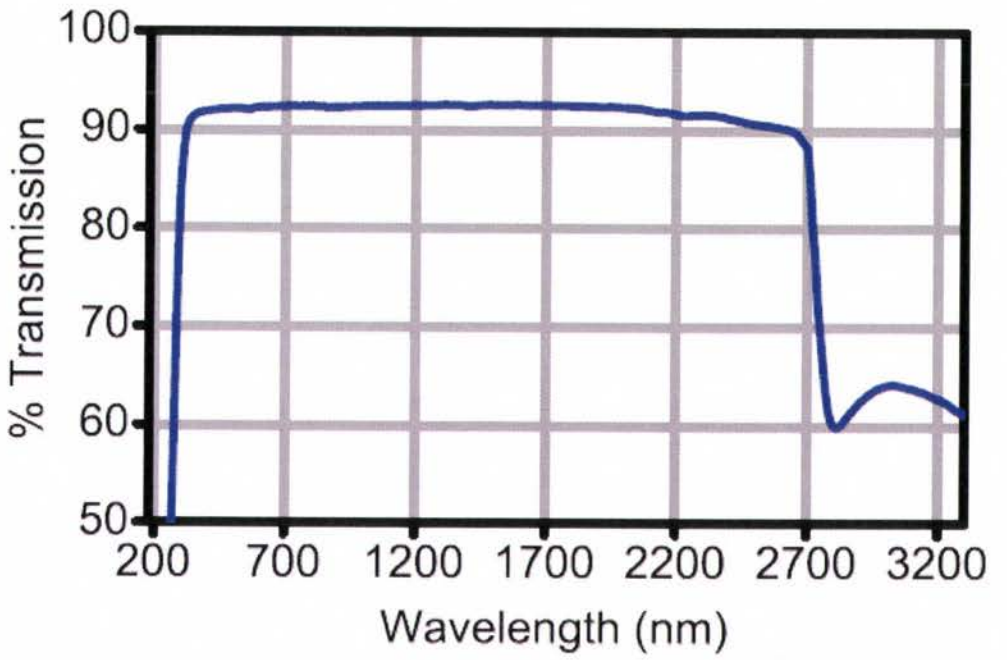

Figure 5.4. Transmission through 1 mm of BK7 glass, including reflections, (graph from manufacturer, Thor Labs).

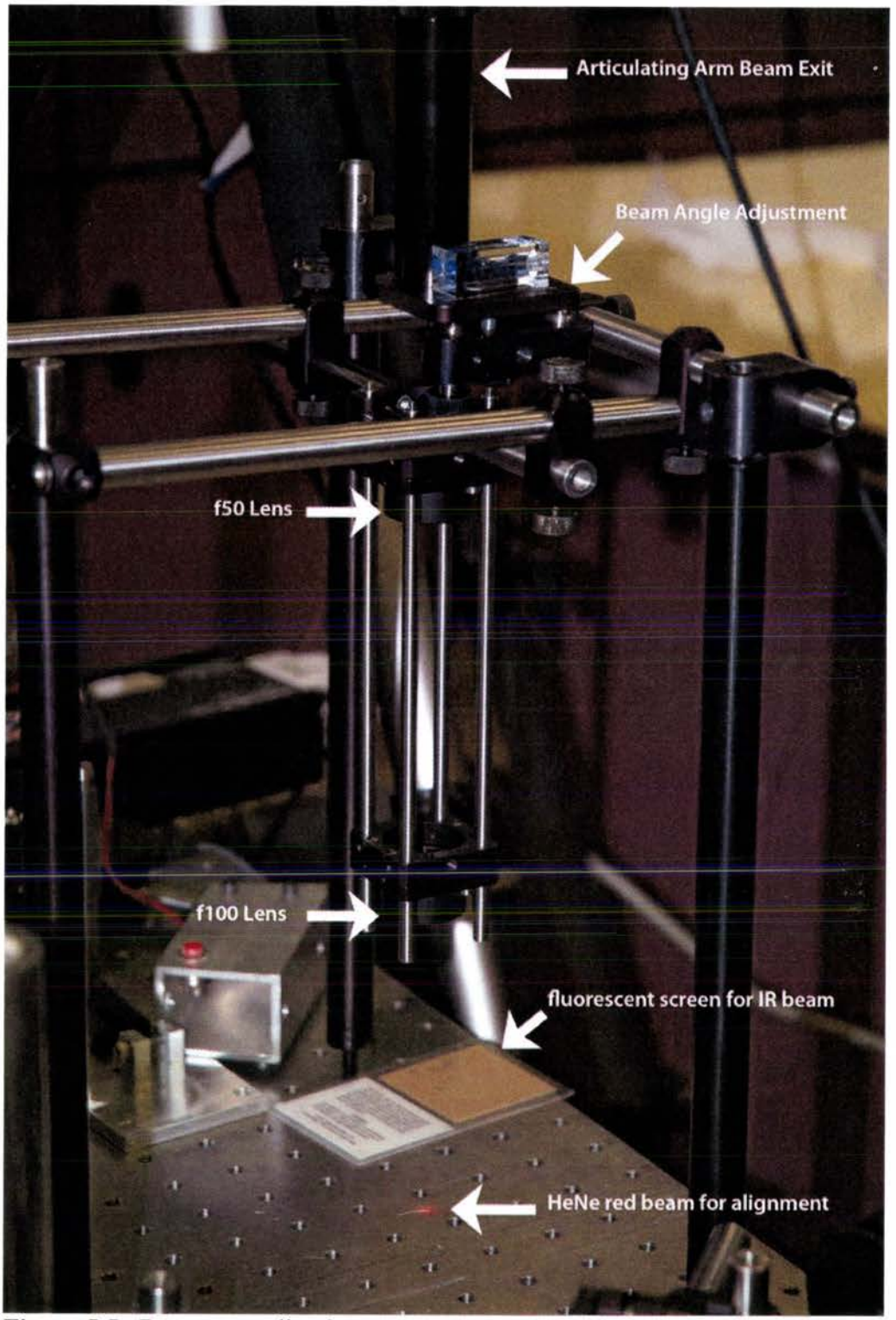

Figure 5.5 Beam expanding lenses mounted under articulating armature. Note the adjustments on both the articulating arm support and the lens rails to direct the beam normal to both lenses and the skin sample. HeNe beam is visible on table where tissue sample was placed.

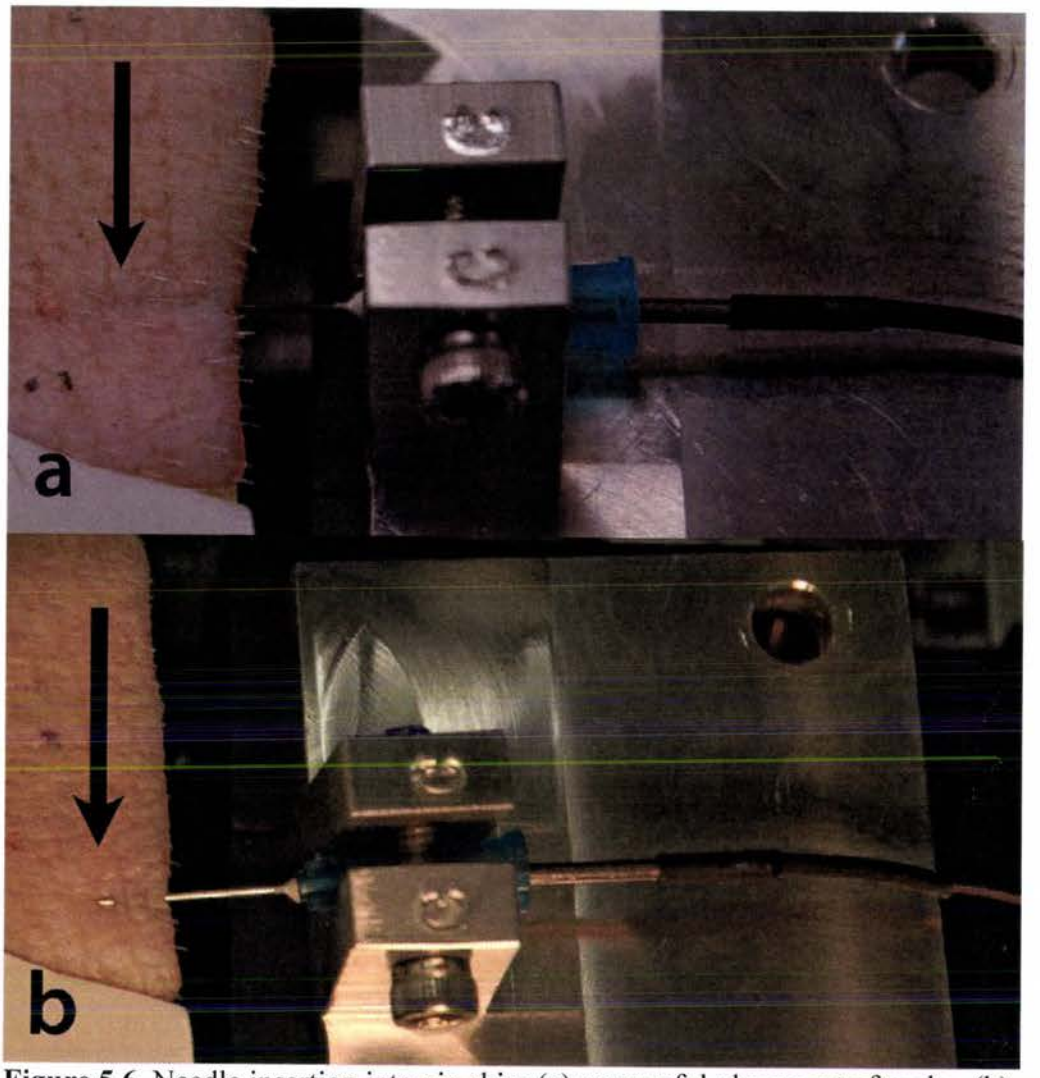

Figure 5.6 Needle insertion into pig skin; (a) successful placement of probe, (b) needle has re-surfaced. Also in (b) the HYP-0 thermocouple can be seen entering the 25 g needle.

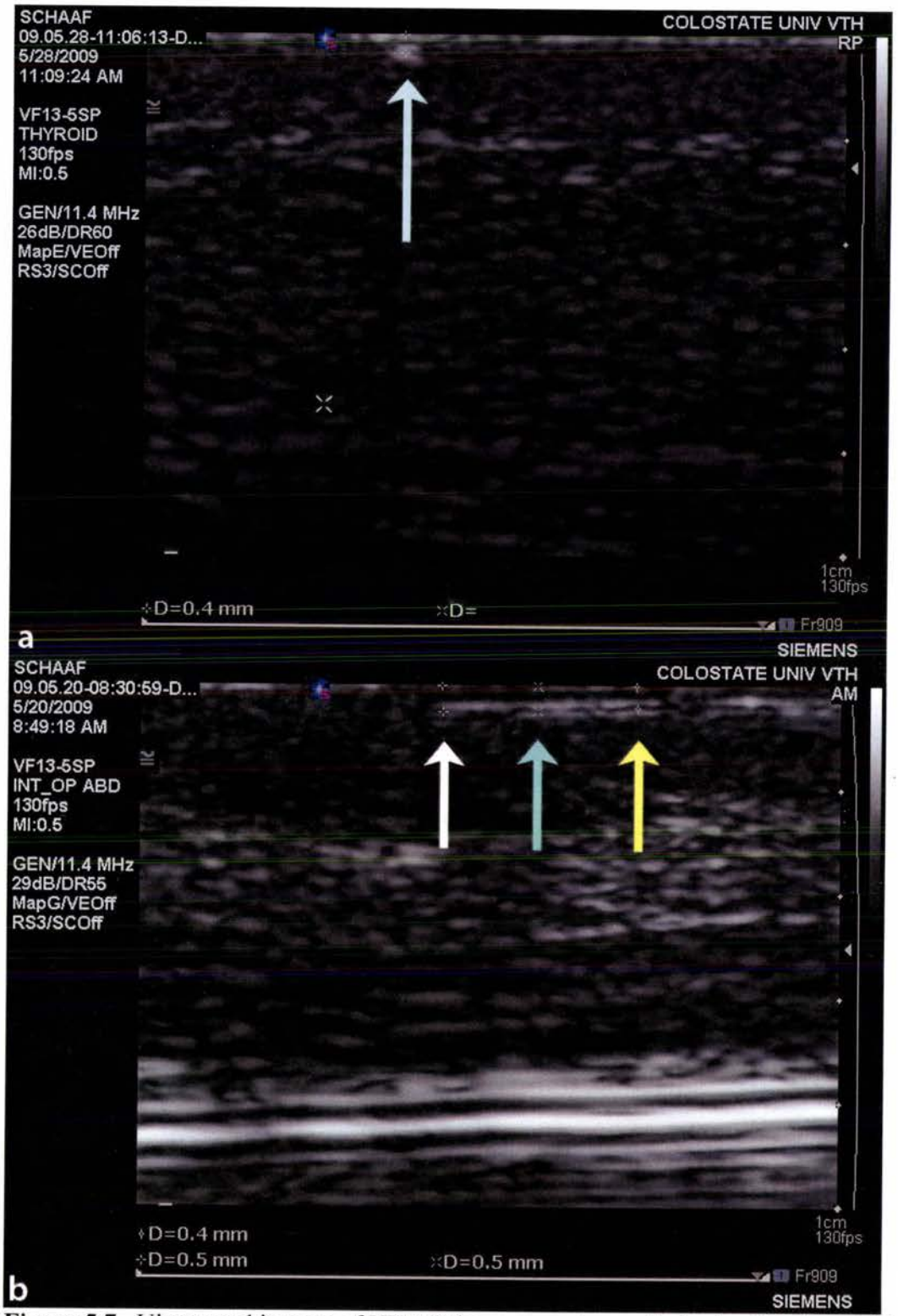

Figure 5.7. Ultrasound images of HYP-0 thermocouple needle in pig skin, imaged in a) transverse plane cross section, and b) long axis cross section.

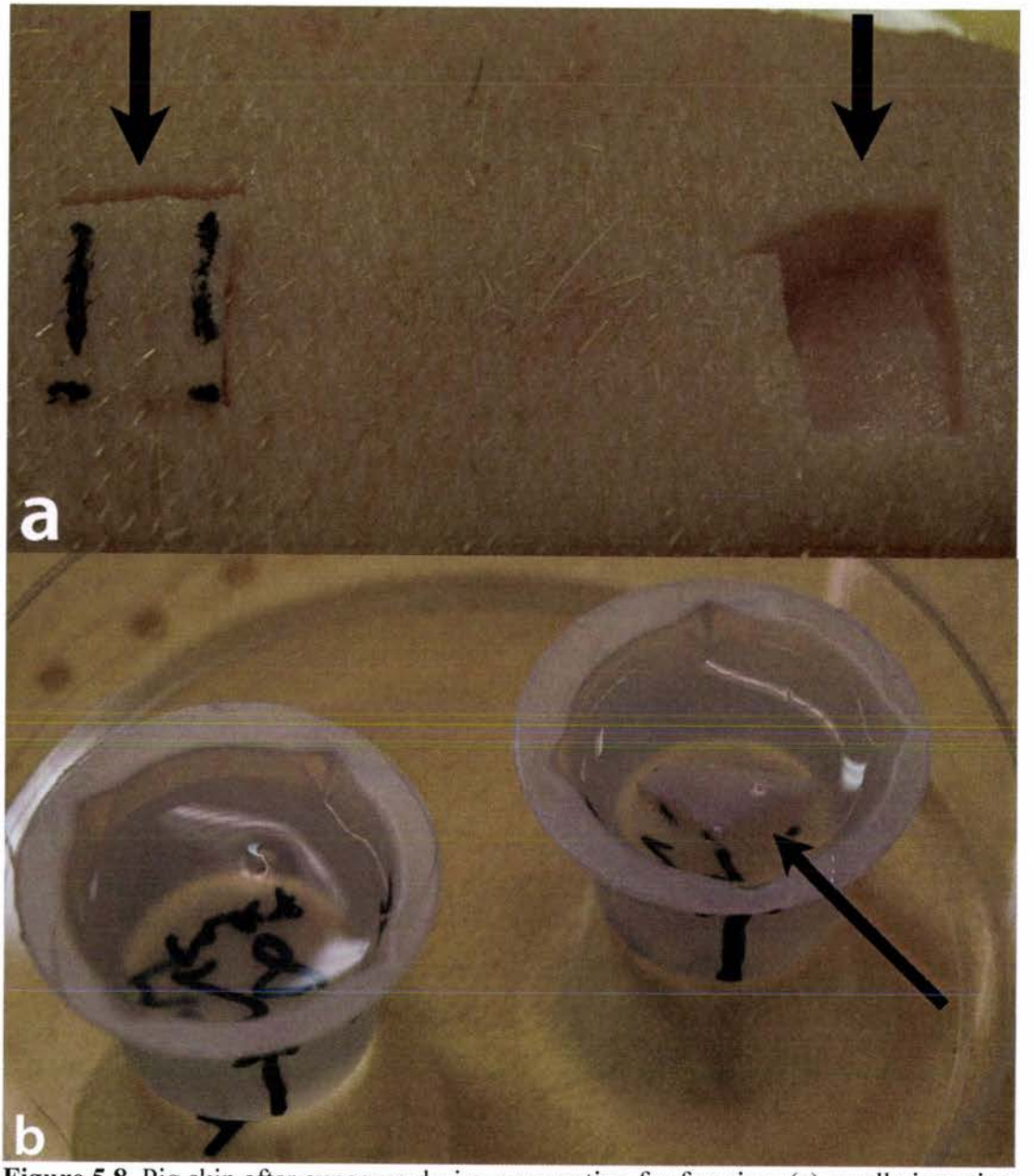

Figure 5.8 Pig skin after exposure during preparation for freezing, (a) needle insertion marked with ink on left (note lines on both sides of needle and dots for sectioning geometry alignment) and sample cut out on right; (b) inked and cut sample in OCT solution in labeled freezing cup on right, at left is OCT for unexposed skin.

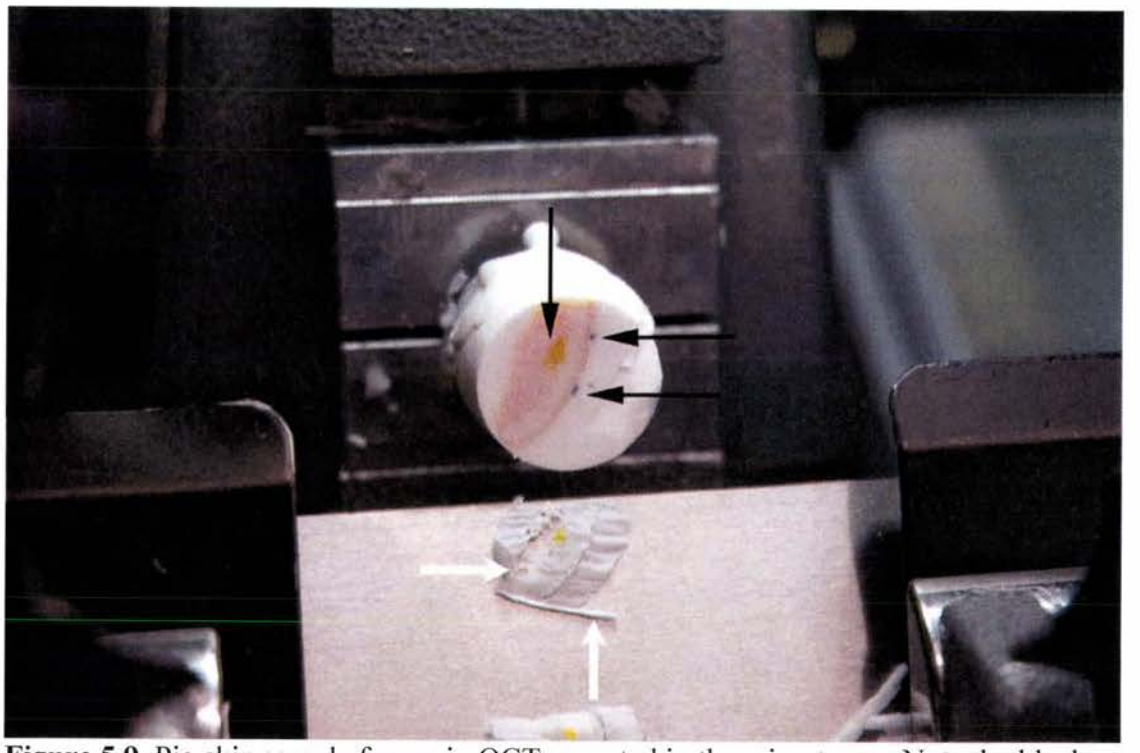

Figure 5.9 Pig skin sample frozen in OCT mounted in the microtome. Note the black ink marks visible on the surface (black horizontal arrows) and the large yellow dye spot (black vertical arrow) from excessive pressure on the syringe during needle withdrawal (yellow dye from successful injection yields inadequate contrast to identify in photographs). Difficulties for successful mounting of a section on a slide are also visible in the section resting on the cutting blade. Curling of the section (white vertical arrow), wrinkles and tearing (white horizontal arrow) were common obstacles to a successful mount.

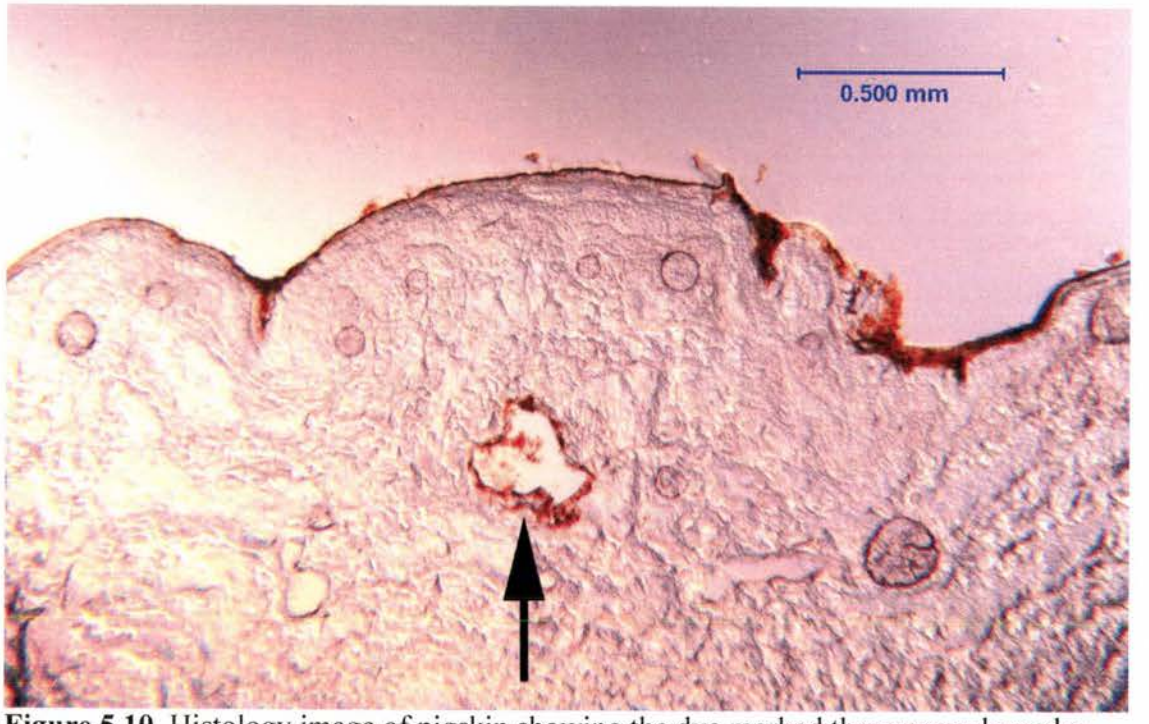

Figure 5.10 Histology image of pigskin showing the dye marked thermocouple probe hole (arrow) and the ink marked surface (ink appears brown in the two valleys on either side of the hole).

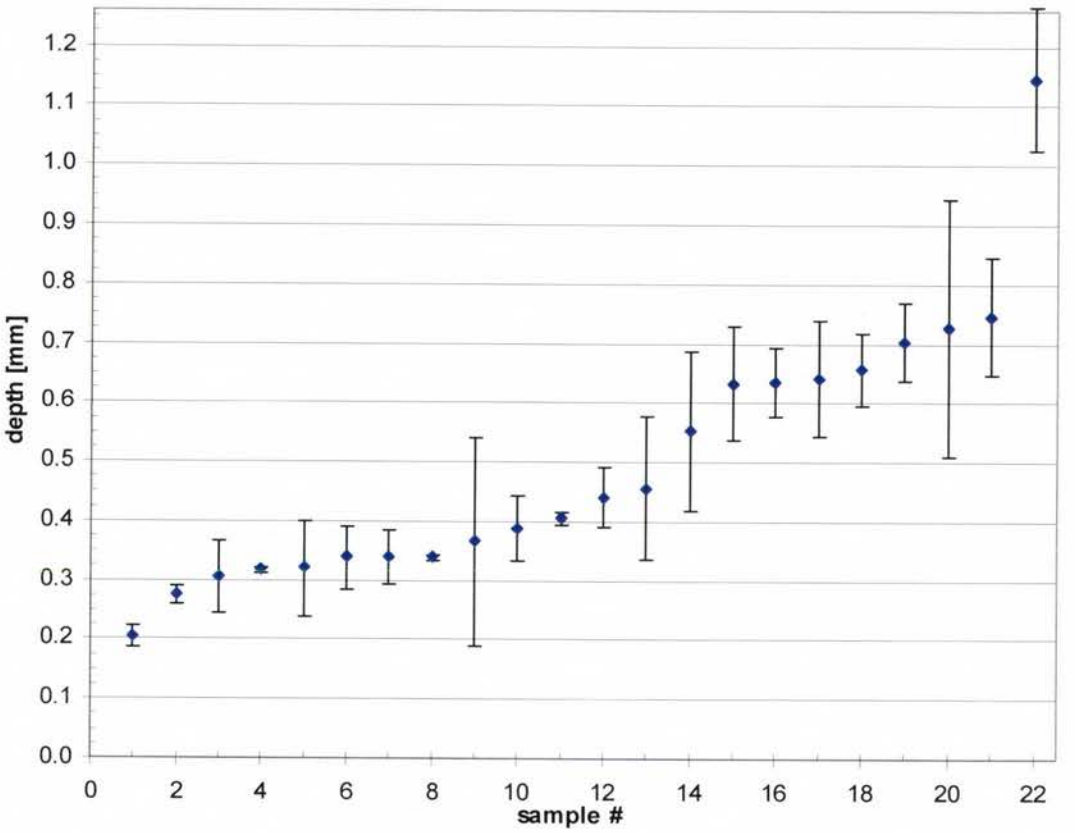

Figure 5.11 Thermocouple measurement depth from histology for CAX pig skin samples with error bars showing one standard deviation of the mean. Each point represents the average depth measured on at least section images of each skin sample.

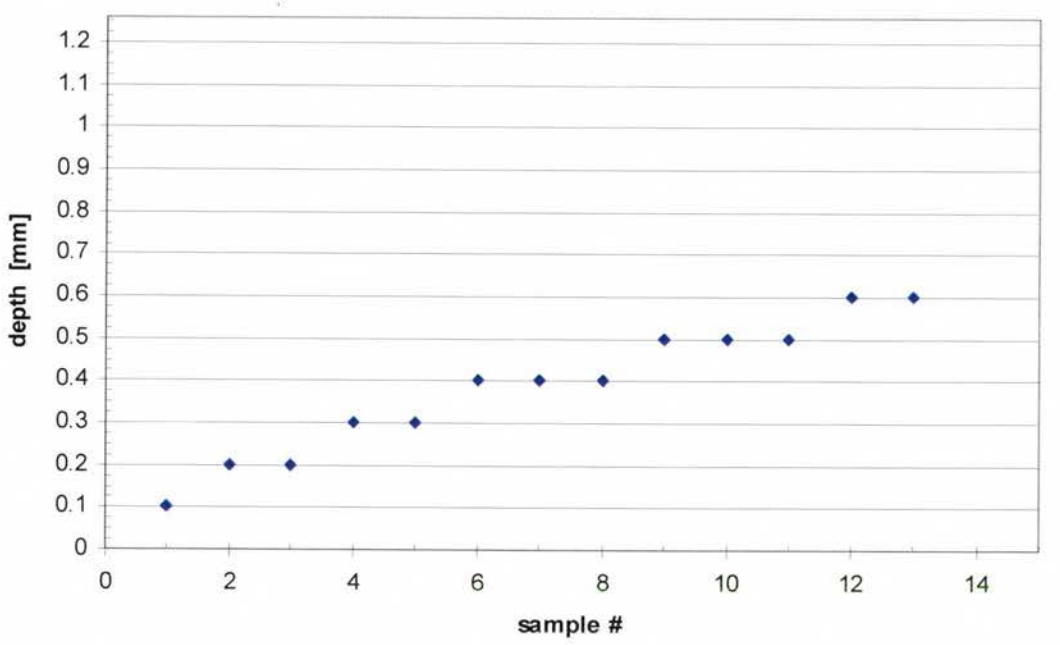

Figure 5.12 Thermocouple measurement depth from Ultrasound imaging for profile pig skin samples.

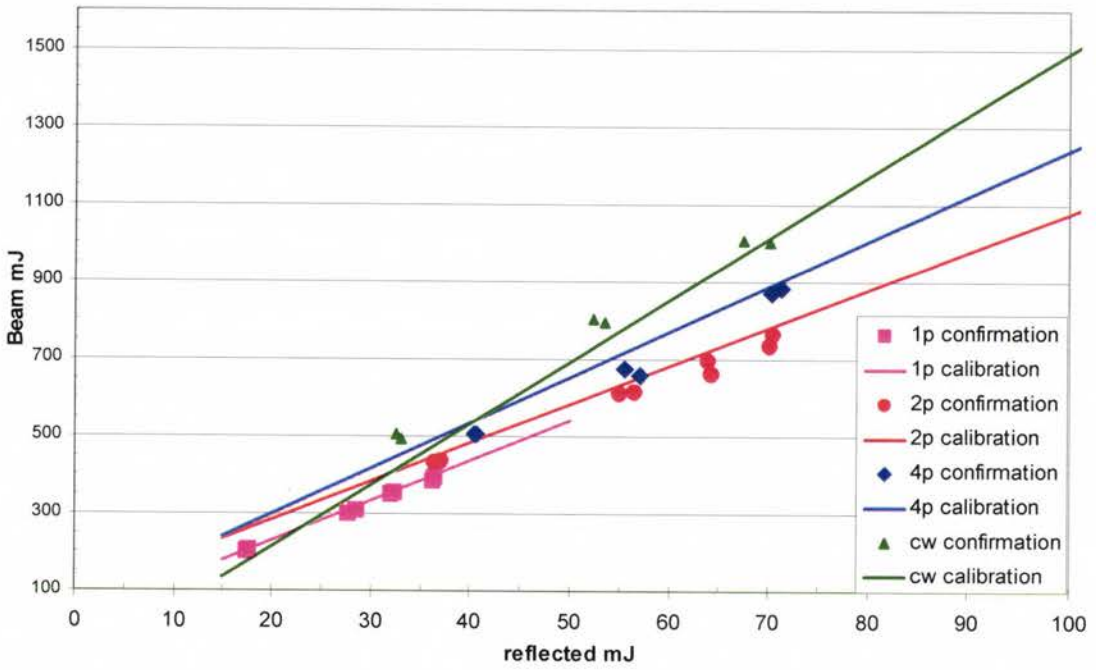

Figure 5.13 Calibration curves of sample irradiation beam relative to reflected beam (straight lines) for four representative pulse sequences and the corresponding consistency data points from post session confirmation measurements (from 16July2009). The pulse sequences are identified in the legend as 1p for single pulse, 2p for two pulse, 4p for four pulse, and cw for continuous wave.

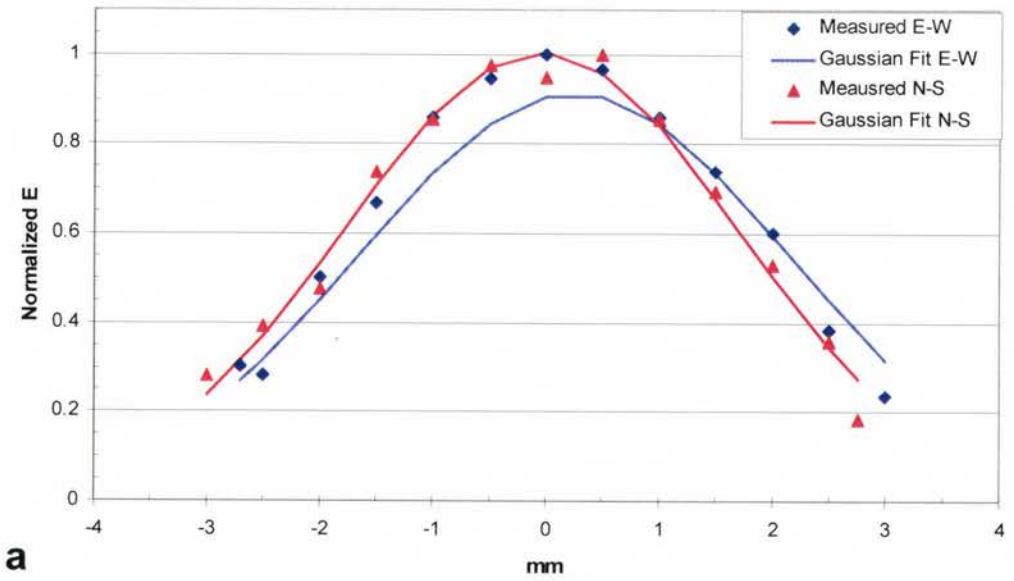

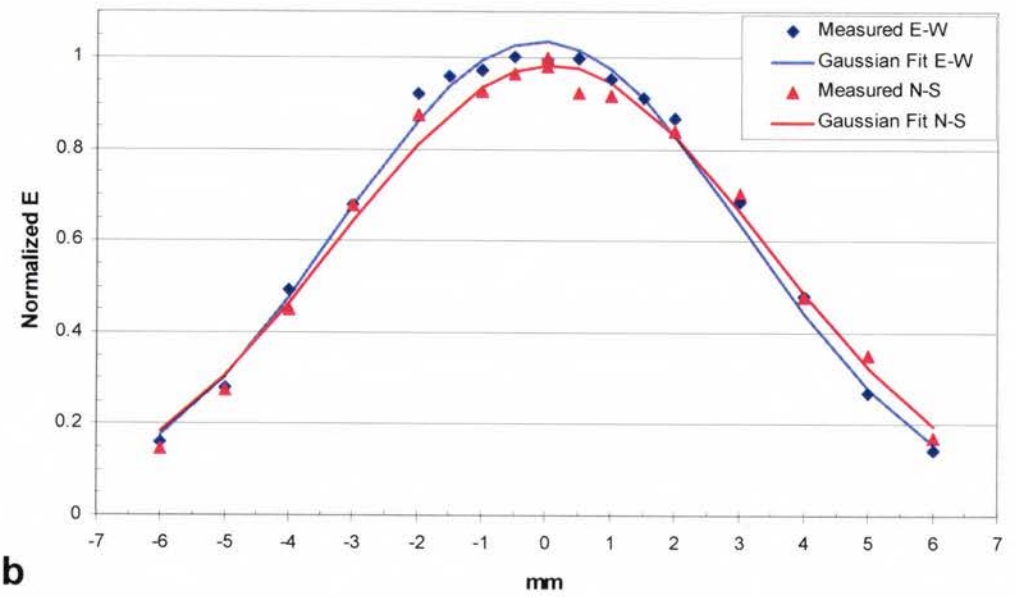

Figure 5.14 Beam profile measurements (diamonds and triangles) and Gaussian fit curves (lines) for a) unmodified beam (r = 3.2 mm) and, b) expanded beam (r=6.3 mm) at the position of tissue sample placement.

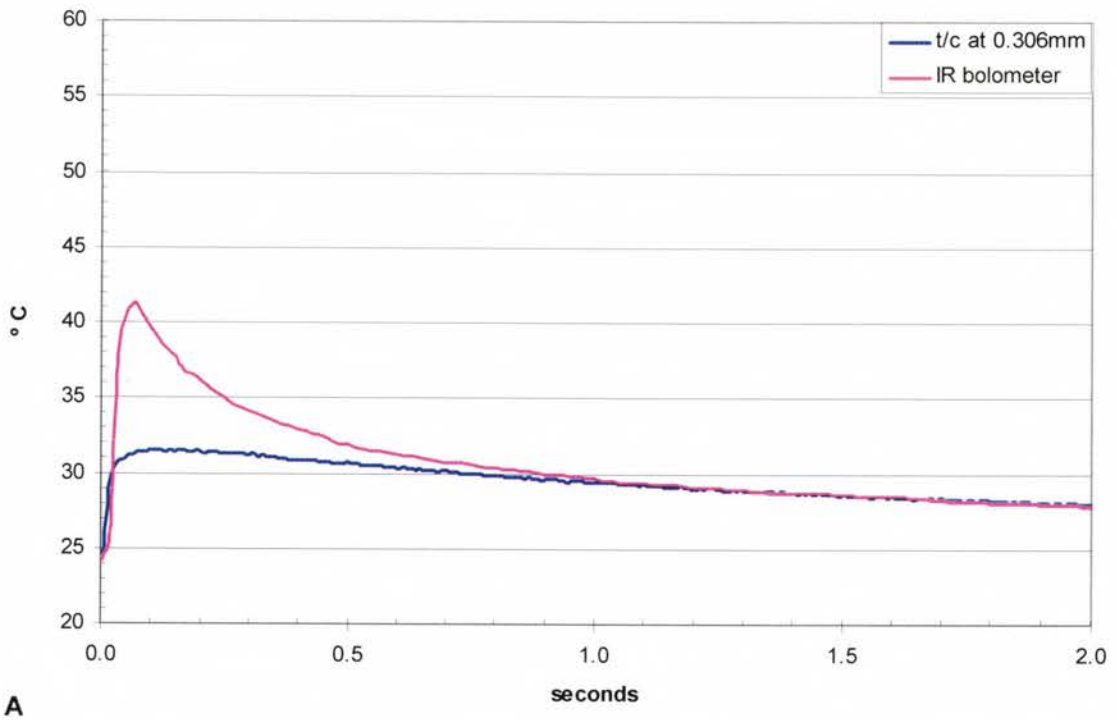
t/c at 0.306mm
IR bolometer
60
55
50
45
40
35
30
25
20
°C
0.0
0.5
1.0
1.5
2.0
seconds

A

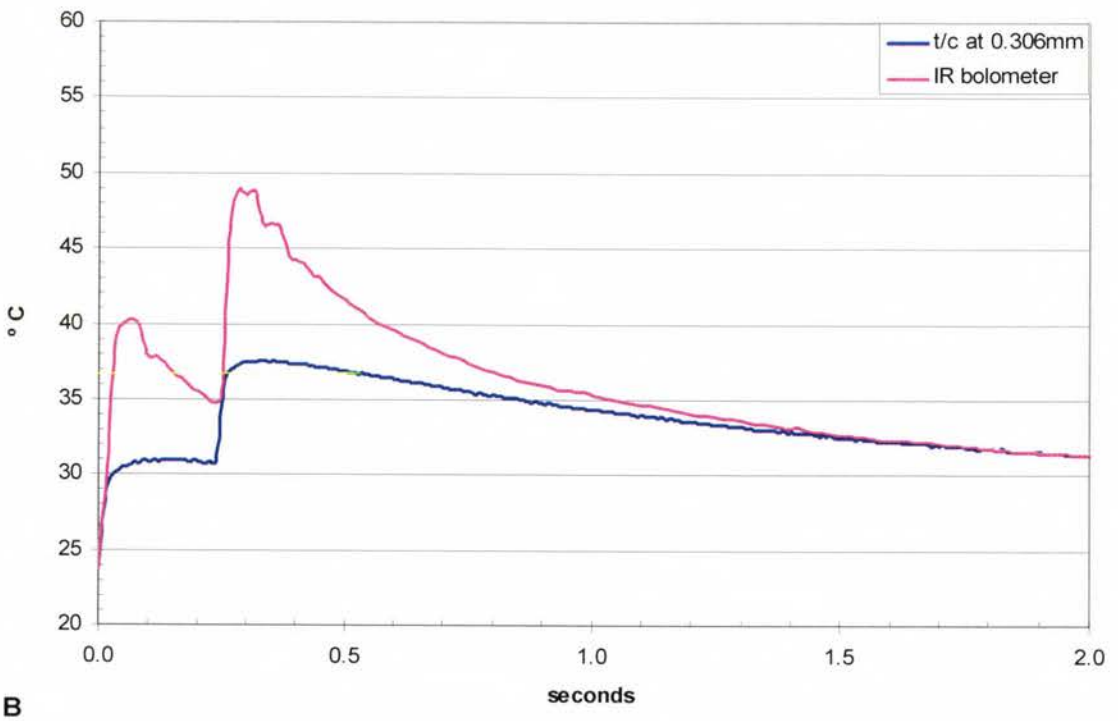
t/c at 0.306mm
IR bolometer
60
55
50
45
40
35
30
25
20
°C
0.0
0.5
1.0
1.5
2.0
seconds

B

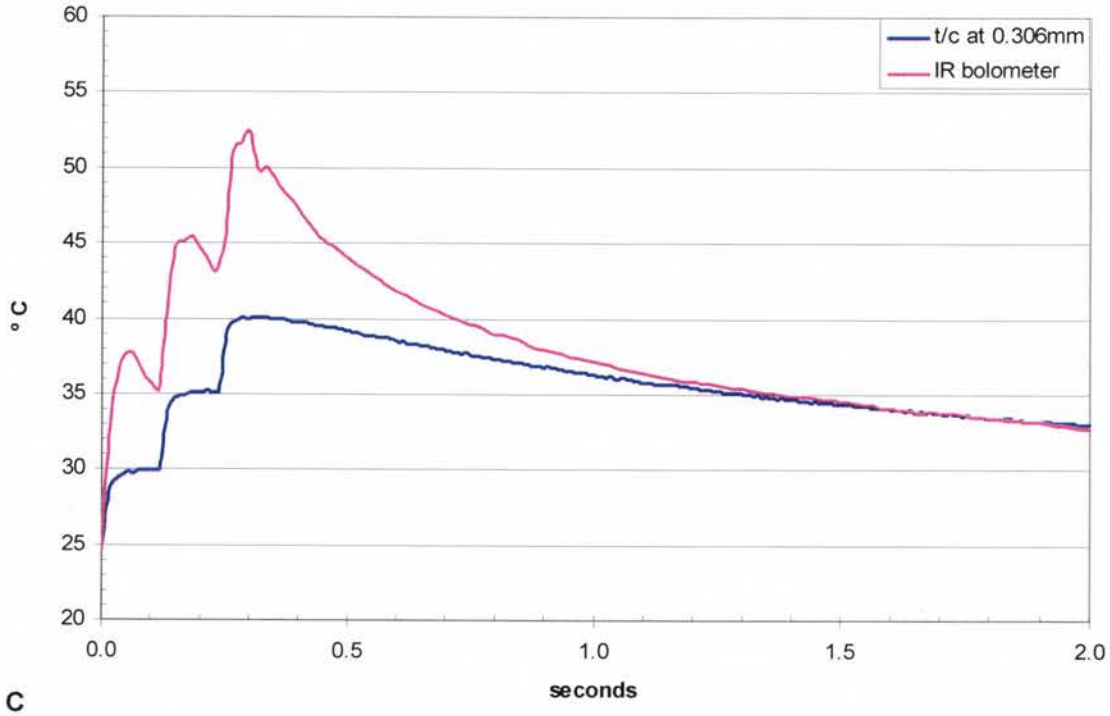
t/c at 0.306mm
IR bolometer
60
55
50
45
40
35
30
25
20
°C
0.0
0.5
1.0
1.5
2.0
seconds

C

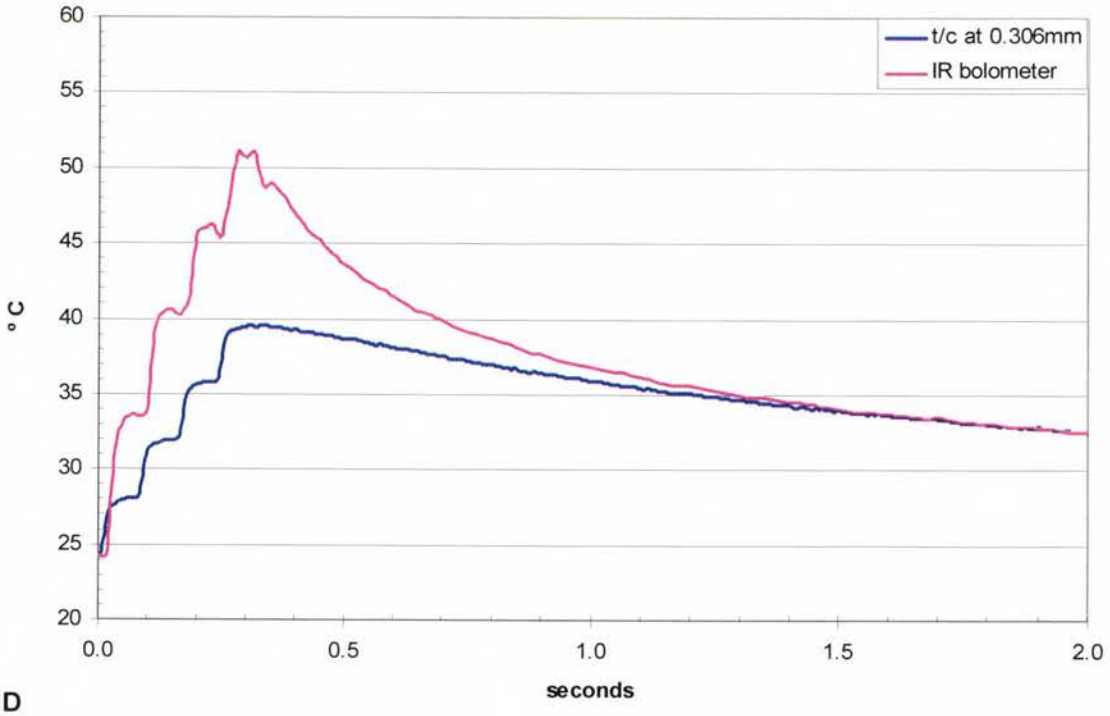
t/c at 0.306mm
IR bolometer
60
55
50
45
40
35
30
25
20
°C
0.0
0.5
1.0
1.5
2.0
seconds

D

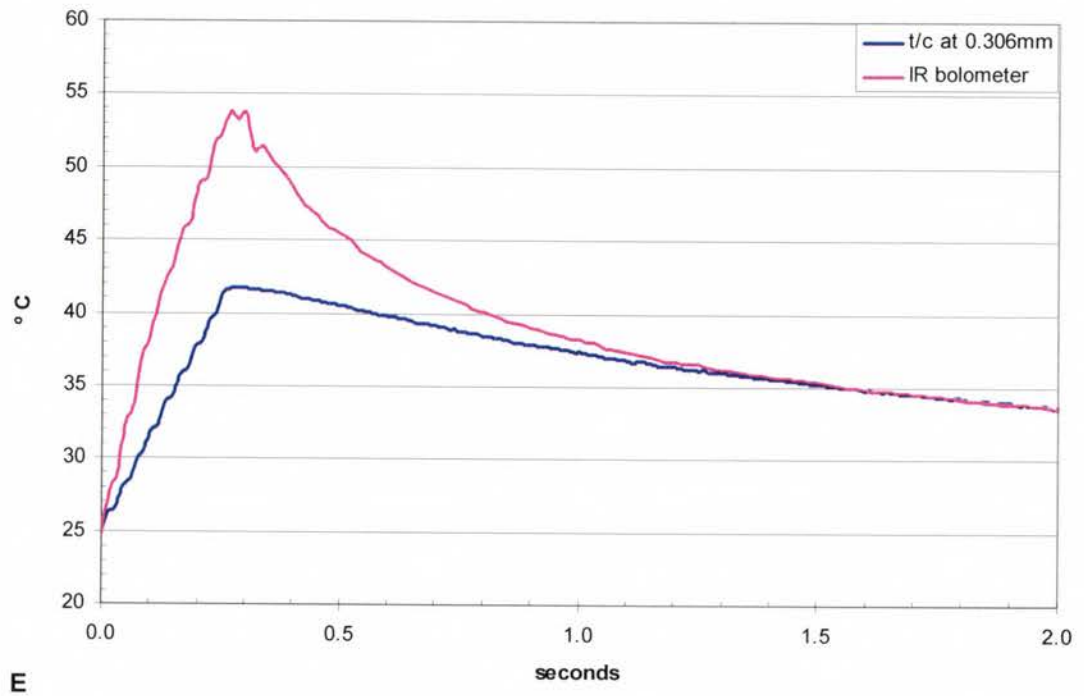

E

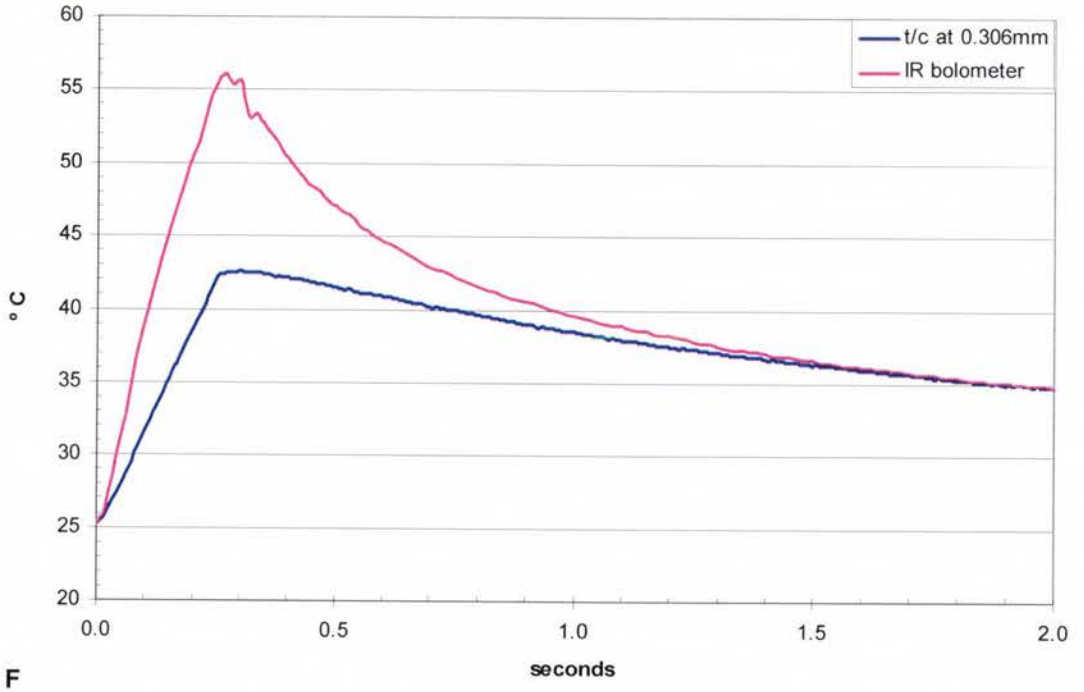

F

Figure 5.15 Temperature rise versus time at "surface" (pink) and at a depth of 0.306 mm (blue) for six pulse sequences: A) single pulse, B) two pulse, C) three pulse, D) four pulse, E) nine pulse, F) 0.25 seconds of continuous wave. The graphs represent roughly equal radiant energy for all sequences except the single pulse which was limited by laser power to about half. In the legends, thermocouple is abbreviated as t/c.

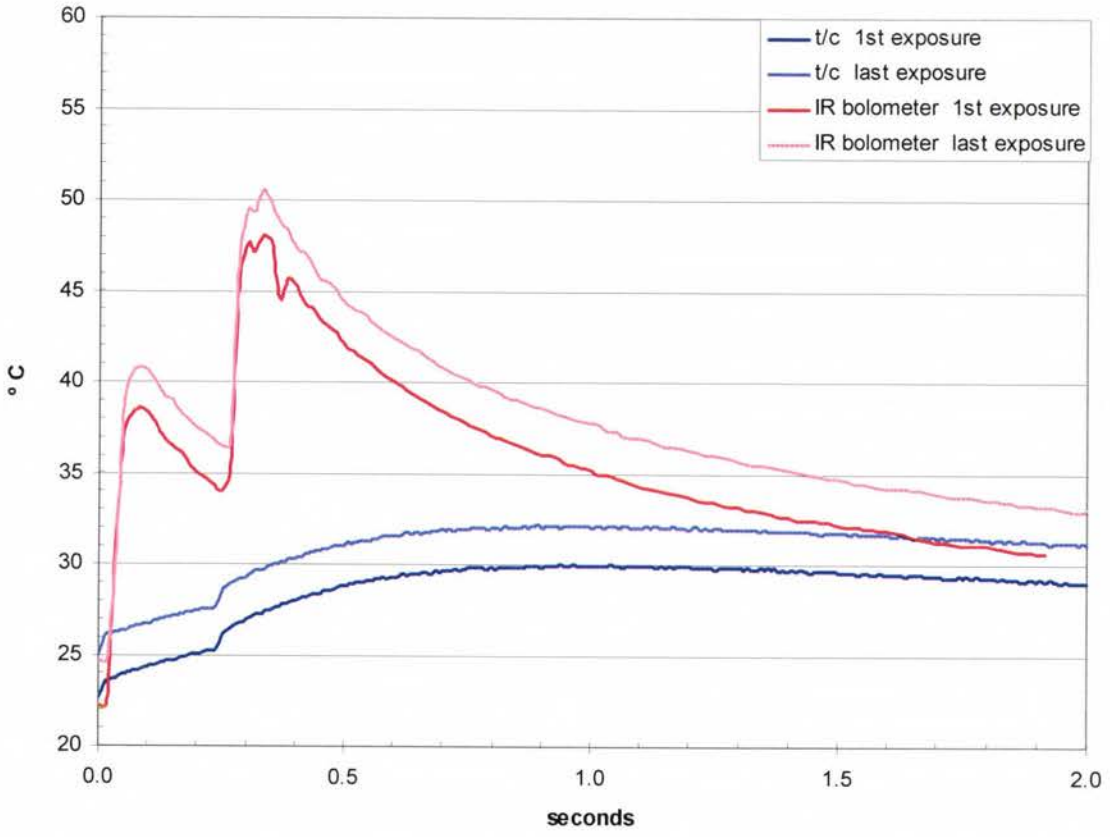

Figure 5.16 First (dark blue for t/c and red for surface) and last (light blue for t/c and pink for surface) exposure of 1st measurement session on 15 July 2009 (depth of thermocouple probe was 440 μm) showing consistency of rise for radiant energy of 883 mJ and 881 mJ respectively.

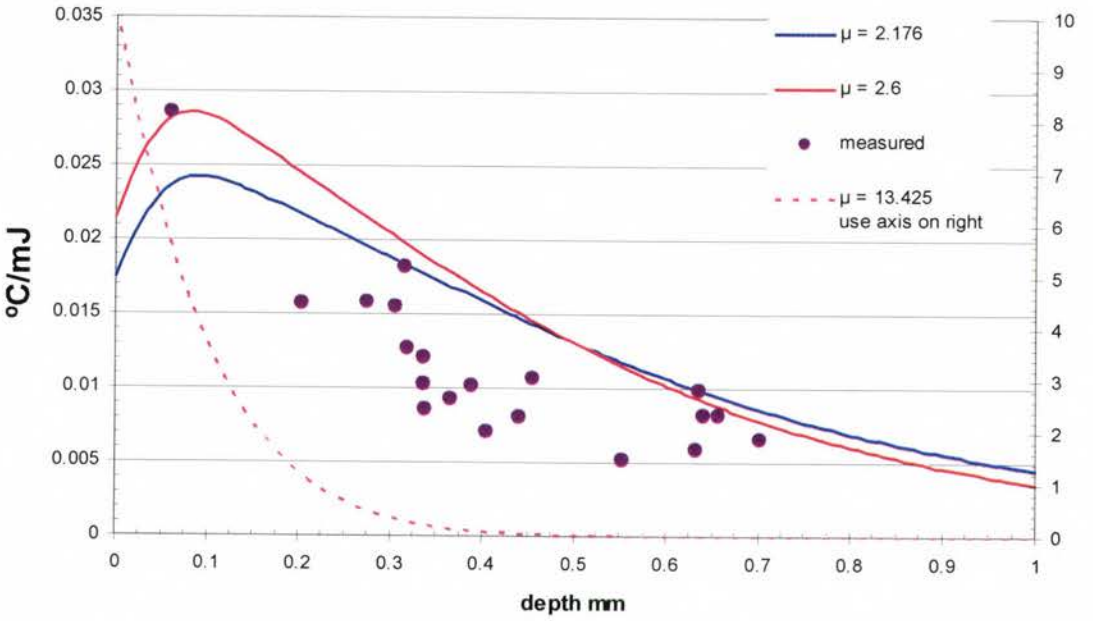

Figure 5.17 Modeled temperature rise per mJ for a two-pulse sequence showing effect of optical absorption coefficient. Lines are model results with solid corresponding to axis on left and dashed to the axis on right hand side. Dots are measured values for two pulse sequences on CAX, corresponding to values on left axis. All model results here used $C = 3.4$, $\rho = 0.00107$, $D = 0.12$.

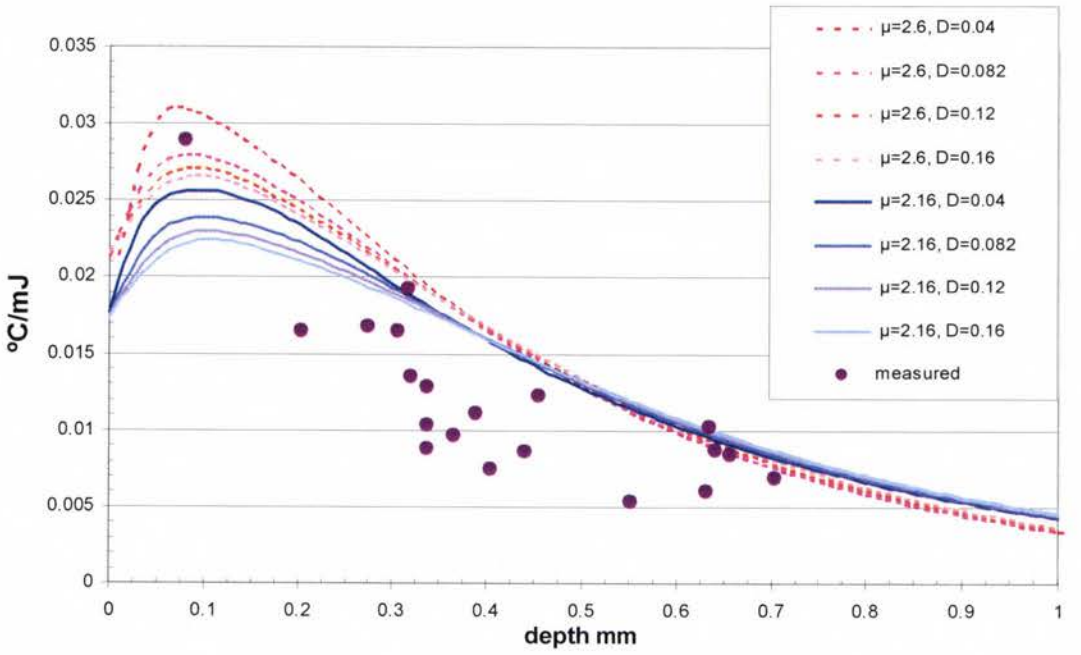

Figure 5.18 Modeled temperature rise per mJ for a three-pulse sequence showing effect of thermal diffusivity constant. Solid lines are model results corresponding to optical absorption coefficient of 2.16 and dashed lines represent optical absorption coefficient of 2.6. Dots are measured values for three-pulse sequences on CAX. All model results here used $C = 3.4$, $\rho = 0.00107$.

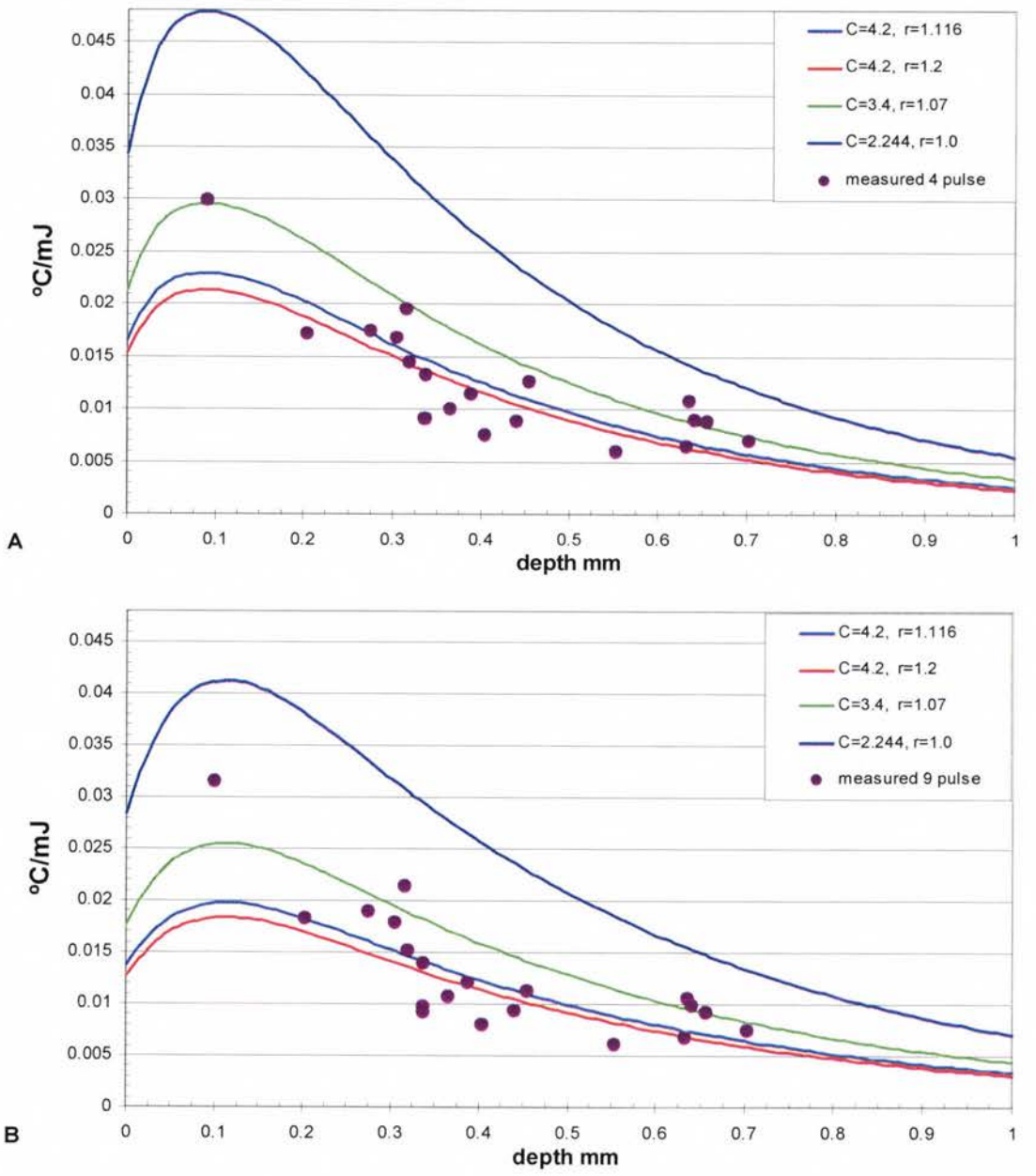

Figure 5.19 Modeled temperature rise per mJ for A) four-pulse sequence corresponding to optical absorption coefficient of 2.6, and B) nine-pulse sequence utilizing optical absorption coefficient of 2.16, showing effect of different values for specific heat constant, C, and relative density, ρ. Solid lines are model results all using thermal diffusivity value of 0.04. Dots are measured values for the four- and nine- pulse sequences on CAX.

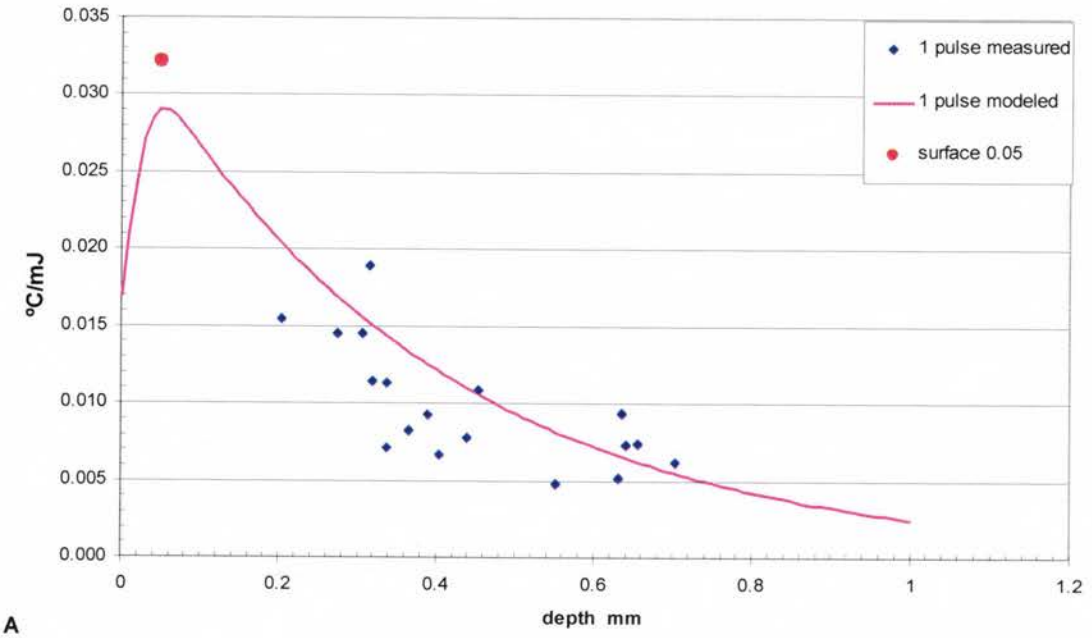
0.035
0.030
0.025
0.020
0.015
0.010
0.005
0.000
°C/mJ
0
0.2
0.4
0.6
0.8
1
1.2
depth mm
1 pulse measured
1 pulse modeled
surface 0.05

A

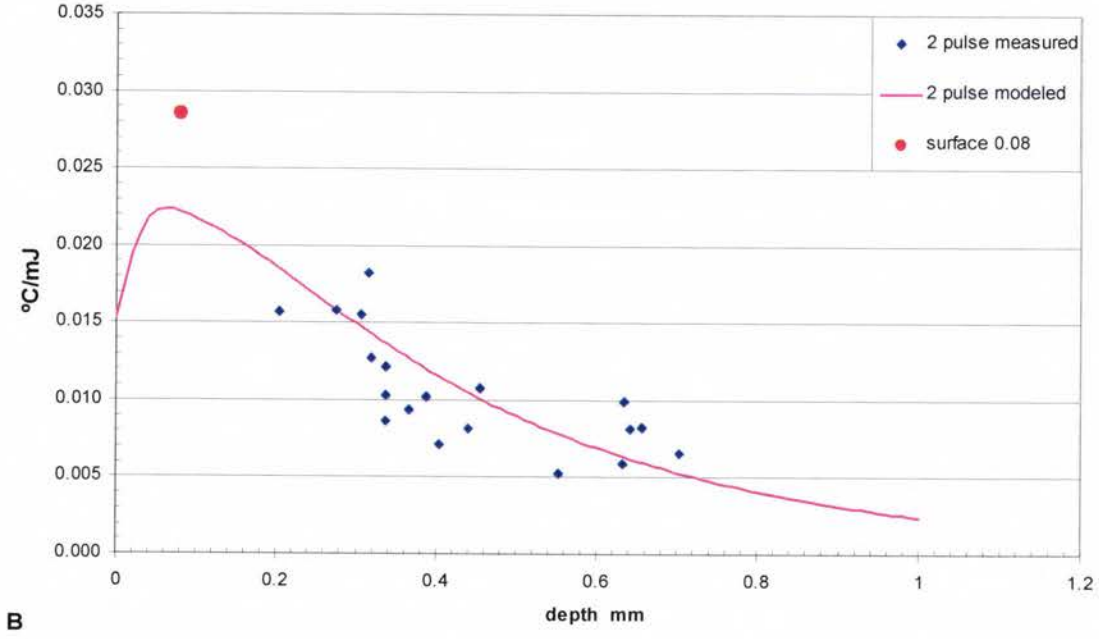
0.035
0.030
0.025
0.020
0.015
0.010
0.005
0.000
°C/mJ
0
0.2
0.4
0.6
0.8
1
1.2
depth mm
2 pulse measured
2 pulse modeled
surface 0.08

B

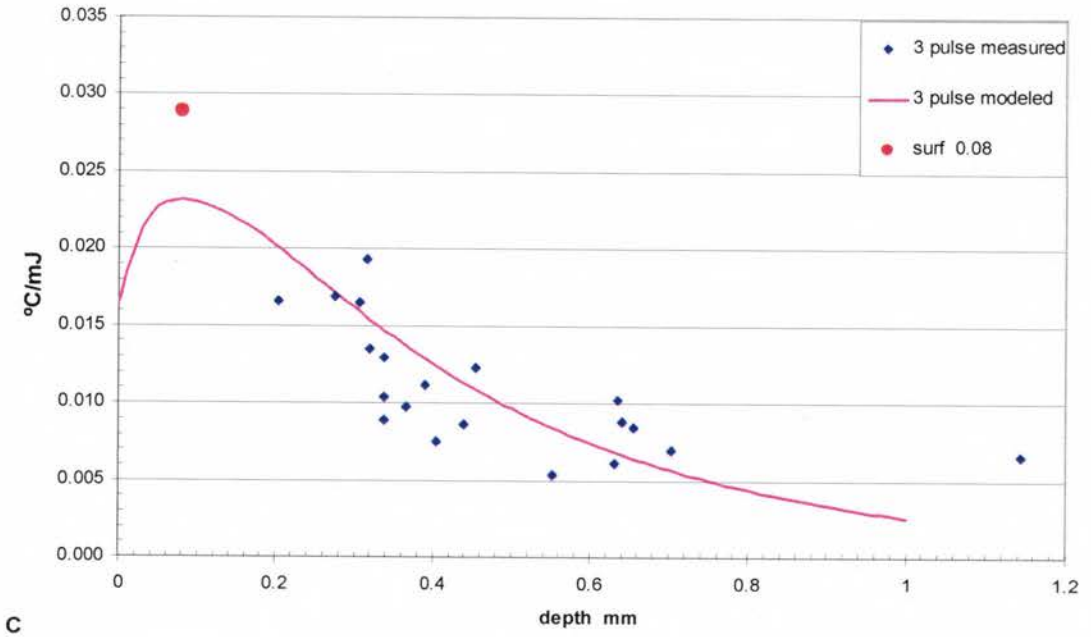
0.035
0.030
0.025
0.020
0.015
0.010
0.005
0.000
°C/mJ
0
0.2
0.4
0.6
0.8
1
1.2
depth mm
3 pulse measured
3 pulse modeled
surf 0.08

C

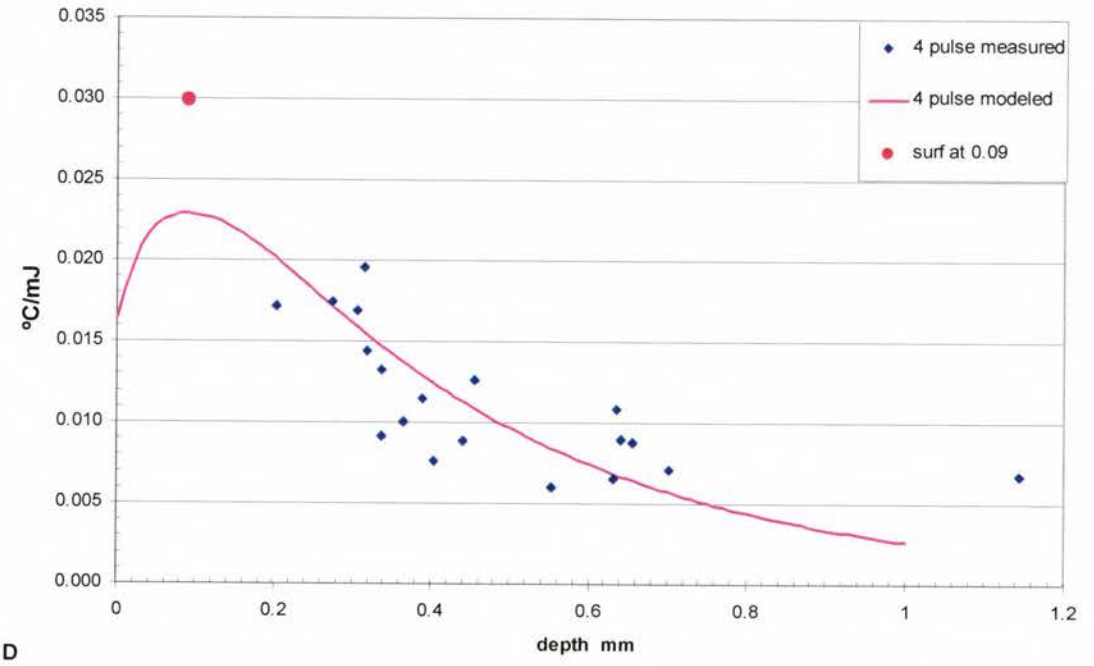
0.035
0.030
0.025
0.020
0.015
0.010
0.005
0.000
°C/mJ
0
0.2
0.4
0.6
0.8
1
1.2
depth mm
4 pulse measured
4 pulse modeled
surf at 0.09

D

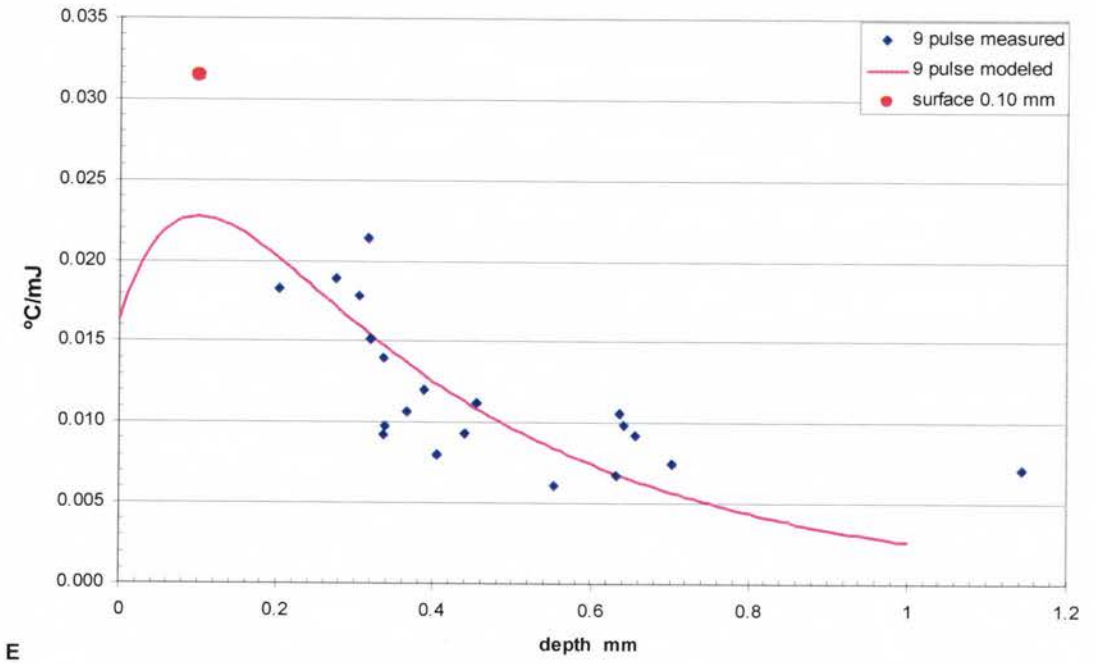

E

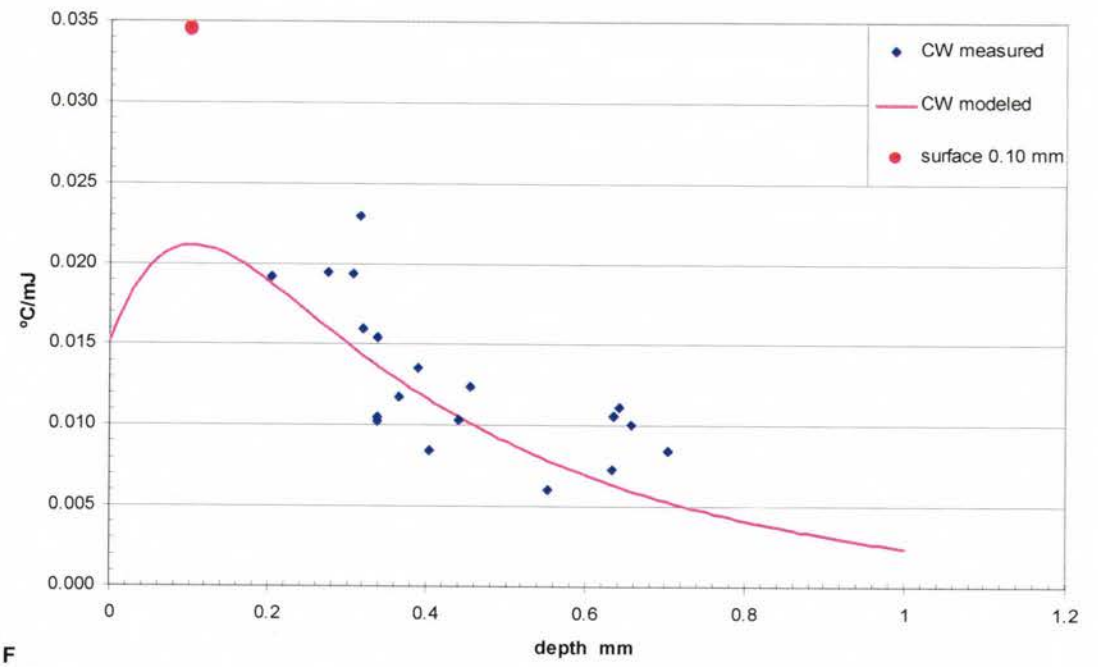

F

Figure 5.20 Modeled temperature rise per radiant exposure for the six pulse sequences using the best fit for all depths with parameters of $\mu = 2.6\ mm^{-1}$ $D = 0.04\ mm^2\ sec^{-1}$, $C = 4.2\ J\ g^{-1}\ °C^{-1}$, $\rho = 0.001116\ g\ mm^{-3}$. Surface measurement is shown at the depth of maximum rise given by the model for the particular pulse sequence.

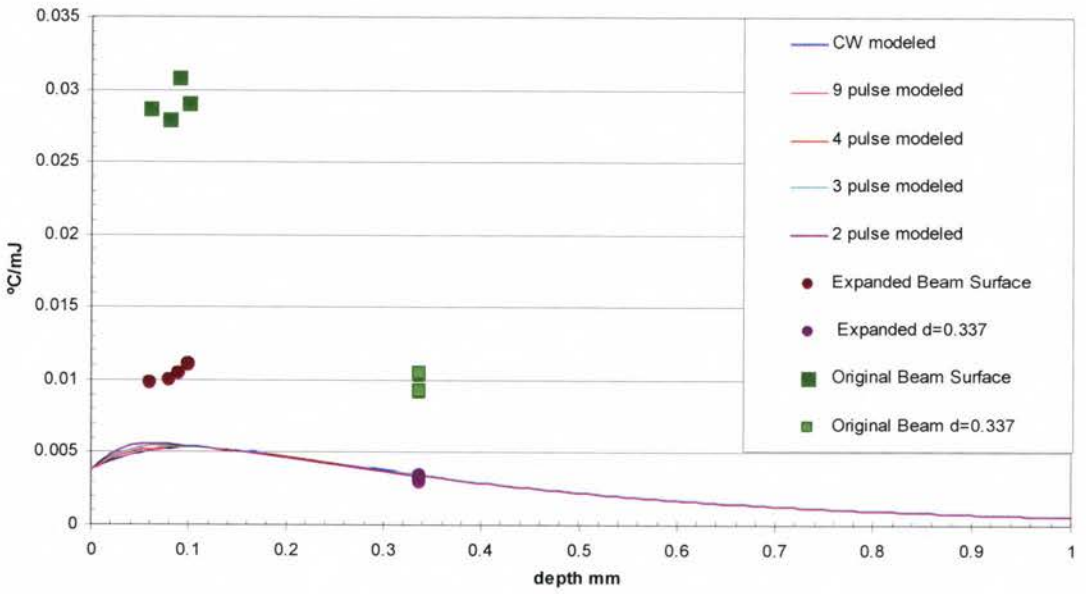

Figure 5.21 Modeled and measured temperature rise per radiant exposure for five of the six pulse sequences using the values determined for the original beam of $\mu = 2.6\ mm^{-1}$, $D = 0.04\ mm^2\ sec^{-1}$, $C = 4.2\ J\ g^{-1}\ °C^{-1}$, $\rho = 0.001116\ g\ mm^{-3}$. Surface measurements are shown at the depth of maximum rise given by the model for the particular pulse sequence. Surface and depth temperature measurements during irradiation with the original beam on the same sample are also shown for comparison.

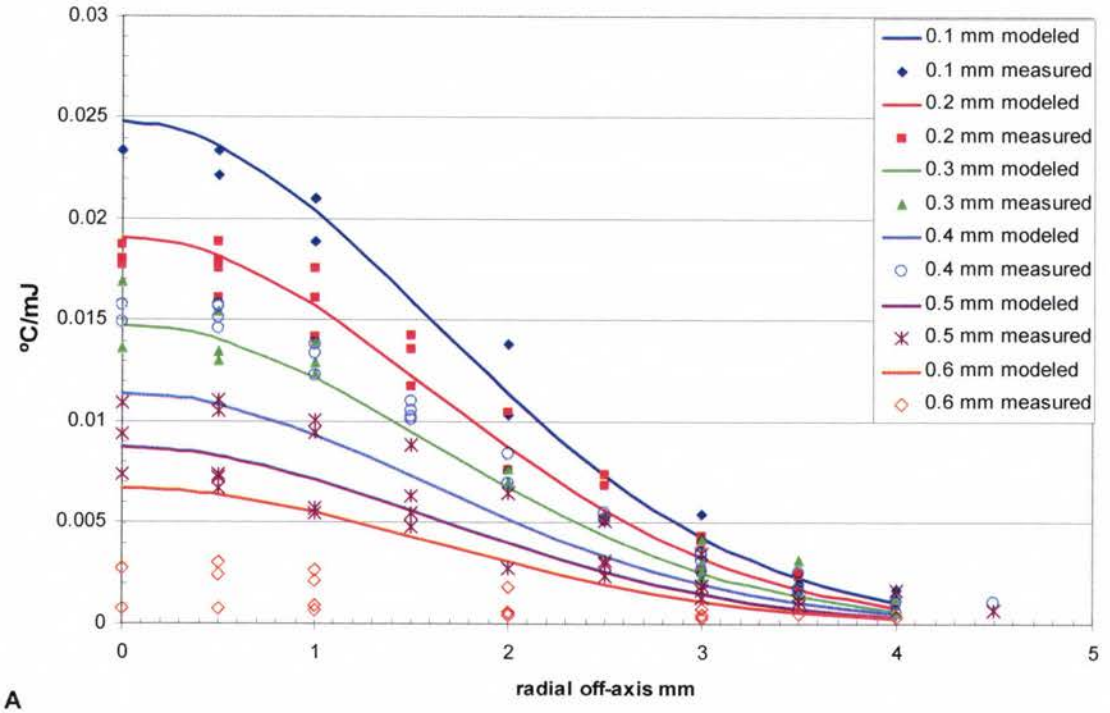
0.03
0.025
0.02
0.015
0.01
0.005
0
°C/mJ
0
1
2
3
4
5
radial off-axis mm
0.1 mm modeled
0.1 mm measured
0.2 mm modeled
0.2 mm measured
0.3 mm modeled
0.3 mm measured
0.4 mm modeled
0.4 mm measured
0.5 mm modeled
0.5 mm measured
0.6 mm modeled
0.6 mm measured

A

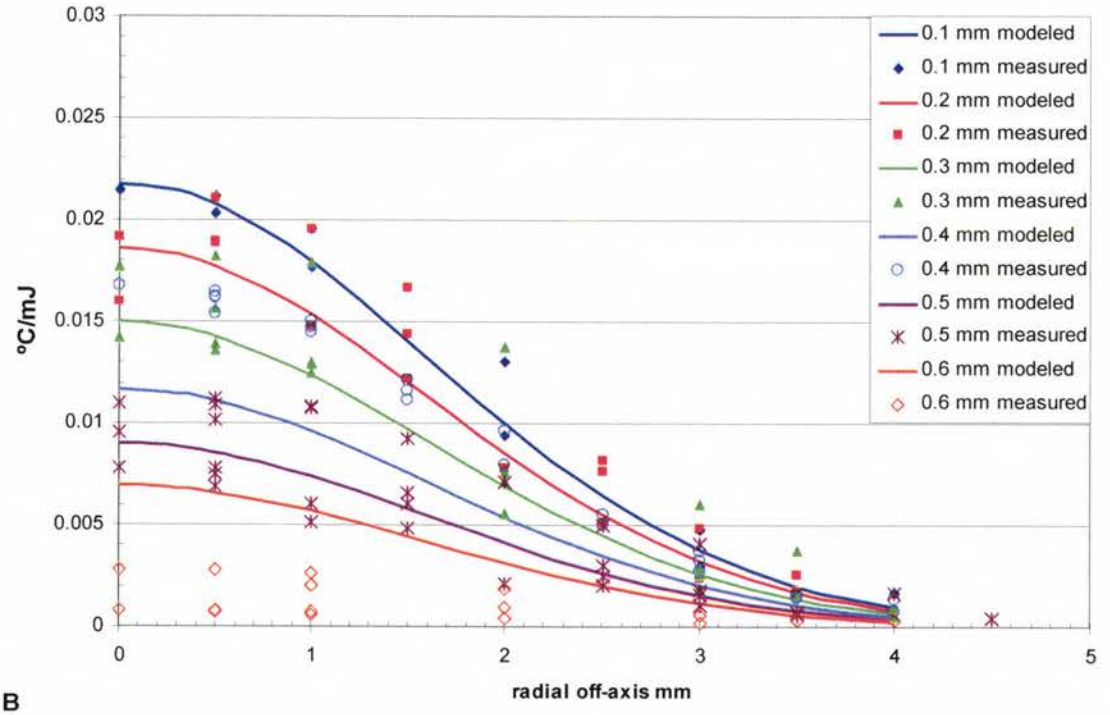
0.03
0.025
0.02
0.015
0.01
0.005
0
°C/mJ
0
1
2
3
4
5
radial off-axis mm
0.1 mm modeled
0.1 mm measured
0.2 mm modeled
0.2 mm measured
0.3 mm modeled
0.3 mm measured
0.4 mm modeled
0.4 mm measured
0.5 mm modeled
0.5 mm measured
0.6 mm modeled
0.6 mm measured

B

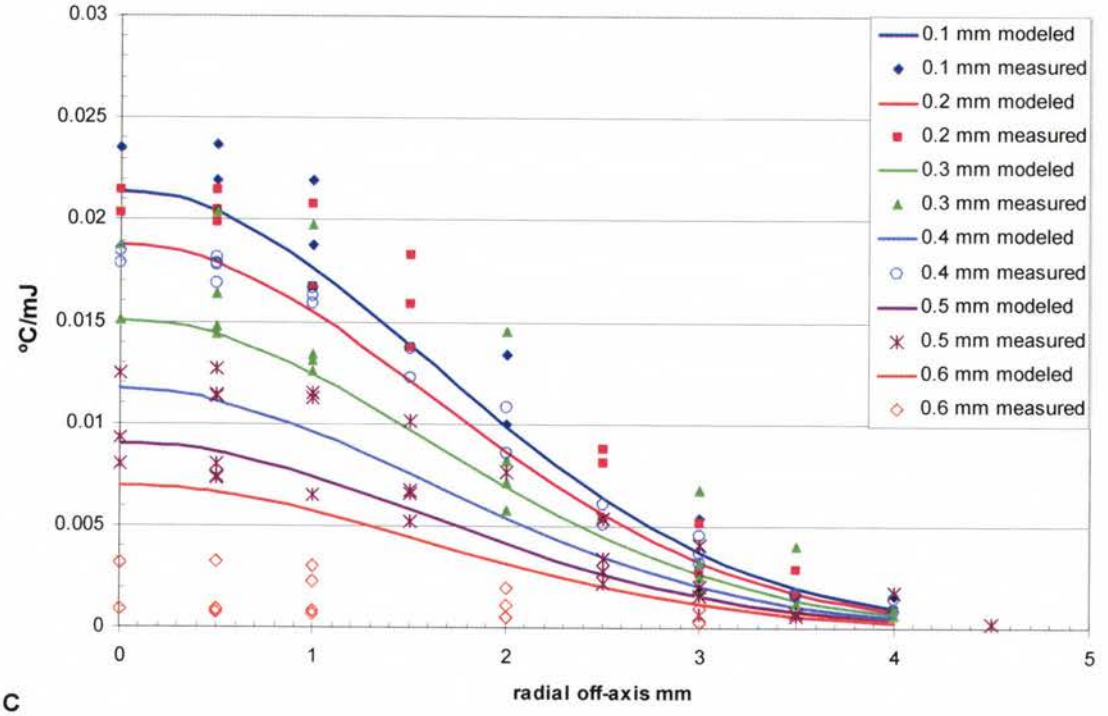
0.03
0.025
0.02
0.015
0.01
0.005
0
°C/mJ
0
1
2
3
4
5
radial off-axis mm
0.1 mm modeled
0.1 mm measured
0.2 mm modeled
0.2 mm measured
0.3 mm modeled
0.3 mm measured
0.4 mm modeled
0.4 mm measured
0.5 mm modeled
0.5 mm measured
0.6 mm modeled
0.6 mm measured

C

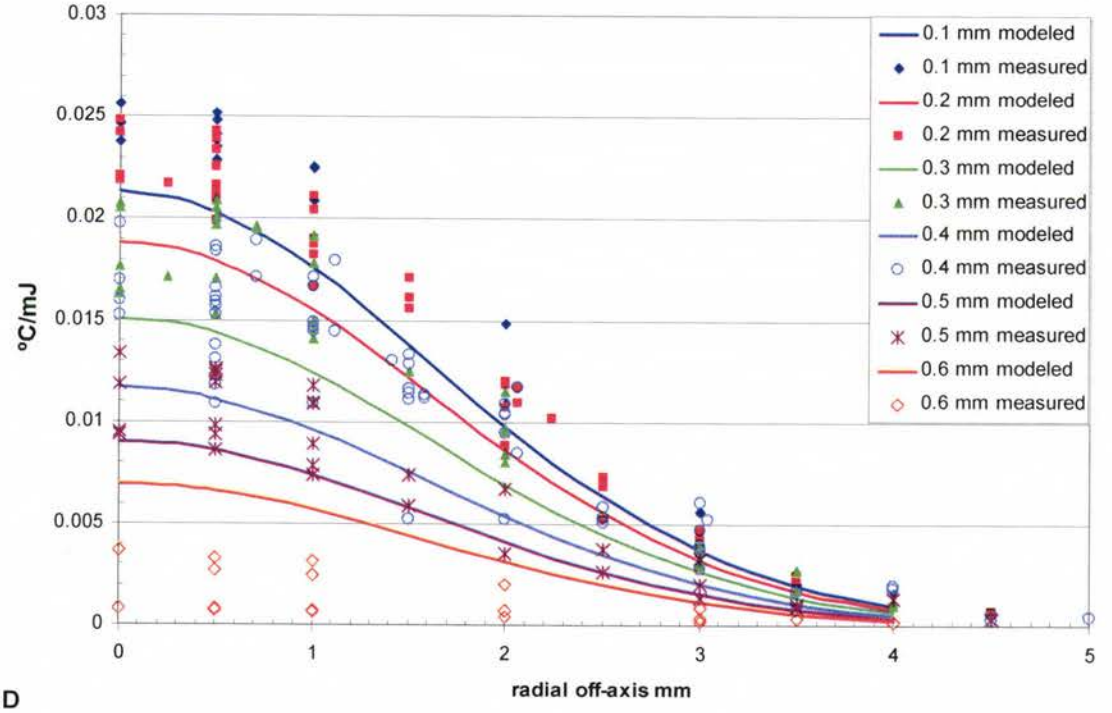
0.03
0.025
0.02
0.015
0.01
0.005
0
°C/mJ
0
1
2
3
4
5
radial off-axis mm
0.1 mm modeled
0.1 mm measured
0.2 mm modeled
0.2 mm measured
0.3 mm modeled
0.3 mm measured
0.4 mm modeled
0.4 mm measured
0.5 mm modeled
0.5 mm measured
0.6 mm modeled
0.6 mm measured

D

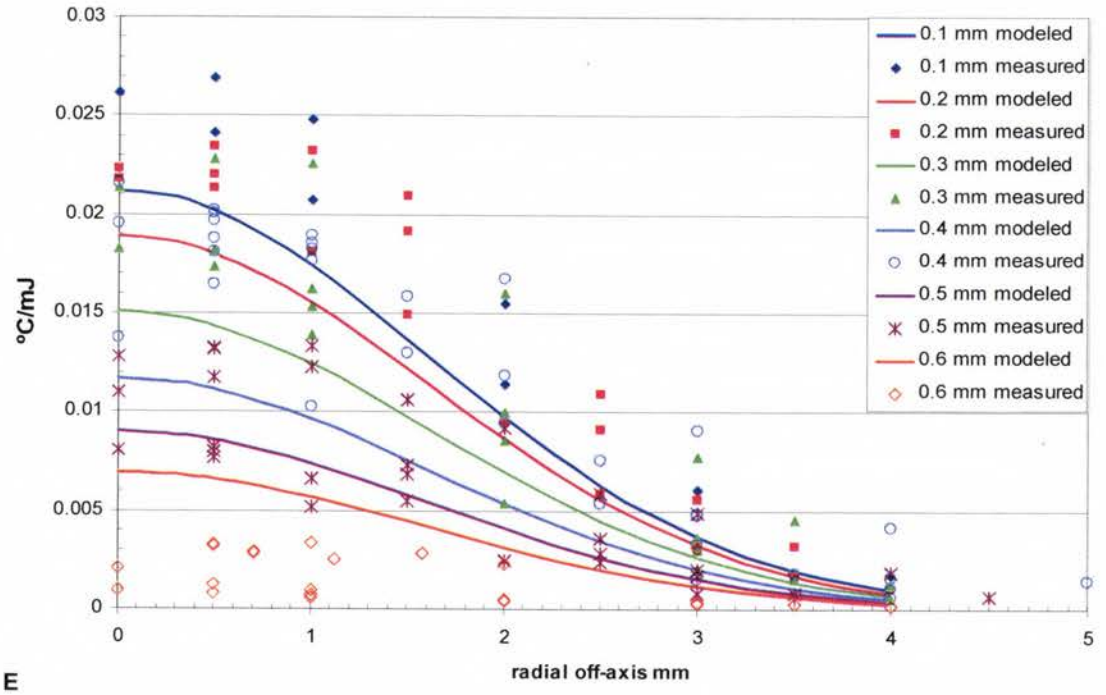

E

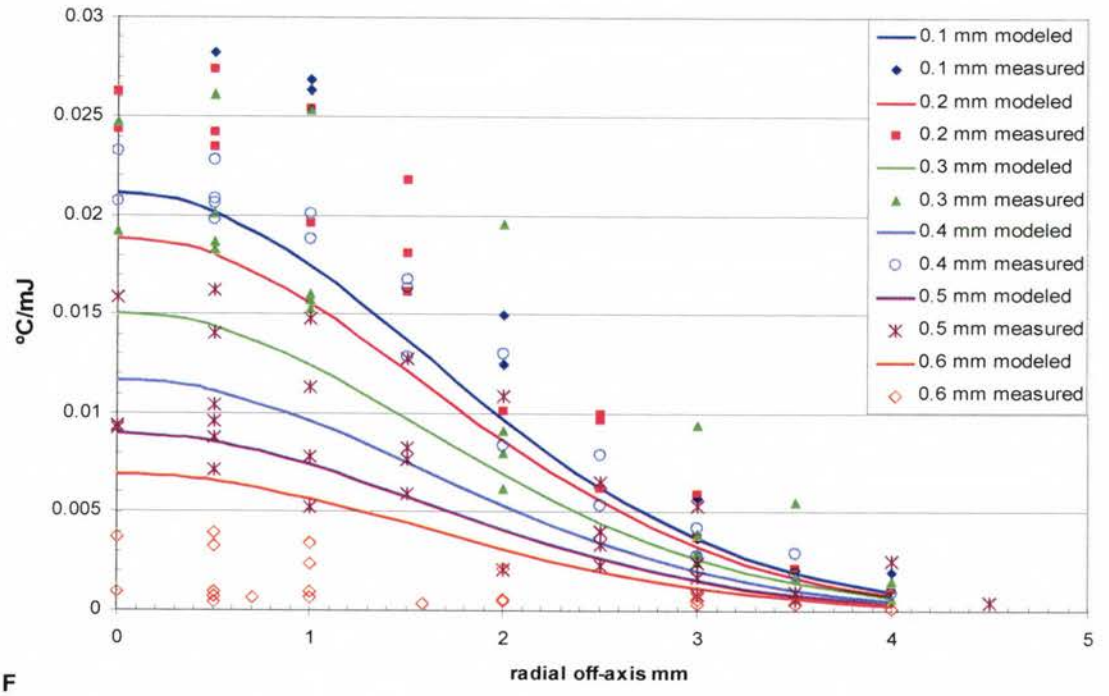

F

Figure 5.22 Modeled (lines) and measured (points) temperature rise per radiant exposure at six depths in pig skin. Graphs are for each of the six pulse sequences studied: A) single 10 msec pulse, B) two pulses, C) three pulses, D) four pulses, E) nine pulses, F) CW for 250 msec.

Chapter 6

Effective Depth of Measurement of Micro-Bolometer Array Infrared Detector

6.0 Abstract

Temperature measurement of biological tissue during and following laser irradiation with a non-contact imaging instrument has proven to be a vital tool for evaluating tissue response. Laser applications in medicine, research, and safety rely on the temperature profiles measured in experiments. For most studies, the temperature measured is assumed to be at the plane of the tissue surface. However, models of tissue heating with mid-infrared lasers show that a distinct heat buildup occurs for some depth below the surface before reaching a maximum. In these cases, the assumption of the detector measuring at the exact surface would significantly bias the measurements. Therefore, some knowledge of the effective depth of measurement would enable the measurements to be more accurately described. The effective measurement depth was between 50 μm and 120 μm for 2.0 μm laser light on pig skin.

6.1 Introduction

Temperature measurement has been important in medicine and biology since Hippocrates discussed fever.[1] However, infrared radiation was not identified as behaving like light until 1800.[2] Laser irradiation of tissue is often studied with a non-

contact heat measurement instrument sensitive to this "dark heat". The first electronic imaging of heat radiated by humans waited for over one and a half centuries.[3-4] The benefit of visualizing the heat energy deposited by lasers is offered by instruments recording measurements in two dimensions, that is the thermal camera. The popularity of lasers in medicine raised the standard of imaging relative temperatures to measurement of absolute temperatures and changes in temperatures.[5] While the thermal camera has since become very popular, there are several unresolved issues regarding their results.

Some issues are particular to the type of thermal imaging and laser irradiation study. One is the influence of extremely high temperatures of the ejected material during laser ablation studies.[6] Laser welding of blood vessels has become one of the most rigorously investigated types of tissue irradiation.[7] Studies of skin cooling are often perturbed by the IR shielding of the cooling agent.[8] Other clinical applications of IR thermal imaging such as detecting inflammation of infected wounds, injured joints, or life-threatening pneumothorax do not require the precision necessary for laboratory research.[9-11]

One of the most common issues left unaddressed is the effective depth or region from which the thermal camera is receiving its IR signal.[12-17] In some cases, the temperature is simply reported as the surface of the tissue, without any information on the type of detector used in the camera.[13,18-20] Thermal cameras are not the only non-contact instruments to assume measurement at the exact surface of the tissue rather than from a finite volume.[21-22] The use of thermal cameras relies on the emission of IR

radiation from the tissue. Yet some laser – tissue heating models depend on an assumption of zero heat flux at the boundary of the tissue – air interface.[23]

One of the few studies to evaluate thermal imaging camera measurement depths claims that if thermal gradients are not significant with the first 100 μm of tissue, the measurement will approximate the surface temperature.[24] Another study gives a cursory treatment to the question of "surface" measurement depth by defining it to be the inverse of the tissue optical absorption coefficient for the incident light on the specific tissue.[25] Finally, a study integrated the IR emissions from all depths to calculate a theoretical temperature at the detector location, but reported the measurements simply as "surface temperatures".[26] The only published study dedicated to performance characteristics of thermal cameras simply claims results are surface temperature.[27]

Thermal imaging cameras have also been used to determine incident beam shape and size based on the assumption that the detector is measuring the interface plane and not a volume.[28-29]

The hypothesis investigated in this project is that a verified thermal model of laser irradiation can estimate the effective depth of measurement of a non-contact IR thermal camera nominally measuring surface temperature of *ex vivo* pig skin.

6.2 Materials and Methods

6.2.1 Irradiation and Measurement

Irradiations of pig skin with a 50 W Tm:YAG fiber laser operated with moderate pulse length sequences of 250 msec total duration were measured with an infrared

micro-bolometer array thermal video camera as described in Chapter 5. The sequences were evenly spaced 10 msec pulses as shown in Figure 5.1. There were six different pulse sequences. The first was a single 10 msec pulse. The intermediate four sequences were two pulses (duty factor 0.08 of the 250 msec period), three pulses (duty factor 0.12), four pulses (duty factor 0.16), and a nine-pulse sequence (duty factor 0.36). The last sequence was a 250 msec period of Continuous Wave (CW) irradiation. The 2.0 μm wavelength laser beam had a $1/e^2$ radius of 3.2 ± 0.28 mm as measured with a pin-hole method, for irradiations of 35 pig skin samples. The laser beam was expanded with a set of f50 and f100 lenses positioned at the sum of their focal lengths into a nominally parallel beam with a $1/e^2$ radius of 6.3 mm for irradiation of one pig skin sample. The beams were verified to have a Gaussian shape in the lowest order mode prior to each measurement session. In addition, the preparatory steps of each measurement session included calibrating a small reflection from the optics to determine the exact radiant exposure for each individual irradiation as described in section 5.2.1. The experimental arrangement is shown in Figure 6.1.

Temperature rise during irradiation and cooling after irradiation was measured with a non-contact thermal imaging video camera model S65HSV (FLIR Systems, Weisbaden Germany). The camera's detector was a 320 × 240 array of micro-bolometer elements. The camera was calibrated by the manufacturer with a sensitivity specification of ± 0.05 °C with NIST traceable blackbody sources (certificate shown as Appendix 6.A). The emissivity was set to 0.98 for skin imaging.[30-34] Images were transferred from the camera to a PC via IEEE 1394 at 60 frames per second with no inter-leaf of pixels. The micro-bolometer responds to infrared radiation in the spectral

range of 7.5 to 13 μm with a change in resistance to applied bias. The thermal camera was mounted on a secure tripod at one meter from the pig-skin surface at an angle of approximately 30° off of normal. The raw data was extracted from the thermal images using the manufacturer's software, Researcher Pro version 2.8 (FLIR Systems, Wiesbaden Germany).

6.2.2 Data Analysis

Baseline skin temperature was subtracted from all recorded temperatures to ameliorate the effects of slight fluctuations in the ambient room and tissue sample temperatures from one measurement session to another. All temperature rise data was normalized to the radiant energy of the Tm:YAG laser exposing the tissue in order to allow comparison between pulse sequences and between different samples of pig skin.

Measured temperature rise per radiant energy for the six different pulse sequences were compared with predicted values calculated using the Vyas approach as described in Chapter 5.2.5. The predicted values were judged on three criteria when a range of optical and thermal constants were employed in the calculations. The first was to match measured temperatures at all depths in Chapter 5. The second criterion for best prediction was to only match the maximum predicted temperature rise to the IR camera reading of "surface" temperature. The last basis for evaluation was to match the maximum predicted temperature to the IR camera "surface" measurement for a larger beam size. In this comparison the beam diameter was doubled so the beam energy was distributed over four times the area compared to the previous experiments. The depth at which the model calculated the maximum temperature rise for the six different pulse

sequences was interpreted to be the depth at which the IR surface camera was effectively measuring temperature. The IR energy radiated from skin in the micro-bolometer's response range has a water attenuation coefficient roughly ten times greater than that of the incident 2.0 μm laser light (Figure 6.2, data from Wieliczka et al).[35]

The thermal response of pig skin as measured by the thermal camera was also compared to the direct incident beam intensity. Beam intensity profiles were measured with model PM10 thermopile probes (Coherent, Santa Clara CA) read by a model EPM2000 meter (Coherent, Santa Clara CA). Beam intensity profiles were measured on ten separate occasions during the course of the experiments and the average $1/e^2$ radius was 3.2 ± 0.28 mm using a pinhole method.[36-37] The $1/e^2$ radius was expanded to 6.3 mm for one session. In comparison to the beam intensity pinhole method, thermal images were analyzed for temperature intensity profile. Raw pixel arrays of temperature were extracted from thermal images and converted to temperature profiles over distance with the pixel size calibration value of 1.25 mm $pixel^{-1}$ at camera distance of 1 m as shown in Chapter 3. The $1/e^2$ radii of the temperature profiles were determined using a cubic spline interpolation on both sides of the maxima and then averaged.

6.3 Results

The modeling of skin temperature rise from irradiation by a 2.0 μm Tm:YAG laser was performed for six pulse sequences of increasing duty factor. The model results were calculated with a range of values for thermal and optical constants optimized to best match measured data. Modeled temperatures were also examined to identify the effective depth of measurement from a non-contact microbolometer thermal imaging

camera data. The camera was used to record (as described in Chapter V) over three thousand pig skin laser irradiations. The measured temperature rise per incident energy was compared to predicted temperatures for six pulse sequences. Three sets of thermal and optical constants were found to best predict the measured temperatures based on the three criteria. The depths at which the microbolometer measurement best matched modeled temperatures are shown in Figure 6.3.

The first criterion considered the model which best fit the measured temperature rise at all skin depths from the surface to 1000 μm. The best match was calculated with the optical and thermal constants from Takata ($\mu = 26\ cm^{-1}$), Deng ($C = 4.2\ J\ g^{-1}\ ^{o}C^{-1}$), Xu ($\rho = 0.001116\ g\ mm^{-3}$), and Bowman ($D = 0.04\ mm^2\ sec^{-1}$). The second criterion was to produce the best match between the non-contact micro-bolometer thermal camera measured temperature rise and the near-surface predicted maximum temperature rise. The model predicted a significant buildup of temperature from the air – tissue interface (depth = 0 μm) to the maximum temperature at a deeper point in the skin for all combinations of thermal and optical constants, producing results on the same order of magnitude as the measurements. Because the maximum temperature rise from the models were in all cases significantly closer to the IR camera measurements than the zero depth model predictions, the modeled maximum temperature was used, as seen in Figure 6.4. The values of optical and thermal constants giving the best match to the IR camera were not the same for all six pulse sequences, as seen in Table 6.1. The third criterion for evaluation was to match the measured temperature rise from the six pulse sequences when the beam radius was doubled. The model was less successful in predicting temperatures at both the "surface" and at a depth of 337 μm with the larger

irradiation area. Under the expanded conditions, the modeled maximum temperature rise was only half of the IR camera measured temperature rise. However, the expanded beam model matched the measured temperature rise at the 337 μm thermocouple depth.

The impact on the depth at which the model predicts the maximum temperature by the optical and thermal constants is demonstrated in Figure 6.5. For example, the temperature rise in skin from a two-pulse irradiation sequence was modeled near the surface using five combinations of values. The micro-bolometer thermal camera measured temperature is shown at the depth predicted by the model using Takata's optical absorption coefficient ($\mu = 2.6$ mm^{-1}), Svaasand's thermal diffusivity of skin ($D = 0.12$ mm^2 sec^{-1}), tissue density from Sandhu ($\rho = 0.00107$ g mm^{-3}), and heat capacity from Crochet ($C = 3.4$ J g^{-1}) because this combination of values best matched the measurement. The value of the optical absorption coefficient has the most effect on the magnitude of the peak, as seen between the solid and dashed curves of the same color. Using some of the published optical absorption coefficients for TmYAG lasers, the model produced an unrealistic temperature rise in Figure 6.6 requiring two different scales for the measured and modeled temperature rise. The value of the thermal diffusivity constant of the tissue has the greatest impact on the depth at which the maximum temperature rise is predicted by the model, as seen between the solid or dashed curves of different colors. The blue and red curves were all modeled with the same values of heat capacity from Deng ($C = 4.2$ J g^{-1}) and tissue density value from Xu ($\rho = 0.001116$ g mm^{-3}). The tissue density and heat capacity in the Vyas model serve as a scaling factor and do not alter the shape of the curve. This is reflected in Table 6.1 in

which the values of the tissue density and heat capacity are the same for all pulse sequences while the optical absorption and thermal diffusivity values change.

The IR camera images produced "surface" beam profiles close to the beam intensity profiles measured with the pinhole method, but not exactly the same. The thermal images from irradiations with the original beam (nominally 3.2 mm radius) produced heat profiles larger than the IR beam intensity profile by more than one standard deviation. With the expanded beam (nominally 6.3 mm), the thermal images from all pulse sequences produced Gaussian shaped heat profiles smaller than the laser beam intensity profile measured with the pinhole-masked power meter. The results for all pulse sequences are listed in Table 6.2.

6.4 Discussion

The estimation of the effective depth of measurement of the micro-bolometer array thermal camera was based on the predicted temperatures from the Vyas Green's function bioheat model. Optimizing the model results by selecting values for the optical and thermal constants it employs, to match the camera measurements reveals three conclusions. First, the depth at which the model best matched measurements was between 50 μm and 120 μm for all three criteria. When the model was optimized for any of the matching criteria, the maximum temperature was found at increasing depth with increasing pulse sequence duty factor. As the duty factor approached one (i.e. as the sequence nears CW), the depth of maximum temperature was asymptotic to 100 μm. To generalize, for the relative absorption of 2.0 μm IR and emission of 7.5 – 13 μm IR,

the micro-bolometer effectively measures from the tissue at depths between 50 μm and 120 μm.

Second, as the pulse sequences increased in duty factor, the model followed a trend opposite to the trend of the IR camera measurements. The micro-bolometer measured increasing "surface" temperatures as the sequences approached CW. The model trended to predict lower maximum temperatures as the number of pulses in a sequence increased. This was seen when the model was optimized to best match all depths or when it focused only on the IR camera reading. This was surprising especially for the case of surface optimized modeling where the single pulse and the CW sequences were best fit to measurements with the same optical absorption and thermal diffusion values to produce the best match to measurements.

Third, when the model was optimized to match all depths, the thermocouple measured temperatures dominated the fit and produced a lower modeled temperature for all pulse sequences. This caused the difference between modeled and measured maximum temperature to increase. Lastly, the temperature rise modeled at the zero depth air – skin interface is roughly 70% of the maximum temperature for all pulse sequences optimized for either all depths or just the surface reading.

The non-contact thermal camera was found to be unsuitable as an instrument for beam profile description. The heat profile recorded was different from the direct beam intensity profile by over one standard deviation. Furthermore, for the original beam, the heat profile was larger than the direct beam profile for all pulse sequences while for the expanded beam the heat profile was smaller than the pin-hole measured beam intensity.

The depth of effective measurement of a thermal camera sensitive to far IR (7.5 – 13 μm) has been shown to be between 50 to 120 microns below the surface of the tissue – air interface for 2.0 μm laser irradiation of pig skin. The generalization of this effective depth to irradiations with other lasers, or other tissues, or other detectors would not be appropriate because all three factors influence the relationship of where the IR signal is generated from heat and to what extent it is able to reach the detector. As Figure 6.2 shows, there are a vast number of combinations of optical absorption coefficients possible between the incident laser penetrating tissue to generate heat and the resulting IR radiating out of the tissue to reach the detector.

6.5 References

1. E. F. J. Ring, "The historical development of temperature measurement in medicine," Infrared Physics & Technology **49** (3), 297-301 (2007).

2. W. Herschel, "Experiments on the refrangibility of the invisible rays of the sun. " Philosophical Transactions of the Royal Society of London **90**, 284-292 (1800).

3. P. Wright, "Neue apparate für diagnostik und therapie," Biomedizinische Technik/Biomedical Engineering **10**, 150-152 (1965).

4. R. J. Young, "Application of thermography to the problem of placental localization: Preliminary communication," British Medical Journal **2** (5415), 976.974 (1964).

5. T. J. Rockstroh and J. Mazumder, "Infrared thermographic temperature-measurement during laser heat-treatment," Applied Optics **24** (9), 1343-1345 (1985).

6. B. Choi, J. K. Barton, E. K. Chan, and A. J. Welch, "Imaging of the irradiation of skin with a clinical CO_2 laser system: Implications for laser skin resurfacing," Lasers in Surgery and Medicine **23** (4), 185-193 (1998).

7. G. E. Kopchok, R. A. White, G. H. White, R. Fujitani, J. Vlasak, L. Dykhovsky, and W. S. Grundfest, "CO2 and Agon-laser vascular welding - acute histologic and thermodynamic comparison," Lasers in Surgery and Medicine **8** (6), 584-588 (1988).

8. J. Kennet, N. Hardaker, S. Hobbs, and J. Selfe, "Cooling efficiency of 4 common cryotherapeutic agents," Journal of Athletic Training **42** (3), 343-348 (2007).

9. P. B. Rich, G. R. Dulabon, C. D. Douillet, T. M. Listwa, W. P. Robinson, B. L. Zarzaur, R. Pearlstein, and L. M. Katz, "Infrared thermography: A rapid, portable, and accurate technique to detect experimental pneumothorax," Journal of Surgical Research **120** (2), 163-170 (2004).

10. B. F. Jones, "A reappraisal of the use of infrared thermal image analysis in medicine," IEEE Transactions on Medical Imaging **17** (6), 1019-1027 (1998).

11. D. J. Ben-Eliyahu, "Infrared thermographic imaging in the detection of sympathetic dysfunction in patients with patellofemoral pain syndrome," Journal of Manipulative and Physiological Therapeutics **15** (3), 164-170 (1992).

12. J. Mnitentag, E. F. Marques, M. P. Ribeiro, G. A. Braga, M. R. Navarro, A. B. Veratti, E. Armelin, R. Macruz, and A. D. Jatene, "Thermographic study of laser on arteries," Lasers in Surgery and Medicine 7 (4), 307-329 (1987).

13. W. Gorisch, K.P. Boergen, R. C. McCord, W. Weinberg, and F. Hillenkamp, "Temperature measurements of isolated mesenteric blood vessels of the rabbit during laser irradiation," presented at the International Symposium on laser surgery, Dallas, TX, 1978.

14. E. D. Jansen, T. H. Le, and A. J. Welch, "Excimer, Ho-YAG, and q-switched Ho-YAG ablation of aorta - a comparison of temperatures and tissue-damage invitro," Applied Optics **32** (4), 526-534 (1993).

15. R. Hibst, K. Stock, and R. Kaufmann, "Ablation and controlled heating of the skin with Er:YAG laser," Lasers in Surgery and Medicine **20**, S40 (1997).

16. R. Hibst and R. Kaufmann, "Effects of laser parameters on pulsed Er-YAG laser skin ablation," Lasers in Medical Science **6** (4), 391-397 (1991).

17. J. H. Torres, J. S. Nelson, B. S. Tanenbaum, T. E. Milner, D. M. Goodman, and B. Anvari, "Estimation of internal skin temperatures in response to cryogen spray cooling: Implications for laser therapy of port wine stains," IEEE Journal of Selected Topics in Quantum Electronics **5** (4), 1058-1066 (1999).

18. E. M. B. Sorensen, S. Thomsen, A. J. Welch, and A. F. Badeau, "Morphological and surface-temperature changes in femoral arteries following laser irradiation," Lasers in Surgery and Medicine **7** (3), 249-257 (1987).

19. C. Cain, T. Milner, S. Telenkov, K. Schuster, K. Stockton, D. Stolarski, C. Condit, B. Rockwell, W. Roach, and A. J. Welch, "Porcine skin thermal response to near-ir lasers using a fast infrared camera," in *Laser interaction with tissue and cells xv*, edited by S. L. Jacques and W. P. Roach (2004), Vol. 5319, pp. 313-324.

20. C. P. Cain, G. D. Polhamus, W. P. Roach, D. J. Stolarski, K. J. Schuster, K. L. Stockton, B. A. Rockwell, B. Chen, and A. J. Welch, "Porcine skin visible lesion thresholds for near-infrared lasers including modeling at two pulse durations and spot sizes," Journal of Biomedical Optics **11** (4), 041109 (2006).

21. A. C. Tam and B. Sullivan, "Remote-sensing applications of pulsed photothermal radiometry," Applied Physics Letters **43** (4), 333-335 (1983).

22. M. H. Al-Saadi, V. Nadeau, and M. R. Dickinson, "A novel modelling and experimental technique to predict and measure tissue temperature duringco(2) laser stimuli for human pain studies," Lasers in Medical Science **21** (2), 95-100 (2006).

23. C. P. Wang, "The mathematical foundation and the boundary conditions encountered in laser energy diffusion in a solid and skin simulant temperature rise," Report NATICK/TR-96/029, (1996)

24. B. Choi, J. A. Pearce, and A. J. Welch, "Modelling infrared temperature measurements: Implications for laser irradiation and cryogen cooling studies," Physics in Medicine and Biology **45** (2), 541-557 (2000).

25. M. Ishihara, T. Arai, S. Sato, Y. Morimoto, M. Obara, and M. Kikuchi, "Nanosecond-time-response temperature measurements using radiation thermometry during 193 nm and 247 nm pulsed light irradiation: Comparison of corneal surface temperature histories," Proceedings of SPIE **4257**, 298-302 (2001).

26. B. Anvari, T. E. Milner, B. S. Tanenbaum, and J. S. Nelson, "A comparative study of human skin thermal response to sapphire contact and cryogen spray cooling," IEEE Transactions on Biomedical Engineering **45** (7), 934-941 (1998).

27. J. H. Torres, T. A. Springer, A. J. Welch, and J. A. Pearce, "Limitations of a thermal camera in measuring surface-temperature of laser-irradiated tissues," Lasers in Surgery and Medicine **10** (6), 510-523 (1990).

28. B. Chen, D. C. O'Dell, S. L. Thomsen, B. A. Rockwell, and A. J. Welch, "Porcine skin ED50 damage thresholds for 2,000 nm laser irradiation," Lasers in Surgery and Medicine **37** (5), 373-381 (2005).

29. B. Chen, D. C. O'Dell, S. L. Thomsen, B. A. Rockwell, and A. J. Welch, "Threshold damage of in vivo porcine skin at 2000 nm laser irradiation - art. No. 60840c," in *Optical interactions with tissue and cells xvii*, edited by S. L. Jacques and W. P. Roach (2006), Vol. 6084, pp. C840-C840.

30. W. L. Wolfe, "Handbook of military infrared technology," (University of Michigan, Ann Arbor MI, 1965).

31. T. Togawa, "Noncontact skin emissivity - measurement from reflectance using step change in ambient radiation temperature," Clinical Physics and Physiological Measurement **10** (1), 39-48 (1989).

32. T. Togawa, "Non-contact skin emissivity measurement by switching two shades of different temperature," Phys. Med. Biol **33** (S1), 409 (1988).

33. D. Mitchell, C. H. Wyndham, and T. Hodgson, "Emissivity and transmittance of excised human skin in its thermal emission wave band," Journal of Applied Physiology **23** (3), 390-& (1967).

34. D. J. Watmough and R. Oliver, "Wavelength dependence of skin emissivity," Physics in Medicine and Biology **14** (2), 201-& (1969).

35. D. M. Wieliczka, S. Weng, and M.R. Querry, "Wedge shaped cell for highly absorbent liquids: Infrared optical constants of water," Applied Optics **28**, 1714-1719 (1989).

36. P. J. Shayler, "Laser-beam distribution in focal region," Applied Optics **17** (17), 2673-2674 (1978).

37. R. Birngruber, "Laser output characteristics," Health Physics **56** (5), 605-611 (1989).

38. B. Chen, H. W. Kang, S. L. Thomsen, and A. J. Welch, "Modeling thermal response of skin to 2000 nm laser irradiation," Lasers in Surgery and Medicine, s**18,** 274 (2006).

39. A. Takata, "Development of criterion for skin burns," Aerospace Medicine **45** (6), 634-637 (1974).

40. T. S. Sandhu, "Measurement of blood-flow using temperature decay - effect of thermal conduction," International Journal of Radiation Oncology Biology Physics **12** (3), 373-378 (1986).

41. H. F. Bowman, E. G. Cravalho, and M. Woods, "Theory, measurement, and application of thermal properties of biomaterials," Annual Review of Biophysics and Bioengineering **4** (1), 43-80 (1975).

42. H. Bowman, "A new technique utilizing thermistor probes for the measurement of thermal properties of biomaterials," Cryobiology **13**, 572-580 (1976).

43. L. O. Svaasand, T. Boerslid, and M. Oeveraasen, "Thermal and optical-properties of living tissue - application to laser-induced hyperthermia," Lasers in Surgery and Medicine **5** (6), 589-602 (1985).

44. J. J. Crochet, S. C. Gnyawali, Y. C. Chen, E. C. Lemley, L. H. V. Wang, and W. R. Chen, "Temperature distribution in selective laser-tissue interaction," Journal of Biomedical Optics **11** (3) (2006).

45. V.V. Tuchin, *Tissue optics*, 2nd ed. (SPIE Press, Bellingham WA, 2007).

Table 6.1 Values of optical and thermal constants for 2.0 μm IR light on pig skin used in modeling to most closely predict the measured "surface value" for each of the six pulse sequences. (Values taken from the following references: [38-45])

Constant	1 pulse	2 pulse	3 pulse	4 pulse	9 pulse	CW	
Optical Absorption	2.16	2.6	2.6	2.6	2.6	2.16	mm^{-1}
Specific Heat Capacity	3.4	3.4	3.4	3.4	3.4	3.4	$J\ g^{-1}\ ^{o}C^{-1}$
Tissue Density	1.07	1.07	1.07	1.07	1.07	1.07	$g\ mm^{-3}$
Thermal Diffusivity	0.04	0.12	0.082	0.082	0.04	0.04	$mm^2\ sec^{-1}$

Table 6.2 Thermal camera average heat profile radii of 2.0 μm laser irradiations of pig skin [mm].

Pulse Sequence (Duty Factor)	Original Beam (3.2 ± 0.28 mm pinhole method)	Expanded Beam (6.3 mm pinhole method)
1 pulse (0.04)	3.50	---
2 pulse (0.08)	3.70	6.02
3 pulse (0.12)	3.55	5.86
4 pulse (0.16)	3.68	6.09
9 pulse (0.36)	3.63	5.93
CW (1.00)	3.53	6.29

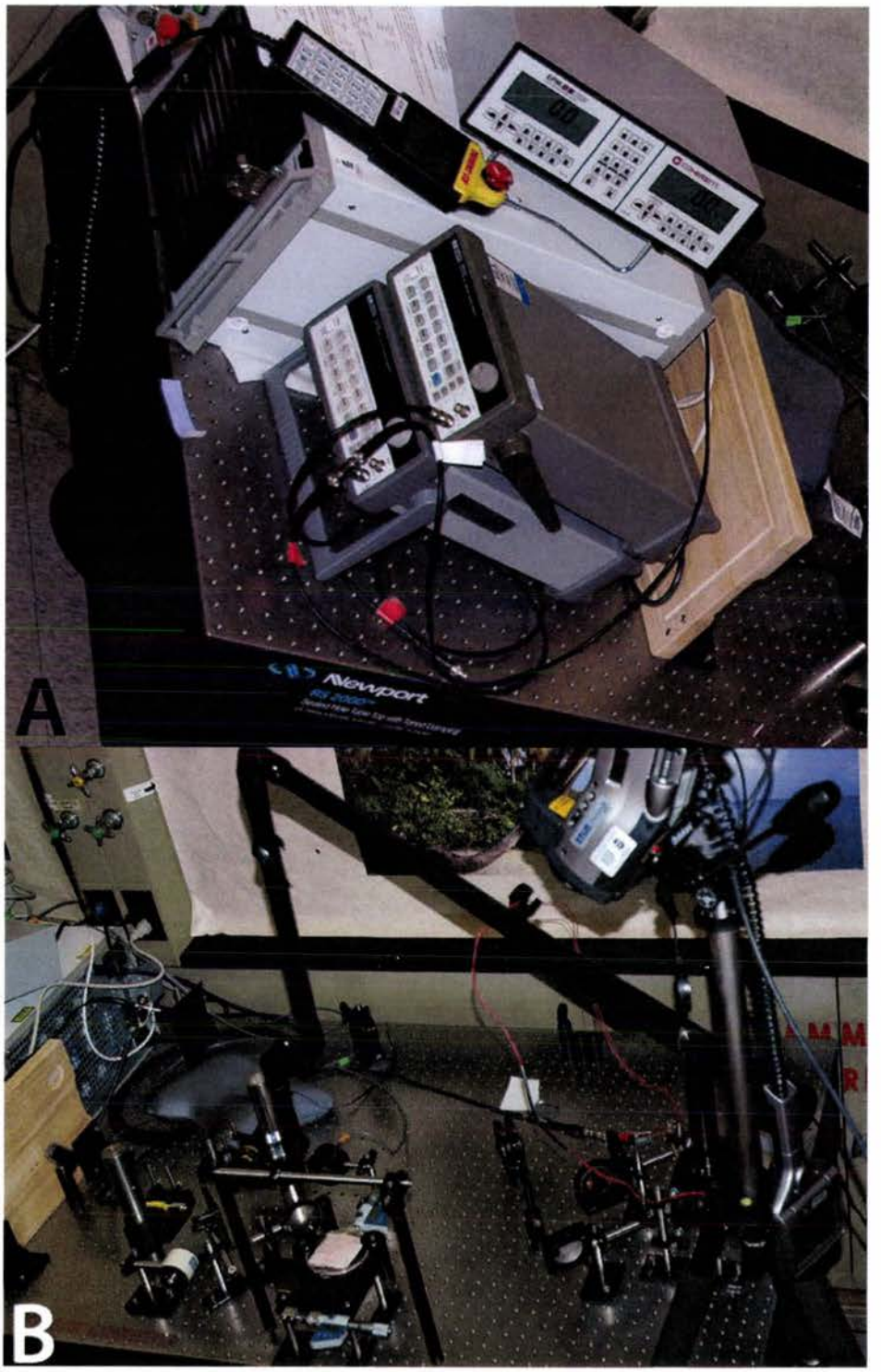
A
Newport
B

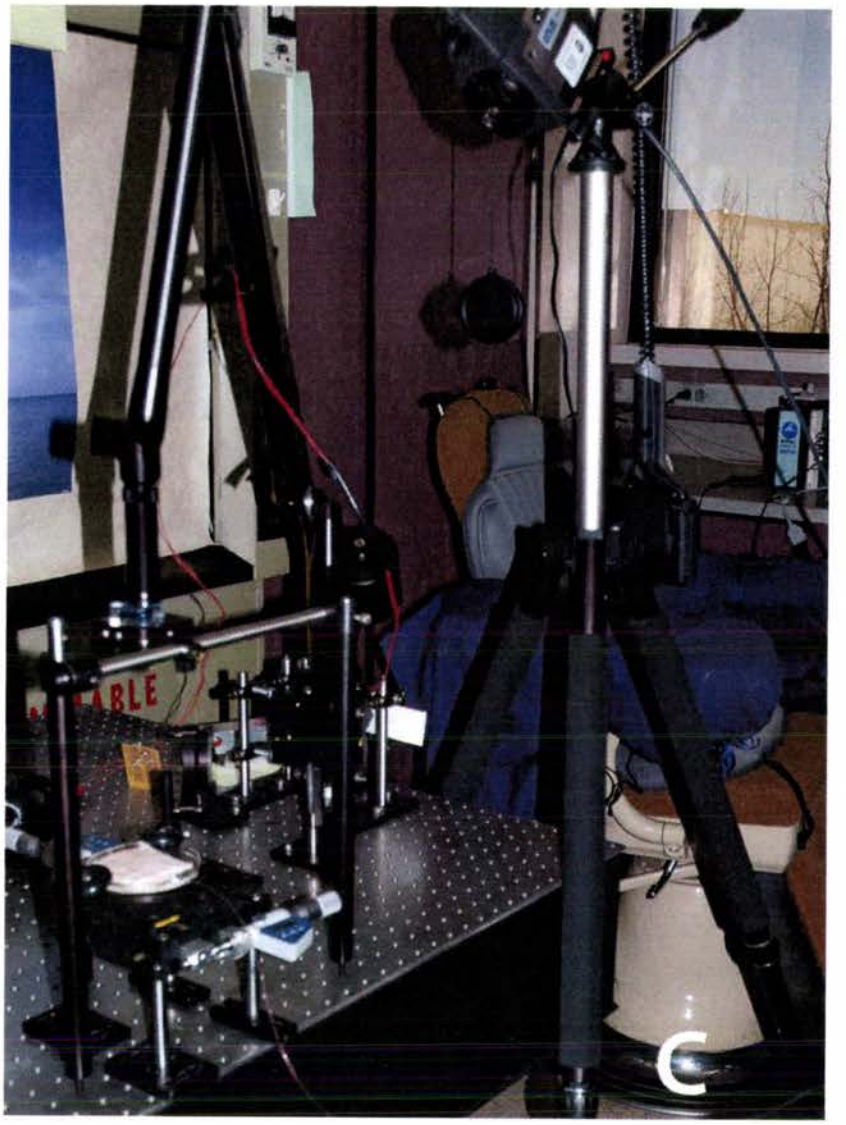

Figure 6.1 Optical and electronic set-up for pig skin irradiation showing a) Tm:YAG laser, pulse generators, and power meter, b) combining IR laser with HeNe with mirrors, thermopile and photodiode probes measuring reflection off of cold-mirrors and centering into articulating arm, c) articulating arm delivering both beams to be normal to the tissue sample surface mounted on micrometer optical stage with microbolometer thermal camera in measurement position.

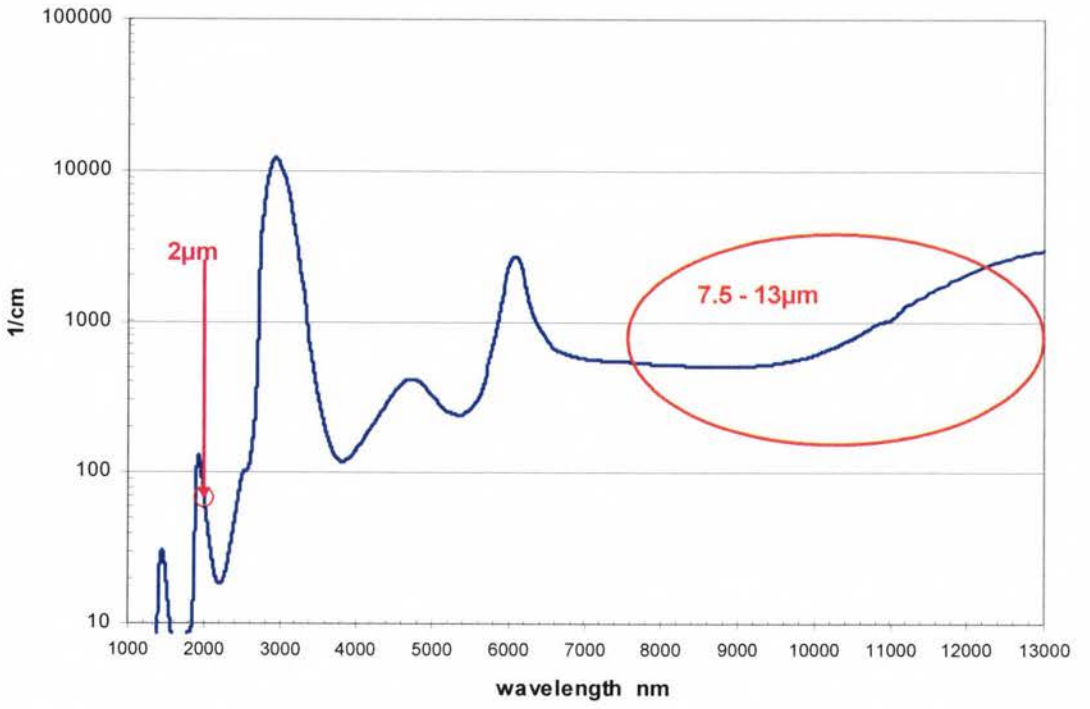

Figure 6.2 IR attenuation coefficient in water over spectrum of interest to Tm:YAG (2,010 nm indicated by red arrow) irradiation of skin measured by micro-bolometer array thermal camera sensitive over 7,500 to 13,000 nm (orange). (Spectrum data downloaded from http://omlc.ogi.edu/spectra/water/abs/index.html July 2008)

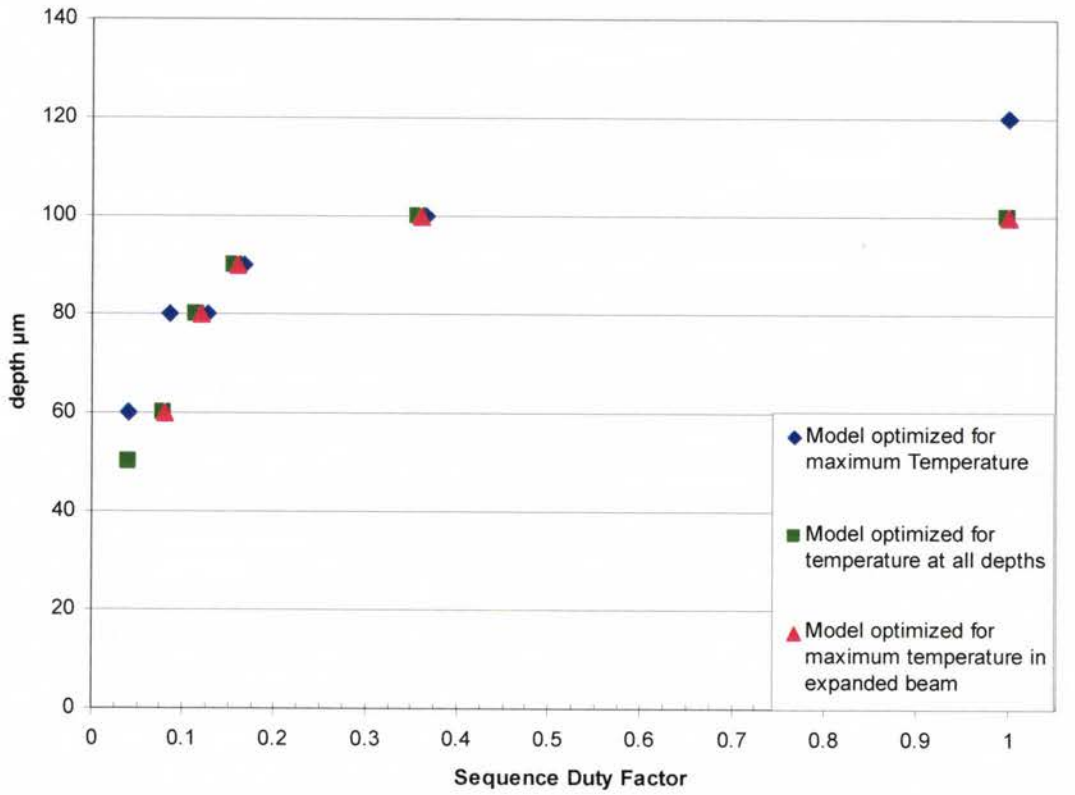

Figure 6.3 Depth at which model predicts the maximum temperature for each pulse sequence. Depth varies slightly when model was optimized for best match by three separate criteria listed in graph legend. Optical and thermal constants used in the model are listed in Table 6.1.

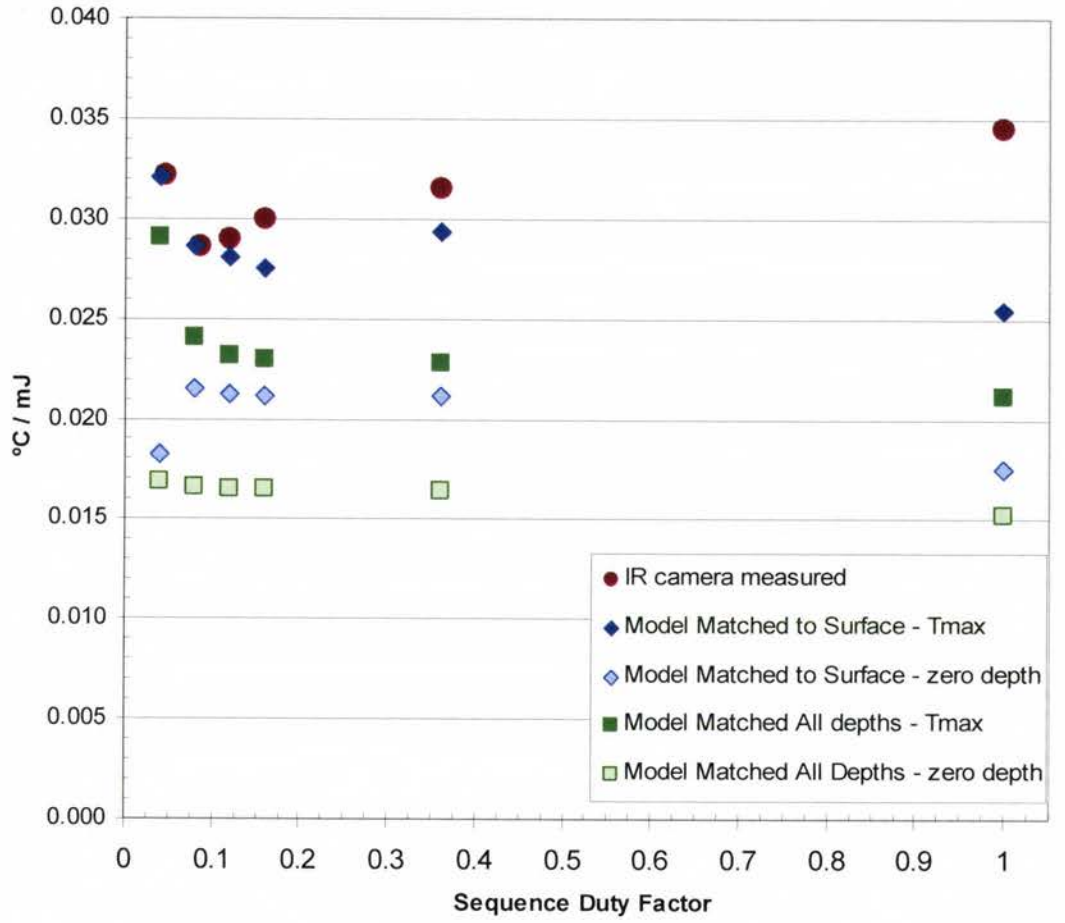

Figure 6.4 Modeled temperature rise per radiant energy on pig skin for two modeling criteria. Temperature rise given for both criteria at two depths. Measured "surface" temperature by microbolometer IR camera for six pulse sequences studied (single pulse DF =0.04, CW DF = 1.0).

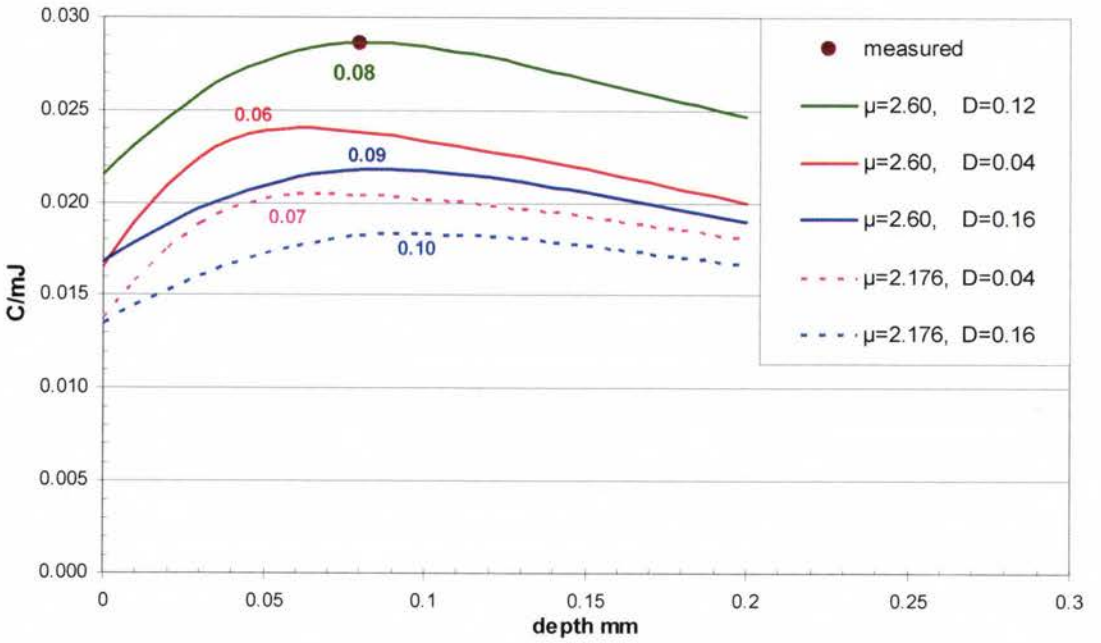

Figure 6.5 Modeled temperature rise per radiant exposure in a two pulse sequence using different published values for the optical absorption and thermal diffusivity constants of pig skin (heat capacity $C = 3.4$ J g^{-1}, tissue density $\rho = 0.001116$ g mm^{-3}). Depth at which the model reaches maximum is labeled in color corresponding to the curve.

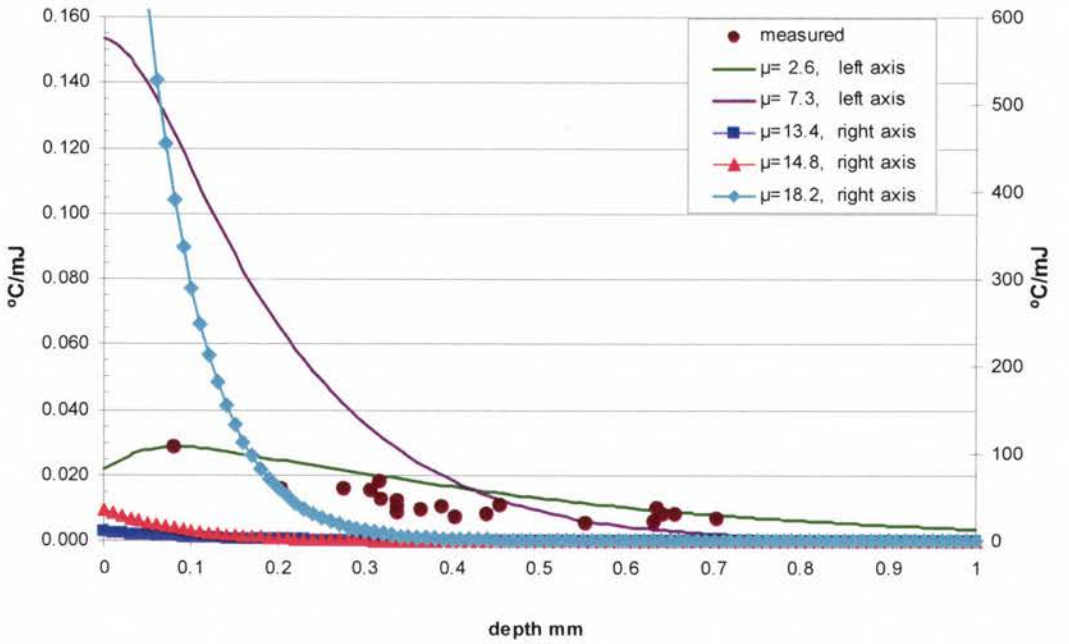

Figure 6.6 Impact of optical absorption coefficient value. Modeled temperature rise per radiant exposure in a two pulse sequence using different published values for the optical absorption coefficient of pig skin (thermal diffusivity D = 0.12 mm^2 sec^{-1}, heat capacity C = 3.4 J g^{-1}, tissue density ρ = 0.001116 g mm^{-3}). Measured temperature rise from thermocouple probe and IR micro-bolometer array camera. Curves with markers refer to vertical axis on right, smooth curves refer to vertical axis on left.

Chapter 7

Summary and Conclusions

7.1 Summary of Results

The large differences in reported values of optical absorption coefficients for 2.0 μm laser light incident on skin prompted an investigation into methods of measuring this constant. A method was successfully developed to grow human keratinocytes in vitro into a uniform optically thin sample for transmission, scattering, and reflection measurements. The histology of the cultured cells demonstrated that the cells could be grown without holes or large variations in thickness. The collagen growth medium was shown to influence the optical properties at varying rates in different parts of the spectrum. This method has the advantage and limitation of excluding melanin from the sample. In the visible portion of the spectrum where melanin is a dominant chromophore, the absence of melanin could be useful in conjunction with measurements of natural skin to isolate the melanin contribution to absorption of light. Cultured optical samples avoid the mechanical, thermal, and chemical changes produced by freezing, homogenization, or compression introduced in conventional sample preparation and handling. Overall the method of culturing tissue samples proved to be useful for measurements of optical properties.

Investigations of the performance capabilities of two non-contact IR temperature measurement instruments have been performed. The tests were similar to those performed on another type of thermal imaging camera using a single detector when possible. In other tests, new approaches were developed to determine the instruments' capabilities. The tests found that the pyrometer had a Signal to Noise Ratio too low to measure skin irradiations with TmYAG lasers at power levels set low enough to avoid injury to the tissue.

Pig skin samples that were irradiated with six pulse sequences with increasing duty factor from a TmYAG laser were measured for temperature rise at four depths from zero to 650 μm within the skin. The analysis found that the different sequences produced values of temperature rise per unit exposure which were statistically different with a p-value less than 0.001. The common assumption of linearly additive heat from thermally confined impulses of laser energy has been shown to break down for 2.0 μm infrared pulses in the millisecond range.

Pig skin samples' temperature rise during and following pulsed laser irradiation were measured from the surface to a depth of over 1 mm. The depths were relatively evenly spaced in 22 intervals. In addition, temperature measurements within pigskin samples were taken across the beam profile. These measurements were used to determine the set of values for optical and thermal constants used in an analytical thermal model which best predicted the temperature rise in skin from pulsed TmYAG laser irradiation.

The analytical model of pig skin temperature rise from pulsed TmYAG laser irradiation was used to estimate the skin depth at which a micro-bolometer array

measured temperatures. The effective depth of measurement was determined by matching the non-contact thermal camera measurements of "surface" temperature during irradiation with the modeled temperatures through time and depth. The depth at which the modeled temperature best matched the camera's measurements during the irradiation sequence changed from 50 μm to 120 μm as the laser pulse sequence duty factor increased from 0.04 to 1.0.

7.2 Conclusions

The cultured keratinocytes offer a new methodology for measurement of biological tissue optical properties. Cultured optical samples avoid the mechanical, thermal, and chemical changes produced by freezing, homogenization, or compression introduced in conventional sample preparation and handling.

The tests of the IR temperature measurement instruments found that the pyrometer had an unacceptably low SNR for skin irradiation experiments which would use exposures less than the visible lesion threshold. Therefore, it was unable to provide the temporal resolution of 5 msec which it was specified to offer. The pyrometer also required a target area of uniform temperature larger than its focal spot of 4.4 mm in order to give accurate measurements. This also disqualified the pyrometer from laser skin injury sub-threshold studies. The micro-bolometer was shown to provide a very low noise measurement suitable to 10 msec laser pulses producing temperature increases of 5 °C.

The ability to lower the maximum temperature rise of a laser exposure to skin through manipulation of laser pulse width and pulse sequence duty factor is useful. For

several clinical fields such as neurology, diabetes, and pain management, lasers are a common tool to produce sensation in specific nerves in the extremities. Delivering the laser energy in pulse sequences with reduced maximal temperature rise offers a larger margin of safety to these procedures. The statistically different temperature rise produced by varying the laser pulse sequences to deliver the same total energy opens the possibility to perform these irradiations with greater margins of safety.

The different values of optical absorption and thermal diffusivity of a tissue at a particular wavelength which are published in literature can produce thermal predictions spanning several orders of magnitude. This uncertainty in modeled results requires experimental validation of a model, and the constants used in the model, to give credible predictions of laser – tissue interactions.

The common assumption of IR thermal camera temperature measurements is that measurements represent the temperature at the air – tissue interface. The analytical heat model has shown that the camera is responding to far infra-red thermal radiation in the range of 7.5 to 13 μm which measures the temperature of skin at depths from 50 to 120 μm when heated with pulses of Tm:YAG laser light.

7.3 Further Investigation

The experiments and research undertaken in this dissertation raise questions as well as finding answers. Some of these questions merit further research to complete the work initiated in this dissertation, and are discussed as follows.

The first problem which should be addressed is determination of the combined transmission, scatter, and reflection measurements of cultured keratinocytes to determine

values of optical absorption and scatter coefficients. Arrangements for using an optical integrating sphere detector would need to be coordinated with the growth of the cell cultures for this to succeed. In addition, many more cell cultures would be required to provide adequate numbers for averaging of histological thickness measurements to use in the calculations.

The second question which would be useful to the scientific community would be to compare the temporal and spatial resolution of thermal imaging cameras which utilize the several types of infrared detector. The micro-bolometer array is a common detector, but so are flying spot cooled HgCdTe detectors and InSb detectors. A common method of determining the temporal resolution of the system would benefit camera users and manufacturers. The small diameters of many laser beams, combined with their Gaussian intensity profile, suggests that spatial resolution of thermal cameras should be reported with more detail than the angular spread of the field of view or the lens focal spot. The Modulation Transfer Function is a method to describe the comprehensive spatial resolution of the entire thermal imaging system, including lenses, detector, and electronics. A standard protocol for measuring MTF would enable comparison of measurement systems between studies.

The differences in temperature rise per incident radiant energy demonstrated for different pulse sequences has significant implications for efforts to use mid-infrared lasers to produce sensation in human skin. The current study employed one beam size, one wavelength, one pulse sequence duration, and all sequences were composed of multiple 10 msec pulses. Further investigation of this phenomenon would be useful to explore these additional variables. In addition, pulse sequences in which the power of

successive pulses is varied should be investigated to determine combinations which could maintain a temperature producing sensation without exceeding tissue damage thresholds.

The many, and widespread, values of thermal and optical constants of biological tissue have been shown to predict temperatures varying by orders of magnitude with analytical models. Further investigation is warranted to determine if the values of these thermal tissue constants (C, D, ρ) found to match measured temperatures with the Tm:YAG laser would also predict temperatures from other lasers.

The effective depth of measurement of a micro-bolometer thermal camera has been found for Tm:YAG laser pulses incident on pig skin. Similar techniques could be used for thermal imaging cameras which employ other types of IR detectors. Additionally, pig skin irradiations with other wavelength lasers should be measured with the micro-bolometer camera. The results matched to similarly predicted temperatures from the analytical heat model would allow the effective depth of measurement to be either generalized to other wavelengths or limited to specific combinations of detector and incident laser. This information could be very important to evaluations of laser effects. Knowledge of the depth at which the measurements represent the tissue temperature will improve the physiological understanding of laser injury.